Bioconjugation Study of Upconversion Nanoparticles for Cancer Detection

By

Yu Shi

Department of Chemistry and Biomolecular Sciences

MACQUARIE University
SYDNEY·AUSTRALIA

A thesis submitted for the degree of Doctor of Philosophy

June 2016

To my parents

To my wife

To my forthcoming baby

I certify that the work in this thesis has not previously been submitted for a degree nor has it been submitted as part of requirements for a degree to any other university or institution other than Macquarie University.

Yu Shi

Acknowledgements

First of all, I sincerely acknowledge my supervisors Prof. Helena Nevalainen, Prof. Nicolle H. Packer and Dr. Bingyang Shi who have always been inspiring, encouraging and supporting me during my candidature. I appreciate everything they have done in assisting to design my PhD project and spending a lot of time to structure and polish my thesis and paper. In addition, the most valuable thing I learnt from Prof. Helena Nevalainen is responsibility and how to be independent and impartial. Prof. Nicolle H. Packer taught me logical thinking in academic research and what is the true science. Dr. Bingyang Shi always sticks up for me like an elder brother particularly in my toughest times. Not only the knowledge, but also the truth in life I learnt from my supervisors will benefit for my future career.

I would also like to thank all my group members and lab colleagues. In particular, Dr. Liisa Kautto and Dr. Tom Lawson offered me with a lot of help in my experiments and helped to formulate my PhD research especially when I started the project. Dr. Run Zhang, Dr. Arun Everest Dass and Dr. Nima Sayyadi provided their profession advice on my PhD project. Dr. Yiqing Lu, Dr. Lixin Zhang and Mr. Xianlin Zheng kindly helped and supported me to debug the confocal microscope system. Mr. Deming Liu, Mr. Shihui Wen and Ms. Chenshuo Ma selflessly shared their knowledge of materials science with me. I couldn’t have completed my thesis without their knowledge and experience.

I also received a lot of support from my project collaborators in Minomic Int. Dr. Brad Walsh, Ms. Irene Justinian and other members in the company provided antibodies, cell lines and experimental protocols to me. I am grateful for their generous help.

I would like to acknowledge the China Scholarship Council (CSC) and Macquarie University for the finance support of my PhD study.

I must express my sincerely acknowledgements to my parents for their care, understanding and great support throughout my life. Their love is the fundamental motivation for keeping me moving forward.

In the end, I want to thank my wife Faye, for her understanding and endless love.

Abstract

Over the past decades, nanotechnology and fluorescence imaging techniques have become increasingly attractive for early detection of cancer. The high sensitivity required for differentiating abnormal cells from normal cells presents a challenge to existing diagnostic protocols. Among other types of nanomaterials, lanthanide-doped upconversion nanoparticles (UCNPs) have unique optical properties and thus hold a great promise in cancer detection at a very early stage using fluorescence imaging. Large Stokes and anti-Stokes shifts, long luminescence lifetime and excellent photostability make UCNPs a good choice for biological and biomedical applications.

On the other hand, biological detection based on UCNP-probes is seriously limited by aggregation of the UCNPs when interacting with biomolecules and by non-specific binding in cell-based detection assays. This thesis explores a series of novel UCNP bioconjugation strategies to overcome the current barriers in bioapplications of UCNPs by enhancing their water dispersibility and stability and decreasing the non-specific binding of UCNP-biomolecule conjugates.

In this research, $NaYF_4$: Yb^{3+}/Er^{3+} and $NaYF_4$: Yb^{3+}/Tm^{3+} UCNPs were synthesized and a $NaYF_4$: Yb^{3+}/Er^{3+}@$NaGdF_4$ core-shell structure was used to improve the upconversion luminescence intensity (Chapter 2). Various surface modification methods including ligand attraction, ligand oxidation, ligand exchange and silica coating were tested and compared to identify a suitable approach for the subsequent bioconjugation study (Chapter 3). Two novel bioconjugation strategies will be presented in detail. Chapter 4 illustrates conjugation of UCNPs to the MIL-38 antibodies through a biotin-streptavidin bridge. Chapter 5 demonstrates a modified one step bioconjugation strategy between UCNPs and MIL-38 antibodies by using a poly(ethylene glycol) (PEG)

linker and orientation controlled functionalization of antibodies. Both novel UCNP-biomolecule conjugation strategies produce water-stable and dispersible products and the biomolecules tested retained their biological activity during the conjugation process. In addition, a fabricated UCNP-antibody complex specifically targeting DU145 prostate cancer cells without detectable non-specific binding was achieved.

Key words: upconversion nanoparticles, cancer early detection, bioconjugation, non-specific binding

List of Acronyms (in alphabetic order)

ABL	abelson murine leukemia viral oncogene homolog 1
ADIBO	aza-dibenzocyclooctyne
APTES	(3-aminopropyl)triethoxysilane
α-CD	α-cyclodextrin
BCR	breakpoint cluster region
BRAF	v-raf murine sarcoma viral oncogene homolog B1
BSA	bovine serum albumin
CCD	charge-coupled device
CD	cluster of differentiation
CFTR	cystic fibrosis trans-membrane conductance regulator
CTC	circulating tumor cell
CTL	cytotoxic T lymphocytes
CYP	cytochrome P450
CV	coefficient of variation
DAPI	indole-6-carboxamidine
DBO	dihexyloxybenzene
DEG	diethylene glycol
DELFIA	dissociation-enhanced lanthanide fluorescent immunoassay
DLS	dynamic light scattering

DMEM	Dulbecco's modified Eagle's medium
DMF	dimethyl formamide
DMSO	dimethyl sulfoxide
DNA	deoxyribonucleic acid
DSPE	1,2-distearoyl-sn-glycero-3-phosphoethanolamine
EDC	1-ethyl-3-(3-dimethylaminopropyl) carbodiimide
EDTA	ethylenediaminetetraacetic acid
ELISA	enzyme-linked immunosorbent assay
FBS	fetal bovine serum
FITC	fluorescein isothiocynate
FRET	fluorescence resonance energy transfer
FT-IR	Fourier transform infrared spectroscopy
GFP	green fluorescent protein
HBO	hydroxyphenyl benzoxazole
HIV	human immunodeficiency virus
HHV	human herpesvirus
CO-520	polyoxyethylene (5) nonylphenylether
IFA	immunofluorescence assay
IR	infrared
LED	light-emitting diode

LOD	limit of detection
LOQ	limit of quantitation
LRET	luminescence resonance energy transfer
MOFO	monofluorinated cyclooctyne
MTT	3-(4,5-dimethylthiazol-2-yl)-2,5-diphenyltetrazolium bromide
NC	nitrocellulose membranes
NHS	N-hydroxysuccinimide
OA	oleic acid
OM	oleylamine
ODE	1-octadecene
OPEA	O-phosphorlethanolemine
OSAM	orthogonal scanning automated microscopy
PAA	poly(acrylic acid)
PAGE	polyacrylamide gel electrophoresis
PBS	Phosphate-buffered saline
PCDA-ABA	pentacosadiynoic acid-aminobutyric acid
PCR	polymerase chain reaction
PEG	poly (ethylene glycol)
PEO	poly (ethylene oxide)
PMT	photomultiplier tube

PNA	peptide nucleic acid
POC	point of care
PSA	prostate-specific antigen
PSCA	prostate stem cell antigen
RNA	ribonucleic acid
SA	streptavidin
SDS	sodium dodecyl sulphate
SNR	signal-to-noise ratio
TAT	trans-activator of transcription
TAMRA	tetramethylrhodamine
TEM	transmission electron microscopy
TEOS	tetraethyl orthosilicate
TGL	time-gated luminescence
TP53	tumor protein 53
TRACE	time-resolved amplified cryptate emission
UC	upconversion
UINBs	upconversion immune-nanohybrids
UV	ultraviolet
WB	Western blot
XRD	X-ray diffraction

Contents

Chapter 1: Introduction

This thesis focuses on the development of novel bioconjugation approaches for upconversion nanoparticles (UCNPs). These nanoparticles can be used as efficient detection probes to interact with biomolecules in order to overcome critical limitations of conventional detection methods. Working towards achieving a high water dispersibility and stability of the nanoparticles and capped biomolecules in biological applications hold great promise in biomedical diagnosis of cancer at a very early stage.

This chapter provides an overview of using UCNP based fluorescent probes for cancer detection. It discusses the current status of cancer detection and motivation for developing new detection techniques. In addition, advantages and progress of biological applications of UCNP fluorescent probes and surface chemistry of the functionalization of UCNPs will be discussed.

1.1 Challenges in Cancer Detection and Fluorescence Based Nanotechnology

Cancer is the second most common cause of death and causes more than one in four of all deaths in the United States annually (DeSantis, Lin et al. 2014; Siegel, Miller et al. 2015). In Australia, one in two men and one in three women are diagnosed with cancer before the age of 85 (Stewart and Wild 2015). The high mortality rate of cancer is in part a reflection of the difficulties associated with its treatment as it is a complex disease involving genetic instability and dysregulation of cell growth where changes in gene expression allow abnormal cells to grow in an uncontrolled manner (Pantel, Brakenhoff et al. 2008). Despite the high incidence and lethality, detection of the presence of cancer early enough can greatly reduce the rate of mortality. As an example, the 5-year survival

rate of a breast cancer patient is 85% for stage II patients (small areas of cancer cells are detected in the lymph nodes) but merely 20% for patients who are at stage IV (cancer has spread to other parts of body) (Hanahan and Weinberg 2000; Hanahan and Weinberg 2011). In contrast, a patients' 5-year survival rate can be increased to 98% if the tumor is recognized and therapy started at the 0 stage (cancer cells localized in the breast) or stage I (cancer cells starting to invade normal surrounding breast tissue) (Ferrari 2005; Pantel, Brakenhoff et al. 2008; Higgins and Ettinger 2009; Chikkaveeraiah, Bhirde et al. 2012).

Similarity between benign tissues and diseased tissues proposes a challenge to differentiate and identify a cancerous cell (Backman, Wallace et al. 2000). Current clinical diagnostic methods depend mainly upon imaging and morphological detection techniques (Hayat 2008; Stewart and Wild 2015). Imaging techniques can involve X-rays, ultrasound imaging (UI), computed tomography (CT), magnetic resonance imaging (MRI), positron emission tomography (PET), single photon emission computed tomography (SPECT) and optical imaging, but these procedures can suffer from low sensitivity and can be expensive to perform (Mettlin, Lee et al. 1991; Pastorino, Bellomi et al. 2003). Morphological analysis including cytology and histopathology face a similar issue of low sensitivity, which does limit the ability to differentiate between healthy and diseased tissues and may thus miss early stage detection (Wulfkuhle, Liotta et al. 2003; Choi, Kwak et al. 2010; Xing, Todd et al. 2010). Therefore, there is an ongoing and pressing need to develop a new class of screening techniques to allow highly sensitive early stage cancer detection.

1.1.1 Cancer Nanotechnology

In recent years, nanotechnology has emerged as a new field of multidisciplinary

research involving biology, chemistry, biochemistry, material science, engineering and physics and has been used to address some of the limitations of the current detection techniques (Ferrari 2005; Nie, Xing et al. 2007; Yao, Yang et al. 2014; Wolfbeis 2015). Materials with at least one or more dimensions at the nanoscale exhibit several unique physical and biochemical properties which can be exploited in nanodevices (Bertrand, Wu et al. 2014). Nanoparticles possess many advantages as probes for biological and biomedical applications (e.g. bioimaging and biosensing). The small size of nanoparticles permits access across biological barriers such as the blood-brain barrier and cell membranes, so they can readily interact with various biological systems at a molecular level. Their size allows them to stay in blood and the body fluid circulation system for a relative long time in part because they are larger than the renal clearance threshold (at 10 nm) (Bertrand, Wu et al. 2014). Another advantage is their multivalent nature, which enables simultaneous targeting of multiple molecules or proteins (Ferrari 2005; Misra, Acharya et al. 2010). Multivalent properties also can increase the binding ability of receptors and decrease chances for their dissociation. Multiple targeting ligands or therapy ligands can be conjugated to the surface of one nanoparticle simultaneously which offers a possibility of combination of diagnostics and therapy (Ehdaie 2007). The therapy response can be monitored in real-time with these dual functional particles. In addition to these advantages, nanoparticles can also provide higher sensitivity in biological applications when compared to organic dyes due to their unique optical properties, such as long fluorescence lifetime and resistance of photobleaching (Wolfbeis 2015). In summary, by taking advantage of the unique optical properties and surface functionality, nanoparticle-based probes can be used to target and monitor biological events and have been used in reports elsewhere for cancer diagnostics. As such, nanotechnology has a broad prospect in cancer detection, because of its enhanced sensitivity and because of the versatility of fluorescence-based detection techniques that can be made part of the approach (Srinivas, Barker et al. 2002; Wang, Shin et al. 2007).

Nanotechnology can be combined with fluorescent detection techniques. As an optical phenomenon, fluorescence can occur when a material absorbs photons at one energy level and then emits them at another, usually lower level (although some particles can now emit at a higher level) (Berezin and Achilefu 2010). Fluorescence spectroscopy takes advantage of this feature of fluorescence and has been frequently used in biological applications of biomolecule detection (Lian, Litherland et al. 2004). For example, it can be used in solution based assays for cancer biomarker detection. Fluorescence microscopy can be applied for *in vitro* cell imaging and biosensing or *in vivo* animal imaging. Flow cytometry allows for high-throughput single cell detection which has potential to be applied in clinical diagnosis (Akers, Berezin et al. 2010). Application of fluorescence techniques for cancer detection relies on the unique optical properties (e.g. quantum yield, fluorescent lifetime and photostability) of various fluorophores, such as organic dyes, quantum dots or upoconversion nanoparticles (Chen 2008; Yao, Yang et al. 2014). Nanoparticle-based fluorophores will be discussed in detail in the following sections.

1.1.2 Nanoparticles for Cancer Detection

In the past decades, organic dyes and fluorescent proteins have been extensively investigated as fluorescent probes for biological and biomedical detection approaches (Hoffman 2005; Luo, Zhang et al. 2011). These traditional fluorophores exhibit several important characteristics such as small size, high fluorescence intensity and good biocompatibility. However, their application in biological detection is normally limited by a series drawbacks, such as high photobleaching characteristics, low photostability, high risk of chemical degradation, narrow absorption with broad emission and short detection time (Resch-Genger, Grabolle et al. 2008). To overcome these drawbacks, a wide range of nanoparticles with better optical properties are being continually developed for cancer detection (**Table 1.1**) (Choi, Kwak et al. 2010). The most widely

used nanoparticles in cancer diagnosis will be briefly discussed in the following (Alok, Panat et al. 2013; Vinhas, Cordeiro et al. 2015).

Types of Nanoparticles	Advantages	Disadvantages	Applications
Quantum Dots (QDs)	• Brighter and more stable signal intensity than organic fluorescent molecules • Predictable range of emission frequencies	• Composed of heavy metal • Exposed to UV may release cytotoxic heavy metal irons	• Fluorescent imaging assays to detect cell surface antigen • *In vivo* cancer detection • Live cells *in vitro* labeling for gene expression study
Magnetic Nanoparticles (MNPs)	• Easy to manufacture • Chemical stable • Biocompatible • Magnetism in external magnetic field allows control over distribution • Low toxicity	• Aggregation may lead to embolization and thrombosis	• Magnetic cell separation for cancer diagnosis • Used as MRI contrast agents • Drugs and genes delivery • Thernotherapy
Gold Nanoparticles (AuNPs)	• Toxicity is surface modification dependent • Size confinement effect • Gold has approved for treating humans	• Poor biocompatibility • Uncertain fate *in vivo*	• Controlled drugs, proteins, DNA release • *In vivo* imaging in photoacoustic tomography, X-rays • Used as fluorescence quencher
Polymer Dots (PDs)	• Biodegradable • Ultrabrightness • High photostability • Nonphotoblinking • Low toxicity	• Low efficiency of delivery • May cause complement activation related pseudo allergy	• *In vitro* and *in vivo* imaging • Plasmid DNA, proteins, peptides, drugs and contrast agents delivery

Table 1.1 Summary of nanoparticles for cancer diagnosis. Sourced from Alok, Panat et al. 2013 and Vinhas, Cordeiro et al. (2015).

Quantum dots (QDs). When compared to organic dyes (e.g. fluorescein isothiocyanate (FITC), 4',6-diamidino-2-phenylindole (DAPI)) and fluorescent proteins (e.g. green fluorescent protein, GFP), semiconductor quantum dots (QDs) have some desirable properties, which can be used in the development of novel applications for cancer diagnosis and biological imaging (Chan and Nie 1998; Alivisatos, Gu et al. 2005; Burda,

Chen et al. 2005; Michalet, Pinaud et al. 2005). For instance, QDs have much higher brightness than organic dyes, and this can be attributed to the molar absorption coefficients that are 30-50 times higher than those of organic dyes. In addition, the fluorescence lifetime of QDs can last up to 10 ns, which is much longer than that of organic dyes (1-5 ns). This feature allows QDs to display an improved signal-to-noise ratio in bioimaging because a time-gated measurement can separate the fluorescence of QDs from any background autofluorescence that is present in the biological spectrum (Smith, Duan et al. 2008; Kairdolf, Smith et al. 2013). Therefore, the application of QDs in cancer detection can bring a greater sensitivity to the detection of cancer biomarker or abnormal tumor cells. Moreover, QDs have broad absorption spectra and narrow emission spectra compared to organic dyes (**Figure 1.1A**) and the emission wavelength of QDs is size-tunable (**Figure 1.1B**) (Jaiswal and Simon 2004). Together these unique properties can enable a single excitation to generate multiple emissions from a range of QDs made to different sizes, which can facilitate multicolor imaging for the detection of multiple targets simultaneously from a single particle (Michalet, Pinaud et al. 2005; Xing and Rao 2008; Wegner and Hildebrandt 2015).

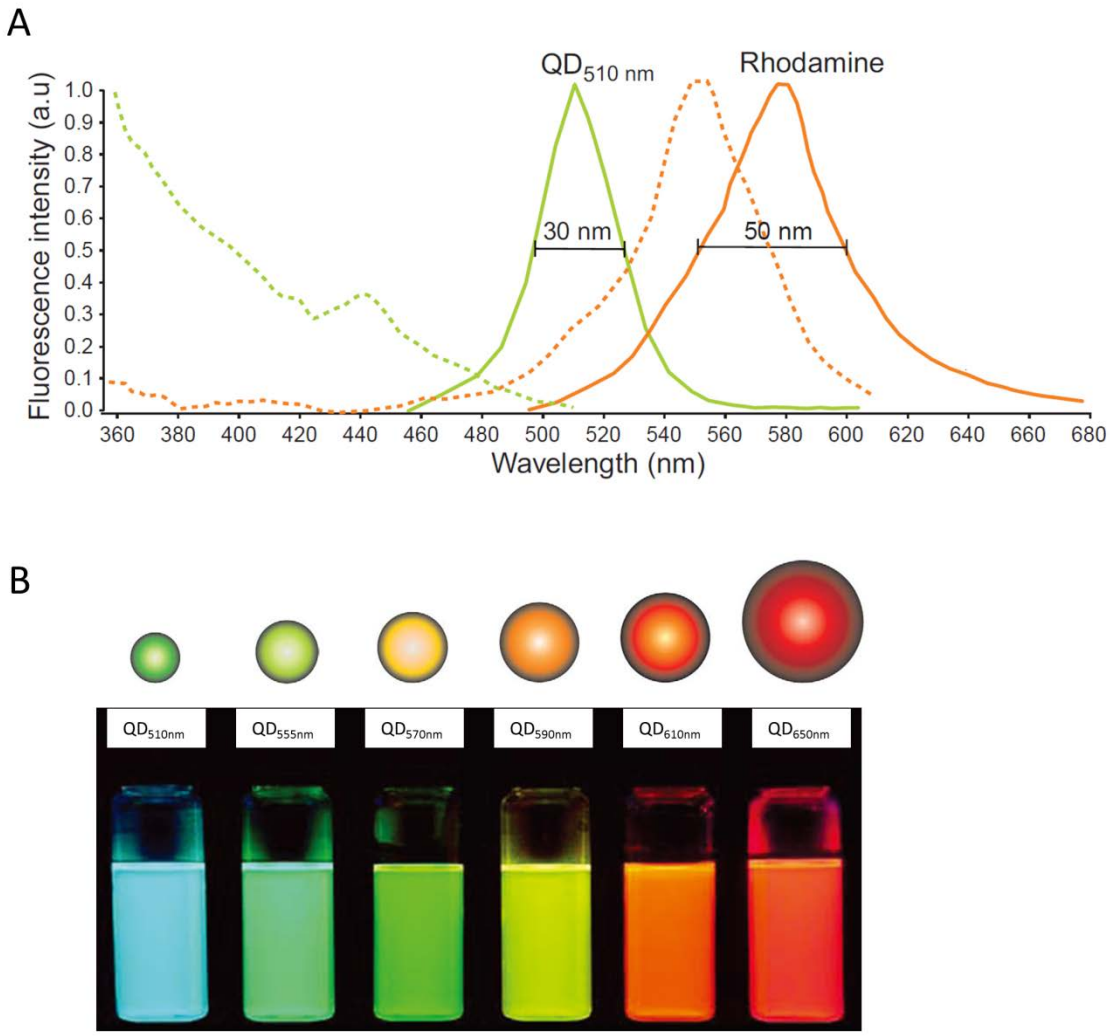

Figure 1.1 (A) A comparison of fluorescence excitation and emission characteristics of QDs and an organic fluorescent dye-Rhodamine. QDs (green broken line) excitation spectrum is broader than that of an organic dye (rhodamine, orange broken line). The emission spectrum of QDs (solid green line) is narrower than that of organic dyes (rhodamine, solid orange line). Numerical values (as nanometers) show the full spectral width at half-maximum intensity; (B) Schematic representation of size-tunable emission properties of QDs (emission wavelength increases with the increase of particle size). Reproduced from Jaiswal and Simon (2004).

Magnetic nanoparticles (MNPs). As a class of engineered particulate material, magnetic nanoparticles (MNPs) can be manipulated under the magnetic field and have been investigated in biomedicine as a contrast probe in magnetic resonance imaging (MRI) (Ito, Shinkai et al. 2005). MNPs consist of various magnetic elements (e.g. Fe, Ni, Co and Mn) and their oxides such as Fe_3O_4, Fe_2CoO_4 and MnO. The magnetic property of MNPs is based on their magnetic susceptibility which depends on the temperature, external field and atomic structure of MNPs and is defined by the ratio of induced magnetization to magnetic field (Kodama 1999; Lu, Salabas et al. 2007). This phenomenon of superparamagnetism of MNPs not only allows them to maintain magnetism after the influence of an external magnetic field, but also helps to reduce the risk of their aggregation. Ultrasensitive MNPs such as this are useful as probes as they have a high chemical stability and biocompatibility, and as such have been applied in the field of cell tracking, liver, lymph node imaging and drug delivery (Pankhurst, Connolly et al. 2003; Tartaj, del Puerto Morales et al. 2003).

Gold nanoparticles (AuNPs) Gold nanoparticles (AuNPs) are another type of nanomaterial that have been investigated and used in fluorescence assays for cancer diagnostics and also possess unique optical properties (Kelly, Coronado et al. 2003; Anker, Hall et al. 2008; Jain, Huang et al. 2008). AuNPs display size confinement effect, which explains their optical and electrical properties. Also, they exhibit a distinct feature, size-dependent absorption in ultraviolet-visible spectra caused by the surface plasmon resonance (SPR). This SPR frequency of Au NPs is a function of the shape, particle size, aggregate morphology, surface modification of the individual particles, and as well a function of the properties of the surrounding solvent (Cai, Gao et al. 2008; Giljohann, Seferos et al. 2010). In addition, AuNPs can be used as a fluorescence quencher that suitable for a variety of biological applications as a model of “on-off” fluorescence probes (Homola 2008). Moreover, AuNPs also can be used for single molecule surface-enhanced Raman scattering (SERS) detection. This effect allows their

incorporation in Au-NP-based biosensors to enhance detection sensitivity in biological applications (Hutter and Fendler 2004; Huang, Jain et al. 2007; Jain, Huang et al. 2008).

Polymer dots (PDs). Semiconducting polymer nanoparticles represent a new class of ultrabright fluorescent probes applied for biological and biomedical imaging (Szymanski, Wu et al. 2005; Wu, Bull et al. 2008; Tuncel and Demir 2010; Cheng, Wang et al. 2013). PDs offer several unique characteristics for various fluorescence studies and optoelectronic appliances such as field-effect transistors, photovoltaic devices and light emitting diodes. Important properties exhibited by PDs include ultra-brightness, high photostability, nonphotoblinking and nontoxicity (Tuncel and Demir 2010; Wu and Chiu 2013). PDs exhibit broad absorption and narrow emission wavelength spectra and offer a significantly higher fluorescence quantum yield in comparison with QDs. The emission spectra of PDs can be easily tuned when altering their composition and this can be useful for *in vitro* and *in vivo* multimodal imaging (Wu, Peng et al. 2006; Wu, Szymanski et al. 2007; Wu, Schneider et al. 2010).

Upconversion nanoparticles (UCNPs). UCNPs have recently emerged as an exciting new class of optical fluorescence probes for biological and biomedical detection. They are essentially nano-sized crystals of inorganic rare earth (lanthanide) (Wang, Banerjee et al. 2010; Barreto, O'Malley et al. 2011). The term "upconversion" is characterized by the conversion of lower energy radiation, which typically is near-infrared (NIR), to higher energy radiation, which is usually in the visible range, via the effect of multiphoton NIR absorption (**Figure 1.2A**) (Gnach and Bednarkiewicz 2012; Chen, Qiu et al. 2014). This is opposite to the conventional downconversion fluorophores such as organic dyes and fluorescent nanoparticles (e.g. semiconductor QDs and AuNPs), which exhibit a Stokes shift of high to low radiation (**Figure 1.2C**).

The anti-Stokes effect is very useful in biological and biomedical applications due to the minimization of autofluorescence of cells and tissues when excited at a 980 nm wavelength. (Cheng, Wang et al. 2013; Chien, Chou et al. 2013; Li, Zhang et al. 2015). For another matter, the discrete emission peaks of UCNPs can be easily separated from the excitation wavelength due to the large anti-Stokes shift and the emission bands are fairly narrow which allows further separation of positive signals (Lim, Riehn et al. 2009; Park, Lee et al. 2015). Thus, the effect of upconversion luminescence enables ultrasensitive detection by increasing the signal-to-noise ratio (Wang, Banerjee et al. 2010) and allows greater tissue-transparent NIR excitation for deeper tissue penetration *in vivo* (Vennerberg and Lin 2011). Besides these unique optical properties, UCNPs also exhibit other important features, including high chemical stability, non-photobleaching and non-photoblinking (in contrast to QDs) (Wang, Banerjee et al. 2010; Vennerberg and Lin 2011). Moreover, the rare earth components of UCNPs are less toxic than heavy metal components of QDs and the NIR excitation wavelength of UCNPs is less cytotoxic (Hardman 2006; Shan, Budijono et al. 2011; Chien, Chou et al. 2013).

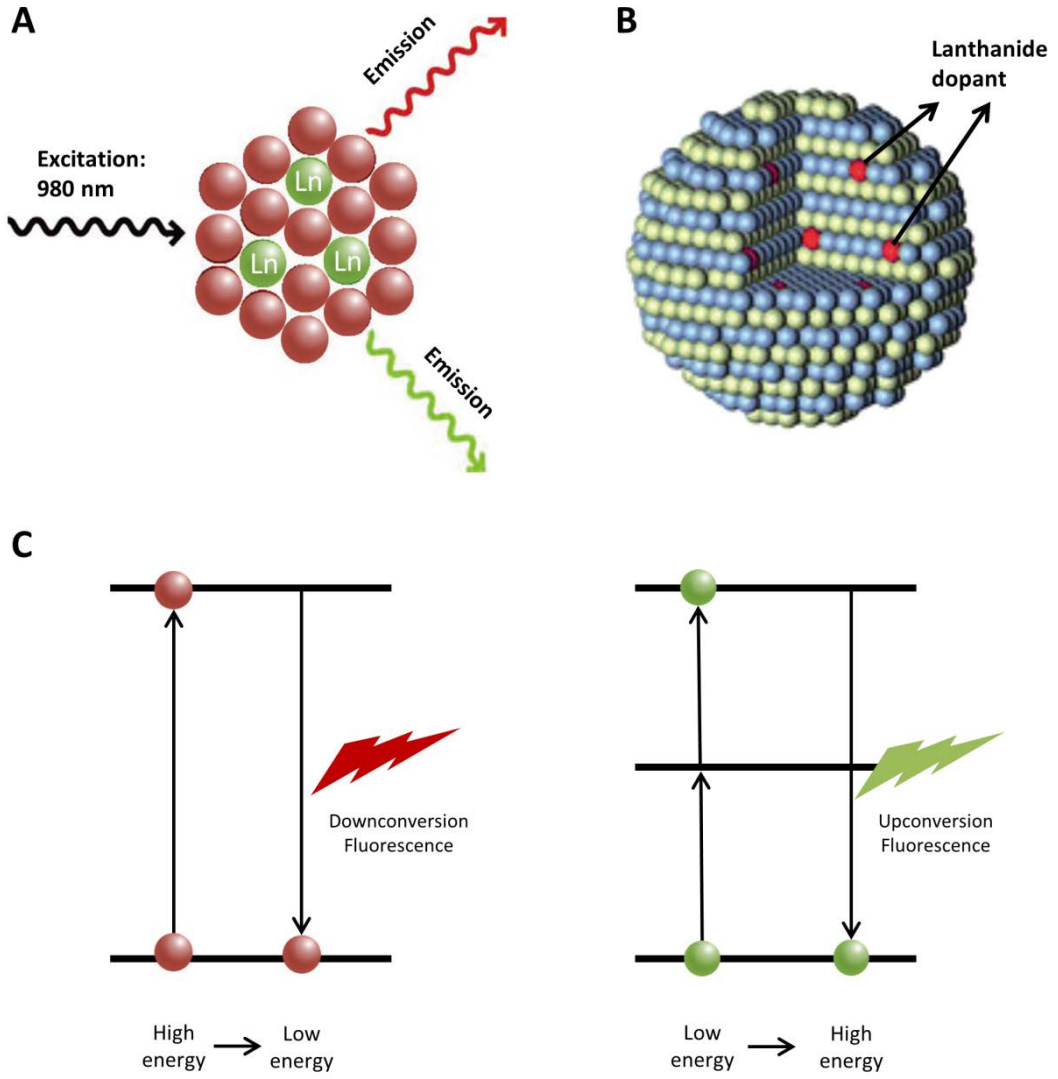

Figure 1.2 (A) Schematic representation of energy upconversion by an UCNP. (B) Schematic representation of rare earth element crystalline host with Ln^{3+} dopant. (C) Comparison of the mechanism of downconversion and upconversion fluorescence. (A) Reproduced from Gnach and Bednarkiewicz (2012). (B) Reproduced from Wang, Banerjee et al. (2010). (C) Reproduced from Vennerberg and Lin (2011).

UCNPs are composed of a rare earth element crystalline substrate, the host matrix, which is doped with small amounts of lanthanide ions (**Figure 1.2B**). There are two

major types of inorganic host matrices used to produce UCNPs, (1) rare earth oxides, such as Y_2O_3 and Y_2O_2S, and (2) rare earth fluorides, such as LaF_3, $NaYF_4$ and $NaGdF_4$ (Wang, Banerjee et al. 2010; Wang, Abbineni et al. 2011). Among different types of crystalline host lattice, $NaYF_4$ and $NaGdF_4$ are the most common and the co-doped sensitizer Yb^{3+} and emitter Ln^{3+} (e.g. Er, Tm and Ho) are the most frequently used. For example in **Figure 1.3A**, $NaYF_4$: Yb^{3+}/Er^{3+} uses Er as emitter and exhibits two predominant emission peaks: green light (at ≈540 nm) and red light (at ≈650 nm) (Wang and Liu 2008; Chen, Qiu et al. 2014). By using the Tm element as emitter, $NaYF_4$: Yb^{3+}/Tm^{3+}, it changes to emission bands close to 480 and 650 nm, respectively and a NIR emission close to 800 nm (Vennerberg and Lin 2011; Xu, Zhan et al. 2013; Wu, Chen et al. 2015). Unlike the size dependent emission colors of QDs, the multicolor emission of UCNPs can be easily tuned, but not necessarily consistently, by altering the various combinations of host crystal and lanthanide dopant ions so that the emission can occur across a broad-spectrum ranging from NIR to violet (**Figure 1.3B**) (Wang and Liu 2008).

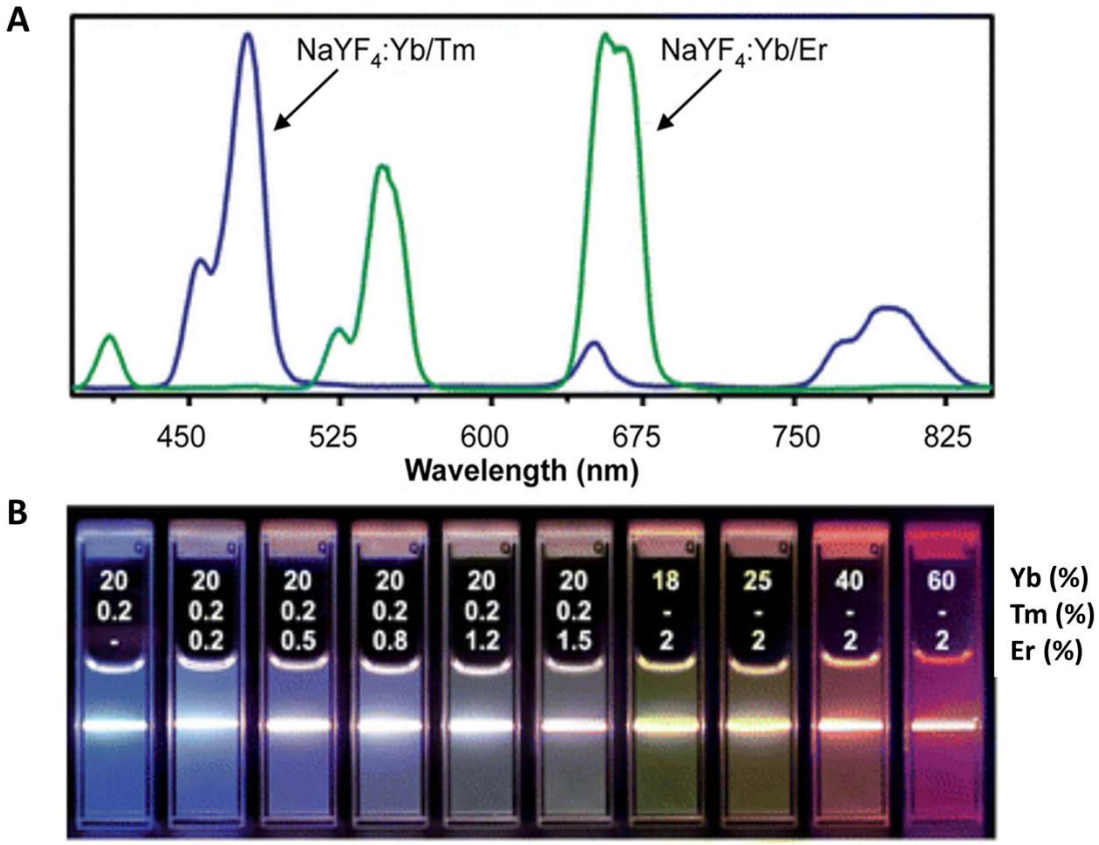

Figure 1.3 (A) Emission spectra of $NaYF_4$: Yb^{3+}/Tm^{3+} compared to $NaYF_4$: Yb^{3+}/Er^{3+} demonstrates the composition- dependent emission profiles of UCNPs. (B) Complied luminescent photos showing colloidal solutions of UCNPs doped with varying ratios of Yb/Tm, and Er are excited at 980 nm. The different colors represent changes in the emission spectra. (A) Reproduced from Chen, Qiu et al. (2014). (B and C) Reproduced from Wang and Liu (2008).

The process of upconversion was proven to be a successful strategy for producing visible emission from NIR excitation. The mechanisms of the upconversion processing including excited state absorption (ESA), energy transfer (ET) and photon avalanche (PA) have been extensively investigated over the past decades (Tsuda, Soga et al. 1999;

Pollnau, Gamelin et al. 2000). Because of the main focus of this thesis, the details of different mechanisms or the various approaches of UCNP synthesis (e.g. coprecipitation method, thermal decomposition method and hydrothermal method) will not be discussed further. More information regarding UCNP synthesis, upconversion mechanism and luminescence efficiency enhancement can be accessed in reports elsewhere (Vetrone, Boyer et al. 2004; Wang, Chatterjee et al. 2006; Li and Zhang 2008; Wang, Wang et al. 2010).

1.2 UCNPs in Cancer Detection

UCNPs with unique optical properties have been extensively reported in various applications in the fields of biomedical imaging, bioassays, biosensors, photodynamic therapy, chemotherapy, gene therapy, thermal sensing and some other applications involving solar cells, photocatalysis and security applications (**Figure 1.4**) (Kim, Nyk et al. 2009; Gu, Yan et al. 2013; Wang, Cheng et al. 2013; Chen, Qiu et al. 2014). However, this work will be only focusing on UCNPs and their use in cancer detection. The topic is divided into three main categories: (1) detection of extracellular cancer biomarkers; (2) detection of cancer cells *in vitro*, and (3) detection of tumor tissue *in vivo*. Details of the detection of extracellular cancer biomarkers will be discussed next.

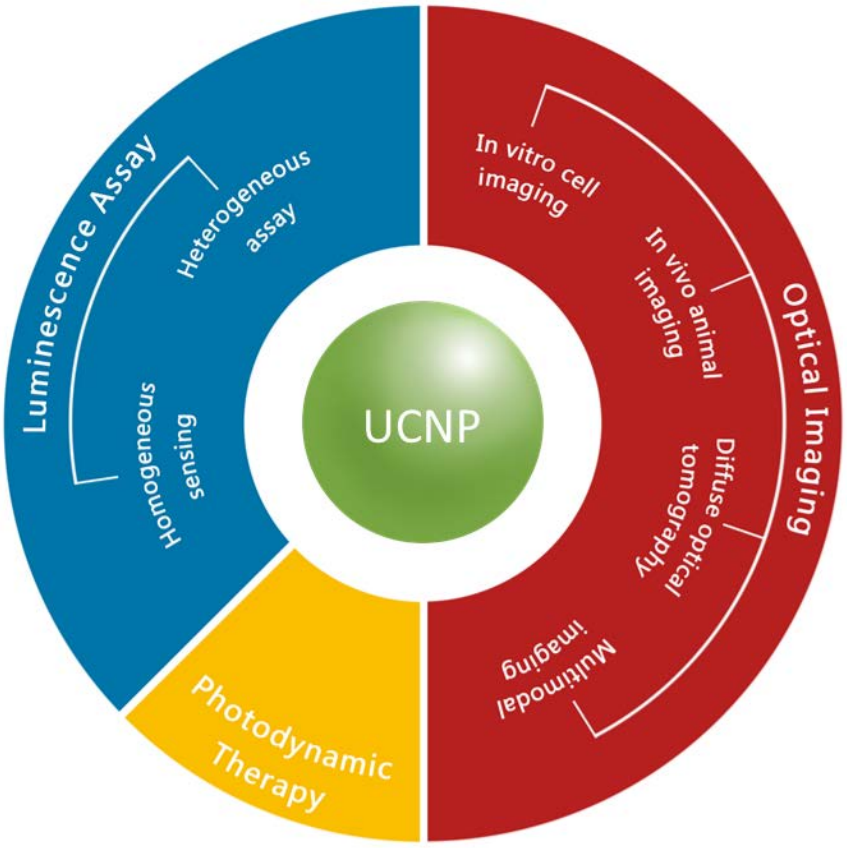

Figure 1.4 Schematic illustration of biological application of UCNPs. Sourced from Wang, Banerjee et al. (2010).

1.2.1 Detection of Cancer Biomarkers with UCNPs

Efficient and early identification and detection of known cancer biomarkers associated with cancerous cells in the blood or other body fluid systems is a central requirement for a cancer probe. Cancer biomarkers associated with cancer cells include secreted proteins, cell surface proteins, nucleic acids or glycans and these can leave clues for cancer diagnosis at a very early stage (Crawley and O'Kennedy 2015; Devi, Doble et al. 2015). Measuring a cancer biomarker in blood, urine, saliva of patients' fluids provides a possibility of detection of cancer at an early stage and predicts tumor recurrence. Proposed challenges are the low abundance of cancer biomarkers in body fluids and the requirement of ultrasensitive probes and screening approaches (Pepe, Etzioni et al. 2001;

Srinivas, Kramer et al. 2001; Rusling, Kumar et al. 2010). Because of their high sensitivity, lanthanide ion-doped UCNPs have been investigated in various bioanalytical assays to solve this issue. These investigations have focused on the heterogeneous upconversion luminescence assay (Wu, Duan et al. 2011; Wang, Wei et al. 2014; Wu, Cen et al. 2014; Huang, Tu et al. 2015) and homogeneous upconversion-FRET assay (Deng, Xie et al. 2011; Yang, Zhao et al. 2012; Wang, Wolfbeis et al. 2013; Chen, Guan et al. 2014).

For the heterogeneous upconversion luminescence assay, Zijlmans et al. reported the application of Y_2O_2S: Yb/Er submicron as a fluorescent reporter to detect the prostate specific antigen (PSA) in human prostate 17 years ago. Considerable studies have attempted to develop monodispersed and uniform-sized UCNPs with high upconversion luminescence to enhance the sensitivity and reduce non-specific binding in bioanalytical assays (Zijlmans, Bonnet et al. 1999). For instance, Liu et al. developed a microplate (96-well plate) assay to detect and quantify various cancer biomarkers (Liu, Tu et al. 2013). They synthesized a $LiLuF_4$: Ln^{3+}@$LiLuF_4$ core/shell UCNPs and conjugated these with avidin to form a sensitive upconversion detection probe which can detect β-hGC as low as 3.8 ng/mL concentration (**Figure 1.5A**). In another study, the $LiLuF_4$: Ln^{3+}@$LiLuF_4$ core/shell UCNPs were conjugated with ATF of uPA to detect H1299 human lung cancer cells by recognizing the overexpressed biomarker uPAR on the H1299 cell membrane (**Figure 1.5B**) (Huang, Zheng et al. 2014). The group also reported a detection assay (Ai, Tu et al. 2013) of PSA, carcinoembryonic antigen (CEA), and alfa-fetoprotein (AFP) with the detection limit down to 20 pM, which is an improvement on the sensitivity compared to other types of conventional immunofluorescence assays, such as a homogeneous time-resolved FRET assay based on ZrO_2: Tb^{3+} nanoparticles with detection limits of 3.0 nM (Liu, Zhou et al. 2012).

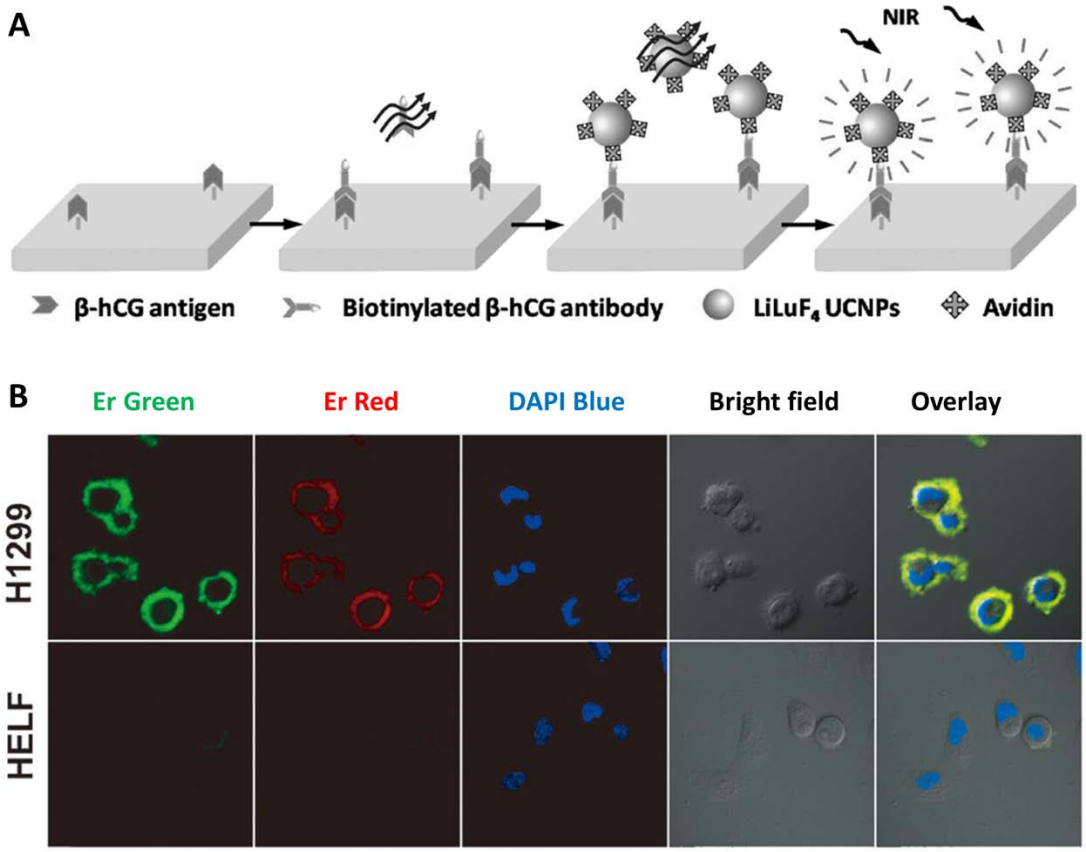

Figure 1.5 (A) Schematic representation of heterogeneous upconversion detection of β-hCG. (B) Fluorescence images of H1299 and HELF cells after incubation with ATF-coupled LiLuF4: Yb/Er@LiLuF4 core–shell UCNPs. Reproduced from Huang, Zheng et al. (2014).

In the homogeneous assay, lanthanide ion-doped UCNPs are commonly used as an energy donor for Förster resonance energy transfer (FRET)-based biological detection (Yang, Zhao et al. 2012). FRET is a mechanism of transfer of the excitation energy from the light sensitive donor molecule (chromophore) to another nearby acceptor molecule (Miyawaki, Llopis et al. 1997; Jares-Erijman and Jovin 2003). Over the past years, FRET-based bioanalytical techniques have gained considerable attention because of their sensitivity and have been extensively applied in biological detection. Moreover,

their use in conjugation with UCNPs which have their own unique optical properties including a large anti-Stokes shift, multiwavelength emission, high flexibility and applicability, have made the UCNP-FRET assay appealing (Wang, Peng et al. 2011; Shi, Tian et al. 2015). After the first report of lanthanide ion-doped UCNPs used in FRET-based detection in 2005, many homogeneous assays have been developed along similar lines for the detection of tumor biomarkers and other molecules (Wang, Yan et al. 2005; Liu, Chen et al. 2013; Wang, Wolfbeis et al. 2013). In 2014, Wang and coworkers demonstrated a NIR UCNP-FRET platform to detect AFP in human serum by using $NaYF_4$: Yb^{3+}/Tm^{3+}@$NaGdF_4$ core/shell UCNPs as an energy donor and gold nanorods as an acceptor (**Figure 1.6A**) (Chen, Guan et al. 2014). In this detection assay, the upconversion luminescence intensity had a linear relation with the concentration of AFP and the detection limit of AFP was measured at a very low level of 0.16 ng/mL. In 2013, Liu's group reported a point-of-care test by applying a paper-based microfluidic system (UC-μPAD) (**Figure 1.6B**). In this UCNP-FRET based detection study, cancer biomarker matrix metalloproteinase-2 (MMP2) and human serum CEA were measured and the detection limit was further reduced to less than 1 pg/mL (He and Liu 2013). Chu and coworkers further elaborated on the UCNP-FRET assay by applying a $NaYF_4$: Yb^{3+}/Er^{3+} as a donor and rhodamine B as an acceptor to detect phospholipase D (PLD) from cell lysate. The studies discussed provide illuminating examples of how the UCNP-FRET based assays can be used to detect cancer biomarkers (Cen, Wu et al. 2014).

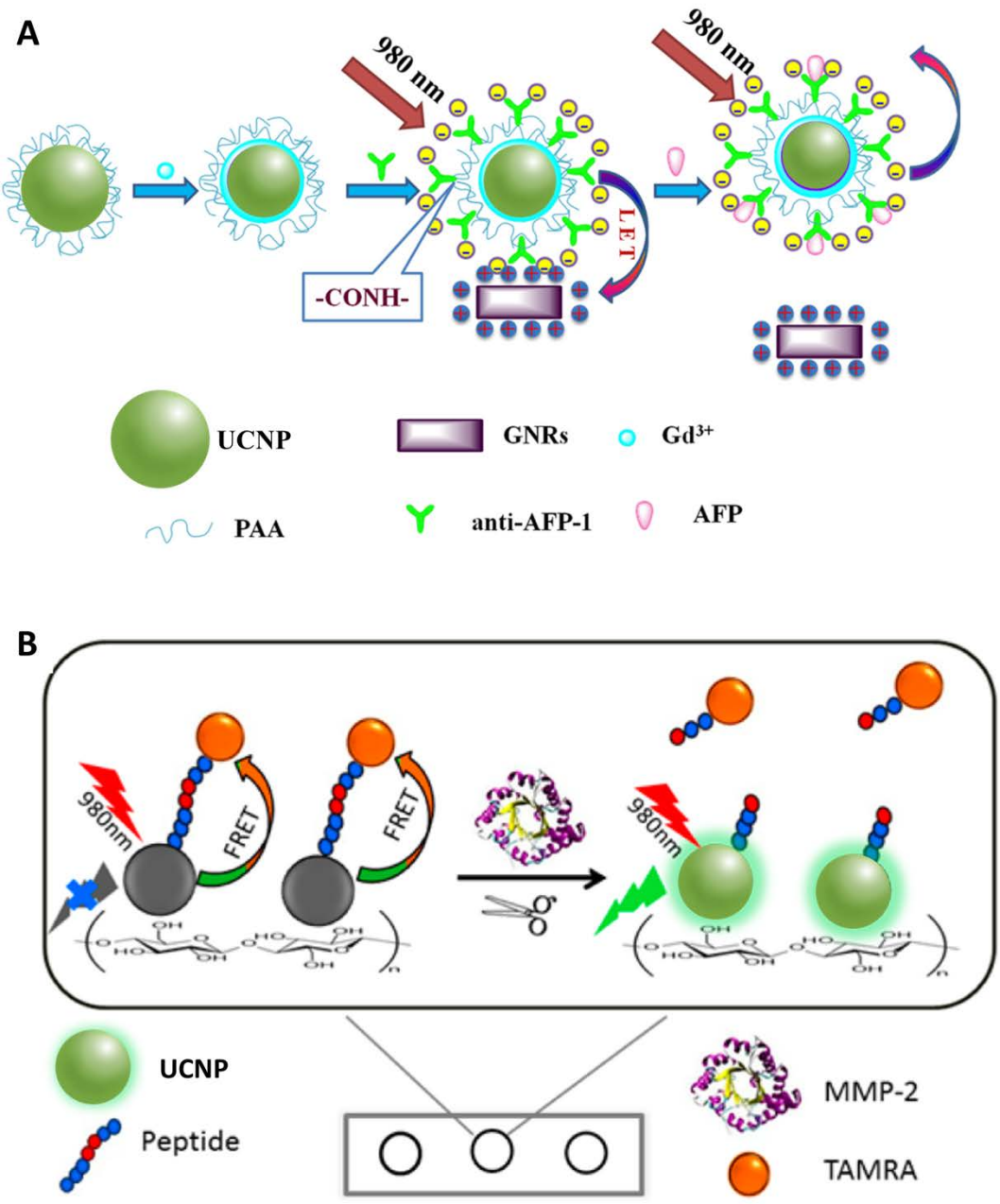

Figure 1.6 (A) Schematic representation of an AFP biosensor based on FRET from anti-AFP conjugated UCNPs to gold NRs. (B) Schematic representation of the UC-μPAD for the MMP-2 assay based on the cleavage of a specific peptide substrate by the target and FRET from UCNPs to TAMRA (tetramethylrhodamine) dye. (A) Reproduced from Chen, Guan et al. (2014). (B) Reproduced from He and Liu (2013).

1.2.2 Detection of Cancer Cells *in vitro* with UCNPs

The tumor cells circulate in body fluids or blood during cancer metastasis when the cancerous cells spread from the primary tumor site to blood or the lymphatic system (Budd, Cristofanilli et al. 2006; Hayes, Cristofanilli et al. 2006). The detection of tumor circulating cells (CTCs) can provide an opportunity to predict and identify cancer metastasis before formation of the second tumor site and thus can provide an opportunity for treatment at the early stage of metastasis (Cristofanilli, Hayes et al. 2005). However, CTCs are found at the frequencies of 1 in 10^5 cells in blood which requires new approach to achieve an effective detection. Nanotechnology with ultrasensitive detection probes and fluorescence techniques has attracted increasing attention to provide solutions for early detection of tumor cells. Over the past decades, many groups have developed UCNPs as fluorescence probes to detect tumor cells by targeting cancer biomarkers on cell membrane (Wang, Cheng et al. 2012; Xu, Zhan et al. 2013; Min, Li et al. 2014). To achieve a successful specific labeling, a variety of recognition moieties such as peptides, antibodies, DNA and small molecules can be conjugated to the surface of UCNPs to provide selective labeling of the targets of interest (Pantel, Brakenhoff et al. 2008; Haun, Devaraj et al. 2010; Mi, Li et al. 2011).

In 2008, Chatterjee and coworkers were the first to demonstrate the use of UCNPs for *in vitro* cell imaging application (**Figure 1.7**) (Chatterjee, Rufaihah et al. 2008). The $NaYF_4$: Yb^{3+}/Er^{3+} UCNPs were conjugated with folic acid and were targeted to HT29 human adenocarcinoma cells and OVCAR3 human ovarian carcinoma cells that express abnormal high levels of folate receptors. The UCNPs as detection probes offered strong upconversion luminescence without background autofluorescence under NIR 980 nm excitation. In a similar study, Jiang and coworkers used folic acid functionalized $NaYF_4$: Yb^{3+}/Er^{3+} UCNPs to detect HT-29 human colorectal cancer cells.

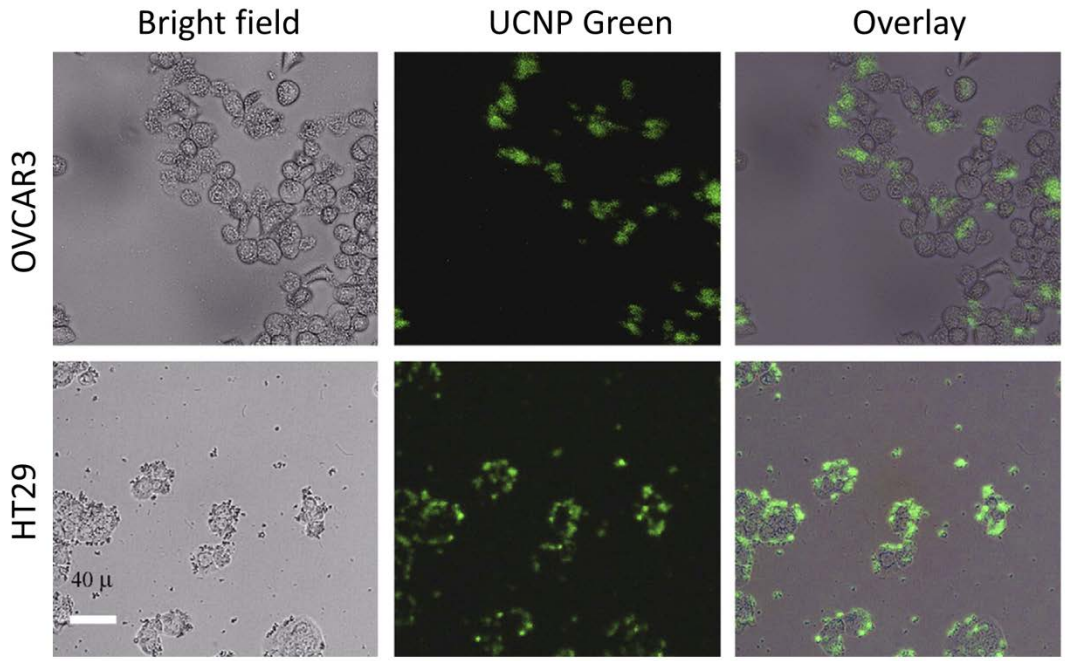

Figure 1.7 Fluorescence images of live human ovarian carcinoma cells (OVCAR3, top row) and human colonic adenocarcinoma cells (HT29, bottom row) after incubation with folic acid modified PEI/$NaYF_4$ UCNPs. The left rows are images in bright-field, the middle rows are fluorescent images under 980 nm excitation, and the right rows are overlays of the left and middle rows. Reproduced from Chatterjee, Rufaihah et al. (2008).

In several other studies, antibodies have been used to modify UCNPs so that they were more efficient in their recognition and this can be attributed to a high affinity of the interaction between an antigen and antibody. Wang and coworkers employed silica coated $NaYF_4$: Yb^{3+}/Er^{3+} and $NaYF_4$: $Er^{3+}/Tm^{3+}/Ho^{3+}$ UCNPs to conjugate with anti-CEA8 antibody. Here the anti-CEA8 modified UCNPs specifically attached to Hela cells due to the high expression of the CEA8 tumor marker on the membranes of cancer cells (**Figure 1.8**). Besides this research, other antibodies have been used to modify UCNPs in cancer detection. Examples include the anti-Her2 antibody conjugated

UCNPs for the detection of SK-BR-3 human breast cancer cells (Jiang, Zhang et al. 2009); anti-claudin 4 and anti-mesothelin antibodies conjugated UCNPs for Panc 1 cell detection (Kumar, Nyk et al. 2009); and (arginylglycylaspartic acid) RGD peptide conjugated UCNPs for detecting $\alpha_v\beta_3$ integrin receptors on U87MG human glioblastoma cells (Xiong, Chen et al. 2009).

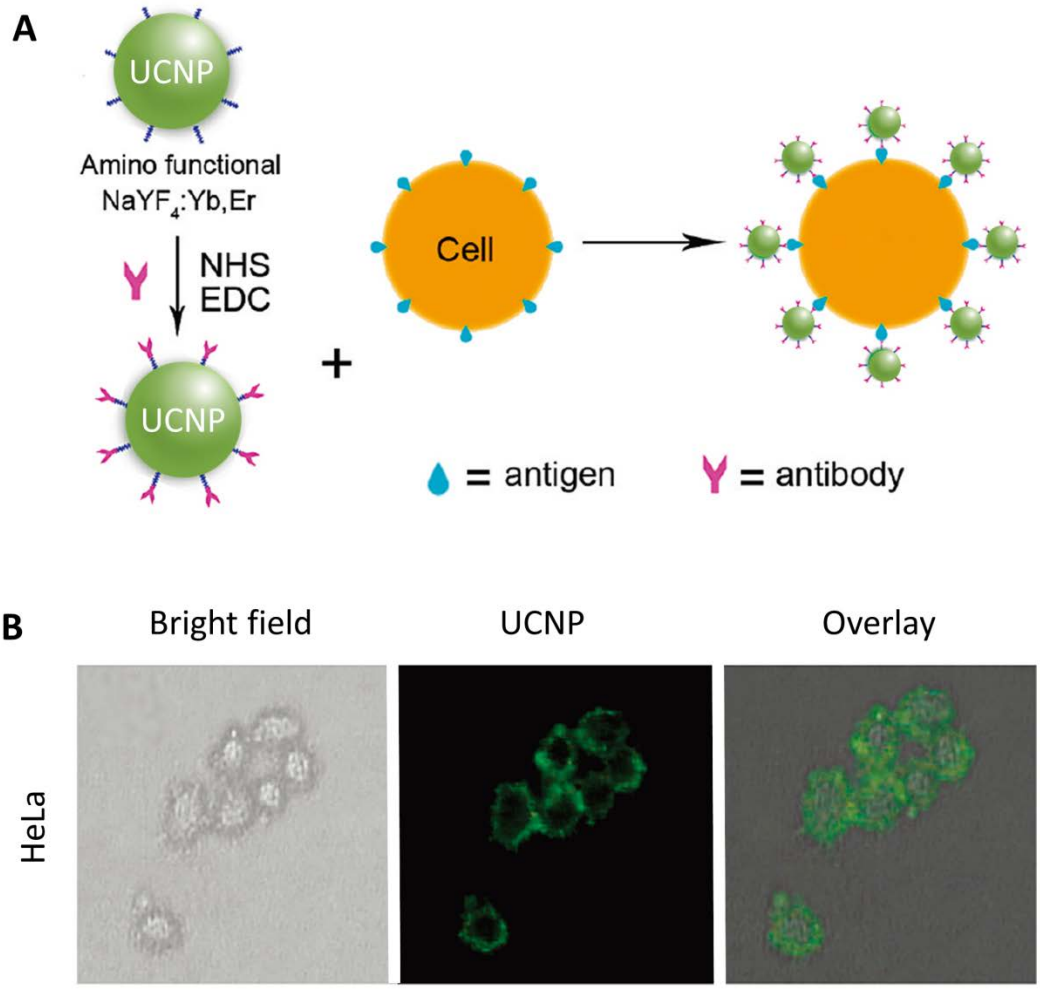

Figure 1.8 (A) Schematic illustration of immunolabeling of HeLa cells using rabbit anti-CEA8 antibody-conjugated NaYF4: Yb^{3+}/Er^{3+}. (B) Confocal upconverted luminescence images of HeLa cells after incubation with rabbit anti-CEA8 antibody-conjugated NaYF4: Yb^{3+}/Er^{3+}. Reproduced from Jiang, Zhang et al. (2009).

In addition to using UCNPs modified with biomolecule recognition moieties, nonfunctionalized UCNPs have also been used for cell imaging through their cell endocytosis. For example, Nyk and coworkers used 3-mercaptopropionic acid (MPA) surface modified UCNPs to incubate with Panc 1 human pancreatic cancer cells and gained high-contrast fluorescence imaging of the cells without autofluorescence (Nyk, Kumar et al. 2008). Similarly, other types of cancer cells, such as MCF-7, SK-BR-3 breast cancer cells, MB49 bladder cancer cells, AB12 mouse mesothelioma cells and Hela cells have also been probed by UCNPs (Hu, Yu et al. 2008; Jalil and Zhang 2008; Wang, Mi et al. 2009).

1.2.3 Detection of Tumor Tissues *in vivo* with UCNPs

In addition to the *ex vivo* cancer biomarker detection and *in vitro* tumor cell detection, a late detection of cancer can also be carried out directly by detecting tumors and other abnormal cancerous tissue growing in the body (Altinoglu, Russin et al. 2008; Agrawal, Strijkers et al. 2010; Cheng, Yang et al. 2011; Choi, Min et al. 2011; Alitalo and Detmar 2012). Due to the unique optical properties of UCNPs that absorb the NIR excitation wavelength and emit light in visible spectrum, NIR excitation provides a higher signal-to-noise ratio, deeper penetration and lower toxicity. UCNP is less harmful than other downconversion nanoparticles (e.g. QDs) and gives a better *in vivo* cancer detection outcome (Lim, Riehn et al. 2006; Yi and Chow 2007; Li, Zhang et al. 2008; Zhou, Liu et al. 2012).

For studies that use UCL imaging of UCNPs in the whole body of small animals, the various detection applications reported can be divided into two main categories: (1) active targeting and (2) passive targeting, each of which depends on the requirement of target-specific recognition. Active targeted imaging assay takes an advantage of the

interactions between a ligand-receptor and antigen-antibody, for which UCNP probes can offer a site-specific tumor detection approach (Choi, Min et al. 2011; Zhou, Liu et al. 2012). Folic acid (FA) is a useful target in cancer detection and functionalized UCNPs have been widely used for *in vivo* tumor targeting due to the high stability and nonimmunogenic feature of FA and the high-level expression of folate receptor (FR) in many types of cancer cells (Chen, Wang et al. 2011; Li and Lu 2013). Li et al. reported creation of FA conjugated UCNPs using (1-ethyl-3-(3-dimethylaminopropyl) carbodiimide) EDC/(N-hydroxysuccinimide) NHS chemistry to successfully target tumor sites in nude mice with Hela tumors (**Figure 1.9A**) (Xiong, Chen et al. 2009). In addition to the *in vitro* cancer cell imaging of RGD functionalized UCNPs, which is based on the high infinity between the RGD peptide and the $\alpha_v\beta_3$ integrin receptor, RGD-modified UCNPs have been utilized for a specific *in vivo* targeting of mice bearing U87MG tumors (overexpressed $\alpha_v\beta_3$ integrin receptor on U87MG cell surface) and these have produced high-contrast images (**Figure 1.9B**) (Xiong, Chen et al. 2009; Zako, Nagata et al. 2009). Similarly, peptide neurotoxin and (C-terminal telopeptide) conjugated UCNPs have also been investigated in live small animal imaging of cancer (Yu, Sun et al. 2010).

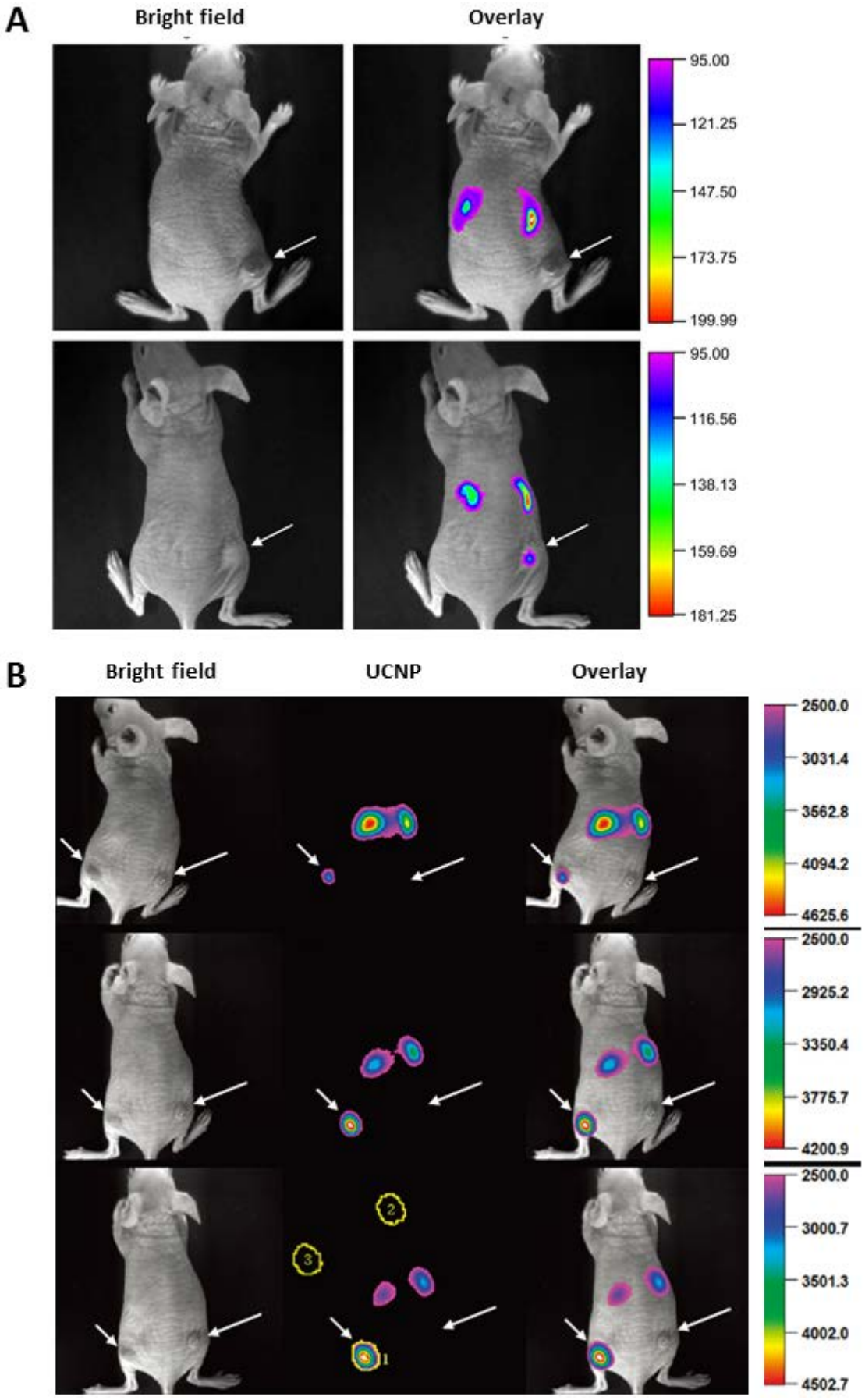
A
Bright field
Overlay
95.00
121.25
147.50
173.75
199.99
95.00
116.56
138.13
159.69
181.25
B
Bright field
UCNP
Overlay
2500.0
3031.4
3562.8
4094.2
4625.6
2500.0
2925.2
3350.4
3775.7
4200.9
2500.0
3000.7
3501.3
4002.0
4502.7
1
2
3

Figure 1.9 (A) *In vivo* UCL imaging of subcutaneous HeLa tumor-bearing athymic nude mice (right hind leg, pointed by white arrows) after intravenous injection of UCNPs-NH_2 (upper panel) and UCNPs-FA (lower panel). (B) Time-dependent *in vivo* UCL imaging of subcutaneous U87MG tumor (left hind leg, indicated by short arrows) and MCF-7 tumor (right hind leg, indicated by long arrows) borne by athymic nude mice after intravenous injection of UCNP-RGD over a 24 h period. (A) Reproduced from Xiong, Chen et al. (2009). (B) Reproduced from Zako, Nagata et al. (2009).

Without attaching to any specific targeting moieties on nanoprobes, a passive imaging assay can utilize the capability that nanoparticles can extravasate blood or the body fluids stream onto tumor site due to poor formation of a tight junction around the tumor tissue (Cho, Wang et al. 2008; Danhier, Feron et al. 2010; Bertrand, Wu et al. 2014). A variety of UCNP imaging studies have been demonstrated including *in vivo* biodistribution tracking, multicolor imaging, lymphatic imaging, vascular imaging and cell tracking (Zhou, Liu et al. 2012; Xu, Zhan et al. 2013; Min, Li et al. 2014; Zeng, Yi et al. 2014). In the literature, biodistribution tracking provides information on the biocompatibility behavior of UCNPs; multicolor imaging utilizes the multi-emission peaks of UCNPs to achieve targeting of different tissues simultaneously; lymphatic imaging enables identification of local lymph nodes which indicates the cancer metastasis status; vascular imaging displays abnormal vessels which commonly occur during tumor proliferation; cell tracking provides real-time monitoring of transplanted myoblast cells.

Besides upconversion luminescence-based *in vivo* imaging, multimodal imaging has attracted increasing attention by incorporation of UCNP probes with current clinical imaging techniques such as CT, MRI and PET, and through this has gained access to their respective advantages (Cheng, Yang et al. 2011; Liu, Sun et al. 2011; Zhou, Yu et

al. 2011; Cheng, Yang et al. 2012; Zhu, Zhou et al. 2012). UCNPs can be further developed by keeping their advantages such as high sensitivity and functionality while compensating for their native drawbacks (e.g. relative low penetration and resolution). Additional imaging techniques are needed to bridge the gap between sensitivity and resolution in tumor imaging (Cheng, Yang et al. 2012; Li, Zhao et al. 2013; Wolfbeis 2015). There are literatures for more information regarding this topic (Zhou, Liu et al. 2012; Xu, Zhan et al. 2013; Min, Li et al. 2014; Zhang, Wei et al. 2014; Wolfbeis 2015).

1.3 Surface Functionalization of UCNPs

In the previous sections, it was demonstrated that upconversion nanoparticles (UCNPs) show significant promise as a tool to address current limitations associated with various biodetections and bioimaging of cancer cells and biomarkers. However, a series of challenges would still need to be overcome for their successful application in biology and these challenges are related to the synthesis of UCNPs.

UCNPs can be produced by various methods (e.g. thermal decomposition method, hydrothermal method) and their surface is generally hydrophobic due to the capping ligands, such as oleic acid (OA) and oleylamine (OM), which are hydrophobic (Wang and Liu 2009; Gnach and Bednarkiewicz 2012; Chen, Qiu et al. 2014). After their synthesis, these original capping ligands allow UCNPs only to be dispersed in a nonpolar organic solvent (e.g. hexane or cyclohexane), but not in an aqueous solution. To use UCNPs successfully in biological applications, such as bioimaging and biolabeling, their surface has to be made hydrophilic so that they can be dispersed in water. Additional further functionalization is necessary to achieve biocompatibility if UCNPs were to be used *in vivo*. Biocompatibility of UCNPs requires that they are

non-toxic and that they have no side effects on the immune system and on cells. Moreover, the particles should be sensitive, highly stable and capable of biotargeting.

As a consequence, a critical step to make use of inorganic, hydrophobic and nonfunctional UCNPs for biological applications is their surface modification and functionalization so that they become water soluble, biocompatible and generation of functional groups for subsequent bioconjugation with different biological molecules. They should also be biorecognizable and capable of biotargeting (Liu, Tu et al. 2013; DaCosta, Doughan et al. 2014; Tsang, Chan et al. 2015). Ideal surface modified UCNPs generally have to satisfy the following characteristics: colloidal stability in a variety of physiological solutions (e.g. PBS buffer and cell culture medium) over a wide pH range, low non-specificity interactions with other species (e.g. molecules, cells and cell culture devices) in biological environments and easy functionalization for further biological or biomedical applications. To make UCNPs hydrophilic, numerous surface modification methods have been developed and reported in the past decade. These include ligand oxidation (Chen, Chen et al. 2008), ligand exchange (Boyer, Manseau et al. 2009; Dong, Ye et al. 2010; Chen, Ohulchanskyy et al. 2011; Chen, Wang et al. 2011), surface santilization (Li and Zhang 2006; Sivakumar, Diamente et al. 2006; Rantanen, Järvenpää et al. 2009; Wong, Chan et al. 2010), ligand removal(Kumar, Nyk et al. 2009), layer by layer assembly (Sukhorukov, Donath et al. 1998) and amphiphilic polymer coating(Johnson, Sangeetha et al. 2010; Jiang, Pichaandi et al. 2012). To make UCNPs biofunctional, various bioconjugation strategies such as physical absorption and chemical covalent linkage strategies have been applied. Furthermore, a large variety of biological molecules such as antibodies (Zhan, Qian et al. 2011), peptides (Xiong, Chen et al. 2009; Lee, Lee et al. 2013), aptamers (Duan, Wu et al. 2012; Chen, Yuan et al. 2013) and small molecules (Wang, Cheng et al. 2011; Ma, Huang et al. 2012) have been conjugated to UCNPs so that they can provide specific targeting and other functions. In the following sections, more details will be provided to demonstrate the importance of

how a hydrophilic, highly stable, highly biocompatible and bioconjugated UCNPs for biological applications can be made.

1.3.1 Hydrophilic Processing of UCNPs

Besides hydrophilic transition, the aim of exploring various surface modification strategies of UCNPs is to address a series of issues: reproducibility of the surface modification of the particles; maintenance of the UCNPs quantum yield in water; control of the particle size; minimization of particle aggregation; and selection of affordable modification reagents (Muhr, Wilhelm et al. 2014). A successful surface modification method for UCNPs has to meet all of these requirements.

Methods for surface modification described for UCNPs, can be classified as follows: (1) UCNP bilayer coating with polymers or amphiphilic molecules; (2) direct modification of the original ligand; (3) complete replacement of the original ligand; and (4) UCNP shell encapsulation with inorganic materials or noble metals (**Figure 1.10**). Each of these approaches will be discussed below.

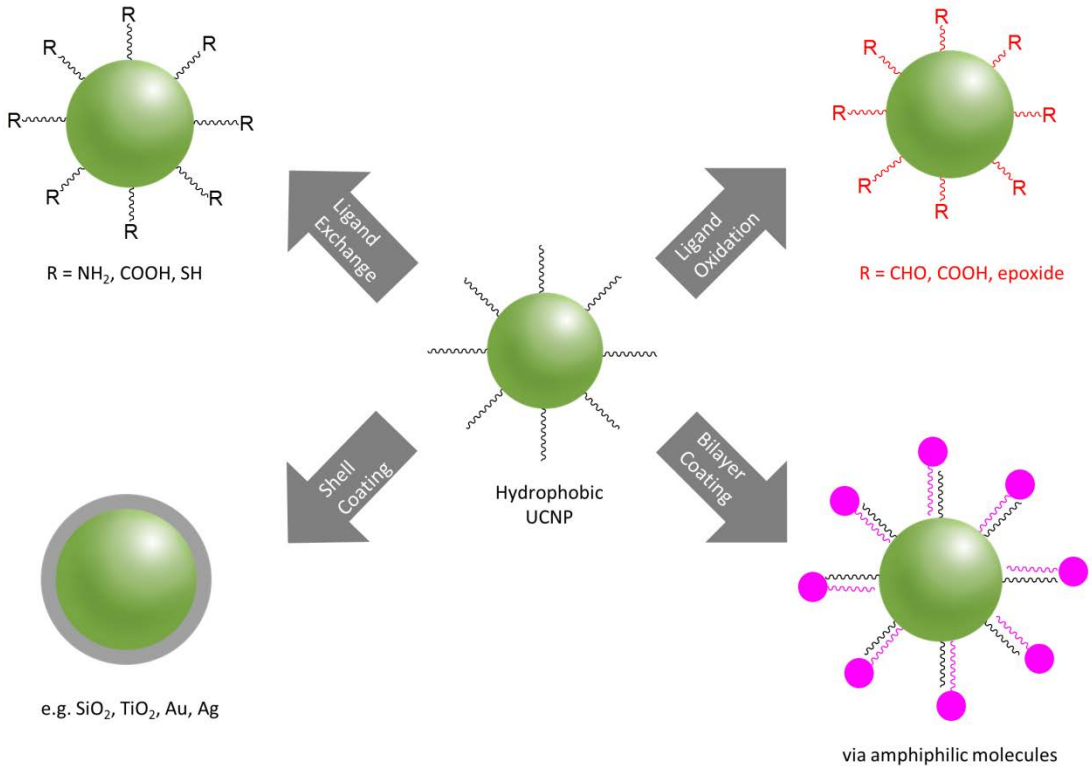

Figure 1.10 Schematic illustration of UCNP surface modification strategies. Sourced from Muhr, Wilhelm et al. (2014).

.

1.3.2 Bilayer Coating with Polymers or Amphiphilic Molecules

Where an extra thin layer is added to the surface of hydrophobic UCNPs, the interaction between polymers or amphiphilic molecules and the original hydrophobic capping ligands typically involves two non-covalent forces: (1) hydrophobic-hydrophobic van der Waals interaction and (2) electrostatic attraction. Based on the type of the interaction force, the method for the additional bilayer coating strategy for surface modification of UCNPs can be further divided into two subgroups: (a) ligand attraction and (b) layer-by-layer assembly.

Ligand attraction strategy takes advantage of the hydrophobic-hydrophobic van-der-Waals interaction between the original hydrophobic ligands (e.g. OA or OM) and selected amphiphilic polymers to achieve the conversion of UCNPs from hydrophobic to water soluble particles. While the hydrophobic part of an amphiphilic polymer interacts with hydrophobic native ligands on the surface of the UCNPs, the hydrophilic part, which is on the other side and induces solubility in water, provides various functional groups to assist in bioconjugation with biological molecules of interest such as specific antibodies or DNA (Johnson, Sangeetha et al. 2010). In addition, polymer coating can provide higher water stability in different solutions as well as help reduce non-specific binding of biological molecules. Additionally, this method can help preserve the optical properties of UCNPs. For example, Liu and co-worker reported a successful polymer attraction method by applying an amphiphilic polymer of octylamine-poly(acrylic acid)-poly(ethylene glyco) (OA-PAA-PEG) to render OA-capped $NaYF_4$: Yb^{3+}/Er^{3+} UCNPs water soluble (**Figure 1.11A**) (Cheng, Yang et al. 2010). Chow and co-workers modified the $NaYF_4$: Yb^{3+}/Er^{3+}@$NaYF_4$ core/shell structure via octulamine and isopropylamine modified PAA as amphiphilic coating molecule to render UCNPs hydrophilic and provide carboxylic functional groups (**Figure 1.11B**) (Yi 2007). Veggel and co-workers developed a simple ligand attraction method by utilizing the poly(maleic anhydridealt-1-octadecene) (PMAO) to transfer the hydrophobic $NaYF_4$ core/shell nanoparticles into a water solution with high stability in different pH conditions and various biological mediums (**Figure 1.11C**) (Jiang, Pichaandi et al. 2012). In addition to these examples, other amphiphilic polymers such as poly(ethylene glyco)-block-poly(carprolactone) (PEG-b-PLC) (Budijono, Shan et al. 2009), 6-aminohexanoic acid (AHA) (Cao, Yang et al. 2011), poly(L-lysine) (PLL) (Nichkova, Dosev et al. 2005) and amphiphilic phospholipids (**Figure 1.11D**) (Yao, Wang et al. 2014) have been reported in the literature.

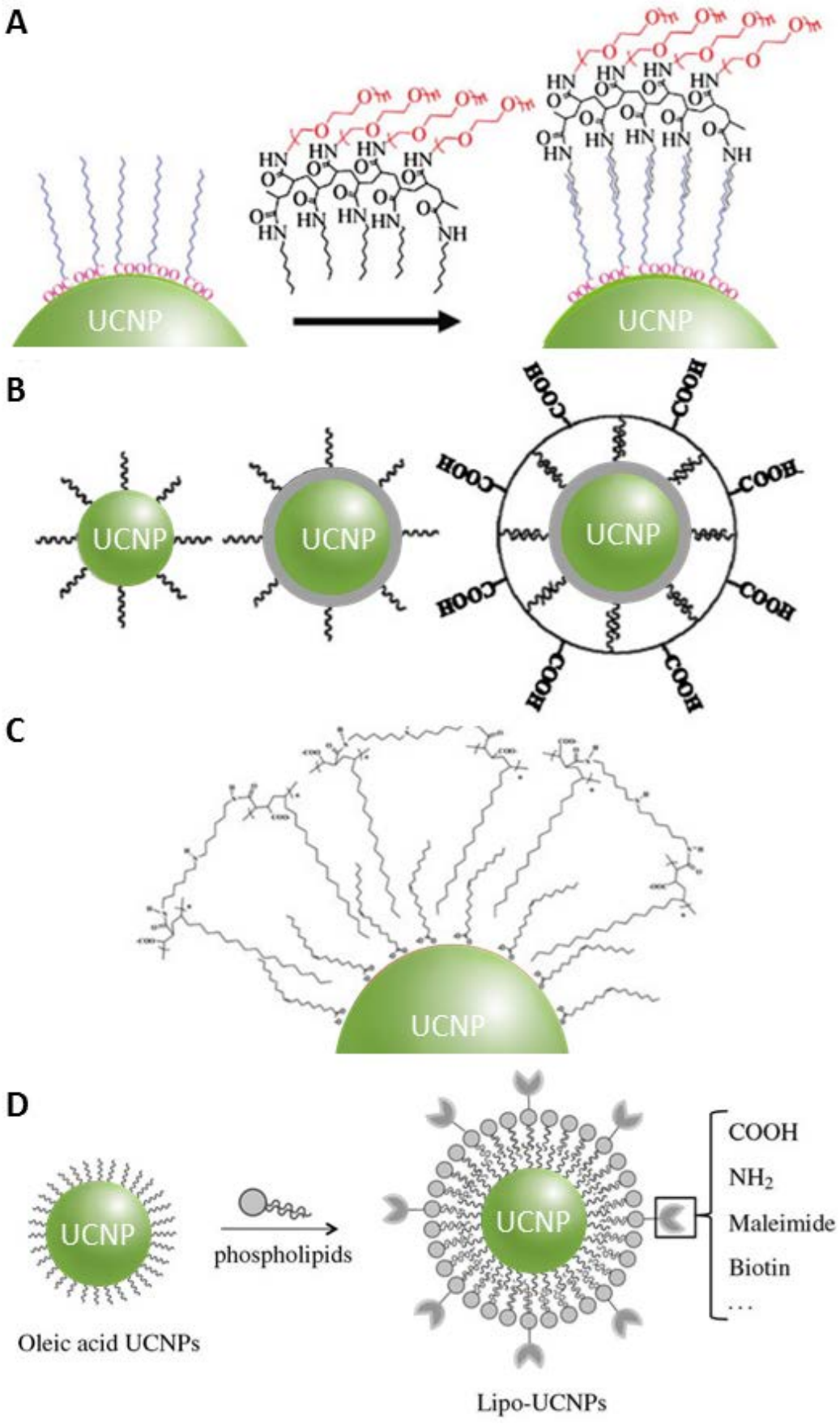
A
UCNP
UCNP
B
UCNP
UCNP
UCNP
COOH
C
UCNP
D
UCNP
phospholipids
Oleic acid UCNPs
UCNP
COOH
NH2
Maleimide
Biotin
...
Lipo-UCNPs

Figure 1.11 Schematic illustration of (A) amphiphilic polymer OA-PAA-PEG coating with OA-capped $NaYF_4$: Yb^{3+}/Er^{3+} UCNPs; (B) PAA attraction with $NaYF_4$: Yb^{3+}/Er^{3+}@$NaYF_4$ core/shell UCNPs; (C) PMAO coating with $NaYF_4$ core/shell UCNPs; (D) bifunctional amphiphilic phospholipid coating OA-capped UCNPs to produce various functional groups. (A) Reproduced from Cheng, Yang et al. (2010). (B) Reproduced from Yi (2007). (C) Reproduced from Jiang, Pichaandi et al. (2012). (D) Reproduced from Yao, Wang et al. (2014).

By taking advantage of electrostatic attraction, layer-by-layer assembly typically applies oppositely charged species between the UCNPs surface and coating molecules to achieve water solubility of UCNPs. Li and co-workers reported that hydrophilic UCNPs with PAH-PSS-PAH coating can be made by sequential depositing of oppositely charged poly(allylamine hydrocloride) (PAH), poly(styrene sulfonate) (PSS) and PAH on UCNPs surface in a PAH-PSS-PAH layer-by-layer manner (**Figure 1.12**) (Wang, Yan et al. 2005). UCNP surface modification using layer-by-layer assembly is not only simple and versatile, but also makes it possible to make surface modified UCNPs of different size, layer thickness and shapes using various composites of coating materials. The disadvantage of this method is that these post-treatments require much time for UCNP functionalization and can greatly increase the hydrodynamic diameter of coated UCNPs which can then limit their biological applications (Bao, Luu et al. 2010).

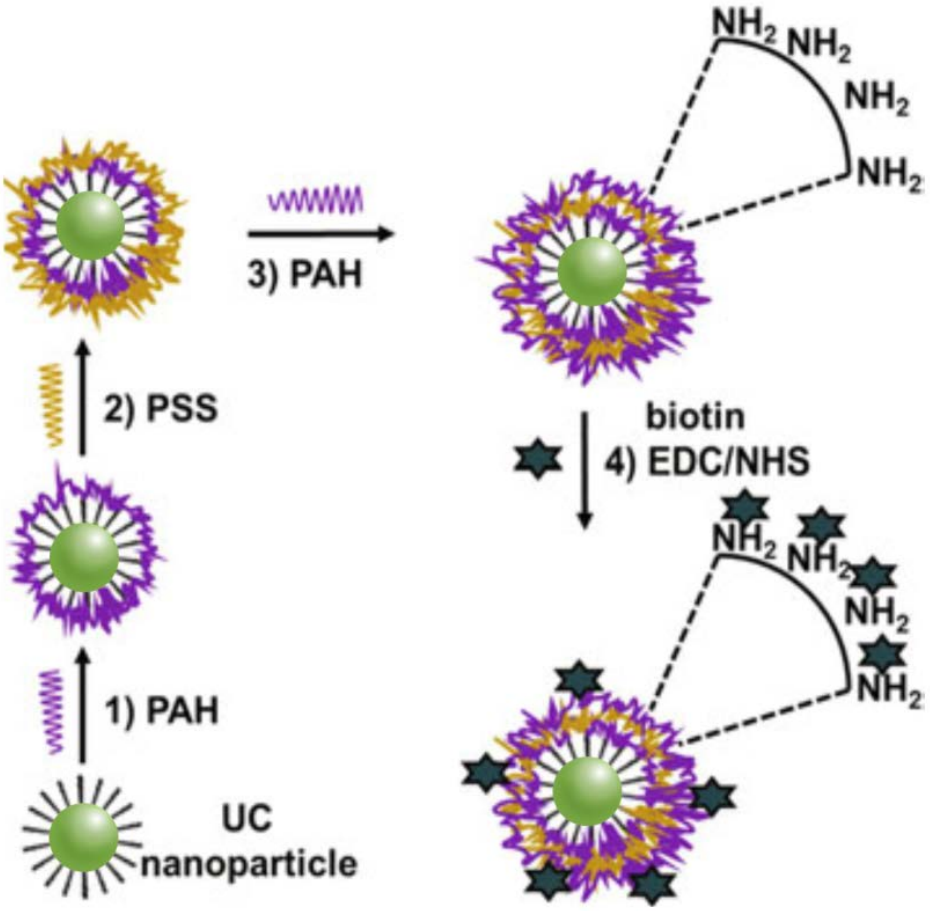

Figure 1.12 Schematic illustration of sequential depositing of PAH, PSS and PAH with UCNPs. Resourced from Wang, Yan et al. (2005).

1.3.3 Direct Modification of the Original Ligand

The concept of direct modification of the UCNPs' original ligand mainly involves selective oxidation of the carbon-carbon double bond of the OA or OM to form azelaic acids, which causes generation of free carboxyl groups on the surface of UCNPs. After this ligand oxidation, OA-capped UCNPs become water dispersible. Oxidation of the UCNPs ligand generally requires application of a strong oxidizing reagent such as Lemieux-von Rudloff reagent and ozone (Chen, Chen et al. 2008; Hu, Yu et al. 2008; Zhou, Xu et al. 2009). In 2008, Li's group firstly reported a simpler and moreversatile

ligand oxidation method which selectively oxidized the OA on UCNPs surface to two carboxylic acids by applying Lemieux-von Rudloff reagent (**Figure 1.13A**) (Chen, Chen et al. 2008). The oxidation method had no obvious negative effects on the UCNP morphology, chemical composition or upconversion luminescence emission capacity. However, this method requires a long reaction time and gives a much lower yield. The group of Yan et al. reported an oxidation method which applied ozone to convert the OA on the surface of UCNPs into azelaic aldehyde or azelaic acid via ozonolysis (**Figure 1.13B**) (Zhou, Xu et al. 2009). This method is clean, simple, straightforward and the ozone is readily available; most importantly, it has no major negative effects on UCNP morphology and optical properties. After ligand oxidation of UCNPs, the free carboxylic acids on the particle surface also make a further covalent conjugation with hydrazine and doxorubicin possible so that they can be used in cancer drug delivery. One disadvantage of ligand oxidation of the UCNPs is that the types of available surface ligands are typically limited due to oxidation of the carbon-carbon double bond of the ligand. Another disadvantage is that dispersion in water solution can have poor colloidal stability (Dai, Yang et al. 2012).

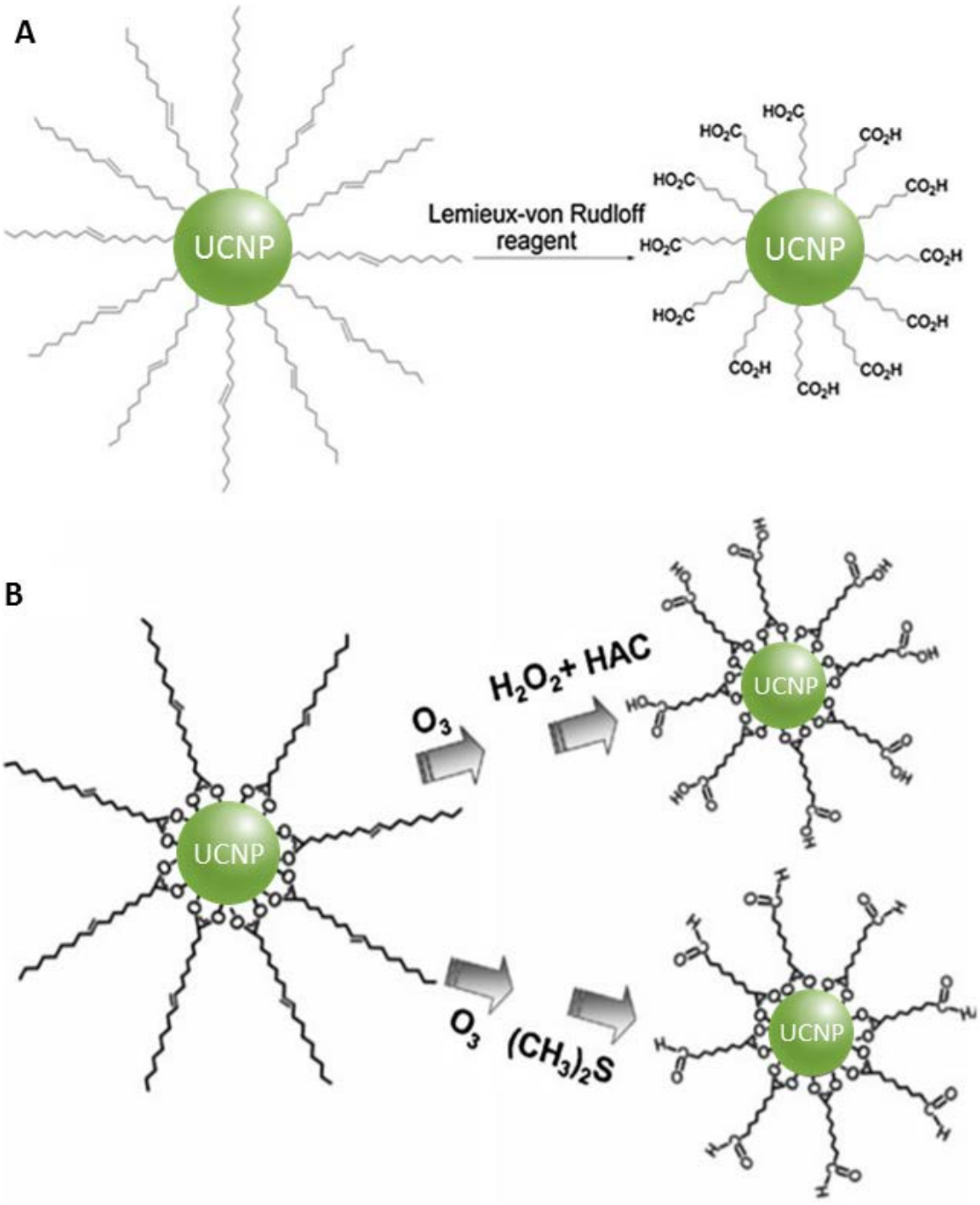

Figure 1.13 Schematic illustration of ligand oxidation of OA-capped UCNPs via (A) Lemieux-von Rudloff reagent and (B) ozonolysis. (A) Reproduced from Chen, Chen et al. (2008). (B) Reproduced from Zhou, Xu et al. (2009).

Ligand removal is another strategy to attain a hydrophilic surface and can simply involve the removal of OA surface ligands by direct acid (e.g. HCl) or excess ethanol treatment with the assistance of sonication, followed by dispersement of UCNPs in water. The group of Xv et al. reported that OA on the UCNP surface can be released completely by washing with excess ethanol under sonication (Kumar, Nyk et al. 2009). Capobianco et al. also reported that OA of UCNPs can be removed with an acid treatment (**Figure 1.14**) (Bogdan, Vetrone et al. 2011). Under acidic (pH=2-4) and ultrasonic treatment, the carboxylate groups of OA or OM on UCNP surface can be protonated to generate oleic acid and then the free oleic acid can be extracted and removed with diethyl ether. After this treatment, UCNPs can be purified to form a stable colloid in aqueous environment and stored for a long time. However, the disadvantage of the ligand removal method is that any subsequent bioconjugation process is difficult as the surface lacks any functional groups (Bogdan, Rodríguez et al. 2012).

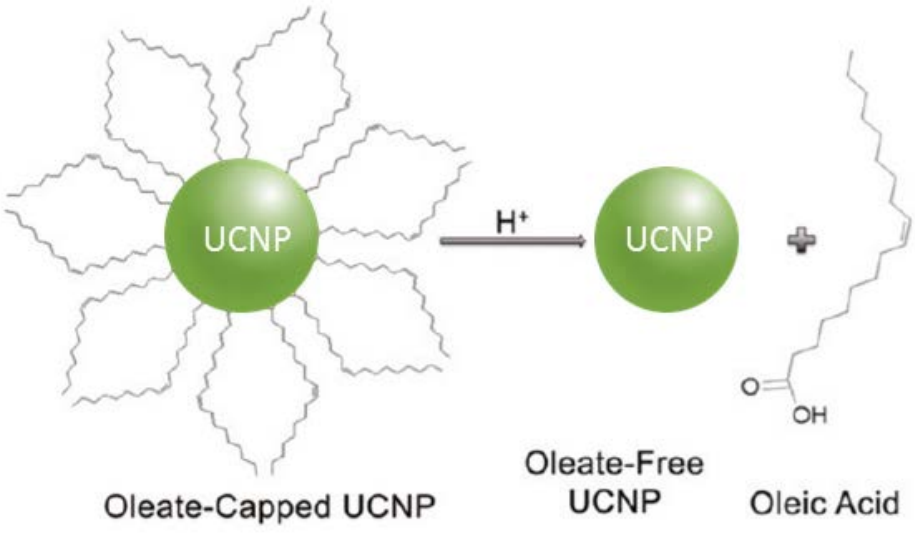

Figure 1.14 Schematic illustration of removal of original capped surface ligands on UCNPs. Reproduced from Bogdan, Vetrone et al. (2011).

1.3.4 Complete Replacement of the Original Ligand

Ligand exchange is an effective and versatile method to modify the UCNP surface. It is considered the most popular strategy for replacing the original hydrophobic ligand (e.g. OA or OM) with various hydrophilic ligands without causing a negative effect on particle morphology or changes to the optical properties of UCNPs. Based on this, the ligand exchange strategy can be categorized into two main subgroups: (1) direct exchange of the original ligands by new ligands; or (2) a two-step replacement using nitrosyl tetrafluoroborate ($NOBF_4$) or another strong acid to generate ligand-free nanoparticles before their further replacement with new ligands.

In the case of direct ligand exchange (one-step ligand exchange), the native surface ligand on UCNPs can be completely replaced by another ligand with stronger lanthanide ions coordinating ability and greater polarity to achieve water solubility. The interaction strength between UCNPs and new ligands has been reported to increase in the following order: -SH＜-NH_2＜-COOH＜-PO_4, however there are no reports which compare the interaction strengths between these hydrophilic capping ligands (Dong, Xu et al. 2011). Most UCNPs are capped by the hydrophobic OA surface ligand with a long chain hydrocarbon and a carboxylate group and this molecular structure can coordinate with lanthanide dopant ions on the UCNP surface. For a successful and efficient surface ligand exchange, a much stronger coordinating capability with lanthanide ions on the UCNPs surface is needed and can be achieved by using single-chelating hydrophilic ligands or a multichelating hydrophilic ligands (Schäfer, Ptacek et al. 2007). For direct ligand exchange, a large number of successful methods have been reported in the literature. These have involved citrate (Cao, Yang et al. 2010), poly(ethylene glycol) PEGylate-phosphate (**Figure 1.15A**) (Boyer, Manseau et al. 2009), poly(amido amine) (PAMAM) (Bogdan, Vetrone et al. 2010), poly(allylamine hydrochloride) (PAH) (Juan, Cheng et al. 2015), mercaptopropionic acid (MPA) (Nyk, Kumar et al. 2008),

poly(acrylic acid) (PAA) (Chen, Ohulchanskyy et al. 2011), poly(vinylpyrrolidone) (PVP) (Jiang, Win et al. 2013), monothiolated heterobifunctional PEGs (Xiong, Chen et al. 2009), 3-dimercaptosuccinic acid (DMSA) (Chen, Wang et al. 2011), mercaptosuccinic acid (MSA) (Zhan, Qian et al. 2011), 1,10-decanedicarbocylic (DDA) (Shen, Sun et al. 2010), and mercaptonudecanoic (MUA) (Shen, Sun et al. 2010). These ligands are most commonly used for UCNP surface ligand exchange to generate particle water solubility and to produce additional functional groups thereby facilitating bioconjugation. For example, the carboxyl groups from PAA coordinate with lanthanide dopant ions on UCNPs surface and the carboxyl groups can be used to provide covalent linkage to primary amine groups on protein surfaces (**Figure 1.15B**). As another example, the thiol groups from MPA on the surface of UCNPs can be used to bind to antibodies.

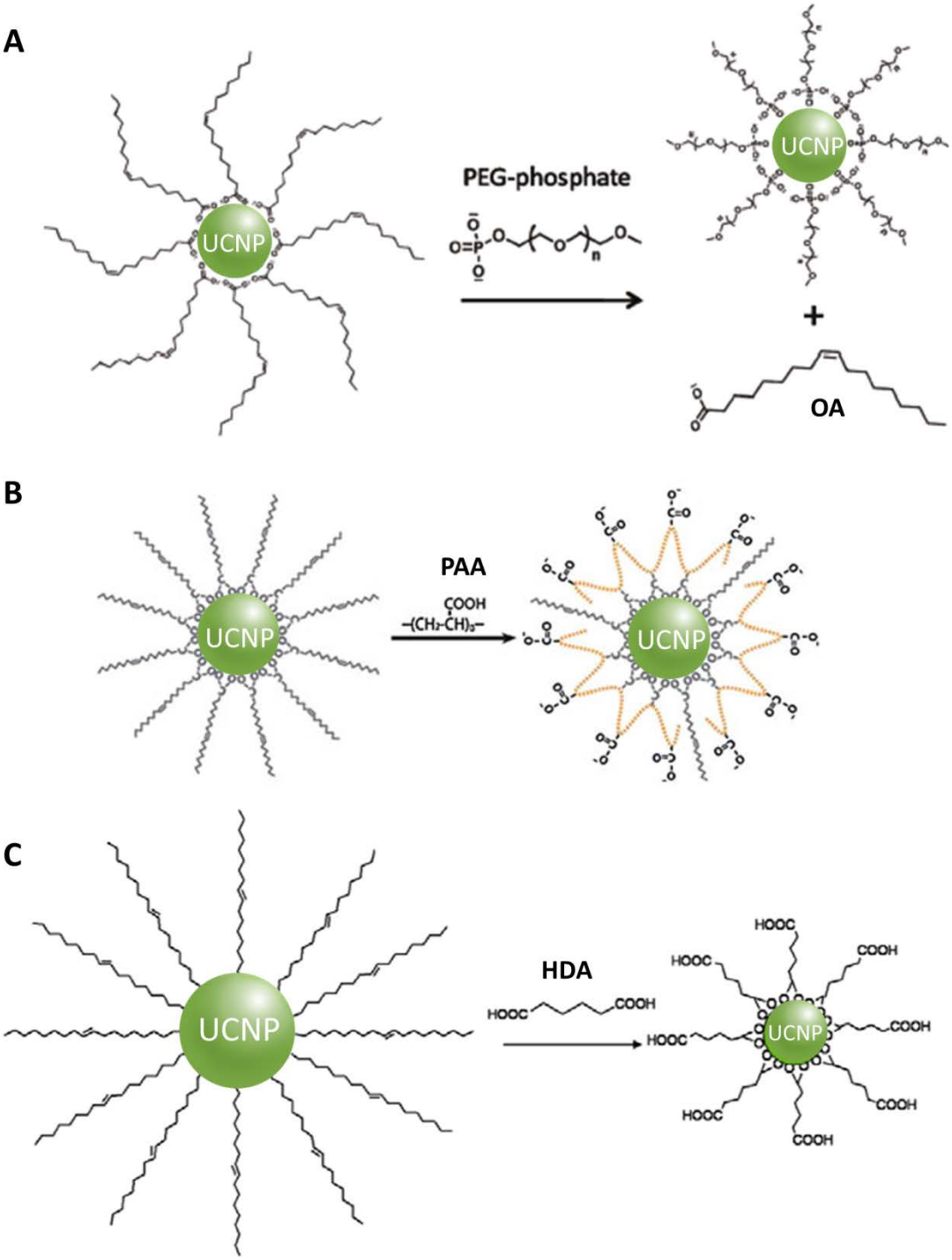

Figure 1.15 Schematic illustration of one-step ligand exchange with UCNPs via (A) PEG-phosphate, (B) PAA and (C) HDA. (A) Reproduced from Boyer, Manseau et al. (2009). (B) Reproduced from Chen, Ohulchanskyy et al. (2011). (C) Reproduced from Dayaker, Durand et al. (2014).

Ligand exchange of hydrophobic OM-capped UCNPs utilizes amino groups to coordinate with the lanthanide dopant ions on the surface of UCNPs. Compared to OA-capped UCNPs, the interaction between OM and UCNP surface is relatively weak and as such may facilitate the ligand exchange process. Various hydrophilic ligands have been reported for this direct ligand exchange of OM-capped UCNPs: hexanedioic acid (HAD) (**Figure 1.15C**) (Dayaker, Durand et al. 2014), PEGylated-carboxylate, thioglycolic acid (TGA) (Dong, Xu et al. 2011), PEGylated-diacid(Yi and Chow 2006), and poly(ethylenimine) (PEI) (Yi, Peng et al. 2011). These capping ligands have been reported elsewhere to facilitate water stability of UCNPs in aqueous condition with the benefit of no obvious change to the optical properties and morphology.

In the case of two-step ligand exchange, UCNPs must first be treated with a $NOBF_4$ reagent and then coordinated with a new ligand to generate water solubility and useful functional groups. Murry and co-workers reported a versatile and widely applicable method for hydrophobic nanoparticle surface modification by utilizing $NOBF_4$ (**Figure 1.16**) (Dong, Ye et al. 2010). $NOBF_4$ was used to completely replace the OA or OM of original ligands attached on UCNPs surface. The OA or OM can be efficiently stripped off and BF_4^- anion replaced and coordinated with lanthanide dopant ions on the surface of UCNPs after treatment at room temperature for several hours. In this step, aggregation during ligand exchange, like in other direct exchange strategies, can be minimized and provide electrostatic stabilization of UCNPs in polar media, such as (dimethylformamide) DMF and (dimethyl sulfoxide) DMSO for long-term storage. In the second step, further functionalization is possible based on this ligand-free state of UCNPs since the BF_4^- counter-ion can be easily replaced by other functional ligands such as phosphate groups that have better coordination abilities with lanthanide ions. With this approach, the interaction of BF_4^- modified UCNPs with various new ligands is simpler and the creation of the desired surface functionalized UCNPs straightforward.

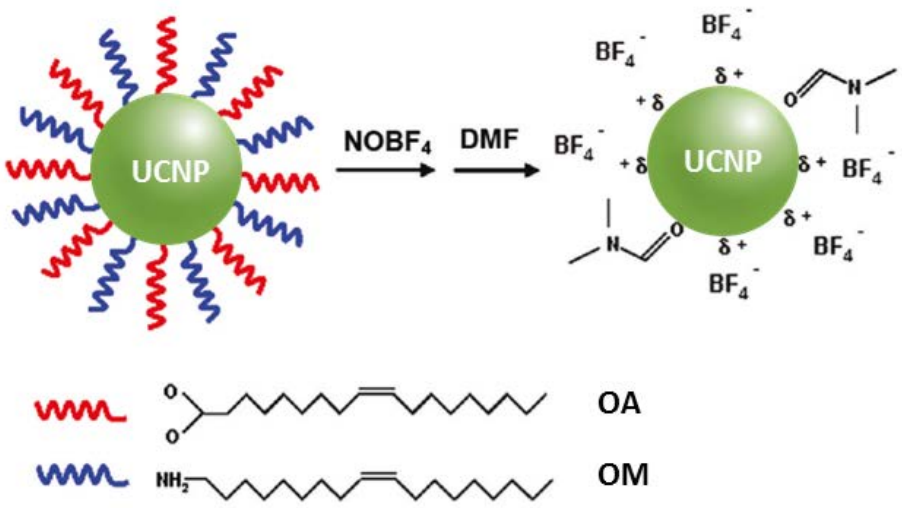

Figure 1.16 Schematic illustration of two-step ligand exchange via $NOBF_4$. Reproduced from Dong, Ye et al. (2010).

1.3.5 Surface Silanization

Water solubility, functionality and biocompatibility can also be achieved by adding an additional shell on top of OA or OM-capped UCNPs. Silica coating of UCNPs is possibly the most frequently used method as it provides high stability, biocompatibility and optical transparency (Li and Zhang 2006; Sivakumar, Diamente et al. 2006). As a useful strategy to produce water dispersible and surface functionalized UCNPs, both the Stober method (Mi, Zhang et al. 2010) and reverse microemulsion method (Xing, Bu et al. 2012) can be applied depending on the polar nature on the capping ligands of UCNP surface. For instance, Stober method can be used to modify hydrophilic UCNPs (Sivakumar, Diamente et al. 2006) by adding tetraethyl silicate (TEOS) in the presence of ethanol and ammonia (Wang, Zhao et al. 2008). The pH of reaction solution and the amount of involved reagent have to be precisely controlled to make a uniform thickness of the silica shell on the UCNPs. The thickness of the silica shell can be easily adjusted to 1-3 nm and can provide a highly uniform surface to the UCNPs (Li and Zhang 2006).

A reverse microemulsion method can also be used to generate a silica shell on UCNPs with hydrophobic capping ligands (Li, Wang et al. 2011). The surfactant Igepal CO-520 (nonylphenol ethoxylate) is introduced here to form a stable reverse microemulsion for polymerization of precursors (Li, Guo et al. 2010). Ammonia is used to control the concentration silicic acid to achieve a steady SiO_2 shell growth. The thickness of the silica shell still can be precisely controlled by changing the reaction time and amount of reagents (Liu, Chen et al. 2013). Li and co-workers reported a 5 nm thickness of the silica shell on the UCNPs surface which demonstrated a good water dispersibility (Hu, Xiong et al. 2009).

Different functional groups further produced on the UCNP@SiO_2 surface. One method is to modify the as-prepared UCNP@SiO_2 is with silanizing reagents(Zhang 2015). Another is to add functional organosilanes during the polymerization step of the silica coating reaction, which then do not require a post-synthetic modification after the silica coating of UCNPs (Chen, Zhen et al. 2013). For example, amino-functionalized UCNP@SiO_2 can be produced by introducing aminopropyltrimethoxysilane (APTMS) (Sivakumar, Diamente et al. 2006; Ramasamy, Chandra et al. 2013) and aminopropyltriethoxysilane (APTES) (Bharali, Klejbor et al. 2005); carboxyl functionalized UCNP@SiO_2 can be produced by using carboxyethylsilanetriol (CEST) (Liu, Zhao et al. 2013; Hlavacek, Sedlmeier et al. 2014). The various functional groups can be flexibly produced by selecting different surface silanization methods to satisfy the different needs of the subsequent conjugation with biological functional molecules (Mader, Kele et al. 2010; Yang, Deng et al. 2010).

Despite considerable functional potential for bioconjugation and the high water solubility of UCNP@SiO_2, this method can sometimes still suffer from classic problems which other surface modification strategies do not have (Wang, Yang et al. 2012). The

UCNP@SiO_2 tend to aggregate and precipitate within several hours after their preparation and display poor water stability in aqueous environments (Wang, Mi et al. 2009). Once UCNP@SiO_2 aggregate, they cannot be redispersed in water even after sonication treatment. A notable difference from other surface modification methods is that the shape and hydrodynamic diameter of nanoparticles can change drastically with the addition of a silica shell and the oversized nanoparticles may become difficult to apply for *in vivo* detection or therapy (Rantanen, Järvenpää et al. 2009; Idris, Gnanasammandhan et al. 2012). In addition, there is another disadvantage of silica coating, which is that the TEOS/APTES modification tends to compromise the upconversion luminescent quantum yield and the brightness of UCNPs is usually weaker in comparison to the same particles without the silica coating (Rantanen, Järvenpää et al. 2009).

1.4 Bioconjugation of UCNPs

Once the as-prepared UCNPs acquire solubility in water and have been functionalized (e.g. –COOH, -NH_2, -SH) as discussed, the next step is to further modify the surface of the UCNPs for their bioapplications. There are several issues that need to be addressed. The first one is the purpose for functionalization of UCNPs. Depending on the nature of the application, for example, cancer detection, tumor imaging, biosensing or drug delivery, hydrophilic UCNPs can be conjugated with antibodies, peptides, aptamers or small molecules. After determining which targeting moieties or drugs will be applied in conjugation of UCNPs, suitable bioconjugation strategies can be selected to achieve the aim. Once the conjugation strategy has been decided, it is needed to choose the chemistry of functional groups to be utilized needs to be chosen to gain a good conjugation outcome. Based on these considerations, details of UCNPs bioconjugation will be discussed next.

1.4.1 Targeting Modes and Biomolecules for Bioconjugation of UCNPs

Understanding the surface functionalization of UCNPs is vital for improving the current limitations, such as aggregation of UCNPs and inactivation of conjugated biofunctional molecules, in cancer detection. A multitude of targeting biomolecules can be attached to UCNPs for cancer diagnosis so that a sensitive and specific targeting of cells or tissues of interest can be achieved (Santra, Zhang et al. 2001; Wilhelm, Hirsch et al. 2013).

Antibodies are the most widely used targeting reagents used in cancer detection for *in vitro* and *in vivo* work (Carter 2006). They are commercially available and their high specificity and binding affinity to the target of interest make antibodies an ideal reagent for cancer specific targeting (Shen, Xu et al. 2012). Small fragments of antibodies, like the single-chain variable fragment (scFv) and the antigen-binding fragment (Fab) can be used either to reduce the size of the antibody molecule or minimize their immunogenicity (Begent, Verhaar et al. 1996; Mayer, Tsiompanou et al. 2000). Peptides are usually used to target cancer cells through the recognition of transmembrane proteins on cancer cell surface. For example, RGD, which consists of arginine, glycine and aspartic acid is the most commonly used peptide (Pierschbacher, Hayman et al. 1983). It has a high affinity for $\alpha_V\beta_3$ integrin, a tumor biomarker which has a very high expression in tumor endothelial cells (Zitzmann, Ehemann et al. 2002). Another example is transferrin, which is a type of glycoprotein with high affinity binding to Fe^{3+} ion in blood and can be used to detect cancer cells (Fletcher 1971). The transferrin receptor which can be recognized by transferrin has a higher expression level in various cancers such as skin, breast, colon, pancreas and lung cancer. when compared to expression in normal tissue (Gatter, Brown et al. 1983). Aptamers are oligonucleotides which can specifically bind to proteins, cells or small molecules of interest and can thus be used as targeting molecules in bioconjugation of UCNPs (Chen, Yuan et al. 2013).

1.4.2 General Bioconjugation Strategies

There are two types of approaches for coupling biofunctional molecules to UCNPs: (1) physisorption or electrostatic absorption and (2) chemical covalent linkage.

Physisorption is a simple and straightforward approach using non-covalent forces (Kumar 2005). Due to the absence of a chemical linkage, the coupling molecules such as proteins or peptides will not lose their biological activities after their attachment to the UCNP surface and the luminescent quantum yield of UCNPs will not change after bioconjugation is completed. Zhang and co-workers reported an electrostatic absorption approach where they used PAH modified UCNPs with a positive surface charge to conjugate to negatively charged anti-CEA8 antibodies (Zhan, Qian et al. 2011). In another work, Capobianco and co-workers successfully conjugated heparin to UCNPs surface (Bogdan, Rodríguez et al. 2012). The physisorption strategy may result in some errors or poor outcomes to the conjugation process. For instance, non-specific binding of UCNP-biomolecules with other species in biolabeling assays cannot be eliminated. The other disadvantage is that the coupling of biomolecules may be disorientated when conjugating to UCNPs and thereby decrease the binding capability with the target of interest (Kumar 2005).

Chemical covalent linkage is another approach to bioconjugation (**Figure 1.17**). Here the linkage resolves the non-specific binding of the coupling biomolecules seen in the physisorption approach and facilitates a higher specific coupling of nanoparticles with biological functional molecules (Kumar 2005). Chemical covalent linkage typically involves chemical reactions between the functional group on the surface of UCNPs and another reactive group on the biomolecules (Gnach and Bednarkiewicz 2012). In some cases, the desired biomolecules can directly couple with UCNPs via pairs of functional

groups. Nucleic acid aptamers and some small molecules such as folic acid can be conjugated to the UCNP surface via a mercapto group and an amine group. Sometimes in this chemical linkage approach, crosslinkers, such as the multifunctional PEG linkers, can be introduced to bring about a better space oriented effect with biomolecules and better water solubility. The crosslinkers bond between the UCNPs surface via chemical or physical absorption and the biomolecules through their pairs of functional groups. Antibodies, streptavidin and some toxic proteins have been utilized as crosslinkers in bioconjugation to gain better bioactivity and water solubility (Wang and Liu 2008; Chen, Ohulchanskyy et al. 2010). However, the introduction of crosslinkers in UCNP bioconjugation does greatly increase the hydrodynamic diameter which again may limit their application if a FRET based biosensing approach is used (Chen, Liu et al. 2008).

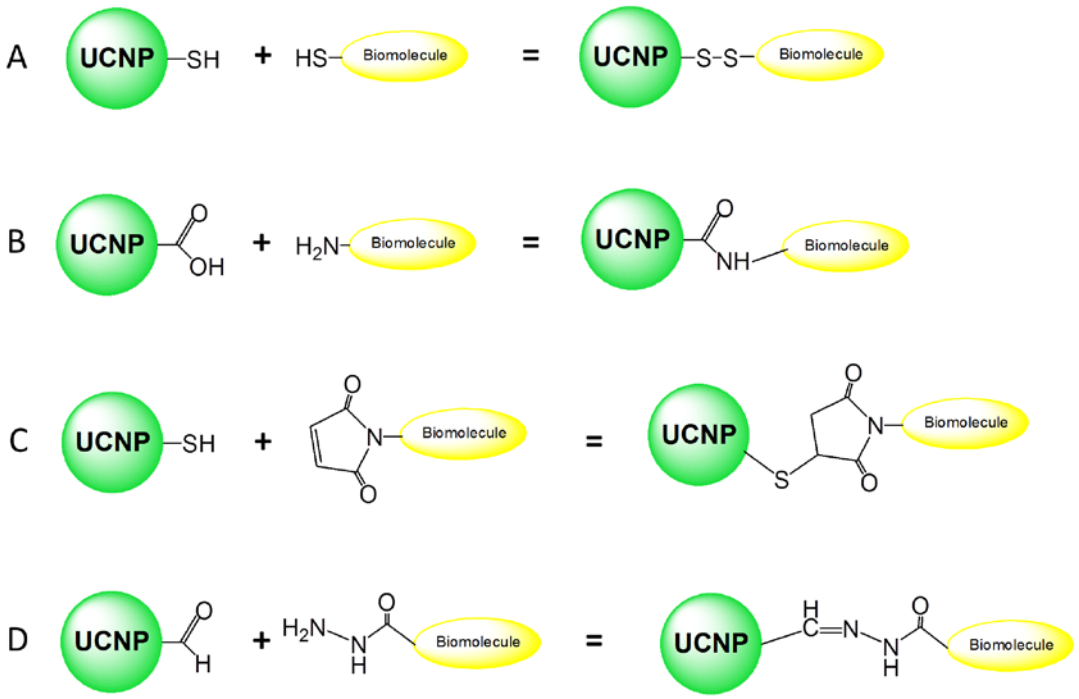

Figure 1.17 Strategies of bioconjugation of UCNPs in view of reactive groups. The coupling reactions between (a) two thiols form a disulfide bond, (b) carboxylic acid and primary amine form amide bond, (c) thiol and maleimide group form thioether bond, (d) aldehyde group and hydrazide group form hydrazide bond. Reproduced from Kumar

(2005).

1.4.3 The Use of Functional Groups of Bioconjugation

To apply covalent linkage reactions for UCNP bioconjugation, a reactive functional group and a crosslinking reagent are needed. The most common approach is to use the chemistry between carboxyl groups and primary amine groups such as the –COOH or –NH_2 which are relatively easy to add during the UCNP surface modification procedure. In this case, EDC and NHS are usually applied as activators in the conjugation reaction between the primary amine group and carboxyl group (Hermanson 2013). Carboxyl groups can be activated by EDC while efficiency of the reaction can be improved by using NHS to yield an amide bond. Carboxylic acid on the surface of UCNPs can be generated by surface modification with PAA (Chen, Ohulchanskyy et al. 2011), DMSA (Chen, Wang et al. 2011), HAD (Dayaker, Durand et al. 2014) or MSA (Zhan, Qian et al. 2011) and can be coupled with biomolecules containing primary amine groups such as streptavidin, folic acid, antibodies or DNA. The amine groups on the UCNP surface can be provided by PEI (Yi, Peng et al. 2011), ADA (Zhou, Yao et al. 2010), APTES (Li and Zhang 2006; Ramasamy, Chandra et al. 2013) and covalently linked to carboxylate containing biomolecules such as antibodies and DNAs.

Another approach is to use a covalent linkage between aldehyde groups and hydrazide groups to form a hydrazide bond between UCNPs and biomolecules. With this approach aldehyde groups can be generated by oxidation of carbohydrates especially in the conjugation of antibodies with polysaccharides in Fc region (Kumar, Aaron et al. 2008).

The reaction between maleimide groups and thiol groups forms a thio-ether bond under

physiological conditions and can be very useful for bioconjugation with proteins that contain –SH groups, while the maleimide groups are commonly introduced by functionalized crosslinkers (Zako, Nagata et al. 2009). The disulfide linkage in bioconjugation is another approach by coupling two thiol groups which can employ a crosslinker with a thiol group at one end of the molecule chain (Ryu, Park et al. 2010). Moreover, interaction and high affinity between biotin (Ju, Tu et al. 2011; Tu, Liu et al. 2011) and avidin/streptavidin (Faure, Hoffmann et al. 2008) can be introduced into UCNP bioconjugation. Streptavidin conjugated UCNPs can also be easily attached to biotinylated molecules or proteins.

1.5 Aims of the Thesis

Several methods of UCNP functionalization have been developed for biological and biomedical applications in the past decade. However, due to limitations of the UCNP-biomolecule platform such as nanoparticle aggregation and protein inactivation, it is necessary to explore new surface modification and bioconjugation strategies of UCNPs to understand the nature of the problems and overcome current obstacles restricting the use of UCNPs in bioapplications.

The aims summarized in the following:

(1) To synthesize and characterize UCNPs which are suitable for biological applications such as cancer detection.

(2) To test a variety of suitable approaches for the surface modification of UCNPs and identify a method that renders the UCNPs with good colloidal stability and potential for subsequent biological functionalization.

(3) To develop reliable strategies for the bioconjugation of UCNPs with special emphasis on high water dispersibility and stability. In addition, maintaining the biological activity of the conjugated biomolecules will also be addressed.

Chapter 2: Synthesis and Characterization of Upconversion Nanoparticles

2.1 Background

Upconversion luminescence (UCL), *i.e.* the emission of one photon upon the excitation of several lower energy photons, has attracted considerable attention in a broad range of applications due to its unique characteristics (e.g. anti-Stokes shift) (Haase and Schäfer 2011). In recent years, the development of nanotechnology has been boosting the scientific interest, especially the interest of the biomedical field in relevant material systems, typically lanthanide ion-doped nanomaterials (Li, Zhang et al. 2015). These nanomaterials, capable of converting near infra-red (NIR) photons to higher energy photons ranging from ultraviolet (UV) to NIR, allow the excitation to fall in the so-called ‘‘optical window’’ (~650-1300 nm), *i.e*. the optimal spectral range for minimal absorption by human tissue and negligible auto-fluorescence of the biological background (Chen, Qiu et al. 2014). They are thus expected to be able to significantly improve the quality of luminescence biomedical imaging, labelling and therapy.

Many different routes for the synthesis of upconversion nanoparticles (UNCPs) have been described recently. For example coprecipitation (Wang, Bu et al. 2008), thermal decomposition (Boyer, Vetrone et al. 2006), solvothermal synthesis (Liu, Tu et al. 2010), and high-temperature coprecipitation (Xu, Zhao et al. 2013) are typically carried out in organic solvents. Some synthetic routes such as hydrothermal synthesis (Hu, Chen et al. 2008), and sol–gel processes (Sivakumar, van Veggel et al. 2005) can also be performed in aqueous media. Chemical vapor deposition (Yang, An et al. 2004) is a less common route that does not belong to either category. Highly monodisperse UCNPs of uniform

size and shape are mainly synthesized in high-boiling organic solvents. For example, oleic acid serves as a solvent and also controls the crystal growth by coordinating to the nanoparticle surface and forms a hydrophobic layer of surface ligands (Liu, Tu et al. 2010). Usually, a subsequent surface modification is necessary to yield a hydrophilic surface composition before these UCNPs can be employed in biological applications.

In this chapter, uniform UCNP $NaYF_4$ doped with Yb^{3+}/Er^{3+} in different sizes and Yb^{3+}/Tm^{3+} were synthesized. The UCL intensity by different sizes were compared at the same dopant concentration in $NaYF_4$: Yb^{3+}/Er^{3+}. In addition, prompted the instrumentation limitations, a strategy to significantly increase the UCL for UCNPs with regard to core-shell structure synthesis has also been studied.

2.2 Experimental Section

2.2.1 Reagents and Materials

Yttrium chloride hexahydrate ($YCl_3 \cdot 6H_2O$, 99.9%), gadolinium chloride hexahydrate ($GdCl_3 \cdot 6H_2O$, 99.9%), ytterbium chloride hexahydrate ($YbCl_3 \cdot 6H_2O$, 99.9%), erbium chloride hexahydrate ($ErCl_3 \cdot 6H_2O$, 99.9%), thulium chloride hexahydrate ($TmCl_3 \cdot 6H_2O$, 99.9%), sodium hydroxide (NaOH, 98%), ammonium fluoride (NH_4F, 99.9%), oleic acid (OA, 90%), oleylamine (OM, 90%) and 1-octadecene (ODE, 90%), were all purchased from Sigma–Aldrich and used as received without further purification.

2.2.2 Synthesis of OA-Capped β-Phase $NaYF_4$: Yb^{3+}/Er^{3+} (or Tm^{3+}) Nanoparticles

Hexagonal phase (β-phase) OA-capped UCNPs were synthesized using an thermal decomposition method as described previously (Boyer, Vetrone et al. 2006). The synthesis of $NaYF_4$: 20% Yb^{3+}/2% Er^{3+} is given as an example. Briefly, YCl_3 (0.78

mmol), $YbCl_3$ (0.18 mmol), and $ErCl_3$ (0.02 mmol) were stirred with 6 mL OA and 15 mL 1-octadecene (ODE) in a 100 mL three-neck round-bottom flask. The resulting mixture was heated at 160 °C under argon flow for 30 min to form a clear light yellow solution. After cooling down to 50 °C, 10 mL of methanol solution containing 0.16 g NH_4F (4 mmol) and 0.10 g NaOH (2.5 mmol) was slowly dropped into the flask with vigorous stirring for 30 min. Then, the slurry was slowly heated and kept at 110 °C for 30 min to remove methanol and residual water. Subsequently, the reaction mixture was quickly heated up to 300 °C (45 min for 15 nm sized nanocrystals, 1 h for 20 nm), 310 °C (45 min for 25 nm, 1 h for 30 nm), and 320 °C, 1 h for 41 nm and protected by an argon atmosphere. The products were isolated by adding ethanol, and centrifuged without size-selective fractionation. The final $NaYF_4$: Yb^{3+}/Er^{3+} nanocrystals were redispersed in cyclohexane at 5 mg/mL concentration after washing with cyclohexane/ethanol several times.

2.2.3 Synthesis of α-Phase Sub 10 nm $NaYF_4$ UCNPs

For cubic phase (α-phase) $NaYF_4$ nanoparticles, YCl_3 (0.78 mmol), $YbCl_3$ (0.18 mmol), and $ErCl_3$ (0.02 mmol) were added to a 100 mL round bottom flask containing 6 mL of OA and 15 mL of ODE. Under argon atmosphere, the solution was stirred and heated to 160 °C for 0.5 h, followed by adding solid sodium oleate (2.5 mmol) and anhydrous NH_4F (4 mmol). The reaction was maintained with stirring for 30 min, followed by adding 5 mL OM, and then heated to 310 °C (45 min for 11 nm), 300 °C (45 min for 7 nm).

2.2.4 Synthesis of Core-Shell Structure UCNP

Preparation the α-phase $NaGdF_4$: α-$NaGdF_4$ nanocrystal seeds were prepared as the precursors of the inert core shell. 2.0 mmol $GdCl_3$ was magnetically mixed with 12 mL

OA, 6 mL OM and 20 mL ODE in a 100 mL three-neck round-bottom flask. The mixture was degassed under argon flow and heated to 160 °C, kept for 60 min to form a clear solution, and then cooled to room temperature. 20 mL methanol solution containing NH_4F (0.296 g) and NaOH (0.2 g) was added into the clear solution and stirred for 60 min at room temperature. The solution was slowly heated to 110 °C and kept for 30 min to completely remove methanol and residual water. The reaction mixture was quickly heated to 280 °C and aged for 45 min. After the solution cooled, 30 mL ethanol was added to precipitate the nanocrystals. The precipitate was washed with cyclohexane and ethanol 4 times, and the α-$NaYF_4$ seeds were re-dispersed in 10 mL cyclohexane. The obtained cyclohexane solution containing α-$NaGdF_4$ seeds was mixed with 1.5 mL OM, 7 mL OA and 11.5 mL ODE in a 100 mL three-neck flask. Then, the mixture was kept at 110 °C for 30 min under Argon flow. After the mixture was cooled to room temperature, α-$NaGdF_4$ ODE solution as the precursor of the inert shell was obtained and stored at 4 °C.

Inert shell coated UCNPs: the original $NaYF_4$: Yb^{3+}/Er^{3+} UCNPs were coated with inert shell using the α-$NaGdF_4$ nanocrystal seeds. In a typical process, 2 mL of $NaYF_4$: Yb^{3+}/Er^{3+} nanocrystals stored in cyclohexane (0.1 M) was magnetically mixed (1000 rpm) with OM (1 mL), OA (5 mL) and ODE (8 mL) in a 100 mL three-neck flask. The mixture was heated to 110 °C and kept for 30 min under argon flow to completely remove cyclohexane and residual water. The reaction mixture was heated to 310 °C (20 °C per min) and 0.3 mL α-$NaGdF_4$ seeds (3~5 nm, 0.1 M in ODE) was quickly injected using a 1 mL syringe. Then, 0.2 mL of α-$NaGdF_4$ seeds in ODE was injected every 10 min. After the last injection, the solution was kept at 310 °C for 10 min and then naturally cooled down to room temperature. 15 mL ethanol was added to precipitate the nanocrystals. The product was washed with cyclohexane and ethanol 4 times.

2.2.5 Transmission Electron Microscopy

The UCNPs were sufficiently diluted (≈0.1 mg/mL) so that visualization of individual particles was possible and 20μL of UCNPs solution was placed on a 50 Å thick carbon-coated copper grid and the excess solution was immediately removed. The TEM images of the UCNPs were then recorded on a PHILIPS CM10 system operating at 100 kV. The TEM images were then processed with ImageJ analysis to obtain the size and size distributions of UCNPs. A black and white binary TEM image was firstly imported to ImageJ and then the nanoparticles on the image were segmented by measuring the segmentation threshold value. A total particle number of 100 segmented UCNPs were analyzed by ImageJ and give the mean particles size.

2.2.6 Fluorescence Spectra Measurement

The UCNPs were diluted to the same concentration of 5 mg/mL and their fluorescence emission spectra were recorded on a Fluorolog®-3 spectrophotometer equipped with a 980 nm VA-II diode pumped solid-state (DPSS) laser (current set at 1.50 A) and a 1200 g/mm grating. The spectra were measured over the range of wavelengths from 350 nm to 850 nm.

2.3 Results and Discussion

2.3.1 TEM Imaging of UCNPs $NaYF_4$: Yb^{3+}/Er^{3+} with Different Size Distribution

OA-capped UCNPs $NaYF_4$: 20% Yb^{3+}/2% Er^{3+} (OA-UCNPs) were synthesis by the thermal decomposition method. By different combinations of temperature and synthesis time, different sizes of UCNPs can be obtained and be well controlled for the biological application. Transmission electron microscopy (TEM) was applied to reveal the morphologies, size and dispersibility of UCNPs after synthesis. TEM images are given

in **Figure 2.1** and show that α-$NaYF_4$ with size 7 nm and β-phase $NaYF_4$ with different sizes at 11, 15, 20, 25, 30 and 41 nm are monodisperse and uniform in cyclohexane. The different shades of gray of UCNPs observed in the TEM images are from different diffraction contrasts of the crystalline materials.

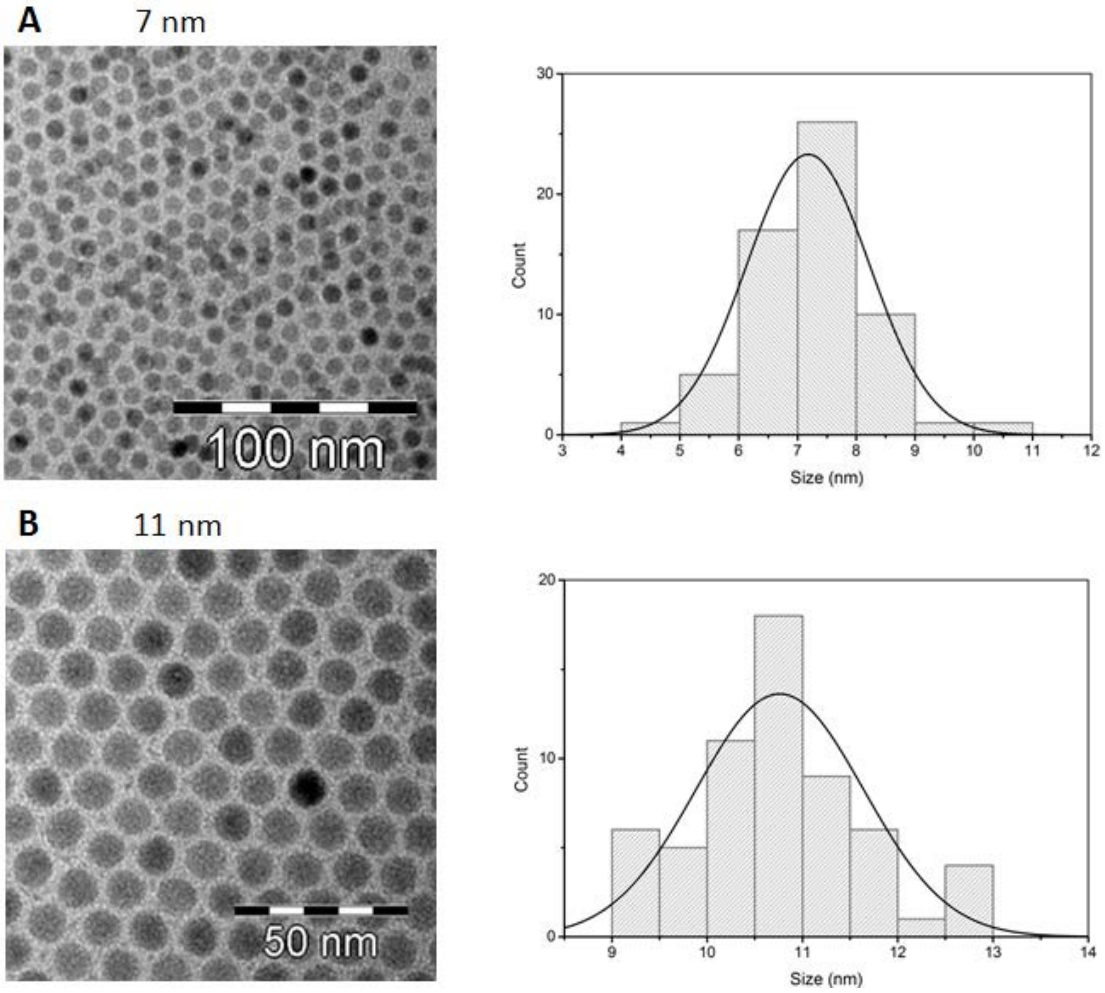

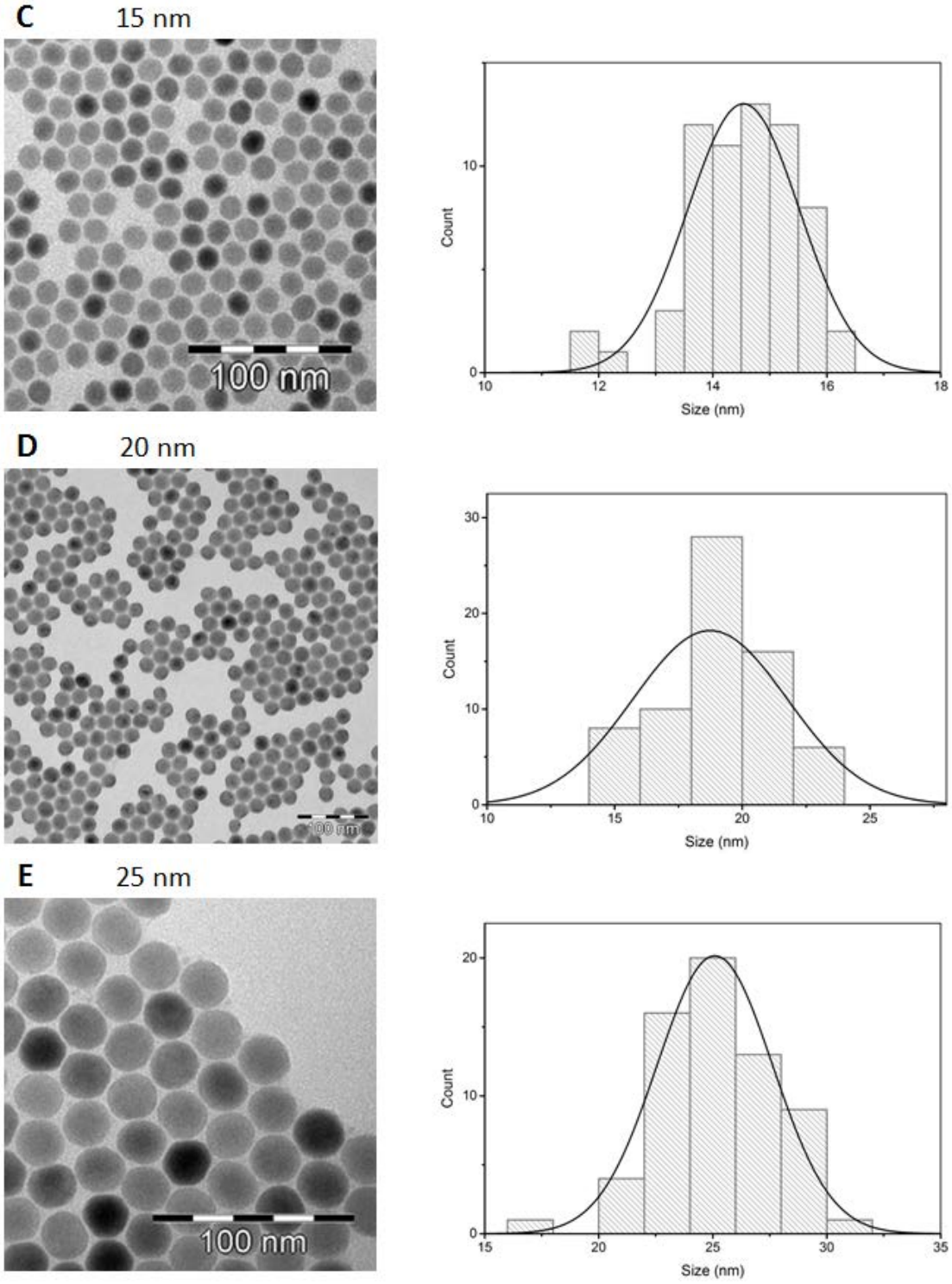
C
15 nm
100 nm
Count
Size (nm)
D
20 nm
Count
Size (nm)
E
25 nm
100 nm
Count
Size (nm)

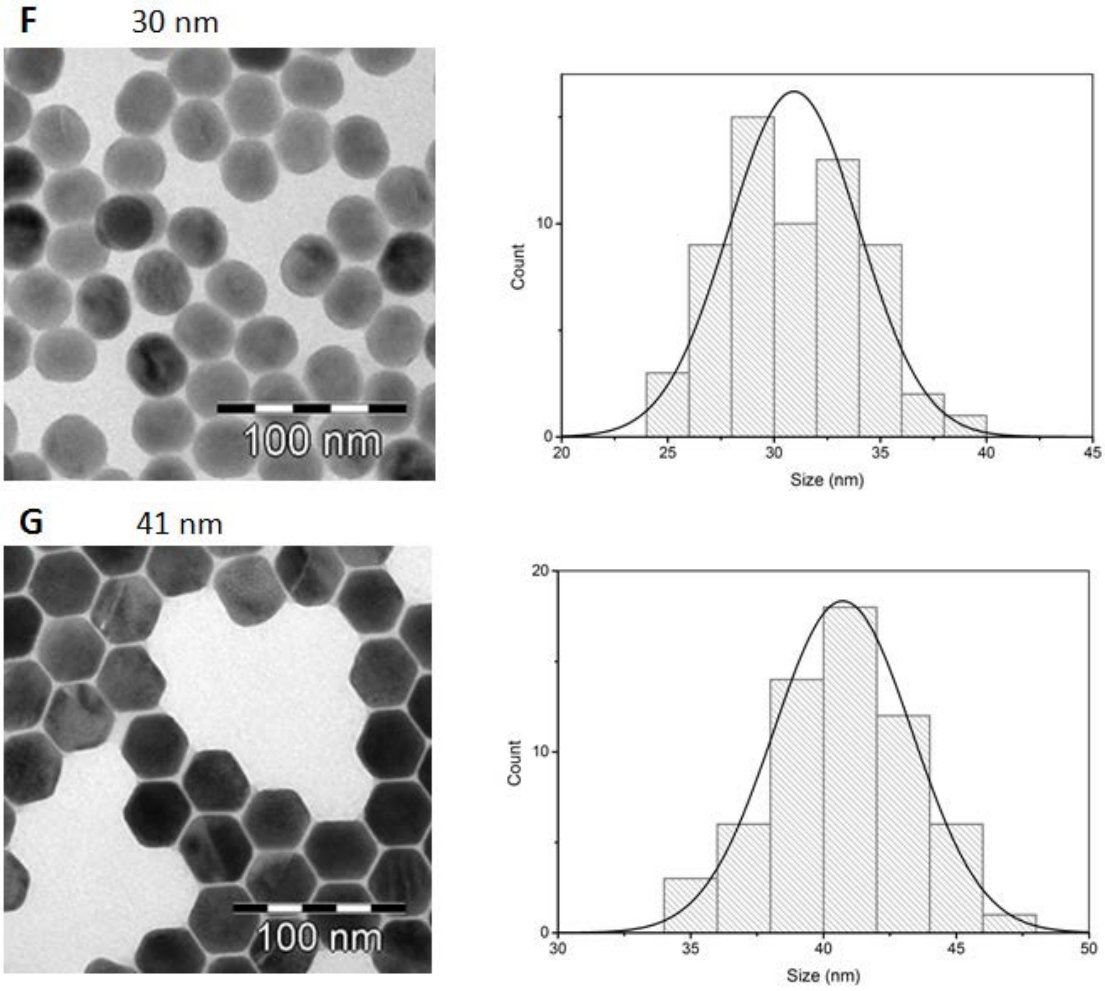

Figure 2.1 TEM images (left panel) of OA-UCNPs $NaYF_4$: Yb^{3+}/Er^{3+} with different sizes (A) 7 nm, (B) 11 nm, (C) 15 nm, (D) 20 nm, (E) 25 nm, (F) 30 nm and (G) 41 nm, along with the size distributions (right panel) determined from the TEM data using ImageJ analysis.

2.3.2 Luminescence Emission Spectra of UCNPs $NaYF_4$: Yb^{3+}/Er^{3+}

Emission spectra of UCNPs $NaYF_4$: Yb^{3+}/Er^{3+} under 980 nm excitation wavelength have peaks in the region from 350 nm to 700 nm that correspond with previous literatures (Boyer, Vetrone et al. 2006). Under continuous near infrared excitation at 980 nm, the visible UCL of UCNPs $NaYF_4$: Yb^{3+}/Er^{3+} appears mainly green in color due to the green emission from Er^{3+} ions doped in UCNPs $NaYF_4$ lattice. Three peaks which are 520 nm,

540 nm and 650 nm predominantly displayed in $NaYF_4$: Yb^{3+}/Er^{3+} emission spectra. The green UCL around 520 nm, 540 nm and red emission around 660 nm are attributed to the transition from $^2H_{11/2}$, $^4S_{3/2}$, and $^4F_{9/2}$ to $^4I_{15/2}$ of Er^{3+}, respectively.

UCNPs with different size diameter ranging from 7 nm, 11 nm, 15 nm, 20 nm, 25 nm, 30 nm and 41 nm were adjusted to the same concentration of 10 mg/mL in cyclohexane for the emission spectra measurement. As shown in **Figure 2.2**, the emission intensity of UCNPs of different size had a non-linear increase with larger nanoparticle size. The values of luminescence intensity, which were collected at 540 nm over the wavelength range, corresponding to diameter size are compared in **Figure 2.2 B**, with the UCNPs of size 41 nm showing 18 times stronger luminescence intensity than UCNPs of size 7 nm due to the fact that more emitters (Er^{3+} ions) can be doped into larger sized nanoparticles that result in stronger emission intensity.

A

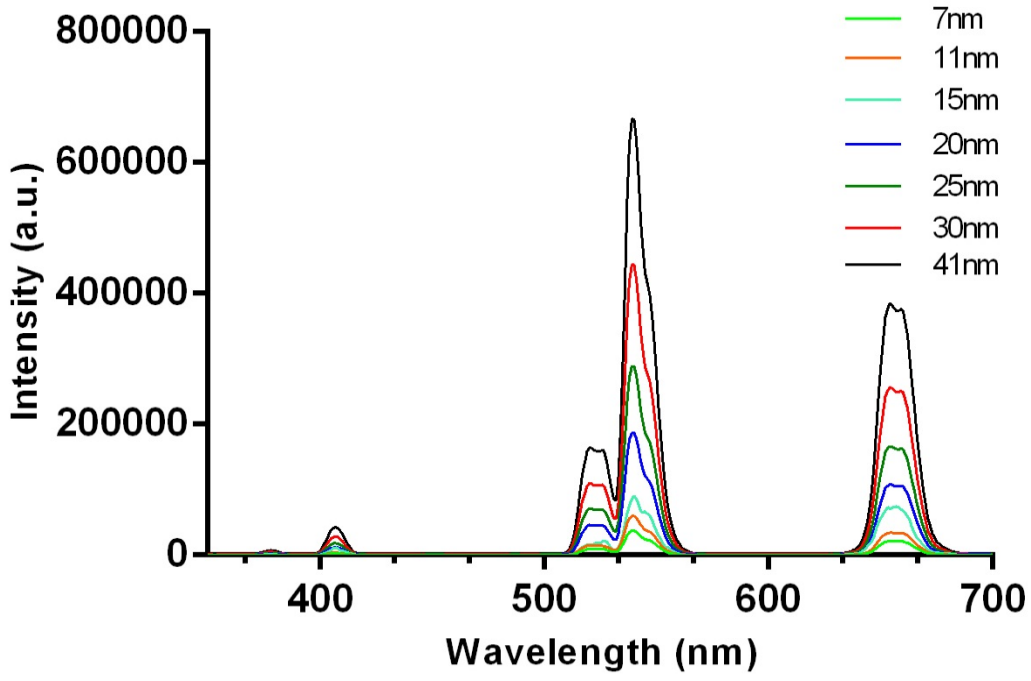

B

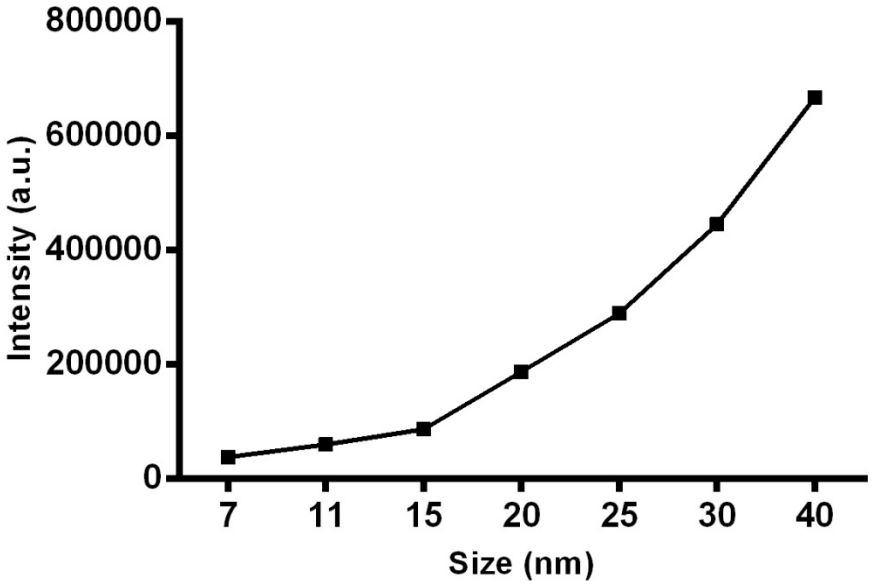

Figure 2.2. (A) Luminescence emission spectra of UCNPs $NaYF_4$: Yb^{3+}/Er^{3+} and the changes of luminescence intensity with different nanoparticle size diameter, excited with 980 nm. (B) Luminescence intensity of the UCNPs increased with the increasing diameter of the nanoparticles.

2.3.3 TEM Imaging of UCNPs $NaYF_4$: Yb^{3+}/Tm^{3+} and Size Distribution

OA-UCNPs $NaYF_4$: 20% Yb^{3+}/2% Tm^{3+} were synthesized by thermal decomposition method. **Figure 2.3** shows that the synthesized hexagonal OA-capped UCNPs $NaYF_4$: 20% Yb^{3+}/2% Tm^{3+} disperse very well in cyclohexane and, in contrast to the $NaYF_4$: Yb^{3+}/Er^{3+} UCNPs, have a uniform size around 33 nm. As above, the different shades of gray of UCNPs in TEM images are from the observation of different diffraction contrast of crystalline materials.

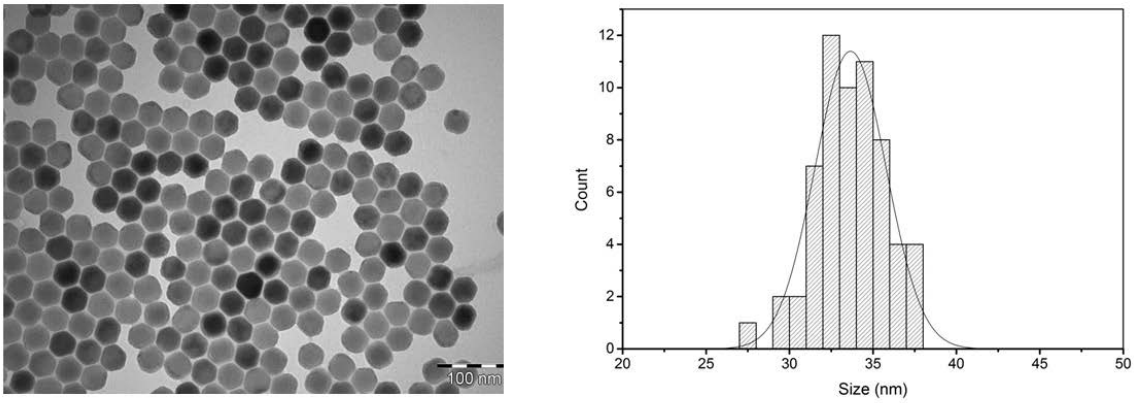

Figure 2.3. TEM images (left panel) of $NaYF_4$: Yb^{3+}/Tm^{3+} UCNPs and the size distributions (right panel) determined from the TEM data using ImageJ analysis shows the average size is 33 nm.

2.3.4 Luminescence Emission Spectra of $NaYF_4$: Yb^{3+}/Tm^{3+}

The emission spectra of UCNPs $NaYF_4$: Yb^{3+}/Tm^{3+} also have peaks in the region from 350 nm to 850 nm that corresponded with previous literatures (Haase and Schäfer 2011). Under continuous NIR excitation at 980 nm, the visible UCL of UCNPs $NaYF_4$: Yb^{3+}/Tm^{3+} appears mainly in blue color due to the blue emission from Tm^{3+} ions doped into the UCNPs $NaYF_4$ lattice. From **Figure 2.4**, four peaks which are 360 nm, 450 nm, 470 nm and 800 nm predominantly displayed in the $NaYF_4$: Yb^{3+}/Tm^{3+} emission spectra in a cyclohexane environment.

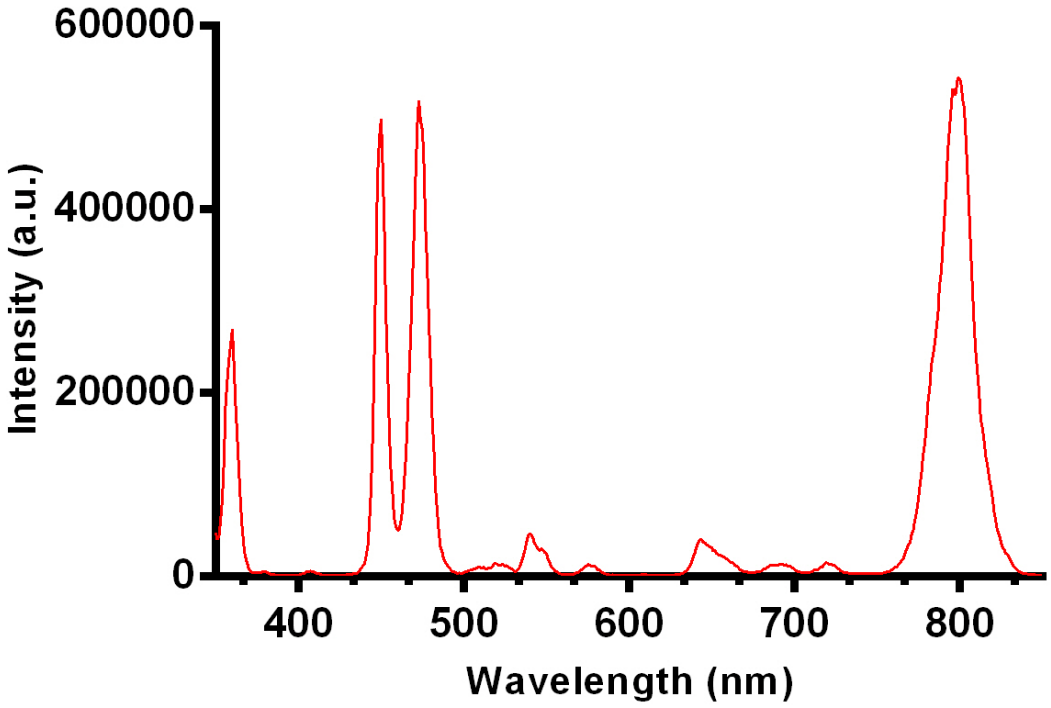

Figure 2.4. Luminescence emission spectra comparison of UCNPs $NaYF_4$: Yb^{3+}/Tm^{3+} with the average size of 33 nm, excited with 980 nm laser .

The results of different sizes of UCNP synthesis have suggested that larger particles yield stronger emission intensity under the same concentration of lanthanide ion dopant (e.g. 20% Yb^{3+} and 2% Er^{3+}). Although larger sized UCNPs provide higher UCL intensity and better outcome in bioimaging or bioanalytical of UCNPs due to the higher signal-noise ratio, the size of nanocrystal is still limited by its bioapplication. Many studies have found that the size of particles plays vital role in the interaction or adhesion with cells. Taking *in vivo* imaging application as an example, nanoparticles with comparable sizes in the range of 5~10 nm are required to target membrane and globular proteins. Much larger sized nanoparticles may block the access of the targeting molecules, interfere with protein functions and limit the accessibility of binding to subcellular structures. (Kobayashi, Ogawa et al. 2009; Lowe, Siegel et al. 2010) The

upconversion fluorescent enhancement procedure (core-shell nanoparticles) and UCNP surface functionalization would greatly increase the size of nanoparticles. Thus, to balance the UCL intensity of UCNPs and their subsequent bioapplication study, selecting suitable size of nanoparticles is very critical. In this study, UCNPs sized around 30 nm were used for the following bioapplications.

2.3.5 TEM Imaging of Core-Shell UCNPs with Increasing Size Distribution

The synthesized UCNPs, especially when monodispersed at low concentration, were difficult to be excited efficiently using our available scanning confocal microscope fitted with a 980 nm laser, when applied to cell imaging. The low power density of the currently set up laser unit was insufficient to excite UCNPs in a fixed scanning time (200 μs/pixel) and this resulted in not being able to collect enough signal. Based on this, a core-shell structural $NaYF_4$ nanoparticles was introduced in this study to achieve the tunable upconversion emission enhancement (Shen, Chen et al. 2013). In this experiment, hexagonal phase (β phase) $NaYF_4$ nanoparticle co-doped with 20% Yb^{3+} and 2% Er^{3+} was used as the core particle since it is the most efficient host material for UCNPs. The cubic phase (α phase) $NaGdF_4$ was chosen as the epitaxial shell due to its good lattice match with $NaYF_4$ (Shen, Chen et al. 2013). In brief, the low efficiency of UCL of UCNPs can be attributed to the non-radiative energy loss due to lack of protection of the host lattice. This limitation can be improved by coating a crystalline shell onto the surface of lanthanide-doped UCNP and the doped ions can be confined within the core $NaYF_4$ particle by the shell (Lin, Zhao et al. 2012). Through a well-defined core-shell structure, the upconversion emission efficiency of $NaYF_4$: Yb^{3+}/Er^{3+}@$NaGdF_4$ nanoparticles can be improved by controlling Gd sublattice-mediated energy migration (Wang, Deng et al. 2011). In this section, the properties of core-shell UCNPs ($NaYF_4$: Yb^{3+}/Er^{3+}@$NaGdF_4$) and core UCNPs ($NaYF_4$: Yb^{3+}/Er^{3+}) were compared.

As shown in **Figure 2.5** upper panel, β phase $NaYF_4$: 20% Yb^{3+}/2% Er^{3+} (OA-UCNPs) nanoparticles (see **Figure 2.1**) and α phase $NaGdF_4$ were firstly prepared following a protocol as literature reported (Boyer, Vetrone et al. 2006). β phase $NaYF_4$: Yb^{3+}/Er^{3+} nanoparticles were then used as seeds for epitaxial growth of α phase $NaGdF_4$ shells (Qian and Zhang 2008). **Figure 2.5** middle panel shows the TEM images of $NaYF_4$: Yb^{3+}/Er^{3+} core compared to $NaYF_4$: Yb^{3+}/Er^{3+}@$NaGdF_4$ core-shell. The average diameter of $NaYF_4$: Yb^{3+}/Er^{3+} core was measure at 30.3 ± 2.9 nm by measuring the particle sizes in TEM images through ImageJ analysis. As expected, the diameter of $NaYF_4$: Yb^{3+}/Er^{3+}@$NaGdF_4$ core-shell increased to 43.6 ± 3.2 nm (**Figure 2.5**, lower panel).

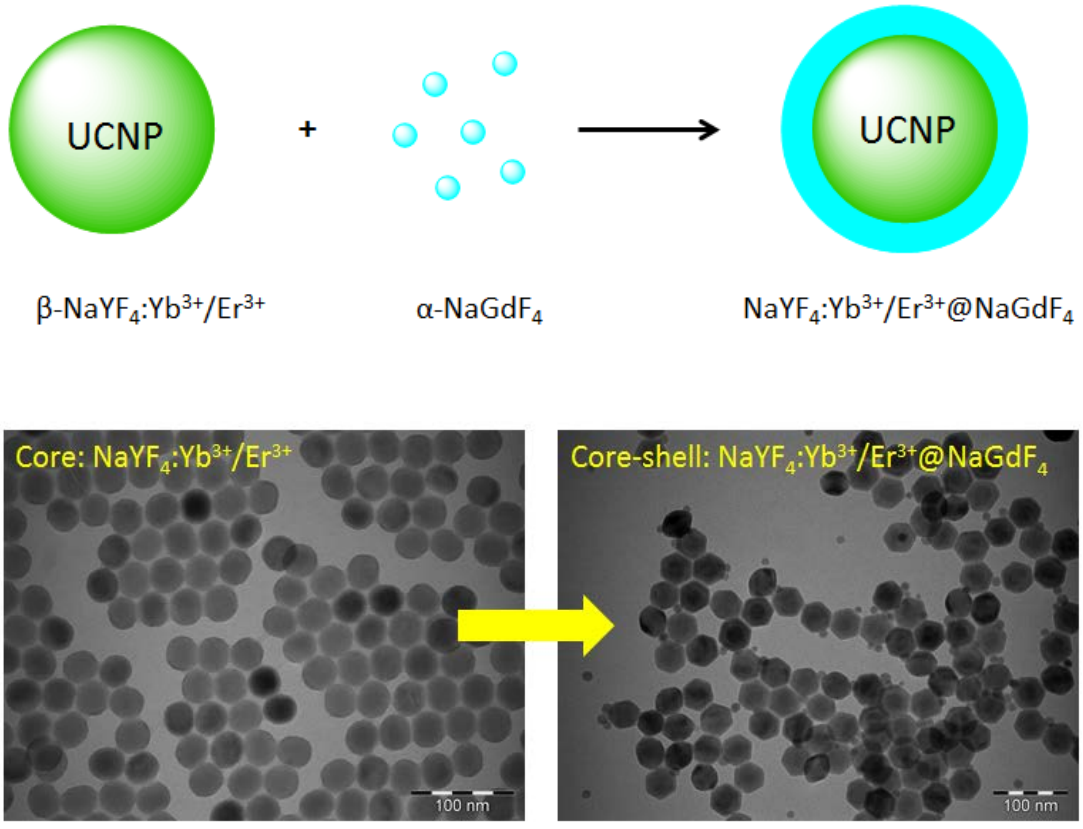

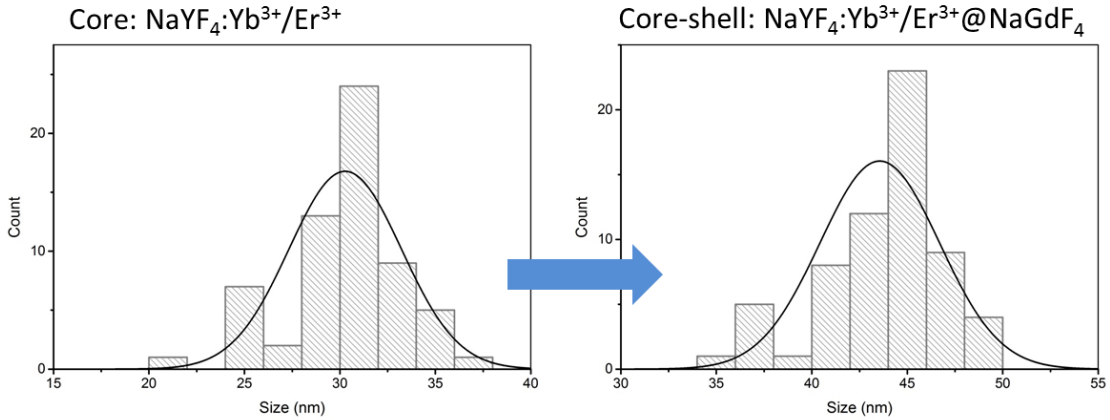

Figure 2.5 The upper panel is a scheme illustrating the synthesis of inert-shell coated UCNPs $NaYF_4$: Yb^{3+}/Er^{3+}@$NaGdF_4$. The middle panel shows TEM images of core UCNPs (left) and (right) core-shell UCNPs in cyclohexane. The lower panel shows the average size of core and core-shell UCNPs measured by TEM at 30.3 ± 2.9 nm and 43.6 ± 3.2 nm, respectively.

2.3.6 Upconversion Emission Spectra Between Core UCNPs and Core-Shell UCNPs

The UCL emission spectra measurement was then performed to view any changes of upconversion efficiency of UCNPs before and after core-shell synthesis. The UCL emission spectra excited by 980 nm laser were compared to quantify the luminescence intensity between $NaYF_4$: Yb^{3+}/Er^{3+} core and $NaYF_4$: Yb^{3+}/Er^{3+}@$NaGdF_4$ core-shell adjusted at the same concentration (20 mg/mL) dispersed in cyclohexane. As compared to $NaYF_4$: Yb^{3+}/Er^{3+} core, there was a significant UCL enhancements of ~3.5 times of the $NaYF_4$: Yb^{3+}/Er^{3+}@$NaGdF_4$ core-shell (**Figure 2.6**). Thus by coating UCNPs with an un-doped $NaGdF_4$ shell the luminescence intensity of the nanoparticles was now detectable by confocal microscopy (**Figure 2.7**).

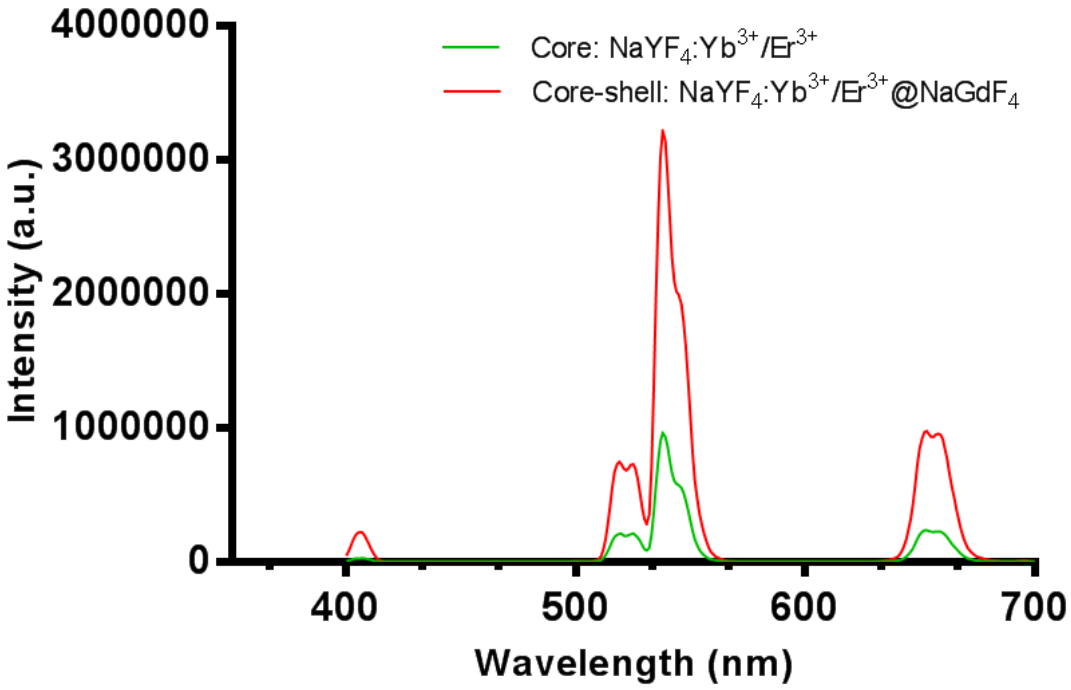

Figure 2.6 Comparison of UCL emission spectra and the changes of luminescence intensity between (green trace) core UCNPs and (red trace) core-shell UCNPs in cyclohexane at 980 nm excitation. The results demonstrate the luminescence intensity increased with the core-shell structure of UCNPs.

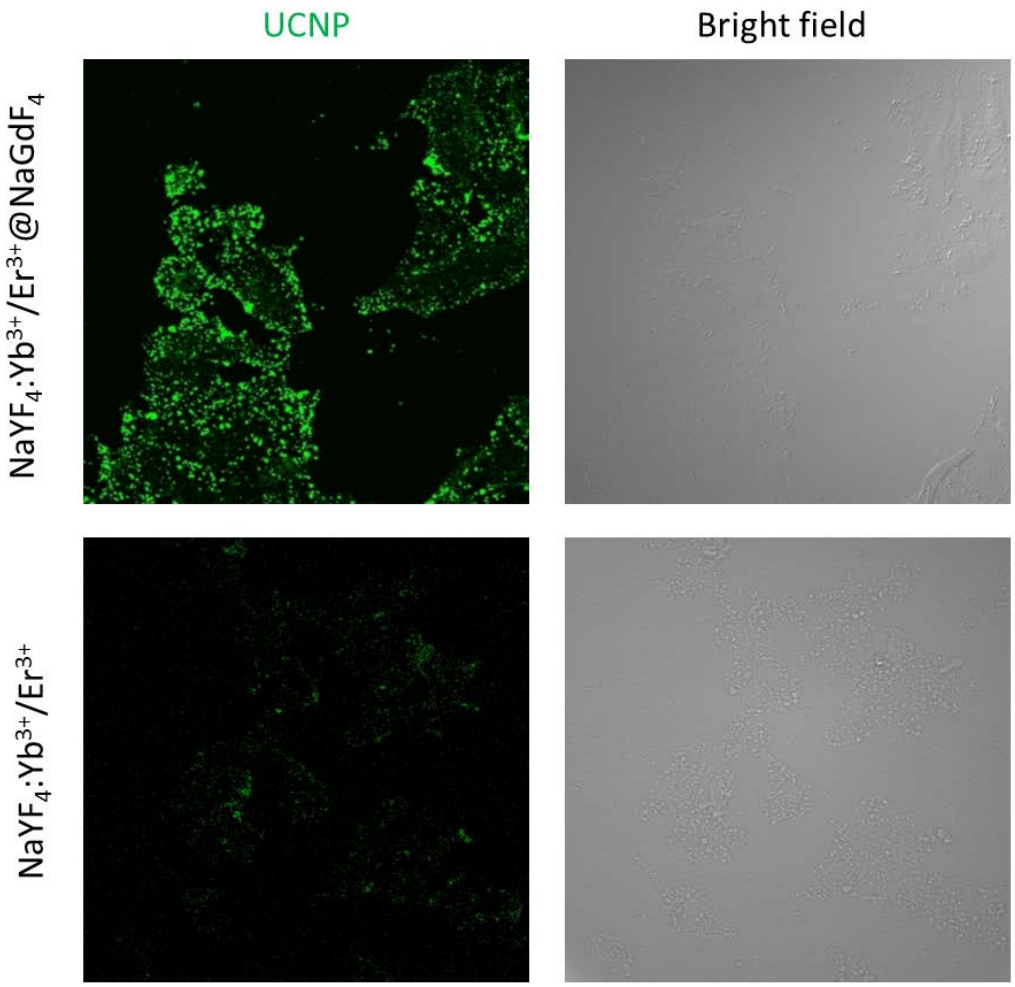

Figure 2.7 Confocal imaging of $NaYF_4$: Yb^{3+}/Er^{3+}@$NaGdF_4$ core-shell and $NaYF_4$: Yb^{3+}/Er^{3+} core (at the concentration of 1 mg/mL) incubated with DU145 prostate cancer cells for 1 h. For UCNPs images, λex=980 nm, and emission was collected at 450 nm.

2.4 Conclusions

In this chapter, different approaches for synthesizing and surface modification of upconversion nanoparticles (UCNPs) were investigated. The method for synthesizing UCNPs chosen in this study was by thermal decomposition which produces highly stable and uniform UCNPs products. While synthesizing by thermal decomposition, the size of UCNPs, which range from less than 10 nm to over 40 nm, can be tuned by

applying different time and temperature during the synthetic reaction. The size tuning of UCNPs enabled us to design nanoparticle probes for bioimaging and biolabeling studies in the following experiments. The smaller size of UCNPs have less steric hindrance ability of conjugation with biological functional molecules (e.g. peptides, antibodies, aptamers and small molecules) and have better accessibility to targeting on cells; on the other hand, the larger size of UCNPs give enhanced UCL emission intensity as they contain more sensitizers and activators, which is reflected as higher brightness than smaller particles with the same dopant concentration (e.g. 20% Yb^{3+} and 2% Er^{3+}). Besides the size, the emission profile of UCNPs was also shown to be tuned by changing the composition of lanthanide dopant ions (Er^{3+} and Tm^{3+}) and this capability was then available for possible simultaneous detection of multiple probes in cell targeting experiments.

A method for enhancing the UCL intensity enhancing approach by the addition of α phase $NaGdF_4$ precursors on β phase $NaYF_4$: Yb^{3+}/Er^{3+} surfaces to form a core-shell structure was also tested. An at least 3.5 times higher luminescence intensity enhancement after $NaGdF_4$ coating was achieved to overcome the low quantum yield limitation of UCNPs.

Due to the fact that OA was used as capping ligand during UCNP synthesis, OA-capped UCNPs were hydrophobic and only dispersed in organic solvent such as hexane and cyclohexane. A hydrophobic to hydrophilic transition procedure is needed to transfer UCNPs into water solutions for the subsequent bioapplications. The following section presents the exploring of different surface modification strategies of UCNPs.

Chapter 3: Surface Modification of Upconversion Nanoparticles

3.1 Background

Upconversion nanoparticles (UCNPs) have emerged as a new type of nanomaterials due to their ability of converting near-infrared (NIR) light into visible fluorescence and have attracted attention to their potential for biological and biomedical applications. However, the method used for efficiently synthesizing UCNPs (Chapter 2) yielded a hydrophobic nanoparticle due to its organic surface surfactant (e.g. oleic acid, OA or oleylamine, OM), whereas water solubility and dispersibility is critical in major fields of biological application of UCNPs.

After nanoparticle synthesis, the hydrophobic UCNPs have to be converted to hydrophilic particle via surface functionalization for their use in bioimaging applications and as biological luminescent labels. The studies described in this chapter were designed to obtain a comprehensive understanding of surface modification of UCNPs for potential bioapplications and to determine the optimal bioconjugation method for further studies. To date, the reported surface functionalization strategies can be roughly categorized into four groups (Chapter 1): (1) extra layer coating of the UCNP surface, such as layer-by-layer assembly (Bao, Luu et al. 2010) and ligand attraction (Jiang, Pichaandi et al. 2012); (2) direct chemical modification of the capping ligand on UCNPs surface, which including the ligand oxidation (Dai, Yang et al. 2012) and ligand removal (Bogdan, Rodríguez et al. 2012); (3) complete replacement of the original ligand by another molecule, which can be divided into two subgroups: the direct ligand exchange (single-step replacement) (Dayaker, Durand et al. 2014) and two-step ligand replacement which needs strong acids or nitrosyl tetrafluoroborate

($NOBF_4$) to produce ligand-free nanoparticles prior to introducing new functional ligands (Dong, Ye et al. 2010); (4) addition of an extra shell on UCNPs surface, for example, silica oxide coating (Hlavacek, Sedlmeier et al. 2014) or metallic gold or silver coating (Alazemi 2014).

In this chapter, a series of surface modification methods among the classification listed above were chosen and tested. Based on (1) to obtain a bilayer coating, α-cyclodextrin (α-CD) (Liu, Chen et al. 2011) and an amphiphilic molecule 1,2-distearoyl-sn-glycero-3-phosphoethanolamine-N-[carboxy(polyethyleneglycol)-2000] (DSPE-PEG-COOH) (Li, Zhang et al. 2012) were used to coat OA-capped UCNPs to test for water dispersibility; Based on (2) to achieve direct chemical surface modification, an oxidizing reagent, ($NaIO_4$-$KMnO_4$, Lemieux-von Rudloff reagent) (Chen, Chen et al. 2008) was used to oxidize the carbon-carbon double bond of OA and generate carboxyl groups; Based on (3) for the ligand exchange strategy, there are two subgroups including the single-step ligand exchange which uses poly(acrylic acid) (PAA) (Xiong, Yang et al. 2010), and the two-step protocol using $NOBF_4$ with O-phosphorlethanolemine (OPEA) (Fedoryshin, Tavares et al. 2014) and PO_4-PEG_{5000}-COOH (Sedlmeier and Gorris 2015). Based on (4) for the addition of a thin shell on top of the UCNP, a silica coating method was used for the modification (Bagwe, Hilliard et al. 2006).

The amphiphilic coating strategy with α-CD was firstly applied to render hydrophobic UCNPs hydrophilic via van-der-Waals interactions between the hydrophobic OA-capped surface and the new coating material. As shown in **Scheme 3.1A**, a general strategy of α-CD coating was performed to achieve the two aims of UCNPs modification: the one is converting the hydrophobic OA-UCNPs surface into a hydrophilic surface; the other is to render functional groups on the UCNPs for the

subsequent molecular conjugation for biological applications. The reaction is based on self-assembly between OA and α-CD. The α-CD contains six glucopyranose rings and one hydrophobic cavity which acts as host molecule while the hydrophobic OA used as capping ligand of UCNPs is the guest molecule. This ligand host-guest attraction strategy is mainly based on the hydrophobic interaction of α-CD and OA and this is simple and rapid method which pull hydrophobic UCNPs into water within 30 s with only shaking.

Scheme 3.1B shows another approach of UCNPs surface modification by coating the OA-UCNPs with multifunctional phospholipids, which afford biocompatibility by mimicking the composition and functionality of a cell membrane. As the properties of amphiphilic structure and biocompatibility can be achieved by phospholipids, the phospholipid based structure can be widely used to provide biofunctionality to various inorganic nanoparticles (Bangham and Horne 1964). As shown in Scheme 1B, the designed phospholipid-like structure contains four parts: two fatty acids, one phosphor group, one PEG molecule and one carboxyl group to realize the biomimetic surface functionalization of UCNPs. The force to conjugate UCNPs and the phospholipid layer is the hydrophobic van der Waals interaction between the hydrophobic OA capping ligands on UCNPs surface and the hydrophobic tails of the phospholipid structure. The fatty acid chains of the phospholipids are embedded into the hydrophobic OA chains on UCNPs surface while the hydrophilic part with carboxylic and phosphorous groups and points out into the aqueous environment to render UCNPs-phospholipid complex water dispersible and carboxyl functionalized.

To directly modify the original ligand on UCNPs surface is very simple. As the OA is widely used as the capping ligand in most synthetic approaches of UCNPs, the molecule structure –CH=CH– can be utilized as the targeting point for oxidation by the

Lemieux-von Rudloff reagent. The Lemieux-von Rudloff reagent oxidation method is known to oxidize selectively a carbon-carbon double bond R–CH=CH-R' to generate two carboxylic acids (**Scheme 3.1C**). This oxidation strategy was expected to result in a simple and versatile way for UCNPs surface modification.

A single-step ligand exchange strategy, which exchanges PAA onto the UCNPs surface was expected to convert hydrophobic UCNPs with OA capping into hydrophilic particles with a polymer spacer and a carboxylic acid-functionalized surface as shown in **Scheme 3.1D**. After ligand exchange, the PAA functionalized UCNPs possess two properties: good dispersibility in an aqueous environment and the carboxylic acid groups on the surface to allow following conjugation with biological molecules for further biological labeling. The surface charge may also play an important role in the interaction of UCNPs with the cell surface.

The two-step ligand exchange strategy is widely applicable by using the reagent $NOBF_4$. $NOBF_4$ was firstly used to strip off the original surface ligand attached to UCNPs and replace their place with inorganic BF_4^- anions, which provide electrostatic stabilization of UCNPs in various polar media, such as dimethyl formamide (DMF) and dimethyl sulfoxide (DMSO) for long time with no observed precipitation and aggregation. A further functionalization is subsequently carried out by using OPEA (**Scheme 3.1E**) or a PEG linker, PO_4-PEG_{5000}-COOH (MW=5000) (**Scheme 3.1F**) to replace BF_4^- anions and generate new capping ligands—=amine groups or carboxyl groups—on the surface of UCNPs.

Surface silanization is another approach which has been seen to be widely used in converting hydrophobic nanoparticles into particles with hydrophilic properties. To

apply a silica coating to UCNPs, a two-step approach was performed in this study to synthesize amino-terminated UCNPs@SiO_2 with a silica shell (**Scheme 3.1G**). After the $NaYF_4$: 20% Yb^{3+}/2% Er^{3+} upconversion nanoparticles were prepared, the silica shell can be deposited onto the nanoparticles surface to form a core-shell structure by the hydrolysis of tetraethyl orthosilicate (TEOS) in the water-in-oil microemulsion method. Then (3-aminopropyl)triethoxysilane (APTES) was used to generate the amino groups on the nanoparticle surface to bring water dispersibility and biological functionality.

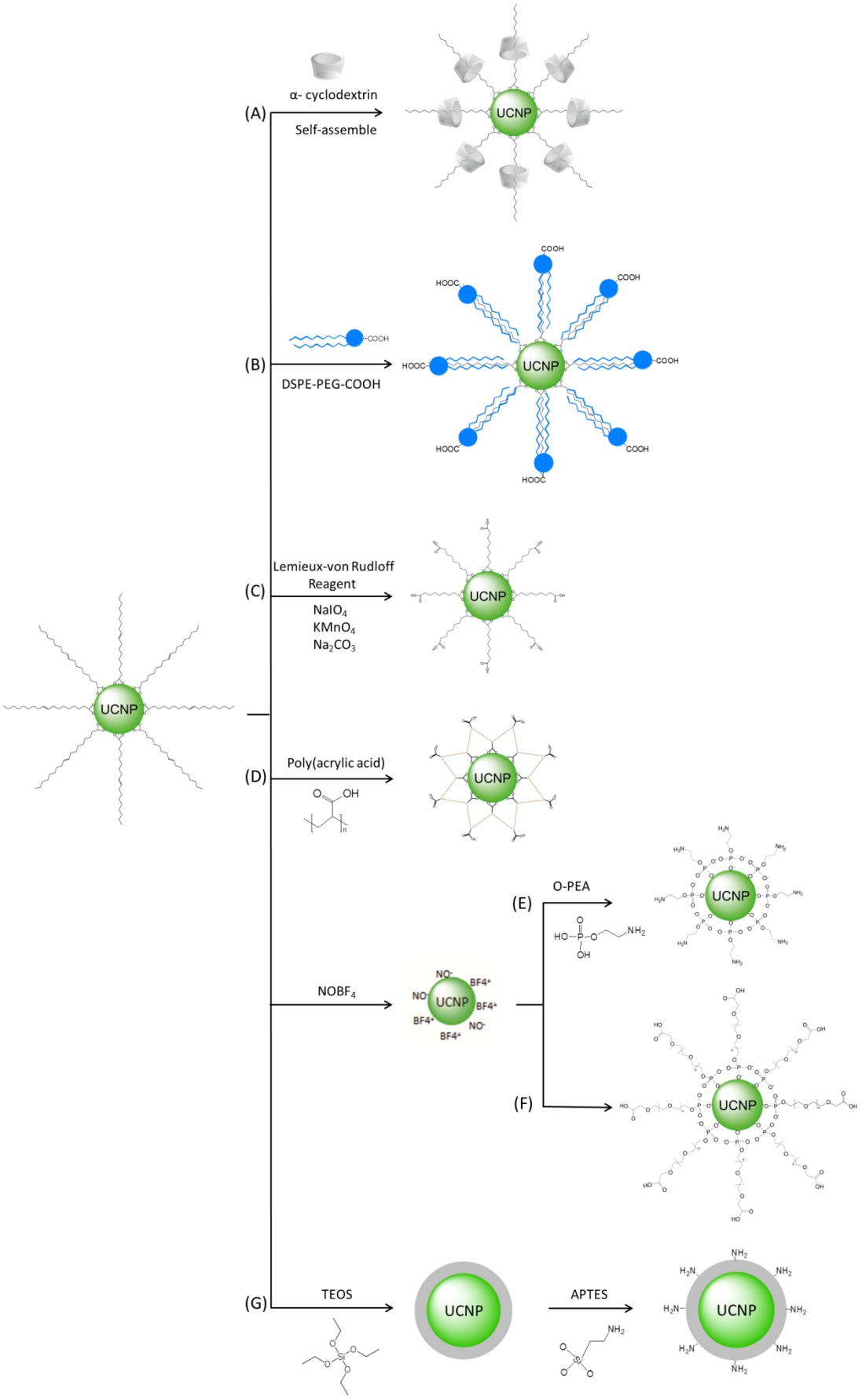
α- cyclodextrin
(A)
Self-assemble
UCNP
(B)
DSPE-PEG-COOH
COOH
HOOC
Lemieux-von Rudloff
Reagent
(C)
$NaIO_4$
$KMnO_4$
Na_2CO_3
Poly(acrylic acid)
(D)
O-PEA
(E)
$NOBF_4$
BF_4^-
NO^+
(F)
TEOS
(G)
APTES
NH_2

Scheme 3.1 Schematic illustration of the methods used to modify and functionalise the UCNP surface: (A) self-assembly of OA-UCNPs with α-CD, (B) self-assembly of OA-UCNPs with DSPE-PEG-COOH, (C) carboxylic acid-functionalized UCNPs from OA-capped precursors oxidation, (D) ligand exchange of UCNPs with PAA, (E) ligand exchange of UCNPs by $NOBF_4$ and OPEA, (F) ligand exchange of UCNPs by $NOBF_4$ and PO_4-PEG_{5000}-COOH and (G) silica coating of UCNPs by TEOS and APTES.

Subsequently a further modification step is commonly performed for binding biomolecules to the surface of UCNPs, which including antibodies (Zhan, Qian et al. 2011), peptides (Lee, Lee et al. 2013), aptamers (Chen, Yuan et al. 2013) and small molecules (Ma, Huang et al. 2012). As every surface functionalization step can change several features of UCNPs, it is not only important to confirm the successful surface functionalization but also to ensure that the modification has no negative impact on the upconversion efficiency or the colloidal stability in aqueous dispersions. Depending on the type of functionalization, several methods can be used for analyzing the functionalization, changes in the size and shape of UCNPs and their dispersibility in aqueous systems.

The following study critically evaluates the advantages and disadvantages conferred by each type of surface modification in regards to the upconversion efficiency, the formation of long-term stable colloids and the capacity for efficient further functionalization with biomolecules. On one hand, transmission electron microscopy (TEM), Fourier transform infrared spectroscopy (FT-IR), dynamic light scattering (DLS), Zeta potential and emission spectra under 980 nm excitation were utilized to characterize the surface modification of UCNPs by the different approaches. Most importantly, the particles were tested for non-specific binding to cells to validate if the surface modification method may be suitable for sensitive biological detection as

minimization of background “noise” is critical. Careful design and optimization of these aspects is essential before UCNPs can be used for bioanalytical applications.

3.2 Experimental Section

3.2.1 Reagents and Materials

Unless otherwise stated, all reagents were purchased from commercial suppliers and used without further purification. Cyclohexane (C_6H_{12}, 99.5%), ethanol (CH_3CH_2OH, ≥99.5%), methanol (CH_3OH, 99.5%), dichloromethane (CH_2Cl_2, 99.8%), toluene ($C_6H_5CH_3$, 99.8%), dimethyl formamide (DMF, 99.8%), α-cyclodextrin(α-CD, 98%), sodium periodate (NaIO4), potassium permanganate (KMnO4), poly(acrylic acid) (PAA), nitrosyl tetrafluoroborate ($NOBF_4$, 95%), O-phosphorylethanolamine (OPEA), tetraethyl orthosilicate (TEOS, 99.9%), polyoxyethylene (5) nonylphenylether (Igepal CO-520), (3-aminopropyl)triethoxysilane (APTES, 98%), ammonium hydroxide solution (NH_4OH, 30%) and RPMI 1640 medium were all purchased from Sigma–Aldrich and used as received without further purification. 1,2-distearoyl-snglycero-3-phosphoethanolamine-N-[carboxy(polyethylene glycol)-2000] (ammonium salt) (DSPE-PEG-COOH) was all purchased from Avanti Polar Lipids. PO_4-PEG_{5000}-COOH was synthesized and purchased from JenKem Technology USA Inc. Prostate cancer cell line DU145 was provided by Minomic Int. Ltd.

3.2.2 Surface Modification by α-CD

The synthesized oleic acid capped upconversion nanoparticles (OA-UCNPs) were washed with cyclohexane/ethanol/methanol (1:2:1, v/v/v), and then air dried at room temperature 10 mg UCNPs was added into 5 mL water containing α-CD (20 mg/mL)

and ultrasonically (20 kHz) treated for 30 min at room temperature. The α-CD coated UCNPs was separated by centrifugation (12000 g) for 5 min, and washed with Milli Q water three times.

3.2.3 Surface Modification by DSPE-PEG-COOH

DSPE-PEG-COOH (5 mg, MW=2000) in 1 mL chloroform was added dropwise to a 2 mL chloroform solution of 5 mg OA-UCNPs. The solution was stirred at room temperature for 2 days to evaporate the chloroform slowly. After heating up to 75 °C for 10 min, the formed film was dissolved into 5 mL Milli Q water by vigorous sonication. After stirring vigorously at 75 °C for another 10 min, the surface modified UCNPs were collected by centrifugation at 12000 g for 10 min. The pellet was washed 3 times with Milli Q water and then dried in vacuum for further use.

3.2.4 Surface Modification by Lemieux-von Rudloff Reagent

A mixture of as-prepared OA-UCNPs sample (0.1 g), cyclohexane (100 mL), tert-butanol (70 mL), water (10 mL) and 5 % K_2CO_3 aqueous solution (5 mL) were stirred at room temperature for about 20 min. Then 20 mL of Lemieux-von Rudloff reagent (5.7 mM $KMnO_4$ and 0.105 M $NaIO_4$ aqueous solution) was added dropwise. The resulting mixture was stirred at 40 °C for over 48 h. The product was then isolated by centrifugation (12000 g) and washed sequentially with deionized water, acetone, and ethanol. Subsequently, the product was dispersed in hydrochloric acid (0.1 M, 50 mL) of pH 4-5, and the mixture was stirred for 30 min. The oxidized product was obtained by centrifugation, washed twice with deionized water and dried under vacuum.

3.2.5 Surface Modification by PAA

Under an argon atmosphere, a diethylene glycol (DEG) solution (10 mL) containing PAA (120 mg, MW=1800) was heated to 110 °C with vigorous stirring for 30 min. The OA-UCNPs (10 mg) in 2 mL toluene were injected slowly into the solution. After stirring at 110 °C for 30 min, the mixture was heated to 240 °C for 2 h. The solution was cooled down to room temperature and excess ethanol was added. The precipitate was recovered by centrifugation (12000 g) and washed with ethanol/water (1:1) and water, 3 times respectively. The PAA modified UCNPs were dried in vacuum for further use.

3.2.6 Surface Modification by $NOBF_4$ and OPEA/PO_4-PEG_{5000}-COOH

20 mg OA-Capped UCNPs in 4 mL cyclohexane was mixed with a solution of $NOBF_4$ (20 mg in 4 mL dichloromethane) with stirring and the mixture was stirred at room temperature overnight. The ligand-free UCNPs was obtained by centrifugation and then washed with toluene: hexane (v/v, 1/1).

OPEA modification: The prepared UCNPs were dispersed into 4 mL DMF, and then, 20 mg of OPEA in 1 mL DMF was added into the solution. The mixture was stirred at room temperature for 24 h before washing with ethanol and ethanol/H_2O.

PO_4-PEG_{5000}-COOH modification: The prepared UCNPs were dispersed into 4 mL DMF, and then, 20 mg of PO_4-PEG_{5000}-COOH in 1 mL DMF was added into the solution. The mixture was stirred at room temperature for 24 h before washing with ethanol and ethanol/H_2O.

3.2.7 Surface Modification by Silica Coating

Silica coating was conducted to obtain a core–shell structure fluorescent nanoparticle via a water-in-oil (W/O) or reverse microemulsion method. 20 mg OA-UCNPs were dissolved into 20 mL of cyclohexane, 0.5 mL of Igepal CO-520 (MW=441) by sonicating for 30min. Afterwards, 100 μL of aqueous ammonia (wt 30%) that was stirred for 30 min at room temperature, and then 100 μL of TEOS was added and followed by vigorous stirring to form a water-in-oil (W/O) microemulsion. The mixture was allowed to stir vigorously for 24 h, and was followed by the addition of 10 μL of APTES for the second post-coating step and producing amino functional groups. The mixture was further reacted for 24 h, and the silica particles were precipitated from the microemulsion by the addition of ethanol. Finally, the particles were separated from the reaction mixture by centrifugation at 12000 g for 15 min and washed four times with ethanol and twice with water.

3.2.8 Transmission Electron Microscopy

The UCNPs were sufficiently diluted (≈0.1 mg/mL) so that visualization of individual particles was possible and 20 μL of UCNPs solution was placed on a 50 Å thick carbon-coated copper grid and the excess solution was immediately removed. The TEM images of the UCNPs were then recorded on a PHILIPS CM10 system operating at 100 kV. The TEM images were then processed with ImageJ analysis to obtain the size and size distributions of UCNPs. A black and white binary TEM image was firstly imported to ImageJ and then the nanoparticles on the image were segmented by measuring the segmentation threshold value. A total particle number of 100 segmented UCNPs were analyzed by ImageJ and give the mean particles size.

3.2.9 Fluorescence Spectra Measurement

The UCNPs were diluted to the same concentration of 5 mg/mL and their fluorescence emission spectra were recorded on a Fluorolog®-3 spectrophotometer equipped with excitation by a 980 nm VA-II diode pumped solid-state (DPSS) laser (current set at 1.50 A) and a 1200 g /mm grating. The emission spectra were measured over a range of wavelengths from 350 nm to 850 nm.

3.2.10 FT-IR Spectroscopy

The IR spectra of UCNPs with different surface functional groups were examined using a Thermo NICOLET6700 Fourier transform infrared spectrometer (FT-IR) at room temperature.

3.2.11 Size Distribution and zeta Potential

The UCNPs size distribution and surface charge were measured by dynamic light scattering analysis (DLS, Zetasizer NanoZS, Malvern Instruments, Malvern, UK). 1 mL of OA-capped UCNPs dispersed in cyclohexane or surface functionalized UCNPs dispersed in PBS buffer was used for the measurement.

3.2.12 Cell Culture and Cell Labelling

Prostate cancer cells DU145 were incubated in RPMI 1640 medium (composition is described in the Sigma-Aldrich catalogue) supplemented with 10% fetal bovine serum (FBS), streptomycin at 100 μg/mL, and penicillin at 100 U/mL. The cells were incubated in Corning® cell culture flasks at 37 ^{o}C in a humidified incubator in the presence of 5% CO_2.

Cells were seeded in Lab-Tek® chamber slides at a density of 4×10^4 cells per well. After allowing cell attachment for 24 h, DU145 cells were washed with PBS, and fixed by 5% paraformaldehyde (PFA). Then DU145 cells were incubated in PBS containing 100 μg/mL surface functionalized UCNPs for 1 h at room temperature in 5% CO_2, and then washed 5 times with PBS to remove excess UCNPs before imaging.

3.3 Results and Discussion

3.3.1 Characterization of UCNP Surface Modification

The $NaYF_4$: 20% Yb^{3+}/2% Tm^{3+} upconversion nanoparticles (UCNPs) utilized in this surface modification study were synthesized by a high temperature thermal decomposition method as mentioned above (Chapter 2). The oleic acid (OA)-capped UCNPs (OA-UCNPs) were firstly purified and dispersed in cyclohexane (**Figure 3.1A**). The average diameter of OA-UCNPs was measure at 29.6 ± 2.2 nm by examining photographic data from the transmission electron microscopy (TEM) to give the mean particle size (lower panel in **Figure 3.1A**).

After α-CD functionalization, the α-CD coated UCNPs (α-CD-UCNPs) still mono-dispersed in PBS buffer (**Figure 3.1B**), while the phospholipid coated UCNPs (DSPE-PEG-UCNPs) did not display a mono-dispersion pattern in PBS buffer with nanoparticles overlaying each other as observed in **Figure 3.1C**. Even more aggregation can be observed of the oxidized UCNPs (Oxi-UCNPs) in TEM (**Figure 3.1D**). PAA treated UCNPs showed good dispersibility in PBS without obvious shape change (**Figure 3.1E**). UCNPs with $NOBF_4$ treatment dispersed well in DMF under TEM (**Figure 3.1F**) and after OPEA and PO_4-PEG_{5000}-COOH replacement, OPEA-UCNPs (**Figure 3.1G**) and PEG-UCNPs (**Figure 3.1H**) were mono-dispersed in PBS without obvious signs of aggregation under TEM. In TEM images of silica coated UCNPs

(Silica-UCNPs) as shown in **Figure 3.1I**, the shell layer coated on the UCNPs cores can be seen clearly under TEM. The diameter of Silica-UCNPs determined by the TEM images was found to have increased to 53.9 ± 3.5 nm. The thickness of silica shell was measured at about 7-8 nm.

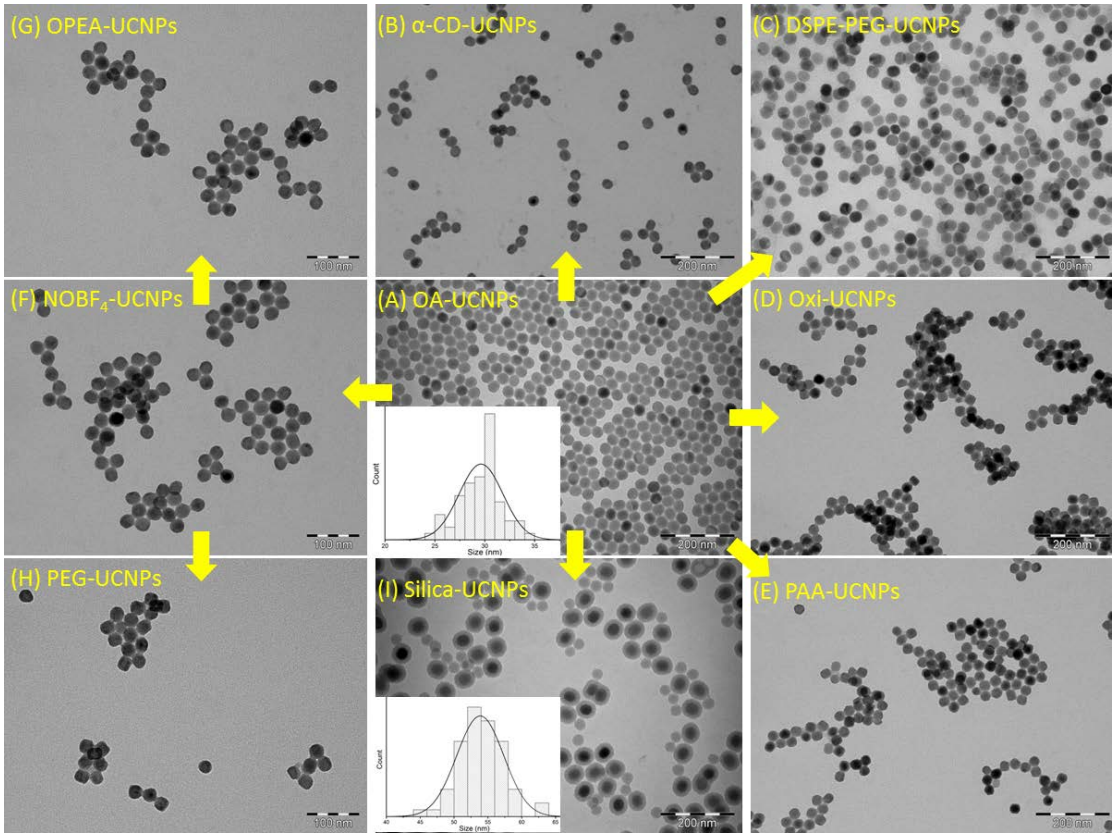

Figure 3.1 TEM images of (A) OA-UCNPs, (B) α-CD-UCNPs, (C) DSPE-PEG-UCNPs, (D) Oxi-UCNPs, (E) PAA-UCNPs, (F) $NOBF_4$-UCNPs, (G) OPEA-UCNPs, (H) PEG-UCNPs and (I) Silica-UCNPs. The average size of OA-capped UCNPs were measured by TEM at 29.6 ± 2.2 nm. The size increased to 53.9 ± 3.5 nm after UCNPs silica coating.

Dynamic light scattering (DLS) measurements (shown in **Figure 3.2**) were performed to monitor the changes of hydrodynamic diameter between OA-UCNPs and various

surface modified UCNPs to determine the surface change. The OA-UCNPs dispersed in cyclohexane were measured to have a diameter of 49.7 nm via DLS which is larger than the size measured by TEM. This difference in size measurement may be explained by the fact that DLS measurements are done in order to determine the true state of particles in media which takes into account the effects of surfactant, surface functional groups on the nanoparticles and the interaction with solvent molecules while TEM only measures the primary particle size of the sample.

After α-CD coating, there were two main peaks observed in the DLS analysis with a shoulder on the first peak (**Figure 3.2B**). The first peak at round 228 nm indicates that the hydrodynamic diameter of α-CD-UCNPs have a great size change compared with the diameter of OA-UCNPs. The shoulder on the peak at about 50 nm indicates there may be some unconjugated UCNPs remaining as 50 nm matches with the original size of OA-UCNPs. The second peak at around 4329 nm indicates that there is a small population of α-CD coated UCNPs aggregating after α-CD coating.

After DSPE-PEG-COOH coating, there are three main peaks that can be observed from the DLS analysis (**Figure 3.2C**). The first peak at approximately 54.1 nm suggests the UCNPs have not been fully functionalized as the diameter has not changed much comparing with the size of OA-UCNPs. The second peak at around 263 nm indicates that the hydrodynamic diameter of DSPE-PEG-UCNPs is significantly larger than the size of OA-UCNPs due to the present of the coated phospholipid-like molecules. The third peak at around 5199 nm again indicates that aggregation of UCNPs after DSPE-PEG-COOH coating occurs.

Figure 3.2D shows the DLS data after UCNPs oxidation, showing there are two main

peaks at 665.5 nm and 2634 nm indicating an increase of hydrodynamic size of the prepared Oxi-UCNPs sample with serious agglomeration happening after surface modification.

A smaller increase of hydrodynamic diameter is observed in the sample of PAA-UCNP at 104.5 nm with a leak at 1737 nm as shown in **Figure 3.2E**. The first peak around at 104.5 nm suggests a well-dispersed population of PAA modified UCNPs in PBS while the peak at 1737 nm indicates the aggregation also happens after PAA surface modification.

In the surface modification method with $NOBF_4$ treatment, the hydrodynamic diameter does not change much at 50.7 nm (**Figure 3.2F**), but the diameter has a great increase to 81 nm (as shown in **Figure 3.2G**) after OPEA modification, which may be attributed to the coating of OPEA molecules. After PO_4-PEG_{5000}-COOH modification, the diameter greatly increased to 125.2 nm (as shown in **Figure 3.2H**) which is larger than OPEA modified UCNPs due to the greater PEG chain length. After silica coating, the hydrodynamic diameter of UCNP@SiO_2-NH_2 increased to 90.1 nm (**Figure 3.2I**) and this change corresponds with the diameter change of these particles as determined by TEM. Little aggregation is observed in these last three UCNP modifications.

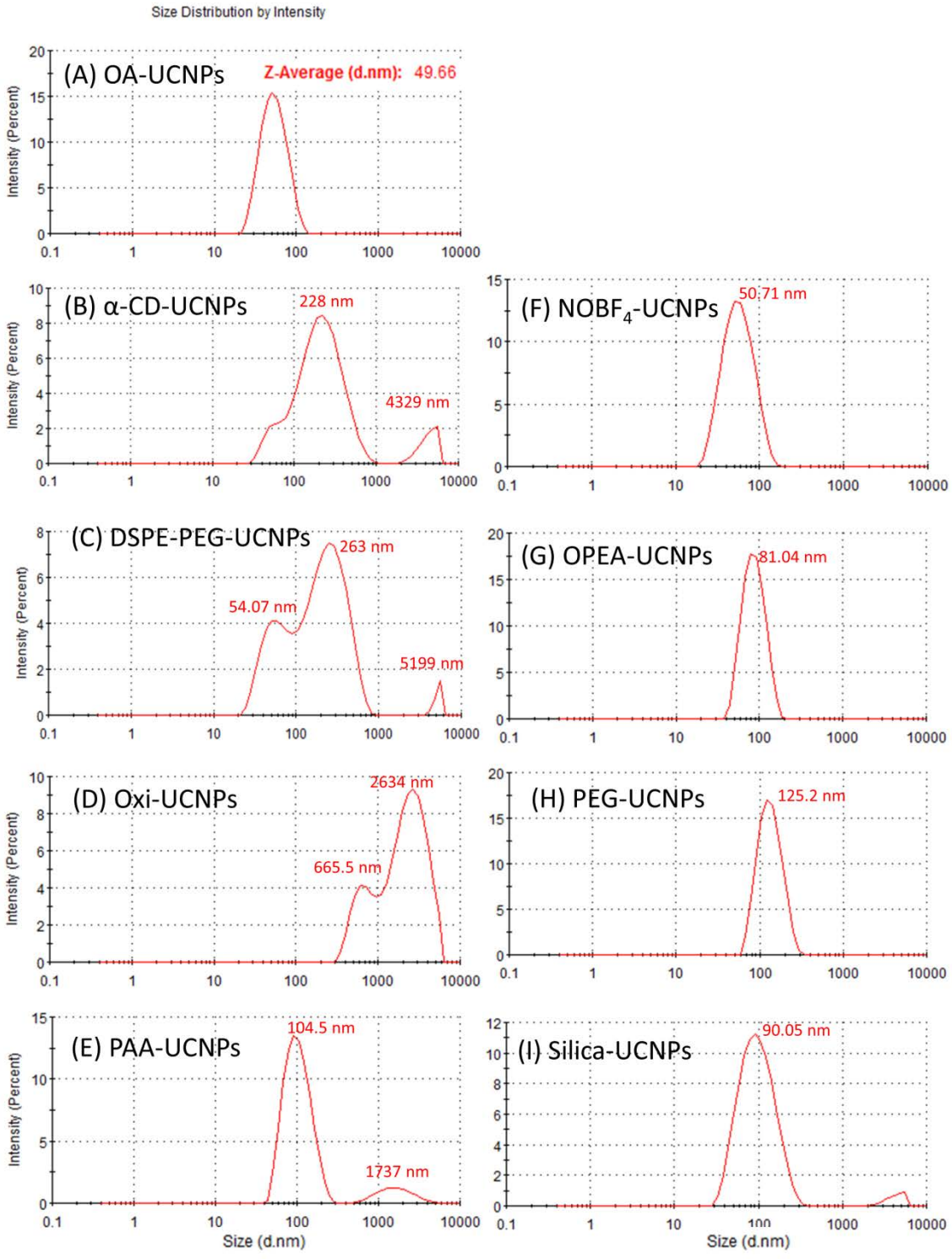

Figure 3.2 Size distribution of (A) OA-UCNPs, (B) α-CD-UCNPs, (C) DSPE-PEG-UCNPs, (D) Oxi-UCNPs, (E) PAA-UCNPs, (F) $NOBF_4$-UCNPs, (G) OPEA-UCNPs, (H) PEG-UCNPs and (I) Silica-UCNPs dispersed in PBS buffer. The

average size of each sample were measured by DLS analysis.

The zeta potential measurement of UCNPs after surface modification was also used to determine the surface change of the surface functionalized UCNPs. Zeta potential of α-CD-UCNPs, DSPE-PEG-UCNPs, Oxi-UCNPs, PAA-UCNPs, OPEA-UCNPs, PEG-UCNPs and Silica-UCNPs dispersed in PBS buffer were measured at -25.2, -10.7, -14.6, -23.1, 24.5, -20.8 and 16.7 mV, respectively (**Figure 3.3**). The mean of zeta potential of various functionalized UCNPs corresponded to the different surface ligands used in UCNP modifications. For example, the negative surface charge (-23.1 mV) of PAA-UCNPs is arisen from carboxyl group modified onto the nanoparticle surface; while the positive charge (24.5 mV) of OPEA-UCNPs is derived from amino groups coating on the surface of UCNPs.

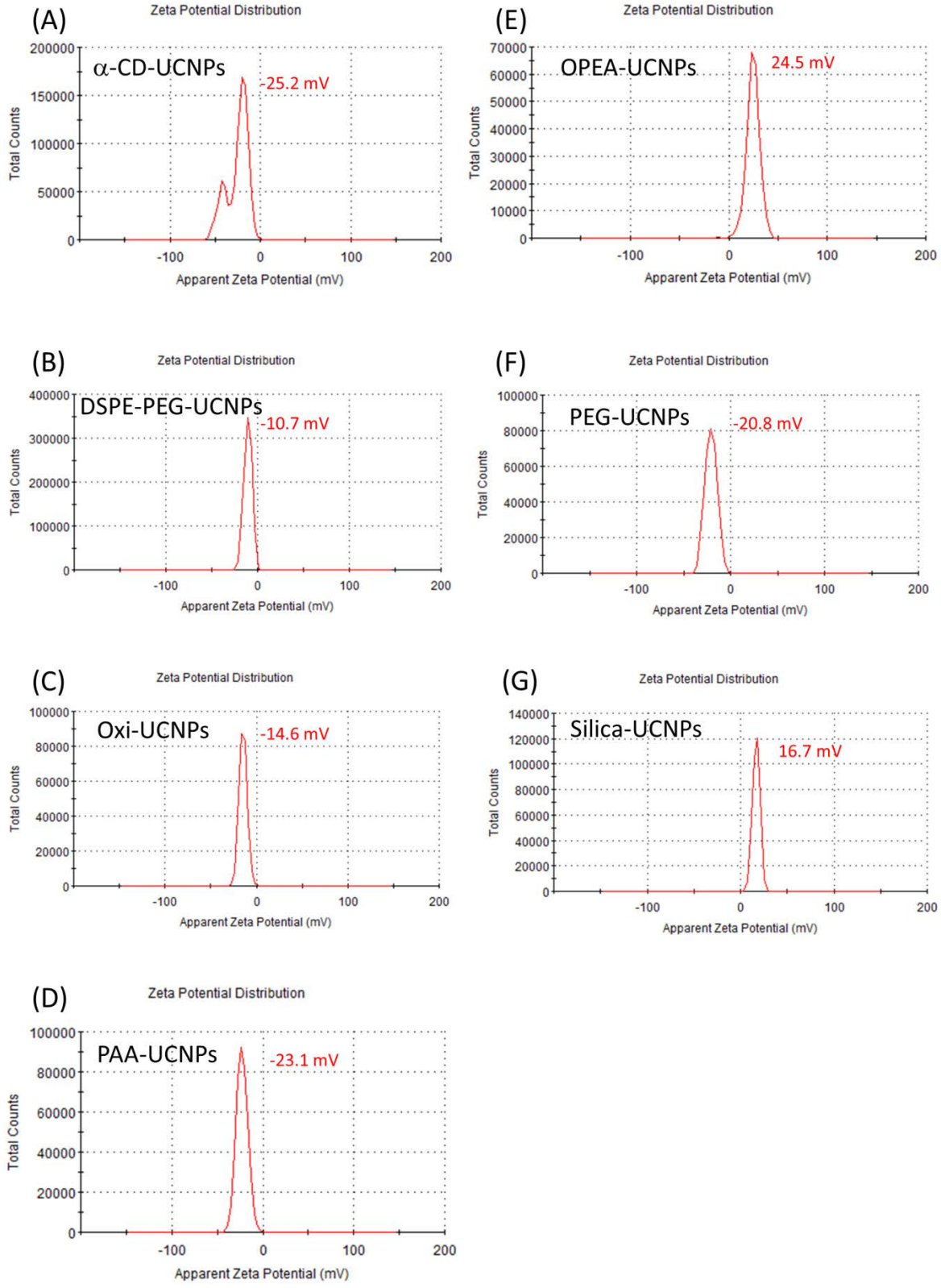

Figure 3.3 Zeta potential of (A) α-CD-UCNPs, (B) DSPE-PEG-UCNPs, (C) Oxi-UCNPs, (D) PAA-UCNPs, (E) OPEA-UCNPs, (F) PEG-UCNPs and (G)

Silica-UCNPs dispersed in PBS buffer.

To further compare the modifications on the UCNPs surface, Fourier-transform infrared (FT-IR) spectra were compared of OA-UCNPs before and after surface modification. As shown in **Figure 3.4A**, two intense bands centered around 1457 cm^{-1} and 1563 cm^{-1} were observed for OA-UCNP, which are due to the C=O asymmetric and symmetric stretching vibration modes of carboxylate anions on the surface of the OA-UCNPs. The strong bands at approximately 2920 cm^{-1} and 2850 cm^{-1} are contributed by antisymmetric and symmetric vibrations of $–CH_2$ as well as the weak stretching vibration at 3005 cm^{-1} associated with the asymmetrical stretching mode of =C-H groups, suggesting the presence of OA on the surface of OA-capped UCNPs.

After α-CD coating (**Figure 3.4B**), some new bands can be observed in the IR spectra of the α-CD-capped UCNPs. The band at 1154 cm^{-1} indicates the antisymmetric glycosidic vibration of C-O-C. Meanwhile, the new band at approximately 1080 cm^{-1} and 1030 cm^{-1} are associated with the coupled stretch vibration of C-C and C-O bond, respectively.

After DSPE-PEG-COOH coating (**Figure 3.4C**), the strong band centered at 1108 cm^{-1} suggested the characteristic absorption band of C-O-C of the PEG molecules. Additionally, the increased absorption band around 1736 cm^{-1} suggested the increased quantity of –COOH groups on the UCNPs surface from the DSPE-PEG-COOH molecules. Meanwhile, the bands at 2920 cm^{-1} and 2850 cm^{-1} associated with the vibration of $–CH_2$ were found to be inconspicuous after DSPE-PEG-COOH coating, which indicated that OA molecules on UCNPs surface had been efficiently blocked by the DSPE-PEG-COOH coating.

In **Figure 3.4D**, after oxidation of the UCNPs, the peak at 3005 cm^{-1} was lost in the

spectrum of the oxidized sample, which indicated the cleavage of the –HC=CH- group. This feature suggested the successful oxidation of UCNPs.

After single-step ligand exchange by PAA (**Figure 3.4E**), the strong band appearing at 1394 cm^{-1} and 1726 cm^{-1} suggested the presence of an increased quantity of the -COOH groups on the UCNPs surfaces. Additionally, the bands at 2920 cm^{-1} and 2850 cm^{-1} as well as the shoulder at 3005 cm^{-1} associated with the asymmetrical stretching mode of =C-H groups of OA became inconspicuous after ligand exchange. This observation indicated that OA molecules had been successfully substituted by PAA.

After the two-step ligand exchange, as shown in **Figure 3.4F**, the featured bands at 2920 and 2850 cm^{-1}, corresponding to $–CH_2$ group, and the bands at 1457 cm^{-1} and 1563 cm^{-1} ,associated with C=O, disappeared in the OPEA-UCNPs sample, which indicated the absence of OA molecules. Meanwhile, the very strong peak centered at 1092 cm^{-1} indicated the distinctive stretching mode of PO_4^{3-} group, and peaks at approximately 3440 and 1580 cm^{-1} were all attributed to stretching and bending vibration of primary amine (N-H). Similarity with the PO_4-PEG_{5000}-COOH replacement in UCNPs ligand exchange (**Figure 3.4G**), the strong peak centered at 1092 cm^{-1} indicated the distinctive stretching mode of PO_4^{3-} group, and the peak located at 961 cm^{-1} is associated with the symmetric stretching vibrations of the P-O mode. In addition, the strong band located around 1715 cm^{-1}, corresponding to the stretching vibration of carboxyl group (C=O), suggested the –COOH groups on the PEG-UCNPs surface. Therefore, the completion of the ligand exchange reaction was supported by the disappearance of bands associated with OA, and appearance of characteristic -COOH peaks.

In the FT-IR spectra of the Silica-UCNPs (**Figure 3.4H**), a strong band centered around

1049 cm^{-1} can be attributed to the symmetrical stretching vibration of Si-O-Si bond which suggested the coated silica layer of UCNPs. The two bands approximately at 3374 cm^{-1} and 1637 cm^{-1} were associated with the stretching and bending vibration of amine groups on the UCNPs surface. Additionally, the two peaks at 2920 cm^{-1} and 2850 cm^{-1} correspond to the antisymmetric and symmetric stretching vibration of the methylene groups ($–CH_2$), which existed in the hydrolysate of APTES. Therefore, the bands at 3374, 2920 and 2850 cm^{-1} together demonstrated that the silica coated UCNPs have been successfully functionalized with amino groups.

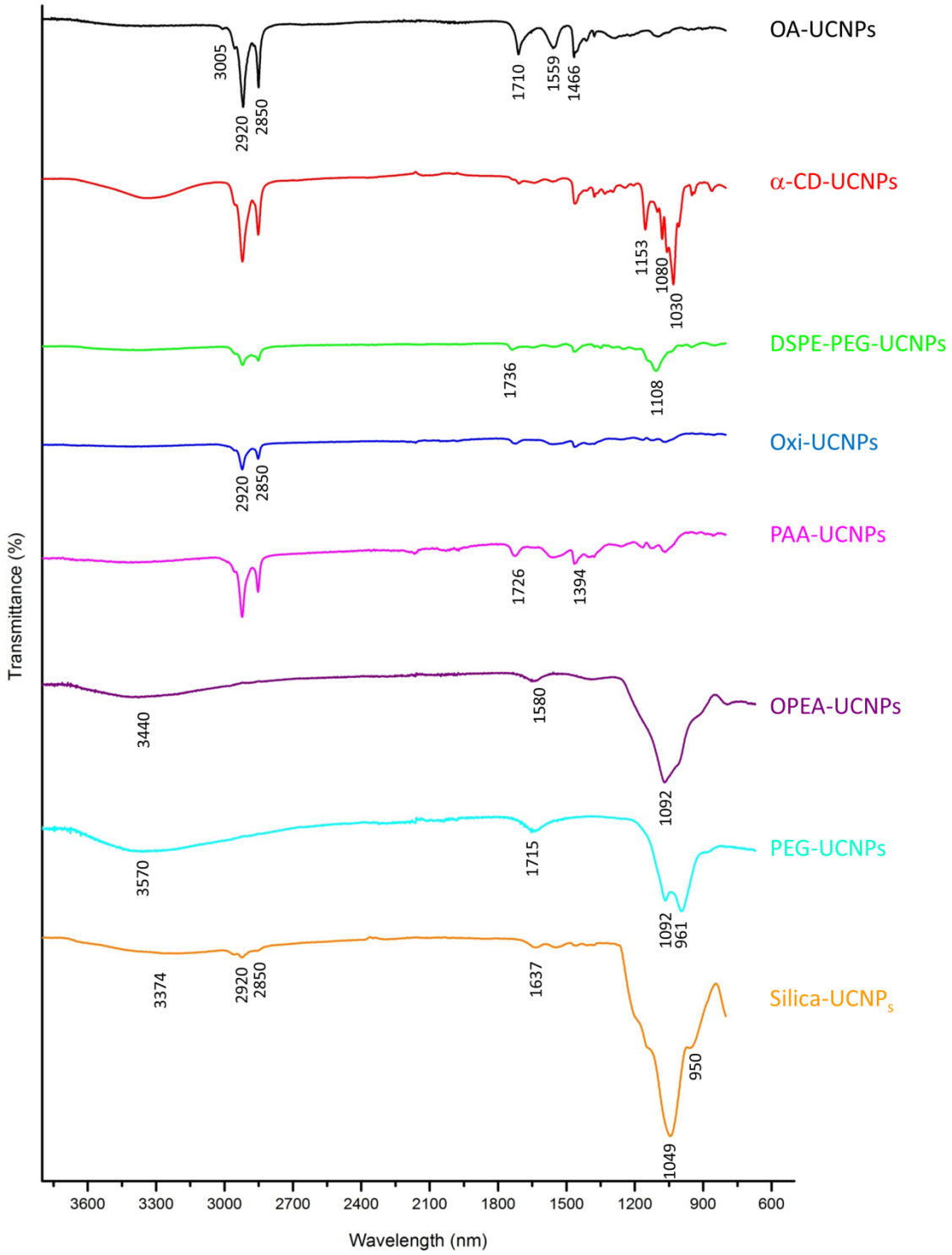

Figure 3.4 FT-IR absorption spectra of (A) OA-UCNPs, (B) α-CD-UCNPs, (C) DSPE-PEG-UCNPs, (D) Oxi-UCNPs, (E) PAA-UCNPs, (F) OPEA-UCNPs, (G) PEG-UCNPs and (H) Silica-UCNPs.

The changes of optical properties of the UCNPs before and after surface modification is vital to evaluate the modification procedure with a successful method expected to retain the upconversion efficiency of the products after surface functionalization in aqueous environments. The upconversion luminescence emission spectra excited by the 980 nm laser were compared to quantify the luminescence intensity between OA-UCNPs and the various surface modified UCNPs at the same concentration (10 mg/mL) dispersed in cyclohexane and PBS buffer, respectively. As compared to OA-UCNPs dispersed in cyclohexane, the emission intensity of α-CD-UCNPs (**Figure 3.5A**), DSPE-PEG-UCNPs (**Figure 3.5B**), Oxi-UCNPs (**Figure 3.5C**) and PAA-UCNPs (**Figure 3.5D**) was only slightly weaker than before functionalization. This may be attributed to the surface quenching effect of water molecules(Li, Zhang et al. 2012). After $NOBF_4$ treatment, the luminescence emission intensity has a significant increase. The enhancement of emission intensity of $NOBF_4$ treated UCNPs might be due to the improved nanoparticle dispersibility in DMF after surface modification. Subsequently, the emission intensity of OPEA modified UCNPs (**Figure 3.5E**) and PO_4-PEG_{5000}-COOH modified UCNPs (**Figure 3.5F**) were only slightly weaker than that of $NOBF_4$ treated UCNPs, which was caused by the change of surface ligands and the surface quenching effect. Compared to OA-capped UCNPs, a significant decrease of emission intensity of silica coated UCNPs (**Figure 3.5G**) can be observed indicating that UCNPs after silica coating will compromise the brightness of the nanoparticles.

To briefly conclude, apart from the UCNP silica coating, other surface modification methods, which included the ligand oxidation, ligand exchange and polymer coating, did not obviously interfere the emission intensity of UCNPs.

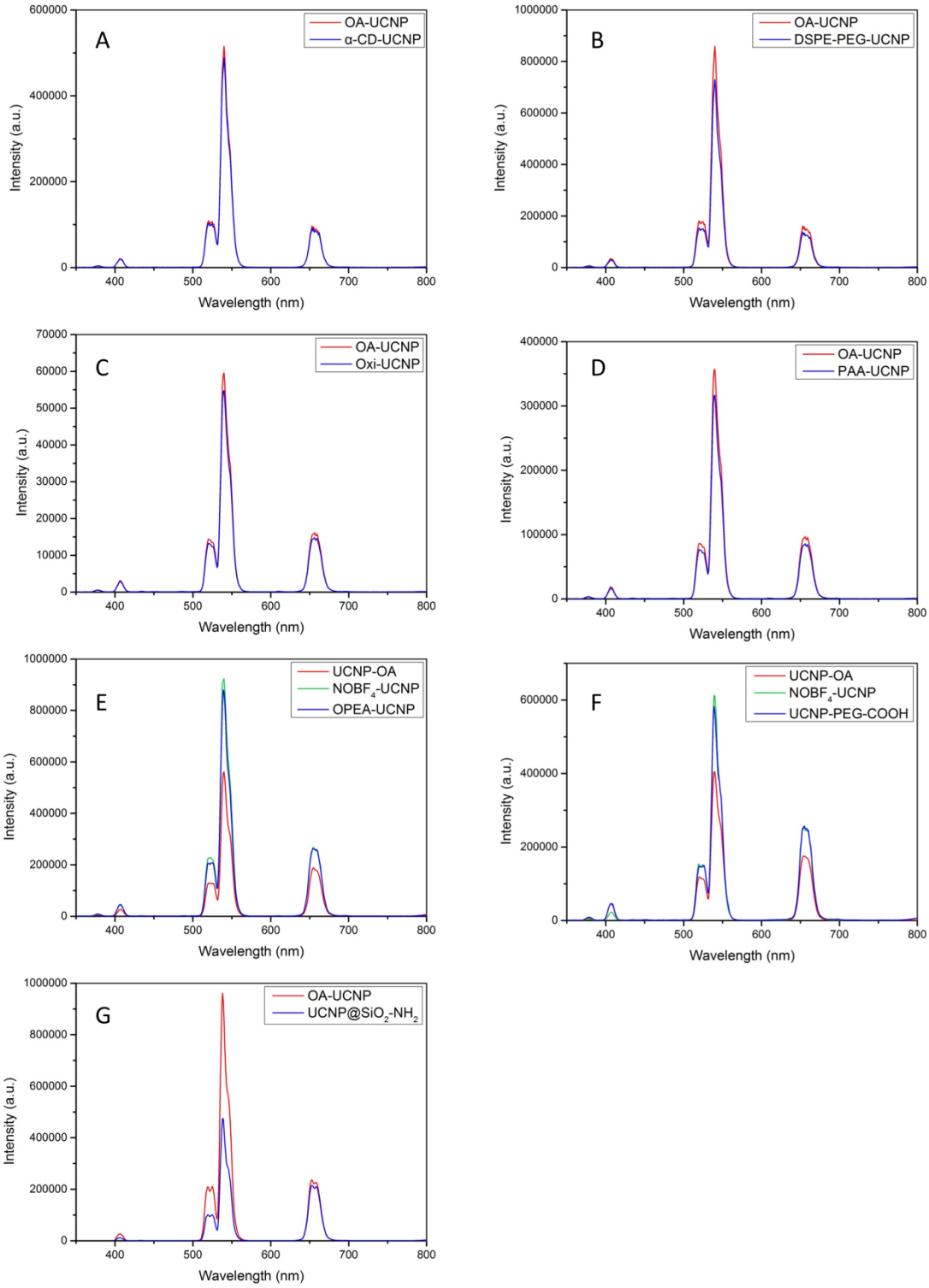

Figure 3.5 Comparison of upconversion fluorescence emission spectra and the changes of luminescence intensity between OA-UCNPs and (A) α-CD-UCNPs, (B) DSPE-PEG-UCNPs, (C) Oxi-UCNPs, (D) PAA-UCNPs, (E) OPEA-UCNPs, (F)

PEG-UCNPs and (G) Silica-UCNPs.

3.3.2 Validation for Application in Bioconjugation and Bioimaging

In order to confirm that the functionalized UCNPs are suitable for biological application, the interaction between hydrophilic UCNPs and cells in biological environment needs to be verified. Some surface modification procedures of UCNPs are not suitable to be used for biological applications as functionalized UCNPs may exhibit non-specific binding and aggregation when interacting with biological cells or tissues. These properties will affect the usefulness of UCNPs as a fluorescence probe in biological labeling. Even though some surface modification strategies produce water dispersible UCNPs, the issue of non-specific binding to cells will complicate the interpretation of their use. A cell based assay in which hydrophilic UCNPs (1 mg/mL) were incubated with DU145 prostate cancer cells (4×10^4/well) for a certain time followed by extensive washing with PBS (at least 5 times) was used to check if most of the UCNPs can be washed off prior to fluorescent microscopy. Due to limitations of the current instrument, the subsequent microscopy imaging requires a longer time to produce quality images; therefore fixed cells were applied in this research. Due to the absence of a targeting compartment in this assay, the fluorescence signal can only result from non-specific binding after PBS wash. A suitably functionalized UCNPs for biological application would either be water dispersible and water stable and would avoid any non-specific binding. Therefore, no fluorescence signal after UCNPs incubation with cells and washing would validate a good surface modification method.

The fluorescent images taken after cell based assay with the different functionalized UCNPs are shown in **Figure 3.6A-3.6D**. Green fluorescence in the images is derived from UCNPs that have serious non-specific binding after the assay. Agglomeration of

UCNPs can be observed sticking onto the cell surfaces with the α-CD-UCNPs, DSPE-PEG-UCNPs, Oxi-UCNPs, PAA-UCNPs functionalization, indicating than the non-specific binding issue might make these nanoparticles unsuitable for the further conjugation for specific biological molecular targeting.

However, the images taken by the fluorescent microscope showed that there was no obvious fluorescence detected after PBS washing of cells incubated with $NOBF_4$/OPEA (**Figure 3.6E**) and $NOBF_4$/PO_4-PEG_{5000}-COOH (**Figure 3.6F**) functionalized UCNPs. These functionalized nanoparticles displayed no detectable aggregation or non-specific binding as no fluorescent signal can be detected after cell incubation with these UCNPs.

Some weak fluorescence signal was detected on the cells after silica coated UCNPs incubation as shown in **Figure 3.6G** suggesting that UCNPs with silica coating are not as good as those modified by the $NOBF_4$ treated ligand exchange method, but are still better than the results from the other methods of functionalization (**Figure 3.6A-3.6D**) that show high levels of non-specific binding.

To summarize, UCNPs functionalized by $NOBF_4$/OPEA and $NOBF_4$/PO_4-PEG_{5000}-COOH by the two-step ligand exchange method appear to have the greatest potential to be applicable to further conjugation with biologically active molecules.

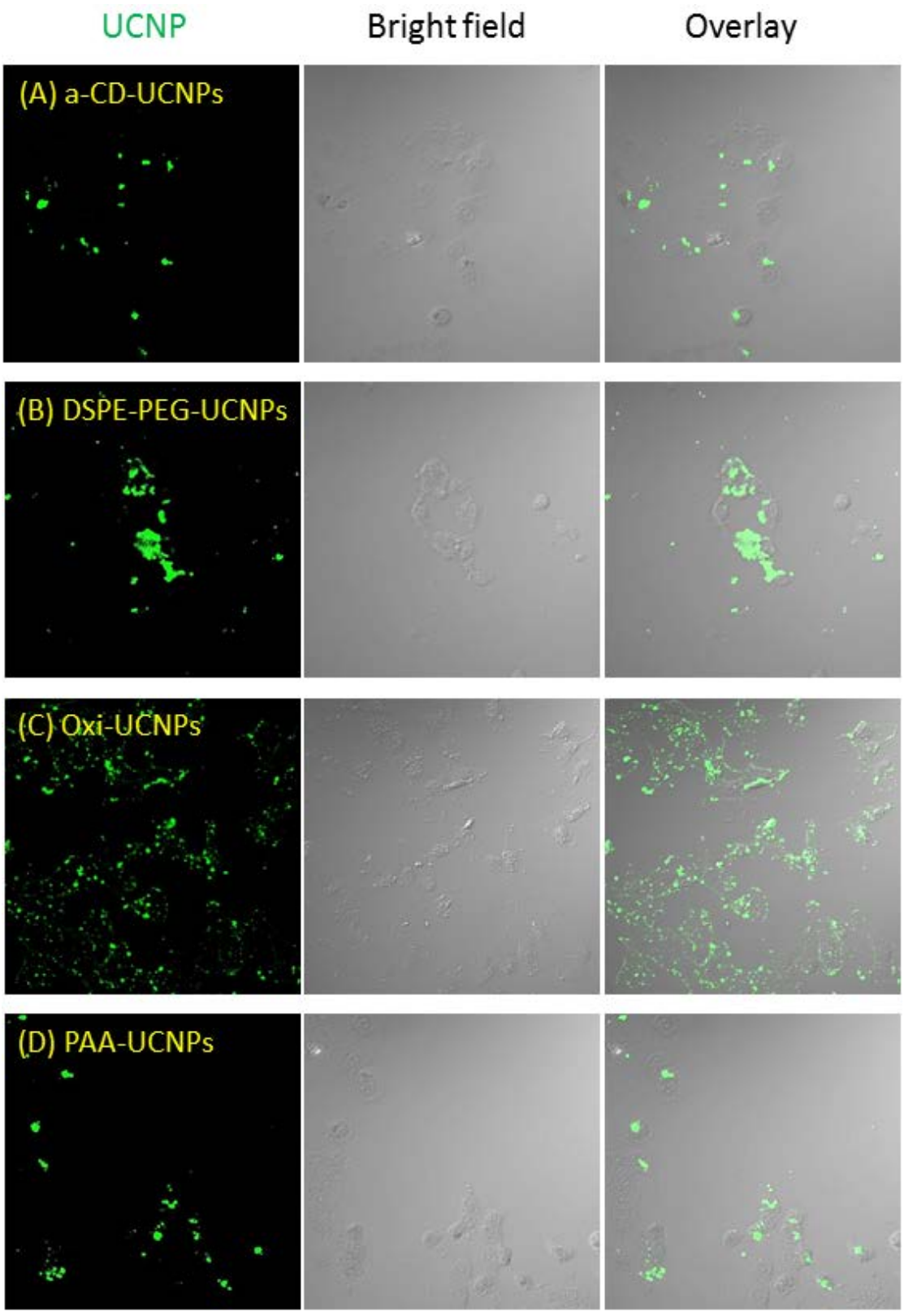
UCNP
Bright field
Overlay
(A) a-CD-UCNPs
(B) DSPE-PEG-UCNPs
(C) Oxi-UCNPs
(D) PAA-UCNPs

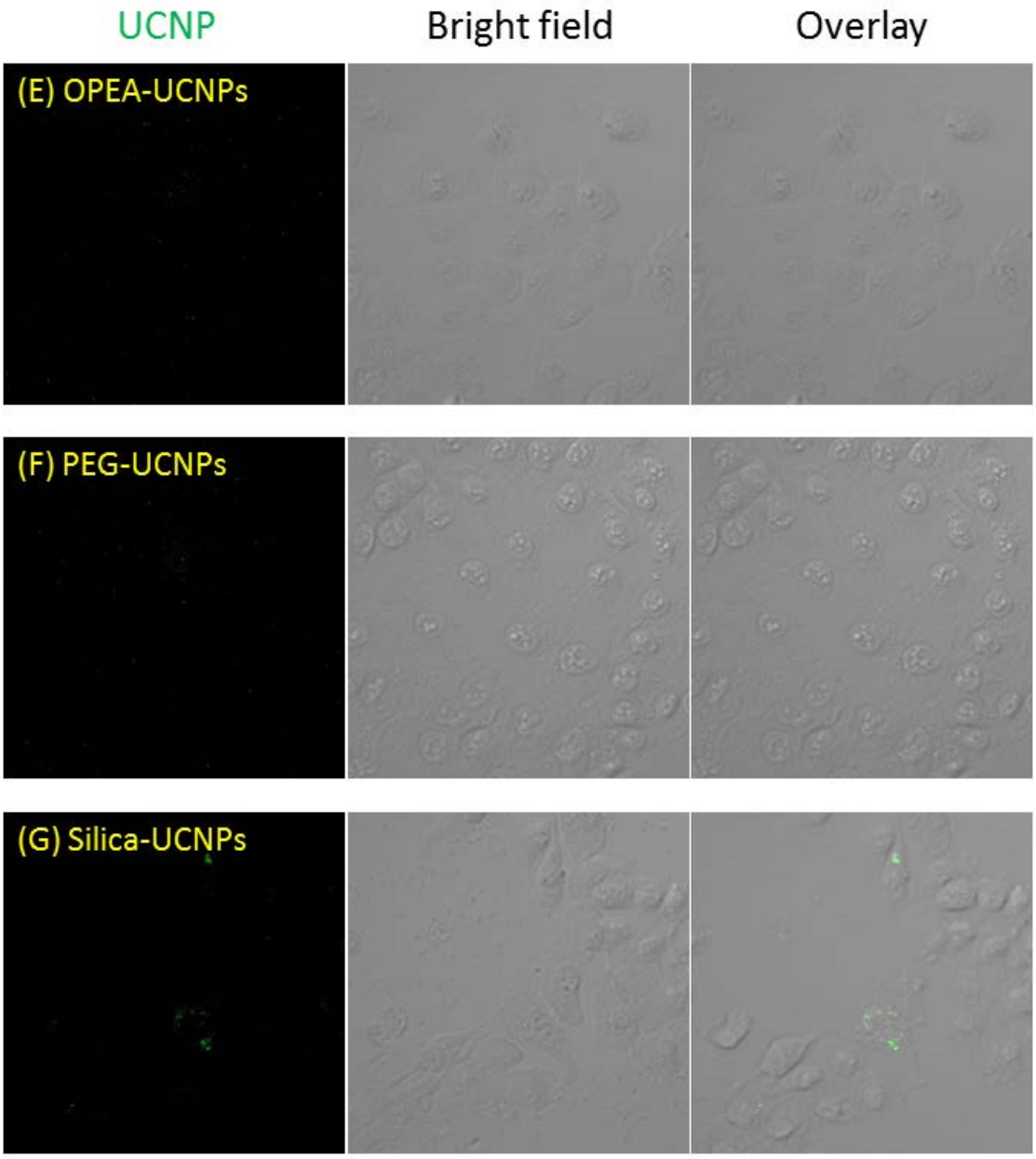

Figure 3.6 Images of incubation with DU145 cells to validate the UCNPs non-specific binding. DU145 cells incubated with (A) α-CD-UCNPs, (B) DSPE-PEG-UCNPs, (C) Oxi-UCNPs, (D) PAA-UCNPs, (E) OPEA-UCNPs, (F) PEG-UCNPs and (G) Silica-UCNPs at the concentration of 1 mg/mL for 1 h and the excess UCNPs was washed off with PBS five times. For $NaYF_4$: Yb^{3+}/Tm^{3+} UCNPs images, λex=980 nm, and emission was collected at 450 nm.

3.4 Conclusions

In this chapter, various approaches for the surface modification of UCNPs were trialed. As such, size and emission tunable UCNPs have been previously acquired by well-investigated approaches (Boyer, Vetrone et al. 2006; Liu, Tu et al. 2010; Xia, Chen et al. 2012; Xu, Zhao et al. 2013), but in this case UCNPs were prepared by thermal decomposition method and are hydrophobic materials. The OA-capped UCNPs were then transited from hydrophobic into hydrophilic particles in order to render them dispersible in the aqueous environment necessary for biological applications. Although numerous simple and versatile approaches to convert hydrophobic surface into hydrophilic surfaces have been reported in past years (Muhr, Wilhelm et al. 2014), aggregation and non-specific binding were seen to be a serious limitation to the application of UCNPs to biological use.

Different strategies were assessed in this work including: (1) ligand attraction--α-CD coating and DSPE-PEG-COOH coating; (2) chemical modification--ligand oxidation by Lemieux-von Rudloff reagent; (3) replacement of original surface ligand by another one—ligand exchange by PAA (single-step replacement) and by $NOBF_4$ and other ligands (two-step replacement); (4) addition of a shell on the surface—silica coating. Although all these strategies have been claimed to be successful in converting UCNPs from hydrophobic to hydrophilic particles, three methods were found to be suitable for the possible application to labeling of cells. These are the two-step ligand exchange which used $NOBF_4$ and OPEA/PO_4-PEG_{5000}-COOH and the silica coating strategy of UCNPs surface modification. These modifications were proven to have good water dispersibility and stability and most importantly, in the cell interaction assay, these UCNPs displayed a clean background in fluorescence signal detection by using NIR laser confocal microscopy, indicating no non-specific lab eling of the cells and showed promising for the further functionalization with specific targeting molecules in the

bioapplications. In addition to the highly stable and dispersible features of the $NOBF_4$ induced surface functionalization approaches, this method is a rapid and simple process for generating other UCNPs with functional groups since the second step of the protocol can be simply started with the stable $NOBF_4$ treated UCNPs dispersed in DMF using any proper ligand for replacement. These UCNP surface modification methods were then used in following chapters to focus on the development of versatile and reliable bioconjugation approaches to render the water dispersible UCNPs functional for use in cell labeling and bioimaging studies.

Chapter 4: Stable Upconversion Nanohybird Particles for Sensitive Prostate Cancer Cell Immunodetection

The previous study in Chapter 3 demonstrated a UCNP surface modification strategy by using $NOBF_4$ and PO_4-PEG_{5000}-COOH. Combined with the good water dispersibility and stability and no obvious non-specific binding of PO_4-PEG_{5000}-COOH modified UCNPs, this strategy holds great promise in developing further studies of bioconjugation. A bioconjugation strategy is reported here to prepare UCNP and streptavidin (SA) conjugates with excellent water stability and biocompatibility under physiological condition. Upconversion immune-nanohybrids (UINBs) was developed to achieve an *in vitro* cancer cells targeting via streptavidin-biotin interaction system between UCNPs and cancer specific antibodies. In this study, a PEG linker PO_4-PEG_{5000}-COOH was employed to modify SA, then the PEG-PO_4 functionalized SA was conjugated to UCNP via ligand exchange method. The UCNP-SA conjugates displayed great stability in aqueous environments for weeks and were successfully applied for the *in vitro* cancer cell targeting and luminesce imaging.

The experimental results and evaluations of this work have been written as a manuscript towards a submission to the *Scientific Reports*.

Stable Upconversion Nanohybird Particles for Sensitive Prostate Cancer Cell Immunodetection

Yu Shi[1], Bingyang Shi [2,3], Arun V. Everest Dass[1,3], Yiqing Lu[3], Robert D. Willows [1], Roger Chung[2], James Piper[3], Helena Nevalainen[1], Bradley Walsh [5], Dayong Jin [3,4], Nicolle H. Packer[1,3]

[1]*Department of Chemistry and Biomolecular Sciences, Macquarie University, Sydney, NSW 2109, Australia*

[2] *Faculty of Medicine & Health Sciences, Macquarie University, Sydney, NSW, 2109, Australia33*

[3]*ARC Centre of Excellence for Nanoscale BioPhotonics, Macquarie University, Sydney, NSW, 2109, Australia.*

[4]*Institute for Biomedical Materials and Devices, Faculty of Science, University of Technology Sydney, NSW, 2007, Australia.*

[5]*Minomic International Ltd, Macquarie Park, Sydney, NSW, 2109, Australia.*

E-mail: bingyang.shi@mq.edu.au

Abstract

Prostate cancer is one of the male killing diseases and early detection of prostate cancer is the key for better treatment and lower cost. However, the number of prostate cancer cells is low at the early stage and it is very challenging to detect. In this study, we successfully designed and developed upconversion immune-nanohybrids (UINBs) with sustainable stability in a physiological environment, stable optical properties and highly specific targeting capability for early-stage prostate cancer cell detection. The developed UINBs were characterized by transmission electron microscopy (TEM), X-ray diffraction (XRD), Fourier transform infrared spectroscopy (FT-IR), dynamic scattering light (DLS) and luminescence spectroscopy. The targeting function of the biotinylated antibody nanohybrid was confirmed by immunofluorescence assay and western blot analysis. The UINB system was able to specifically detect prostate cancer cells with stable and background-free luminescent signals for highly sensitive prostate cancer cell detection. This work demonstrates a versatile strategy to develop UCNP based sustainably stable UINBs for sensitive diseased cell detection.

Introduction

Precision medicine including sensitive early-stage cancer detection holds promising potential for lower healthcare cost and better treatment outcomes (Roychowdhury and Chinnaiyan 2013; Collins and Varmus 2015; Jameson and Longo 2015). The development of cutting-edge techniques in diseased cell immunolabeling (Jain 2007; Wang and Thanou 2010), super resolution imaging (Piliarik and Sandoghdar 2014) and bionanomedicine (Moghimi, Hunter et al. 2005; Peer, Karp et al. 2007) has laid a good foundation and provides powerful toolboxes for advanced theranostics and the realization of personalized medicine. Many commercially available bioreagents including organic dyes, chelates and fluorescent proteins have already been employed in cancer imaging and theranostics as conventional biolabels (He, Wang et al. 2010). Unfortunately, their

application in high sensitivity disease detection has been seriously hindered by some disadvantages, including undesirable photobleaching and photoblinking, chemical and metabolic degradation, and low signal to noise ratio (Alford, Simpson et al. 2009; Luo, Zhang et al. 2011). These shortcomings have been partly overcome by semiconductor quantum dots (QDs) (Chan and Nie 1998), as they can possess high quantum yields, bright photoluminescence, good photostability and narrow emission, leading to their broad applications in molecular labelling as well as in cellular and *in vivo* imaging (Burda, Chen et al. 2005; Kairdolf, Smith et al. 2013). However, there have been wide concerns on the inherent toxicity, chemical instability and uncontrolled life time of QDs (Hardman 2006). Furthermore, the excitation of traditional biolabels (organic dyes, fluorescent proteins, and QDs) usually requires the use of UV or short wavelength radiation for the down conversion photon transfer, which results in a series of drawbacks including low signal-to-noise ratio due to background auto fluorescence, low light-penetration depth inherent to the short wavelength of the UV excitation light, and potential cellular damage caused by long-term irradiation (Michalet, Pinaud et al. 2005; Xing and Rao 2008; Wegner and Hildebrandt 2015). Therefore, it is highly desirable to produce a new class of fluorescent sensors that can label target cells or tissue with higher signal to noise ratio, stronger light penetration capabilities, better photo stability and negligible tissue photo-damage.

Upconversion nanoparticles (UCNPs) are nanoscale crystals doped with rare earth ions. They absorb in a stepwise manner two (or more) low-energy photons in near infrared (NIR) light before emitting one high-energy photon with visible luminescence (Chien, Chou et al. 2013; Park, Lee et al. 2015). Over the past decade, several studies on UCNPs have made tremendous progress, particularly in the controlled synthesis to produce mono-dispersed UCNPs with tuneable nanostructure, sizes, shapes, luminescent emitting colours and life time (Chen, Guo et al. 2011; Liu, Bu et al. 2012; Xia, Chen et al. 2012). Other advantages have been recently discovered including embeddable capacity for

multi-functional hybrid nanomaterials (Lee, Lee et al. 2013; Zhou, He et al. 2014; Li and Lu 2015), negligible cytotoxicity for compatible biomedical devices (Shan, Budijono et al. 2011), robust photo-stability for super stable diagnostics and long-term tracking of molecules and nanocarriers (Yang, Velmurugan et al. 2013; Chen, Ma et al. 2014), high bright luminescent signals with low background for super sensitive detection (Lim, Riehn et al. 2009; Xu, Zhan et al. 2013) and deeper penetration capability for high resolution deep tissue imaging (Zhou, Liu et al. 2012; Xu, Zhan et al. 2013). However, UCNPs are often seriously aggregated in aqueous solutions owing primarily to the presence of hydrophobic capping ligands that are used for the synthetic control of nanostructure, size and shape uniformity (Lim, Riehn et al. 2009; Gnach and Bednarkiewicz 2012; Wu, Chen et al. 2015). To this end, various surface modification approaches have been investigated to transfer such passivated nanocrystals from organic solution into aqueous solutions and to make them amenable for various biomedical applications. These methods, such as, capping ligands removal (Kumar, Nyk et al. 2009), layer-by-layer assembly (Sukhorukov, Donath et al. 1998), optimized salinization chemistry (Rantanen, Järvenpää et al. 2009), silica coating (Li and Zhang 2006; Sivakumar, Diamente et al. 2006; Wong, Chan et al. 2010), polymer encapsulation (Johnson, Sangeetha et al. 2010; Jiang, Pichaandi et al. 2012) and ligand exchange (Boyer, Manseau et al. 2009; Dong, Ye et al. 2010; Chen, Ohulchanskyy et al. 2011; Chen, Wang et al. 2011) have been found to be promising.

To develop super sensitive disease detection for precision medicine, a variety of targeting molecules such as proteins and peptides need to be conjugated onto the surface of UCNPs for specific cell recognition (Santra, Zhang et al. 2001; Liu, He et al. 2013). The functionalization strategies generally involve several chemical modification steps including the introduction of hydrophilic groups and modification of functional ligands on the UCNP surface. These multiple steps ge nerally lead to low yield, poor stability, and low reproducibility (Gnach and Bednarkiewicz 2012; Wilhelm, Hirsch et al. 2013). Moreover, each surface modification will change the interface charge equilibration,

which may result in instability and/or further aggregation of UCNPs (Lü, Guo et al. 2008; Lü, Li et al. 2008). Most importantly, the improper modification of antibody or other functional proteins can decrease the targeting capability of the antibody (Vennerberg and Lin 2011; Xu, Zhan et al. 2013; Yang, Wang et al. 2014; Wu, Chen et al. 2015). The ideal surface modification methods should make the UNCPs stable in the physiological environment and attach the bioactive proteins with high coverage onto the optical nanocrystals without losing their targeting functions. Realizing these requirements is extremely important for high sensitivity disease detection, but is also very challenging.

In this study, we successfully designed and developed upconversion immune-nanohybrids (UINBs) with sustainable stability in a physiological environment, super stable optical properties and highly specific targeting capability for early-stage prostate cancer cell detection. As illustrated in **Scheme 1**, streptavidin was initially conjugated to phosphate-poly(ethylene glycol) (PEG, 5 kDa)-carboxyl (PO_4-PEG_{5000}-COOH) via EDC chemistry and then introduced onto the surface of UCNPs together with excess PO_4-PEG_{5000}-COOH resulting in a one-step ligand exchange strategy. Finally, a highly specific antibody (MIL-38) (Russell, Ow et al. 2004) recognising a prostate cancer antigen was functionalized via biotinylation and introduced onto the surface of the UNCPs through the biotin-streptavidin interaction to give UINBs. The developed UINBs were characterized by transmission electron microscopy (TEM), X-ray diffraction (XRD), Fourier transform infrared spectroscopy (FT-IR), dynamic scattering light (DLS) and luminescence spectroscopy. The targeting function of the biotinylated antibody nanohybrid was confirmed by immunofluorescence assay and western blot analysis. The UINB system was able to specifically detect prostate cancer cells with stable and background-free luminescent signals for highly sensitive prostate cancer cell detection. This work demonstrates a versatile strategy to develop UCNP based sustainably stable UINBs for sensitive diseased cell detection.

Experimental Section

Reagents and Materials

Unless otherwise stated, all reagents were purchased from commercial suppliers and used without further purification. Yttrium chloride hexahydrate ($YCl_3 \cdot 6H_2O$, 99.99%), ytterbium chloride hexahydrate ($YbCl_3 \cdot 6H_2O$, 99.98%), erbium chloride hexahydrate ($ErCl_3 \cdot 6H_2O$, 99.9%), sodium hydroxide (NaOH, 98%), ammonium fluoride (NH_4F, 99.99%), oleic acid (OA, 90%), 1-octadecene (ODE, 90%), cyclohexane (C_6H_{12}, 99.5%), ethanol (CH_3CH_2OH, ≥99.5%), methanol (CH_3OH, 99.5%), dichloromethane (CH_2Cl_2, 99.8%), toluene ($C_6H_5CH_3$, 99.8%), dimethylformamide (DMF, 99.8%), 1-ethyl-3-(3-dimethylaminopropyl) carbodiimide (EDC), *N*-hydroxysuccinimide (NHS), [3-(4,5-dimethylthazol-2-yl)-2,5-diphenyltetrazolium bromide] tetrazolium (MTT) and dimethyl sulfoxide (DMSO) were all purchased from Sigma–Aldrich and used as received without further purification. Pierce™ Streptavidin, EZ-Link® Sulfo-NHS-LC-LC-Biotin, streptavidin-fluorescein isothiocynate (FITC) conjugate, goat anti-mouse IgG (H+L) secondary antibody, FITC conjugate and 2-(4-amidinophenyl)-1H-indole-6-carboxamidine (DAPI) were purchase from Thermo Fisher Scientific. PEG linker PO_4-PEG_{5000}-COOH was synthesized and purchased from JenKem Technology USA Inc. Monoclonal antibody MIL-38 and prostate cancer cell lines DU145 and LNCaP were all provided by Minomic Int. Ltd.

Synthesis of OA-capped $NaYF_4$: Yb^{3+}/Er^{3+} Nanoparticles

Upconversion nanoparticles (OA-capped UCNPs) were synthesized using an organometallic method described previously (Zhao, Jin et al. 2013). Specifically the synthesis of $NaYF_4$: 20% Yb^{3+}/2% Er^{3+} is described here. Briefly, YCl_3 (0.78 mmol), $YbCl_3$ (0.18 mmol), and $ErCl_3$ (0.02 mmol) were magnetically mixed with 6 mL OA and 15 mL ODE in a 100 mL three-neck round-bottom flask. The resulting mixture was

heated at 160 °C under argon flow for 30 min to form a clear light yellow solution. After cooling down to 50 °C, 10 mL of methanol solution containing 0.16 g NH_4F (4 mmol) and 0.10 g NaOH (2.5 mmol) was slowly dropped into the flask with vigorous stirring for 30 min. Then, the slurry was slowly heated and kept at 110 °C for 30 min to remove methanol and residual water. Subsequently, the reaction mixture was quickly heated up to 310 °C for 45 min and protected by an argon atmosphere. The products were isolated by adding ethanol, and centrifuged without size-selective fractionation. The final $NaYF_4$: 20% Yb^{3+}/2% Er^{3+} nanocrystals were re-dispersed in cyclohexane with 5 mg/mL concentration after washing with cyclohexane/ethanol several times.

Streptavidin (SA) PEGlyation

For the PEGylation of SA, primary amines of SA were linked with PO_4-PEG_{5000}-COOH (5 kDa) using EDC/NHS chemistry. 5 mg PO_4-PEG_{5000}-COOH was dissolved in 500 µL MES buffer (0.1 M, pH 5.5) to form a 10 mg/mL solution. The solution was mixed well with 25 mg/mL EDC and 90 mg/mL NHS in MES solution and left to react for 15 min at room temperature. Ultrafiltration was performed by Vivaspin 20 (MWCO 3000) spin columns to remove excess EDC and NHS following buffer exchange into PBS (0.1 M, pH 8.0). The carboxyl activated solution was mixed with 1 mL of 2 mg/mL SA in PBS (SA: PEG molar ratio =1:50) to react at room temperature for 2 h. Then ultrafiltration was performed by Vivaspin 500 (MWCO 50000) spin columns to remove unreacted PO_4-PEG_{5000}-COOH.

Preparation of Streptavidin Conjugated Upconversion Nanoparticles (SA-UCNPs)

20 mg OA-capped UCNPs dispersed in 4 mL cyclohexane were mixed with a solution of $NOBF_4$ (20 mg in 4 mL Dichloromethane) and was stirred at room temperature overnight. Ligand free UCNPs were obtained by centrifugation and then washed with

toluene: hexane (v/v, 1/1). The prepared UCNPs were dispersed into 4 mL DMF (5 mg/mL) for long term storage. 400 µL of 5 mg/mL $NOBF_4$ treated UCNPs in DMF was taken and then added to 250 µL of 2 mg/mL PEGylated SA in 1 mL PBS buffer in a 1:20 molar ratio. After adding 350 µL of 3 mg/mL PO_4-PEG_{5000}-COOH, the solution was stirred at room temperature for 24 h. The SA conjugated UCNPs were washed with PBS buffer after the reaction.

Characterization of the UCNPs

Morphologies and sizes of UCNPs were recorded on a JEOL 2010F Transmission Electron Microscope (TEM) operating at 200 kV. The UCNPs were sufficiently diluted so that visualization of individual particles was possible, 20 µL of the UCNPs solution was placed on a 50 Å thick carbon-coated copper grid and the excess solution was immediately removed. X-ray diffraction (XRD) analysis was carried out on a Bruker D4 X-ray diffractometer using Cu Kα radiation (λ=0.15418 nm). The UCNPs were diluted at the same concentration at 5 mg/mL and their fluorescence emission spectra were recorded on a Fluorolog®-3 spectrophotometer equipped with a 980 nm VA-II diode pumped solid-state (DPSS) laser (current set at 1.50 A) and a 1200 g /mm grating. The spectra were measured over a range of wavelengths from 350 nm to 850 nm. The FT-IR spectra of UCNPs with different surface functional groups were examined using a Thermo NICOLET6700 Fourier transform infrared spectrometer (FT-IR) at room temperature. Dynamic Light Scattering (DLS) and zeta potential were measured to visualize size distribution and surface charge of the UCNPs by Dynamic Light Scattering Zetasizer NanoZS. 1 mL of OA-capped UCNPs dispersed in cyclohexane or surface functionalized UCNPs dispersed in carbonate buffer were used for the measurement.

MIL-38 Antibody Biotinylation

The biotinylation of antibody MIL-38 was performed using EZ-link Sulfo-NHS-LC-LC-biotin according to the manufacturer's specifications. MIL-38 was dissolved in PBS buffer (0.1 M, pH 8) to obtain a 2 mg/mL solution. A 10mM solution of the biotin reagent was prepared by dissolving 2.0 mg of the reagent in 300 μL of ultrapure water. 20 fold molar excess of biotin reagent was used to conjugate to the antibody by incubating at room temperature for 1 h. The excess unreacted biotin was removed by a Vivaspin 500 (MWCO 50000) ultrafiltration spin column.

Cell Culture and Immunofluorescence Assay

Prostate cancer cells (DU145, ATCC) were incubated in RPMI 1640 medium supplemented with 10 (w/v) % fetal bovine serum (FBS), streptomycine at 100 μg/mL, and penicillin at 100 U/mL. The cells were incubated at 37 ^{o}C in a humidified incubator in the presence of 5% CO_2.

Cells were seeded in a Lab-Tek® chamber slide at a density of 4×10^4 cells per well. After cell attachment for 24 h, cells were washed with pre-warmed PBS, and fixed by 5 (w/v) % paraformaldehyde (PFA). For the FITC related IFA labelling, cells were firstly blocked by 2 (w/v) % BSA solution for 30 min, then MIL-38 antibody or biotinylated MIL-38 antibody dispersed in 2 (w/v) % BSA blocking solution was incubated with cells for 1 h. After removed excess antibody solution and washed with PBS three times, FITC conjugated SA (SA-FITC) or FITC conjugated secondary antibody (2^{nd}-FITC) was added and incubated with cells for 1 h. For the upconversion immune-nanohybrids (UINBs, MIL-38-SA-PEG-UCNPs) labelling, UINBs at 100 μg/mL in PBS buffer were incubated with fixed cells for 1 h at room temperature. After incubation the cells were then washed with PBS for three times to remove excess UINBs, SA-FITC or 2^{nd}-FITC

and then stained with DAPI before imaging by Olympus FV1200 confocal microscope.

Western Blot Assay

The DU145 and LNCaP prostate cancer cells cultured in RPMI 1640 cell culture medium over-night were collected and lysed on ice in 500 μL cell lysis buffer (1X PBS buffer, 1 (v/v) % NP40 cell lysis buffer, 0.1 (w/v) % sodium dodecyl sulphate (SDS), 5 mM ethylenediaminetetraacetic acid (EDTA), 0.5 (w/v) % sodium deoxycholate and 1 mM sodium orthovanadate) with 10 μL protease inhibitors.

Equal amounts of cell lysate (20 μL) were loaded and the proteins separated electrophoretically on 4-15 (w/v) % Bis-Tris polyacrylamide gels at 200 V for 50 min, then the proteins were transferred onto nitrocellulose membranes (NC) and blocked with 5 (w/v) % skim milk for 1 h. The membrane was incubated with monoclonal antibody MIL-38 (1:5000 dilution) and SA-FITC/2nd-FITC (1:10000 dilution) to detect the target protein antigen. The immunoreactive bands were visualized on an Odyssey® CLx infrared imaging system according to manufacturer's instructions.

MTT Assay

UCNP cytotoxicity was examined by [3-(4,5-dimethylthazol-2-yl)-2,5-diphenyltetrazolium bromide] tetrazolium (MTT) assay on DU145 prostate cancer cells. DU145 cells were seeded in 96-well plate at a density of 4×10^4 cells per well. The cells were incubated at 37 ^oC in a humidified incubator in the presence of 5% CO_2 until reach the cell confluence at 80%. DMEM cell culture medium was replaced by fresh DMEM containing SA conjugated UCNPs in different concentrations (0, 1, 2, 10, 25, 50, 100 and 200 μg/mL). After incubation at 37

^{o}C in 5% CO_2 for 24 h and 48 h, DMEM was removed and washed by PBS three times. 100 μL of 500 μg/mL MTT solution was added to each well and incubated for 4 h. After removed the excess MTT solution, 100 μL dimethyl sulfoxide (DMSO) was added to cells to dissolve the formed formazan. The optical density of each well was measured at a wavelength of 590 nm by a microplate reader. The cell viability was calculated with following formula:

$$\text{Viability (\%)} = \frac{\text{mean of absorbance value of treatment group}}{\text{mean of absorbance value of control group}} \times 100\%$$

Results and Discussion

Fabrication and Characterization of UINBs

UINBs were fabricated using $NaYF_4$: 20% Yb^{3+}/2% Er^{3+} UCNPs (Zhao, Jin et al. 2013), further functionalized with prepared PEG-Streptavidin (PEG-SA) conjugates and PEG-COOH via a one-step ligand exchange strategy (**Scheme 1A**). The synthesized UCNPs were originally dispersed in the organic solvent (chloroform) and kept stable with the capping agent of hydrophobic oleic acids (OA) (Wang, Han et al. 2010). The uniform morphology (27 ± 8.2 nm) was confirmed with TEM and DLS (**Figure 1A**, **1D** and **1F**). Furthermore, the crystal structures and the phase purity of the OA-capped UCNPs were examined by XRD. Typical XRD patterns of the OA-capped UCNPs are presented in **Figure 1E**. The diffraction peaks of the UCNPs are well defined, and the peak positions and intensities match well with the calculated values for hexagonal $NaYF_4$ (β-$NaYF_4$) (JCPDS No.028-1192), which indicates that the prepared UCNPs are of highly crystalline pure hexagonal phase. To transfer the hydrophobic OA-capped UCNPs into a hydrophilic intermediate for further biomedical applications, $NOBF_4$ was used as an agent to replace the original OA capping and form an intermediate of $NOBF_4$-UCNPs for further ligand exchange functionalization (**Figure 1B**).

Streptavidin (SA) was modified with a PEG linker (PO_4-PEG_{5000}-COOH, ~5 kDa) via EDC chemistry with the formation of amide bonds between carboxylic groups of PEG linker and primary amine groups of SA. The PEG linker modification was used here to reduce the steric hindrance at the surface of the UCNP and increase the stability of the potential biotin-streptavidin interaction. A reaction ratio of 50 (molar ratio: PEG linker to SA) was chosen to keep the balance between product yield and SA biological activity because the less modification, the higher original bioactivity (Cazalis, Haller et al. 2004; Kumar, Aaron et al. 2008). The SA-PEG reaction mixture was analyzed by SDS-PAGE electrophoresis as shown in **Figure S1A**; high molecular weight protein bands were observed at approximately 28 kDa, 38 kDa, 58 kDa and 63 kDa in the PEGylated sample compared with the SA alone (13 kDa, in monomer phase) control, which confirmed the successful SA PEGylation and based on mass, indicated that 3, 5, 9 and 10 PEG linkers have been conjugated on one single SA monomer, respectively. The result from ImageJ analysis of the gel band intensities estimated that there is 57.6% SA modification with PEG and the main product is triply PEGylated SA monomer (50.3%) (**Figure S1B**). Accordingly, 12 PEG chains were estimated to be conjugated on one SA tetramer. The PEG-SA mixtures were further purified by size exclusion chromatography to obtain the highest pure PEG-SA of the main products (112 kDa, with 12 PEG chains per SA), followed by one-step ligand exchange of UCNPs with the purified 12 PEG-SA conjugation in excess unmodified phosphate PEG (5 kDa). This approach replaces the BF_4^- counter-ions on UCNPs with PO_3^{4-} groups on either PEGylated SA or PEG to form water soluble SA-PEG-UCNPs (**Figure 1C**). The excess PO_4-PEG_{5000}-COOH was applied here to coat any remaining bare UCNP surface. This process is used to reduce non-specific interaction and enhance the stability and biocompatibility of the synthesized SA-PEG-UCNPs in the biological solutions by its hydrophilic nature (Kumar, Aaron et al. 2008; Benyettou, Hardouin et al. 2012).

The dynamic size change of the SA-PEG surface-modified UCNPs were measured by

DLS. As shown in **Figure 1F**, the hydrodynamic average diameters of UINBs were significantly increased from 36.7 nm (OA-capped UCNPs) to 161.8 nm (SA-PEG-UCNPs) after surface modification, which is mainly attributed to the diameter of SA and the long PEG chains. On the other hand, the zeta potential was decreased from 23.3 mV to -36.1 mV after conjugation due to the introduction of negative charged PEG molecules and SA protein (**Figure S2**). The SA-PEG-UCNP conjugates can also be verified by checking the typical OD280 absorbance peak from a Nanodrop spectrophotometer (**Figure 1G)**. SA shows a strong ultraviolet (UV) absorption peak at 280 nm while UCNP sample does not have such a typical absorbance. The absorbance curve of UCNP was only used as a control in this experiment. UCNP has relative strong absorption from 220 nm to 330 nm with a decreasing trend. This phenomenon affects the observation of the curve in SA-PEG-UCNP which only has a slight characteristic absorbance peak at 280 nm. This difference between the curve of UCNP only and SA-PEG-UCNP represents the success of bioconjugation. After conjugation, the absorption profile of SA-PEG-UCNPs displays an increasing absorbance at 280 nm. In addition, the functional groups on the surfaces of the bare and SA-PEG-UCNPs before and after bioconjugation were characterized and confirmed by FT-IR spectra (see details in Supporting Information, **Figure S3**). The significant changes in surface properties (size, zeta potential and FT-IR spectra) indicate the success of surface functionalization with SA.

To investigate the effect of the surface modification of UCNPs on the upconversion luminescence (UCL) properties, we measured the photoluminescence spectra of these UCNPs at the same concentration before and after surface modification, by exciting the dispersions in PBS buffer with a 980 nm diode laser. As shown in **Figure 2,** the SA-PEG-UCNPs have good dispersibility in water after functionalization with PEG-SA, and the resulting SA-PEG-UCNPs retained the characteristic upconversion optical properties of the $NOBF_4$ particles with 1.5 fold increased fluorescent intensity, compared

to that of the prepared OA-capped UCNPs in cyclohexane. The two strong green emissions at 520 and 540 nm can be assigned to the $^{2}H_{11/2} \rightarrow {}^{4}I_{15/2}$ and $^{4}S_{3/2} \rightarrow {}^{4}I_{15/2}$ transitions, respectively, whereas the weak red emission at 654.5 nm can be assigned to the $^{4}F_{9/2} \rightarrow {}^{4}I_{15/2}$ transition. The upper panel of **Figure 2** shows the UC fluorescence of the colloidal solution excited with a 980 nm laser appears green in colour and the variation in fluorescence intensity confirmed the result in UCL emission spectra comparison.

Sustainable Stability of UINBs

To investigate the stability of SA-PEG-UCNPs under physiological conditions, the SA-PEG-UCNPs were dissolved at a concentration of 1 mg/mL PBS and Dulbecco's modified Eagle's medium (DMEM with serum) using water as control. The results from the DLS analysis demonstrate that SA-PEG-UCNPs form good colloidal dispersions, with the particle size in water and PBS similar from 1 h to 24 h later, while in DMEM the size increased slightly (from 150 nm to 165 nm) after 24 h' incubation (**Figure 3A**). The sustainable stability of SA-PEG-UCNPs in various physiological buffers was also confirmed by DLS measurement and by exciting the colloidal dispersions with a 980 nm diode laser. As shown in the left panel of **Figure S4A**, strong the UCL emitted from nanoparticles in different solutions (water, PBS and DMEM) was observed with naked eyes from the top layer (left photograph) and bottom layer (right photograph) of the solution when excited with a NIR laser at the top and bottom part of vials, respectively. After 24 h dispersion of UCNPs, green colored fluorescence still can be seen from top layer of solution suggest a good water stability of SA-PEG-UCNPs under physiological conditions as aggregated nanoparticles settle to the bottom rapidly. DLS analysis of SA-PEG-UCNPs in different solutions shows that there is no obvious change of the particle sizes within 24 h (**Figure S4A**). In addition, the size of SA-PEG-UCNPs were tested in PBS at various pH values (4 to 9); no significant change was observed within 1 h,

suggesting stable colloidal dispersions of SA-PEG-UCNPs independent of pH (**Figure 3B**, **S4B**). Even highly concentrated colloidal dispersions of SA-PEG-UCNPs (~5 mg/mL) are stable for several months (data not shown) without sedimentation or precipitation as examined by DLS analysis. Such a sustainable stability of SA-PEG-UCNPs was thus achieved via a one-step ligand exchange, benefiting from the robust attachment of phosphate groups to UCNPs surfaces and the long hydrophilic PEG linker chain. The stability of these SA-PEG-UCNPs allows their application in biological systems. To test their cytotoxicity, the effect of the developed SA-PEG-UCNPs on cell viability was examined by the MTT assay. The results showed that the cell viability was above 90% over 48 h exposure to up to 200 μg/mL of the conjugated UCNPs (**Figure S5**), demonstrating good biocompatibility.

Validating the Antibody-Biotin-SA Conjugation and Specificity

Another key factor for highly sensitive disease detection is the use of highly specific antibody that targets a unique biomarker of diseased cells. MIL-38 (a IgG_1 murine monoclonal antibody) is a prostate cancer antibody (Carter, Sterling-Levis et al. 2004; Khatri, T. Ho et al. 2010) detecting a cell surface glycoprotein and was supplied by our industry partner (Minomic International Ltd). The specific targeting capability of MIL-38 antibody was tested via a standard FITC conjugated immunofluorescence assay on a range of cell lines including one positive cell line (DU145, prostate cancer cell) and four negative cell lines (prostate cancer cell: LNCaP, and breast cancer cells: MCF-7, MDA-MB-231 and SK-BR-3). As shown in **Figure S6**, FITC labelled MIL-38 antibody only targeted DU145 cells with high specificity, with no signal detected on the non-cancer or other cancer cells, indicating the excellent targeting capability of MIL-38 antibody to prostate cancer cells (DU145).

MIL-38 antibody was then biotinylated using EZ-link Sulfo-NHS-LC-biotin through the well-known reaction between primary amine groups on the antibody molecule and NHS activated biotin. The success of the biotinylation of MIL-38 was validated with FITC conjugated SA (SA-FITC) by immunofluorescence assay (IFA) and western blot (WB) analysis using LNCaP cells as negative control. In the IFA assay, DU145 cells (positive) and LNCaP cells (negative) were incubated with biotinylated MIL-38 (MIL-38-biotin) as a primary antibody. Subsequently SA-FITC and FITC conjugated goat anti-mouse secondary antibody (2^{nd}-FITC) were applied to detect MIL-38-biotin on the cell surface. As shown in **Figure 4A(a & b)**, using confocal microscopy, both SA-FITC and 2^{nd}-FITC labelled DU145 cells through specific SA-biotin interaction and MIL-38 antibody-goat anti-mouse secondary antibody recognition, labelled DU145 cells respectively compared to the non-biotinylated MIL-38 control (**Figure 4Ac)**. No signal was detected on the LNCaP cells with MIL-38 labeling under any conditions, suggesting the highly specific targeting capability of MIL-38 was maintained after biotinylation. **Figure 4A(d, e & f)** were confirming that SA does not non-specifically bind to the cells. WB was also performed to further verify the specific targeting capability of MIL-38-biotin. In WB assay, cell lysates proteins of DU145 and LNCaP cells were gel-separated, and SA-FITC and 2^{nd}-FITC were tested with the different MIL-38 conjugates, using common β-actin (one common protein in both cells) as loading control. As shown in **Figure 4B**, the bands at Lane 1 and 4 show the MIL-38 biotinylated antibody binding of a DU145 protein can be detected by both 2^{nd}-FITC and SA-FITC. In addition, the MIL-38 antibody recognition of the DU145 antigen can be targeted by 2^{nd}-FITC alone (band in Lane 5). In addition, none of the immunoblotting assays showed detection in the LNCaP control, indicating there is no MIL-38 antigen in the LNCaP cell lysates and confirms the highly specific targeting capability of MIL-38-biotin and the specific interaction between biotin and SA. These results thus indicate the successful MIL-38 biotinylation and labelling specifically of prostate cancer cells with the traditional FITC fluorophore labelling.

Immunolabeling and Imaging of Prostate Cancer Cells with UCNPs

To facilitate the detection of prostate cancer cells with UINBs, MIL-38-biotinylated antibody was linked to streptavidin coated UCNPs (SA-PEG-UCNPs) as shown in **Scheme 1B**. The resulting MIL38-biotin-SA-PEG-UCNPs were incubated with prostate cancer cells (DU145) in physiological conditions (0.01 M, pH 8.0 PBS buffer in room temperature), with LNCaP cells as negative control. The highly specific immunoreaction between the MIL38-biotin-SA-PEG-UCNPs and cell surface protein expressed on DU145 prostate cancer cell membranes was seen. The cells were washed thrice after incubation with MIL38-SA-PEG-UCNPs and images were captured using a confocal microscope equipped with a 980 nm NIR laser. It can be clearly seen in **Figure 5A** that the DU145 cells exhibited bright green UC fluorescence on their membranes. The shape and position of the cells in bright field and dark field overlapped very well, showing good luminescent signal for detection and imaging. No UC fluorescence was detected on LNCaP cells under the same conditions (**Figure 5D**), confirming the specific labelling of the antibody-UCNP conjugates to the cancer specific surface antigens on prostate cancer cells.

As controls for the specificity of the developed UNIBs, MIL38 antibody-biotin + PEG-UCNPs mixtures and MIL38 antibody + SA-PEG-UCNPs mixtures were incubated with BSA-blocked DU145 cells (positive) and LNCap cells (negative) under the same conditions and detected with a 980 nm NIR laser equipped confocal microscope. Binding of MIL-38 antibody was not seen without SA (**Figure 5B**) or biotin (**Figure 5C**) on DU145 cells or on LNCaP cells (**Figure S7C & D**). It is well-known that the autofluorescence (noise) from cells is very low in the UCNPs based systems due to the unique UC mechanism of the NIR light excited UCNPs, which results in a higher signal-to-noise ratio for bioimaging (Gnach and Bednarkiewicz 2012; DaCosta, Doughan et al. 2014; Wu, Chen et al. 2015).

Optical Stability for Precision Cancer Detection

Another advantage of UCNPs is their photostability compared to conventional fluorophores, which is also a preferred requirement for disease diagnostic detection. To investigate the optical stability of the developed MIL38-biotin-SA-PEG-UCNPs (UNIBs), we compared the UINB-labelled with MIL38-biotin-SA-FITC labelled prostate cancer cells. Both UCNPs and FITC based antibody labelled cell samples were excited under a continuous laser scanning mode at 980 nm (for UCNPs) and 473 nm (for FITC), respectively. As shown in **Figure 6A**, the fluorescent signal from FITC labelled cells is very strong at the beginning, but dropped significantly one minute later and disappeared completely after three minutes under the continual excitation of the 473 nm laser. The UCNPs labelled cells showed stable fluorescent intensity maintained at the same level throughout the 60 minutes of strong NIR excitation (**Figure 6B**). This data suggests that our UINBs have superior, stable optical properties, which is a promising and key feature for improved cellular disease detection and bioimaging.

Conclusions

The demonstrated potential of high-specificity prostate cancer cell diagnostic detection shown in this study benefits from the unique background-free and photostable UCNP properties together with PEG driven colloidal stability and SA-biotin driven antibody conjugation.

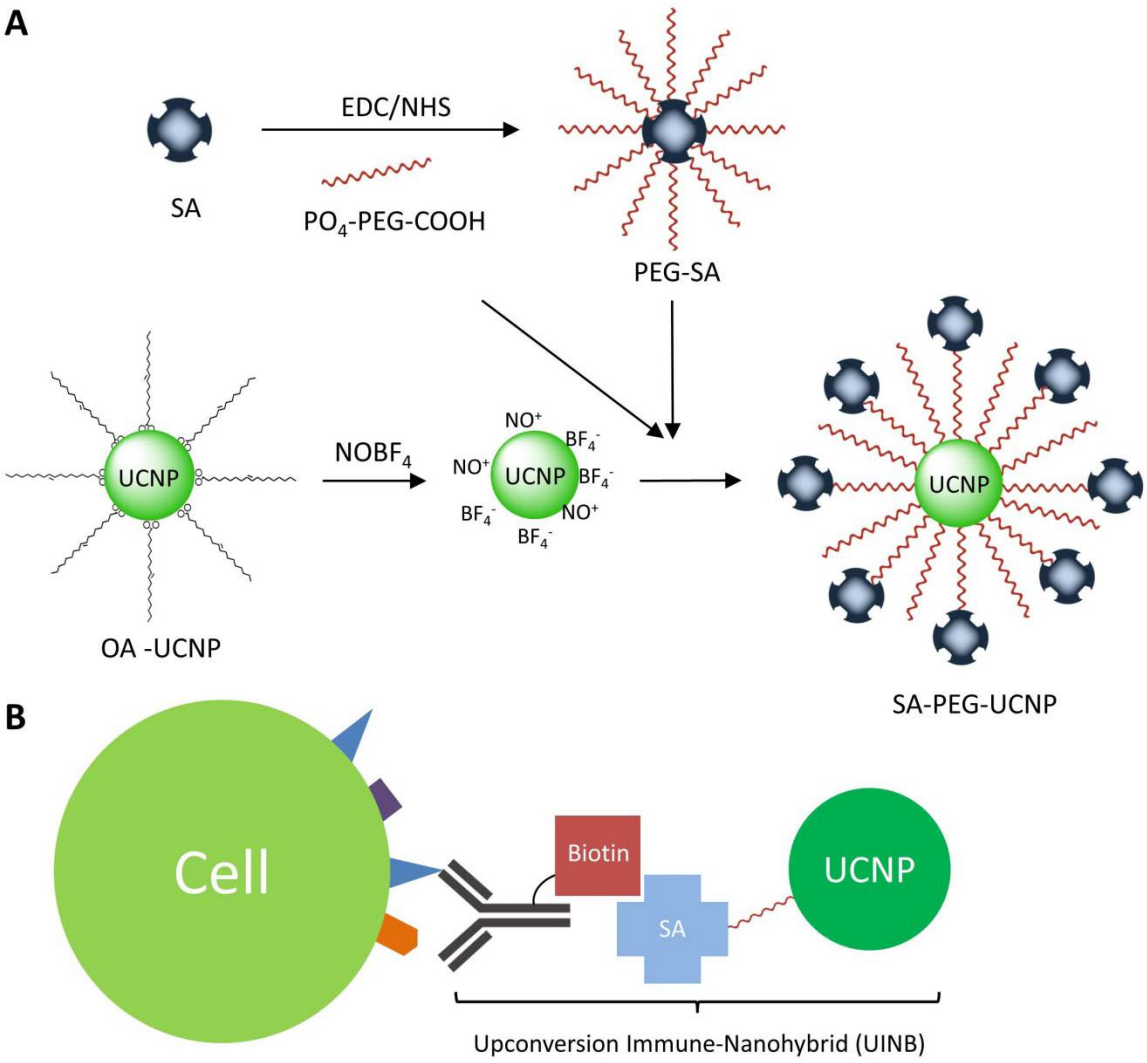

Scheme 1. The schematic illustration of (A) UCNPs and PEGylated SA (PEG-SA) bioconjugation via one-step ligand exchange process. (B) upconversion immune-nanohybrids (UINBs) driven precision cancer cell detection.

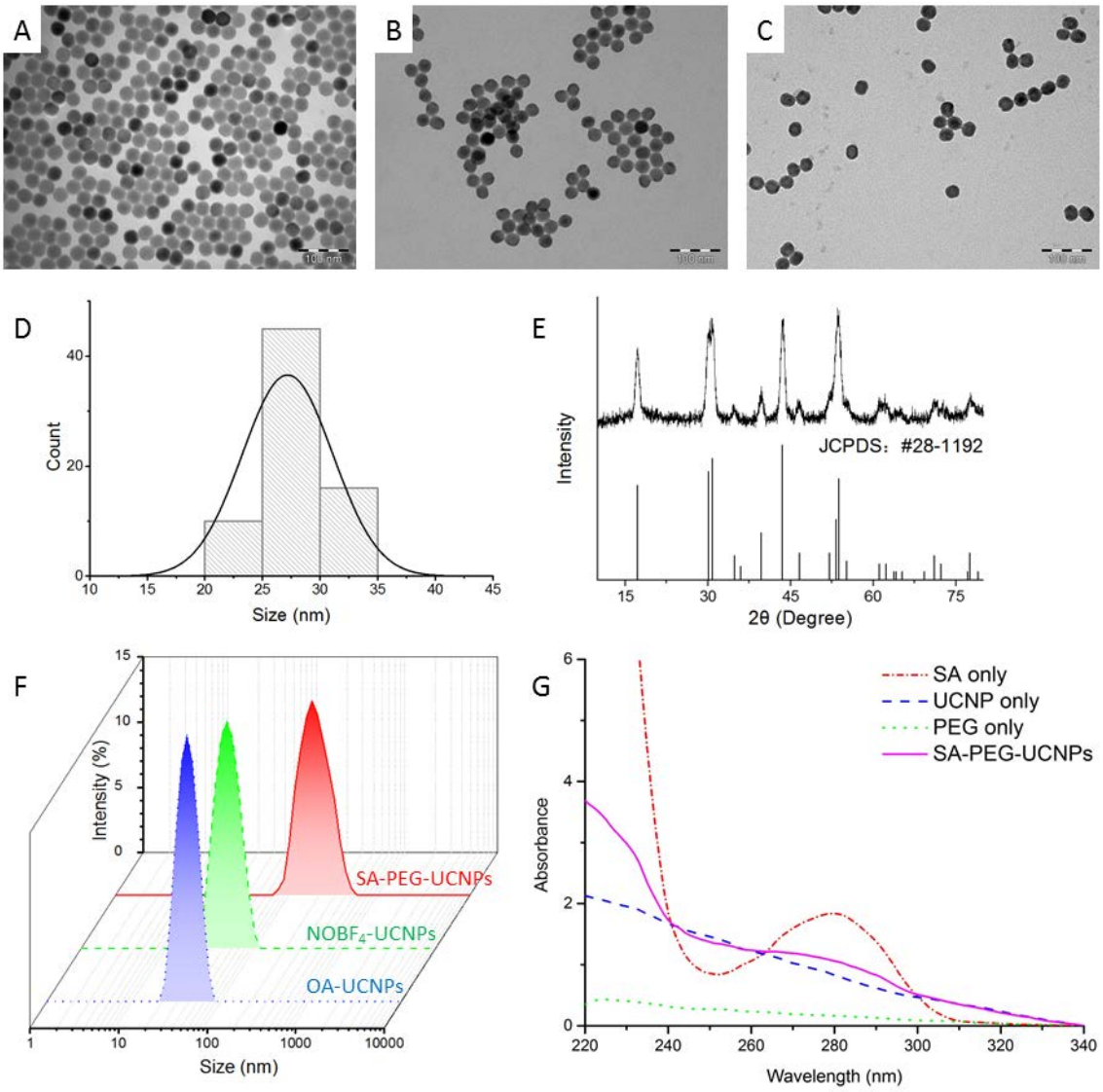

Figure 1. The characterizations of functionalized UCNPs: (A) the TEM image of naked OA-UCNPs; (B) the TEM image of $NOBF_4$-UCNPs; (C) the TEM image of SA-PEG-UCNPs; (D) the size histogram of OA-UCNPs; (E) the XRD spectra of naked UCNPs; (F) the comparison of size distribution of OA-UCNPs, $NOBF_4$-UCNPs and SA-PEG-UCNPs; (G) the comparison of absorbance of OA-UCNPs, $NOBF_4$-UCNPs and SA-PEG-UCNPs.

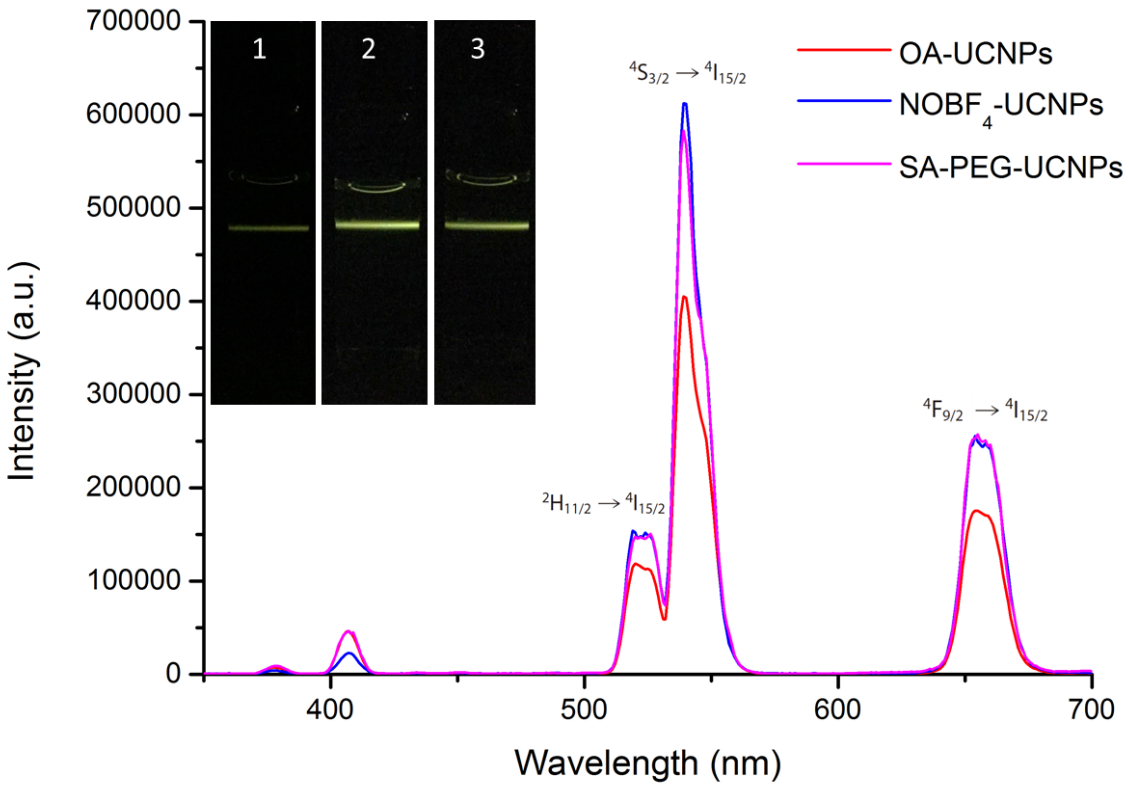

Figure 2. Comparison of upconversion fluorescence emission spectra between (red trace) OA-UCNPs dispersed in cyclohexane, (blue trace) $NOBF_4$-UCNPs dispersed in DMF and (purple trace) SA-PEG-UCNPs dispersed in PBS buffer under 980 nm excitation. The upper panel photographs and lower spectra display the luminescence excited with a 980 nm laser of (1) OA-UCNPs, (2) $NOBF_4$-UCNPs and (3) SA-PEG-UCNPs. All spectra and photographs were obtained at the same concentration of UCNPs (10 mg/mL).

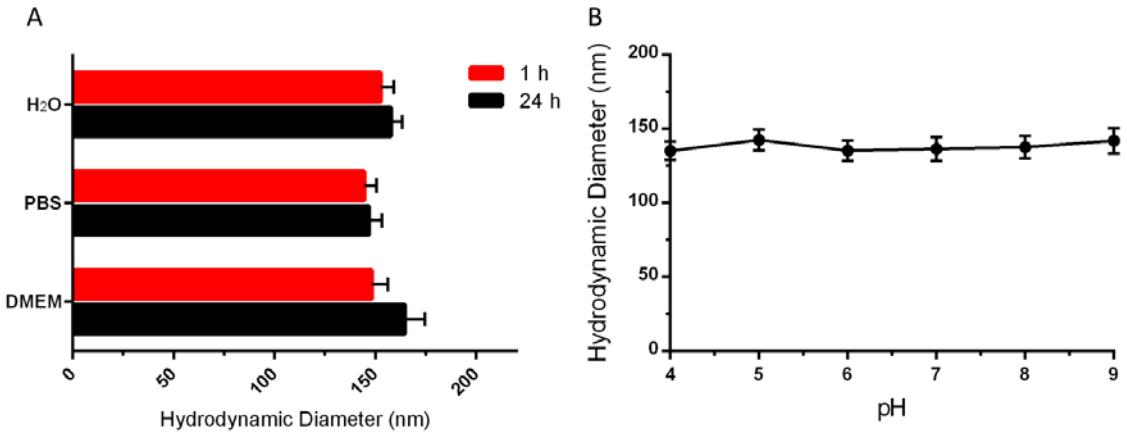

Figure 3. (A) The dynamic light scattering (DLS) of SA conjugated UCNPs dispersed in H_2O, 0.01 M PBS buffer and DMEM cell culture medium with 10% FBS at 1 h and 24 h after preparation. (B) DLS of SA conjugated UCNPs dispersed in PBS buffer at different pH from 4.0 to 9.0 in 1 h.

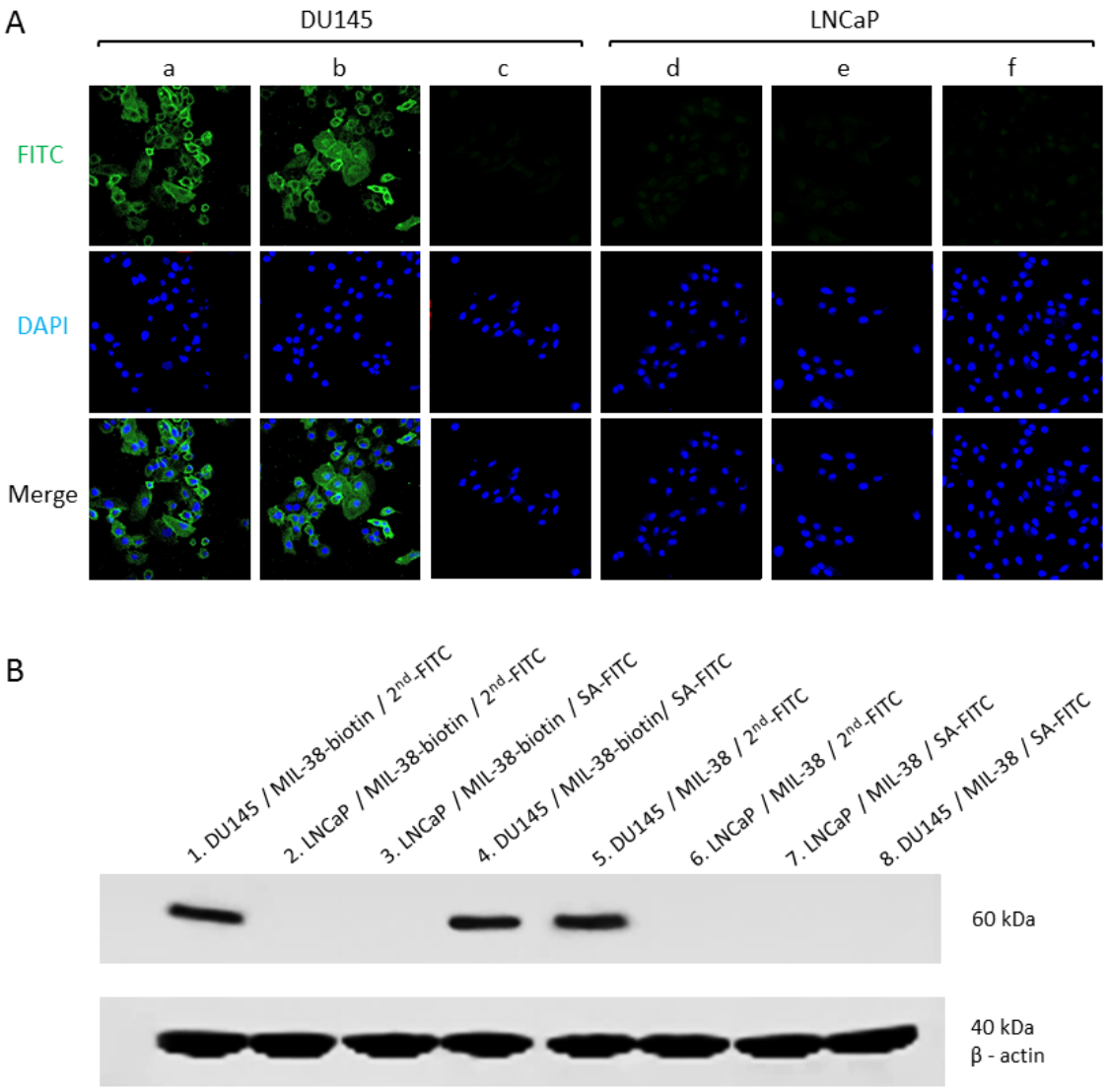

Figure 4. (A) Confocal luminescence imaging of (a) MIL-38-biotin incubated with SA conjugated FITC (SA-FITC), (b) MIL-38-biotin incubated with goat anti-mouse secondary antibody-FITC (2^{nd}-FITC) and (c) MIL-38 incubated with SA-FITC on DU145 prostate cancer cells. (d) MIL-38-biotin incubated with SA-FITC, (e) MIL-38-biotin incubated with 2^{nd}-FITC and (f) MIL-38 incubated with SA-FITC on LNCaP prostate cancer cells. Green and blue colors represent green and blue fluorescence from FITC and DAPI, respectively. (B) Western blot analysis of biotinylated antibody MIL-38-biotin incubated with 2^{nd}-FITC and SA-FITC on the proteins isolated after DU145 and LNCaP cell lysis (1-4); and antibody MIL-38

incubated with 2nd-FITC and SA-FITC after DU145 and LNCaP cell lysis (5-8). Lower panel shows the western blot analysis with β-actin as loading control.

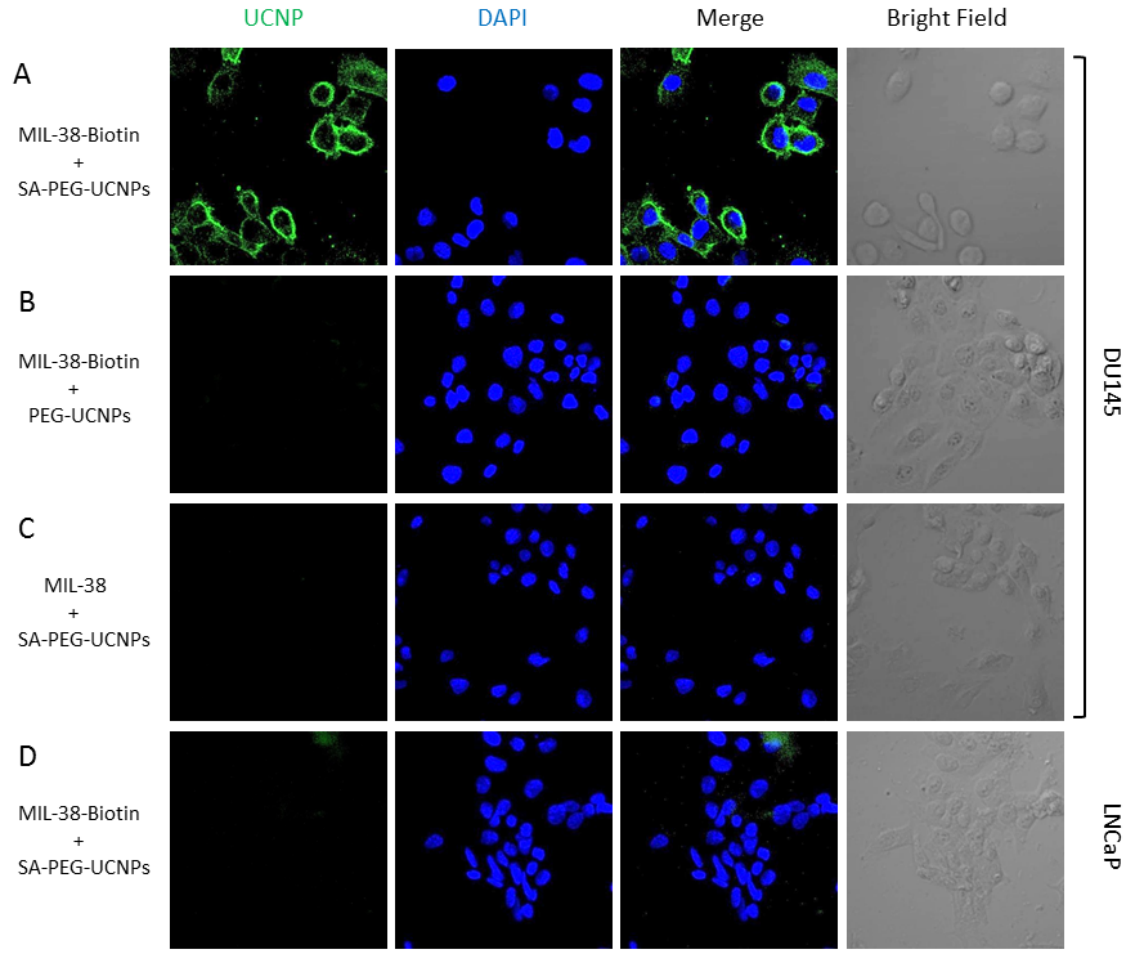

Figure 5. Confocal upconversion fluorescence imaging of (A) SA-PEG-UCNPs + biotinylated MIL-38 (MIL-38-Biotin) labelled DU145 prostate cancer cells; (B) PEG-UCNPs + MIL-38-Biotin labelled DU145 prostate cancer cells; (C) SA-PEG-UCNPs + MIL-38 labelled DU145 prostate cancer cells; (D) SA-PEG-UCNPs + MIL-38-Biotin labeled LNCaP prostate cancer cells. Green and blue colors represent upconversion fluorescence signals and blue fluorescence from UCNPs and DAPI, respectively.

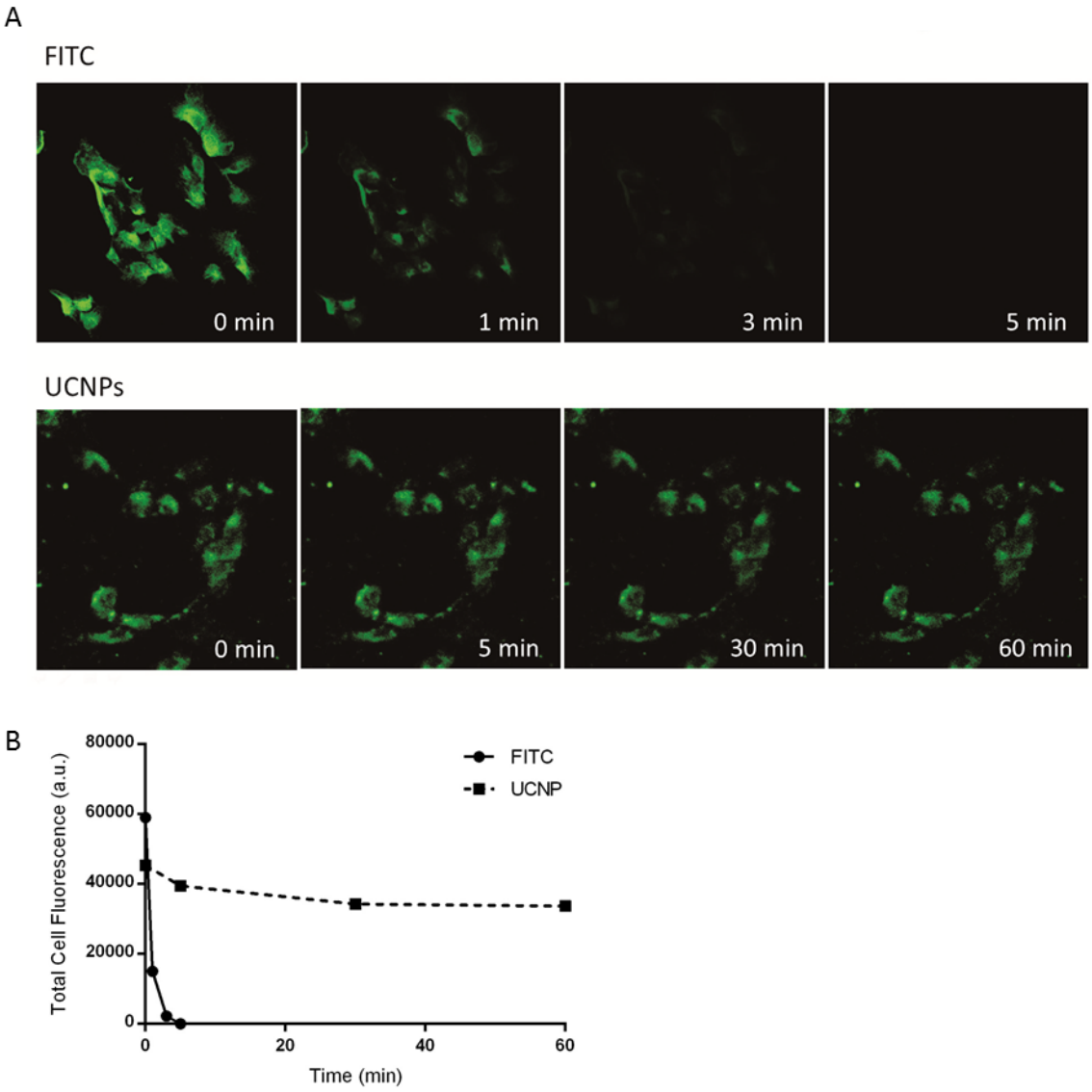

Figure 6. The comparison of photobleaching of fluorescence between FITC and UCNPs conjugated SA in a cell immunofluorescent assay under the excitation of 473 nm (for FITC) and 980 nm (for UCNPs), respectively, with continuous laser scanning mode. (A) The upper panel is the fluorescence serial imaging of FITC-SA in DU145 cells over 60 min. Green colors represent green fluorescence from FITC. The bottom panel is the fluorescence serial imaging of UINBs on DU145 cells over 60 min. Green colors represent UCL signals from UCNPs. (B) Comparison of cell fluorescence intensity determined by ImageJ software between FITC labeling and UCNP labeling over different scanning times.

Supporting Information

Sustainably Stable Upconversion Immune-nanohybirds for High-performance Cancer Detection

Yu Shi[1], Bingyang Shi [2,3], Arun V. Everest-Dass[1,3], Yiqing Lu[3], Robert D. Willows [1], Roger Chung[2] James Piper[3], Helena Nevalainen[1], Bradley Walsh [5], Dayong Jin [3,4], Nicolle H. Packer[1]

[1]*Department of Chemistry and Biomolecular Sciences, Macquarie University, Sydney, NSW 2109, Australia*

[2] *Faculty of Medicine & Health Sciences, Macquarie University, Sydney, NSW, 2109, Australia33*

[3]*ARC Centre of Excellence for Nanoscale BioPhotonics, Macquarie University, Sydney, NSW, 2109, Australia.*

[4]*Institute for Biomedical Materials and Devices, Faculty of Science, University of Technology Sydney, NSW, 2007, Australia.*

[5]*Minomic International Ltd, Macquarie Park, Sydney, NSW, 2109, Australia.*

E-mail: bingyang.shi@mq.edu.au

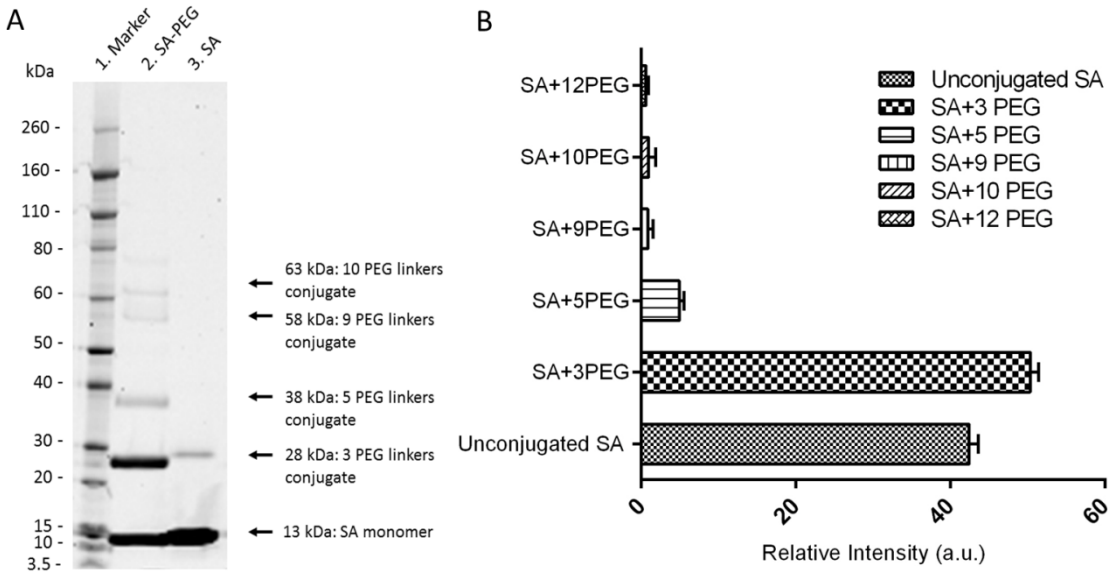

Figure S1. (A) SDS-PAGE analysis of SA and PEGylated SA in reducing condition and stained with coomassie brilliant blue. Lane 1: molecular mass marker. Lane 2: PEGylated SA (20 μg). Lane 3: SA (20 μg). (B) The pixel densities of bands from SA conjugated with six different amount of PEG were quantified using ImageJ software and presented as mean relative intensity. Pixel intensity of SA conjugated with 3 PEG linkers account for 50.3% of all components.

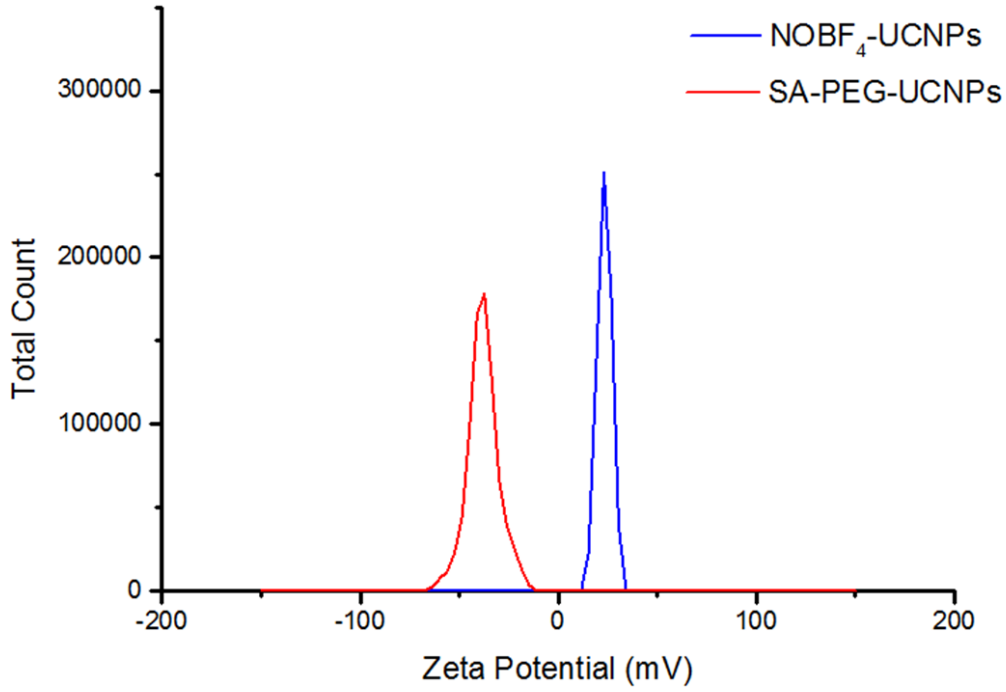

Figure S2. Zeta potential of the $NOBF_4$-UCNPs (blue trace) dispersed in DMF and SA-PEG-UCNPs dispersed in PBS were measured at 23.3 and -36.1 mV, respectively.

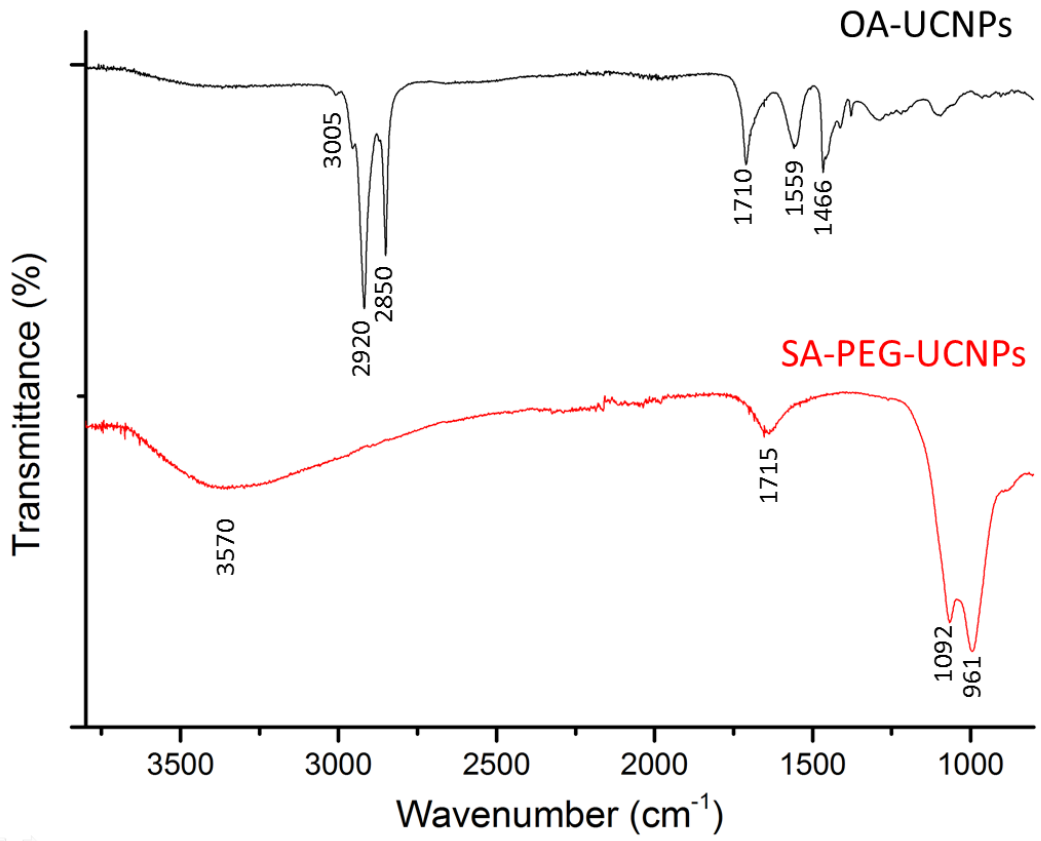

Figure S3. FT-IR absorption spectra of OA-capped UCNPs (black trace) and PEG-UCNPs (red trace) functionalized by $NOBF_4$/SA-PO_4-PEG_{5000}-COOH.

The functional groups on the surfaces of the bare and SA-PEG-UCNPs were identified by FT-IR spectra. The surfaces of the bare NPs are capped with a layer of oleic acid, which acts as the surfactant and capping ligands in this synthesis. The two peaks at 2920 and 2850 cm^{-1} can be assigned to the asymmetric and symmetric stretching vibrations of methylene group, respectively, which exists in the long alkyl chain of the oleic acid molecule. Furthermore, two peaks at 1559 and 1466 cm^{-1} are associated with the asymmetric and symmetric stretching vibrations of the carboxylic group (COO), respectively. After functionalization, the featured bands at 2920 and 2850 cm^{-1} (corresponds to $–CH_2$ group) and bands at 1457 cm^{-1} and 1563 cm^{-1} (associated with

C=O) disappeared indicating the successful removal of OA. Meanwhile, the strong peak at 1092 and 961 cm^{-1} suggests the UCNPs are successfully modified with PO4 groups. Additionally, the strong band located around 1715 cm^{-1} corresponds to the stretching vibration of carboxyl group (C=O), confirming that the –COOH groups on the surface of SA-PEG-UCNPs.

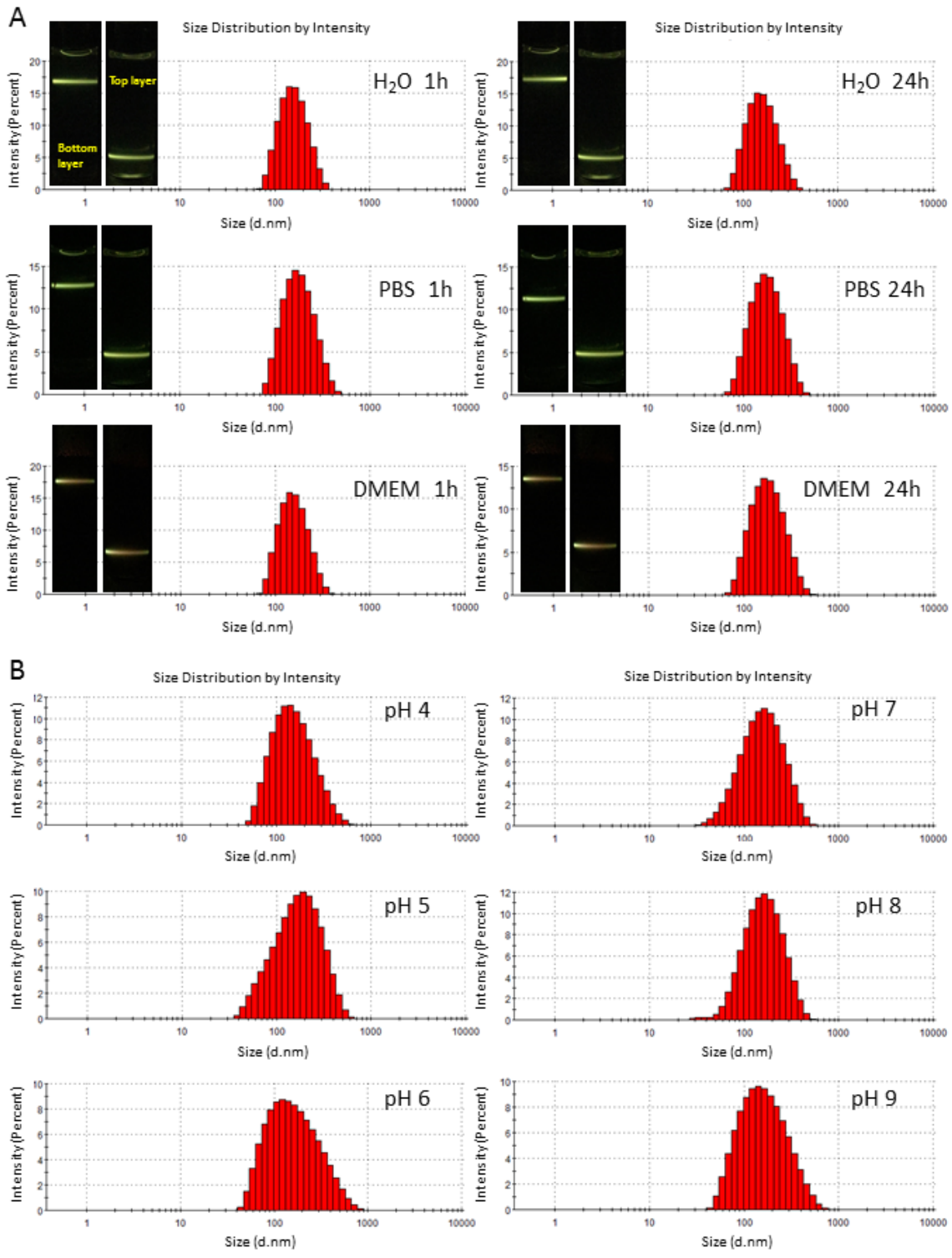

Figure S4. (A) The dynamic light scattering of SA-PEG-UCNPs dispersed in H_2O, PBS buffer and DMEM cell culture medium with 10% FBS at 1 h and 24 h after their respective preparation. Left panel is luminescence photographs of SA-PEG-UCNPs

dispersed in H_2O, PBS and DMEM at 1 h and 24 h after prepared. The top layer (left side) and bottom layer (right side) of UCNP solution are excited at 980 nm laser respectively to monitor water stability. (B) The dynamic light scattering of SA-PEG-UCNPs dispersed in PBS buffer at different pH from 4.0 to 9.0 for 1 h.

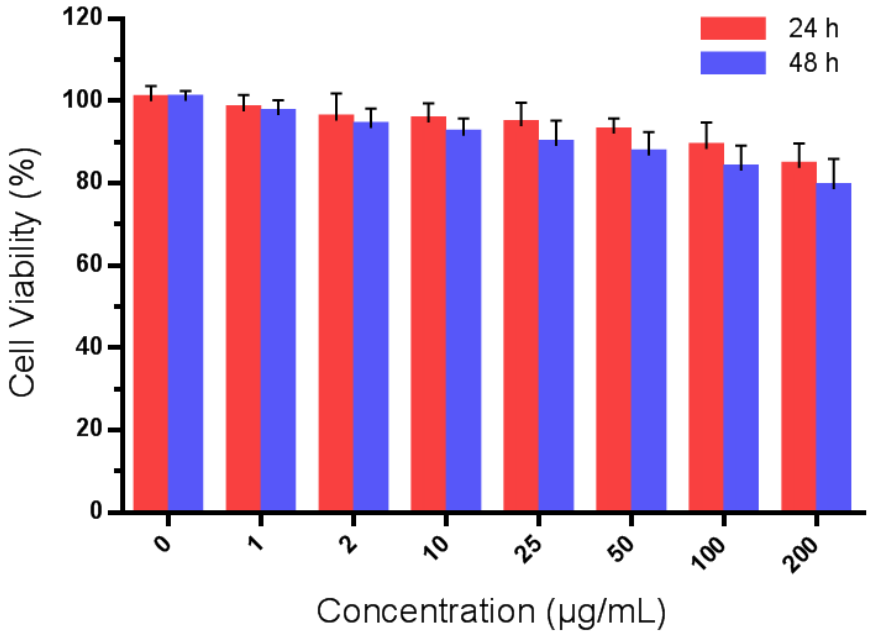

Figure S5. Cell Viability of DU145 cells in the presence of SA-PEG-UCNPs with different concentrations for 24 h and 48 h at 37 °C as measured by MTT assay.

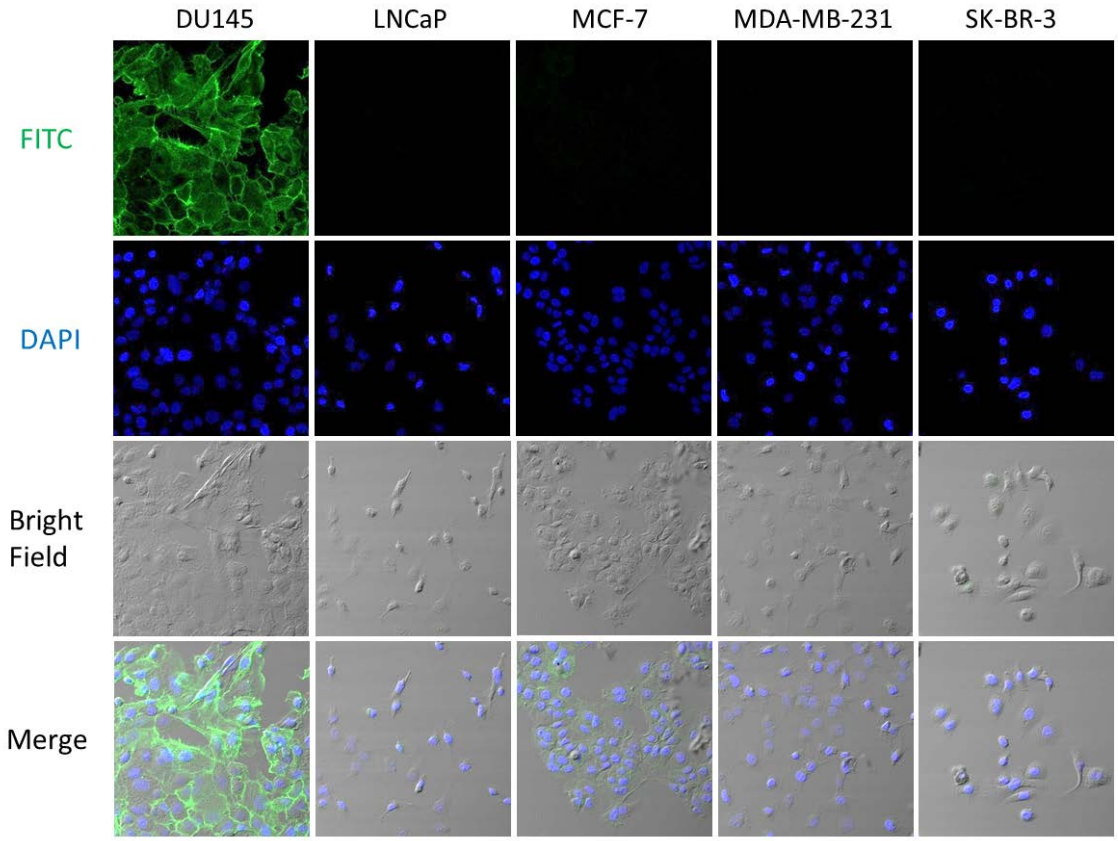

Figure S6. Confocal luminescence imaging of the FITC-conjugated antibody MIL-38 incubated with prostate cancer cell lines DU145 and LNCaP and breast cancer cell lines MCF-7, MDA-MB-231 and SK-BR-3. Green and blue colors represent green and blue fluorescence from FITC and DAPI, respectively.

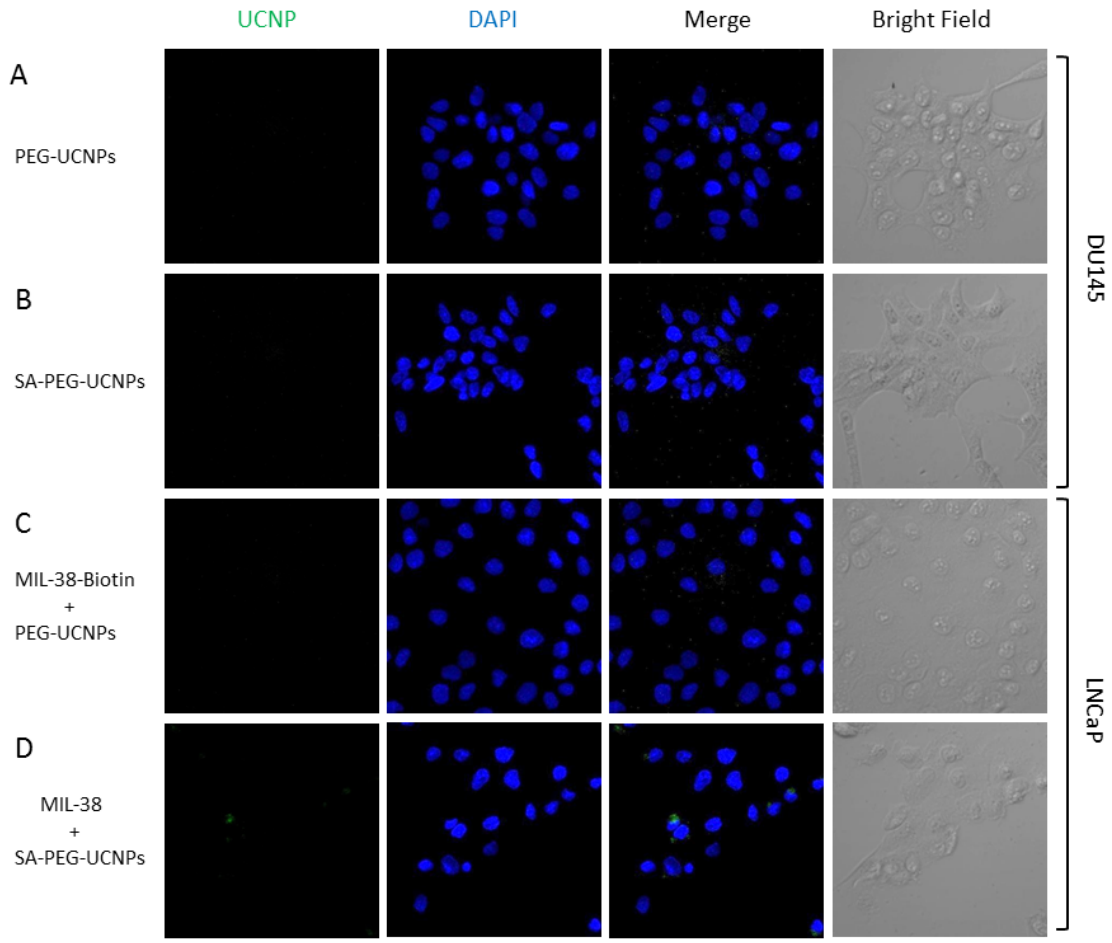

Figure S7. Control experiment of confocal upconversion fluorescence imaging of (A) PEG-UCNPs and (B) SA-PEG-UCNPs incubated with DU145 prostate cancer cells. (C) PEG-UCNPs labeled with MIL-38-Biotin and (D) SA-PEG-UCNPs labeled with MIL-38 on LNCaP prostate cancer cells. All images were taken under the identical instrumental condition and presented at the same intensity scale. Green and blue colors represent UCL signals and blue fluorescence from UCNPs and DAPI, respectively.

Chapter 5: Direct Conjugation of UCNPs via the Fc Glycosylation Site of IgG Antibodies

5.1 Background

The previous results from Chapter 3 indicated that the $NOBF_4$/OPEA functionalized UCNPs provide good colloidal stability and proved to have low non-specific binding when tested in a cell labelling assay. Therefore, there was potential for using these hydrophilic and amino functionalzied UCNPs in subsequent bioconjugations and to establish a UCNP-antibody complex as a fluorescent probe for cell specific targeting. The bioconjugation approach demonstrated in Chapter 4 has provided good stability for upconversion immune-nanohybrids (UINBs); however, it requires multiple steps which may lead to low reproducibility. Considering this, a simple and rapid antibody and UCNP bioconjugation approach which attaches antibodies directly to the UCNPs was investigated. Soduim periodate ($NaIO_4$) was used as a gentle oxidation agent to generate reactive dialdehydes from the oligosaccharides attached at the single site on the two heavy chains of te constant region (Fc) of antibodies. By controlling a proper selection of reaction conditions, such as time, periodate concentration, pH and temperature, two labeling sites per antibody can be obtained without affecting antibody activities (Wolfe and Hage 1995). The oxidized antibody (IgG-CHO) was then reacted with amino functionalized UCNPs through reductive amination (Wagh and Law 2013). This orientational conjugation approach should not affect the antigen binding region (Fab) of antibodies and thus maintain the integrity of their specificity. This direct conjugation strategy, however, resulted in aggregation of the antibodies (data not shown) and was considered not to be a reliable approach. Hence, to maintain the antibody direct modification and achieve high water dispersibility and stability in bioconjugation, it was necessary to develop a new approach.

The outcome from Chapter 4, which demonstrated a ligand exchange conjugation method of UCNPs and streptavidin (SA) with poly(ethylene glyco) (PEG) driven colloidal stability, provided a solution for resolving the problem of the water stability of UCNP bioconjugation. As shown in **Scheme 5.1**, based on IgG-CHO, a bifunctional PEG linker, hydrazide-PEG_{5000}-phosphate (HZ-PEG-PO_4, MW=5 kDa), was introduced to directly add a PEG spacer arm to the Fc region of the antibody via the attached oligosaccharide. This bifunctional HZ-PEG-PO_4 linker, on one hand, can react with the oxidized antibody sugars containing aldehyde groups via reductive amination; and on the other hand, the phosphate group can be used in conjugating to the UCNPs by ligand exchange. To achieve the linkage between UCNPs and PEGylated antibodies, $NOBF_4$ was used to replace the original surface ligands on UCNPs by inorganic BF_4 anions which provided electrostatic stabilization of UCNPs in polar media, such as DMF and DMSO (see Chapter 4). Then the BF_4 counter-ion can be replaced by the phosphate group, which is on the other end of the PEG linker, due to the better coordination ability of PO_4 anions with lanthanide ions on the surface of UCNPs (Liu, Wang et al. 2011; Dong, Korinek et al. 2012). After this bioconjugation, the hydrophilic nature of the PEG linker may provide the most effective surface ligand that improves the biocompatibility of bioconjugation and also leaves the UCNPs and antibodies unhindered by its long spacer arm. The main aim of this work thus was to introduce the PEG-phosphate-based surface ligand (HZ-PEG-PO_4) to hopefully improve the colloidal stability of the UCNP-antibody complex whilst not aggregating in biological environments, such as water, PBS buffer and DMEM cell culture medium. The successful two site functionalization procedure of labeling the antibodies, by polysaccharide oxidation and PEGylation, would maintain the bioactivity of antibodies to provide specific targeting ability of the UCNP-antibody conjugation. In this work, MIL-38 monoclonal antibody was utilized as a targeting agent to specifically recognize prostate cancer cells.

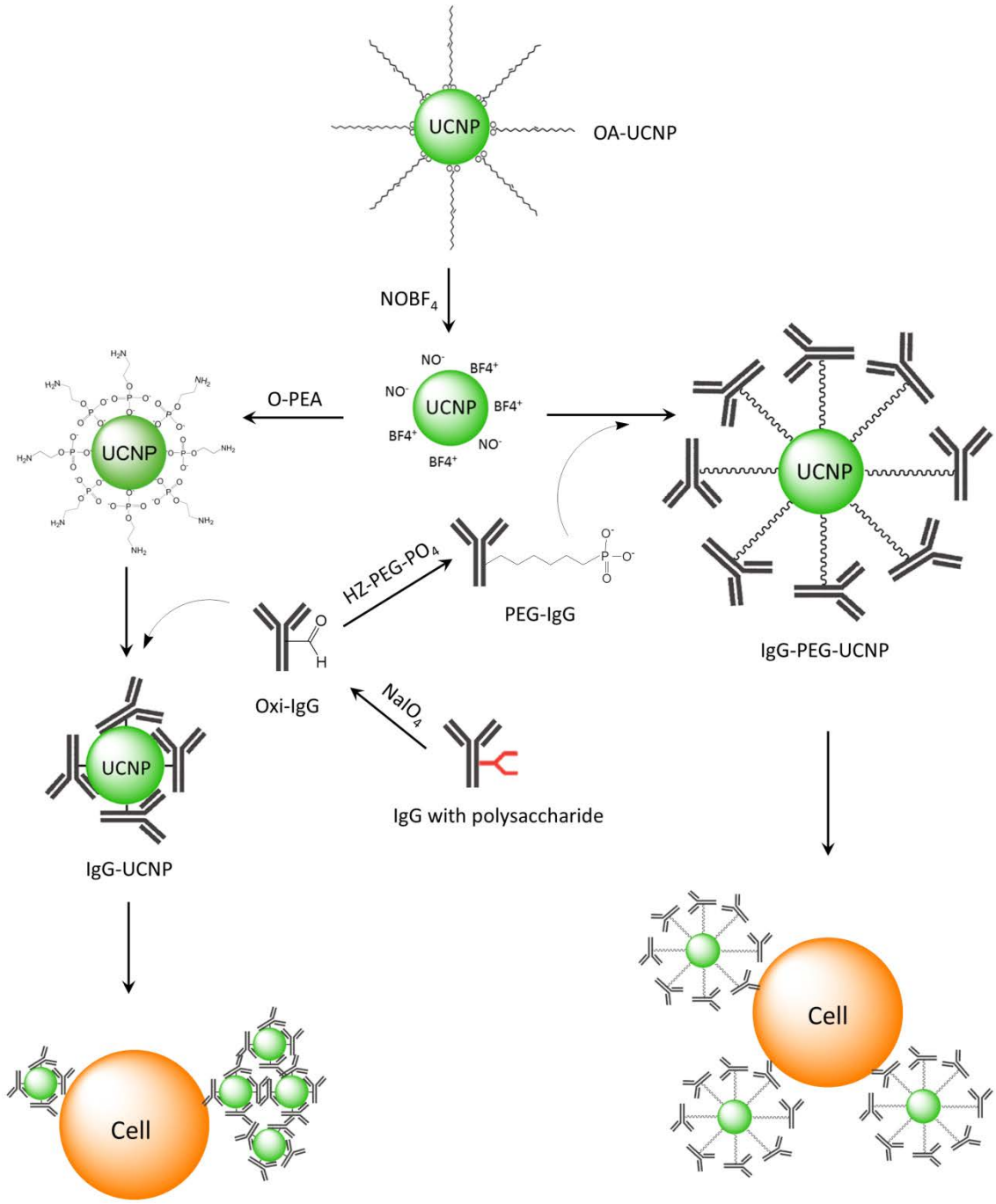

Scheme 5.1 A diagram of the synthetic scheme of antibody and UCNP conjugation via the IgG oligosaccharide protocol with cell specific labeling. The left side shows a conjugation protocol between amino functionalized UCNP and oxidized antibody via

reductive amination. The right side shows a direct conjugation between $NOBF_4$ treated UCNP and PEGylated antibody via ligand exchange.

5.2 Experimental Section

5.2.1 Reagents and Materials

Unless otherwise stated, all reagents were purchased from commercial suppliers and used without further purification. Yttrium chloride hexahydrate ($YCl_3 \cdot 6H_2O$, 99.99%), ytterbium chloride hexahydrate ($YbCl_3 \cdot 6H_2O$, 99.98%), erbium chloride hexahydrate ($ErCl_3 \cdot 6H_2O$, 99.9%), sodium hydroxide (NaOH, 98%), ammonium fluoride (NH_4F, 99.99%), oleic acid (OA, 90%), 1-octadecene (ODE, 90%), cyclohexane (C_6H_{12}, 99.5%), ethanol (CH_3CH_2OH, ≥99.5%), methanol (CH_3OH, 99.5%), dichloromethane (CH_2Cl_2, 99.8%), toluene ($C_6H_5CH_3$, 99.8%), dimethylformamide (DMF, 99.8%) were all purchased from Sigma–Aldrich and used as received without further purification. goat anti-mouse IgG (H+L) secondary antibody, FITC conjugate and 2-(4-amidinophenyl)-1H-indole-6-carboxamidine (DAPI) were purchase from Thermo Fisher Scientific. PEG linker hydrazide-PEG_{5000}-phosphate (HZ-PEG-PO_4) was synthesized and purchased from JenKem Technology USA Inc. Monoclonal antibody MIL-38 and prostate cancer cell lines DU145 and LNCaP were all provided by Minomic Int. Ltd.

5.2.2 Characterization of UCNPs

Protocol can be found in Chapter 4.

5.2.3 Synthesis of OA-Capped $NaYF_4$: Yb^{3+}/Er^{3+} Nanoparticles

Protocol can be found in Chapter 4.

5.2.4 Oxidation and PEGylation of MIL-38 Antibody (Oxi-MIL-38 & PEG-Oxi-MIL-38)

Oxi-MIL-38: For the oxidation of the oligosaccharides on the heavy chains of the IgG antibody MIL-38, 100 μL of 20 mM cold (4 ^{o}C) $NaIO_4$ sodium acetate solution was mixed with 100 μL of cold (4 ^{o}C) MIL-38 solution (1 mg/mL in 0.1 M sodium acetate buffer, pH 5.5) on ice for 30 min. 500μL PBS buffer (0.1 M, pH 8) was added to quench the reaction. Excess $NaIO_4$ was removed with change of buffer to PBS, by using a ultrafiltration spin column, Vivaspin 500 (MWCO 50000, GE). The oxidized MIL-38 (Oxi-MIL-38) was used for conjugation with UCNPs.

PEG- Oxi-MIL-38: For the MIL-38 PEGylation, 10 μL of 7 mM HZ-PEG-PO_4 linker was added to Oxi-MIL-38 and mixed for 2 h at room temperature. Non-reactive linkers were separated by Vivaspin 500 ultrafiltration spin column.

5.2.5 Preparation of Oxidized MIL-38 (Oxi-MIL-38) Conjugated UCNPs

Protocol of amino functionalized UCNPs (OPEA-UCNPs) can be found in Chapter 3.

Oxi-MIL-38 and OPEA-UCNPs conjugation: 100 μL of OPEA-UCNPs was mixed with 1 mL of 2 mg/mL of Oxi-MIL-38 and incubated for 2 h at 37 °C to form the Schiff base intermediates. Then 10 mg $NaBH_3(CN)$ was added to the reaction mixture and further incubated for 30 min at 37 °C to further reduce the intermediates to the

corresponding secondary amines. The resulting antibody conjugated UCNPs (MIL-38-UCNPs) were purified by washing with PBS buffer and centrifugation. The MIL-38-UCNPs were stored in PBS at 4 °C.

5.2.6 Preparation of PEGylated MIL-38 (PEG-Oxi-MIL-38) Conjugated UCNPs

The $NOBF_4$-UCNPs (5 mg) dispersed in DMF added to 2 mg/mL PEG-Oxi-MIL-38 in PBS buffer. The mixed solution was stirred at room temperature for 24 h. The PEG-Oxi-MIL-38 conjugated UCNPs (MIL-38-PEG-UCNPs) were purified by washing with PBS buffer and centrifugation. The MIL-38-PEG-UCNPs were stored in PBS buffer at 4 °C.

5.2.7 Absorption Spectrum

The Thermo Scientific Nanodrop 2000 Spectrophotometer was used to measure the absorption spectrum profiles of different samples, which includes MIL-38-UCNP and MIL-38-PEG-UCNP conjugates, and all the pure antibody, PEG and OPEA-UCNP standards. 2 µL of each sample was dipping onto the lower measurement pedestal to obtain the spectrum profiles.

5.2.8 Cell Culture and Immunofluorescence Assay (IFA)

Protocol of cell culture can be found in Chapter 4.

IFA: Cells were seeded in Lab-Tek® chamber slides at a density of 4×10^4 cells per well. After cell attachment for 24 h, cells were washed with pre-warmed PBS, and fixed by 5 (w/v) % paraformaldehyde (PFA). After blocking with 2% (w/v) BSA solution, cells

were incubated with MIL-38-UCNPs or MIL-38-PEG-UCNPs at 100 μg/mL in blocking solution for 1 h at room temperature. Excess UCNPs were removed by sufficient washing with PBS and the UCNP-labelled antibodies were then incubated with 100 μg/mL of FITC conjugate goat anti-mouse IgG (H+L) secondary antibody (2^{nd}-FITC) for 1 h at room temperature. After incubation cells were then washed with PBS to remove excess 2^{nd}-FITC before imaging.

5.2.9 MTT Assay

Protocol can be found in Chapter 4.

5.3 Results and Discussion

5.3.1 Preparation and Characterization of UCNPs

The preparation, transmission electron microscopy (TEM) imaging, size distribution and X-ray diffraction (XRD) of the oleic acid (OA)-capped $NaYF_4$: 20% Yb^{3+}/2% Er^{3+} UCNPs (OA-UCNPs) were demonstrated in Chapter 4.

To transfer hydrophobic OA-UCNPs into hydrophilic nanoparticles, a two-step ligand exchange method, which was using nitrosonium tetrafluoroborate ($NOBF_4$) and O-phosphorylethanolamine (OPEA), was carried out as illustrated in Chapter 3. The TEM micrographs shows the OPEA functionalized UCNPs were well dispersed in PBS buffer (pH 8.0) with no sign of aggregation (**Figure 5.1C**). To demonstrate the $NOBF_4$/OPEA ligand exchange of OA-UCNPs, the Fourier-transform infrared (FT-IR) spectra were compared with β-$NaYF_4$ UCNPs before and after surface modification (**Figure 5.2**). Detailed description of FT-IR analysis can be referred to Chapter 3. Furthermore, the zeta potential of OPEA-UCNPs was measured to be 33.8 mV in PBS,

which indicated the $–NH_2$ groups presented on UCNPs surface (**Figure 5.3**).

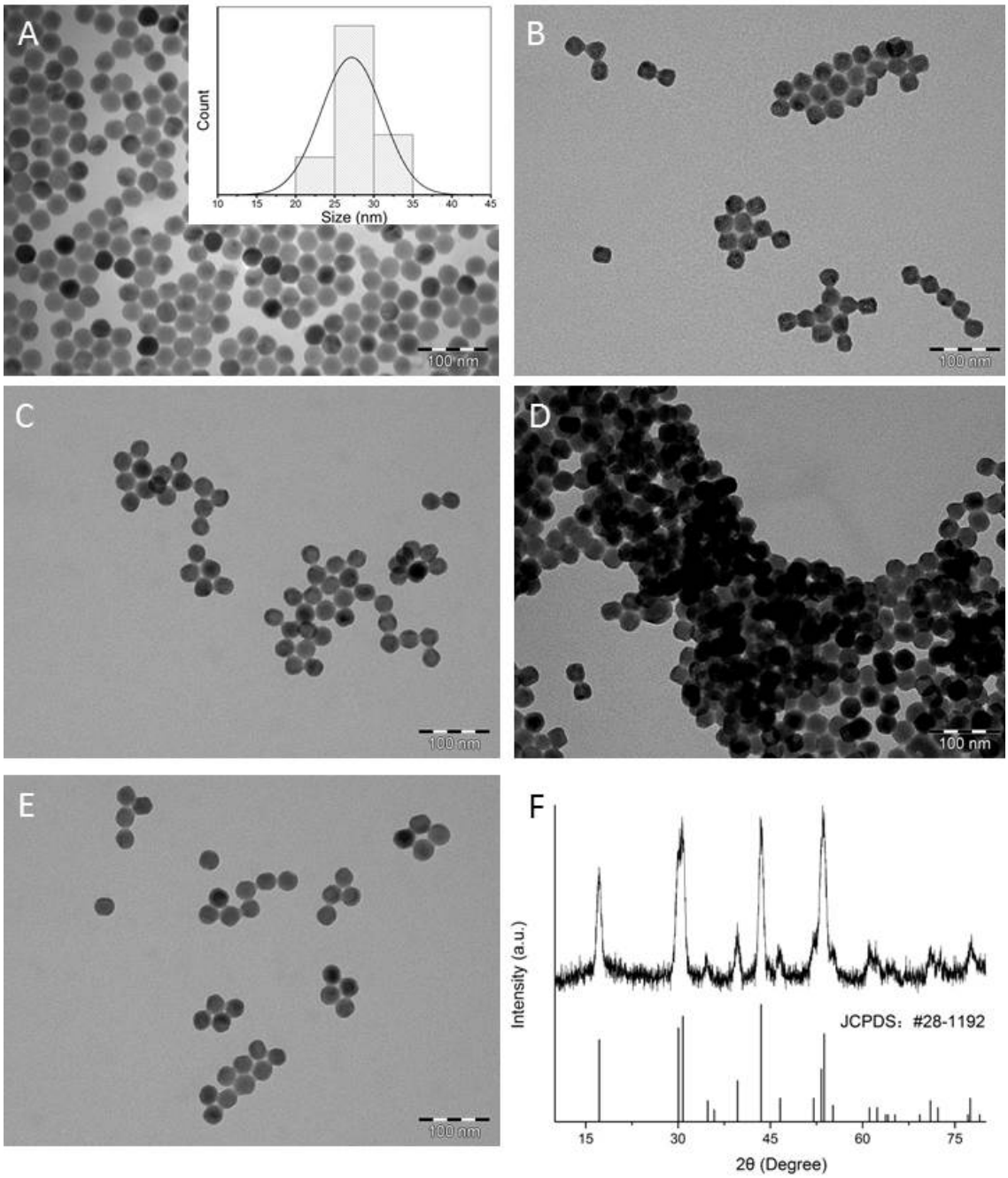

Figure 5.1 TEM images of (A) OA-capped UCNPs (OA-UCNPs) dispersed in cyclohexane, (B) $NOBF_4$ treated UCNPs ($NOBF_4$-UCNPs) dispersed in DMF, (C)

OPEA functionalized UCNPs (OPEA-UCNPs), (D) MIL-38 antibody conjugated UCNPs (MIL-38-UCNPs) and (E) PEGylated MIL-38 antibody conjugated UCNPs (MIL-38-PEG-UCNPs) dispersed in PBS buffer. The average size of OA-UCNPs which was measured by TEM at 27.2 ± 3.9 nm is shown in (A). (F) X-ray diffraction (XRD) pattern for upconversion nanoparticles $NaYF_4$: 20% Yb^{3+}/2% Er^{3+}.

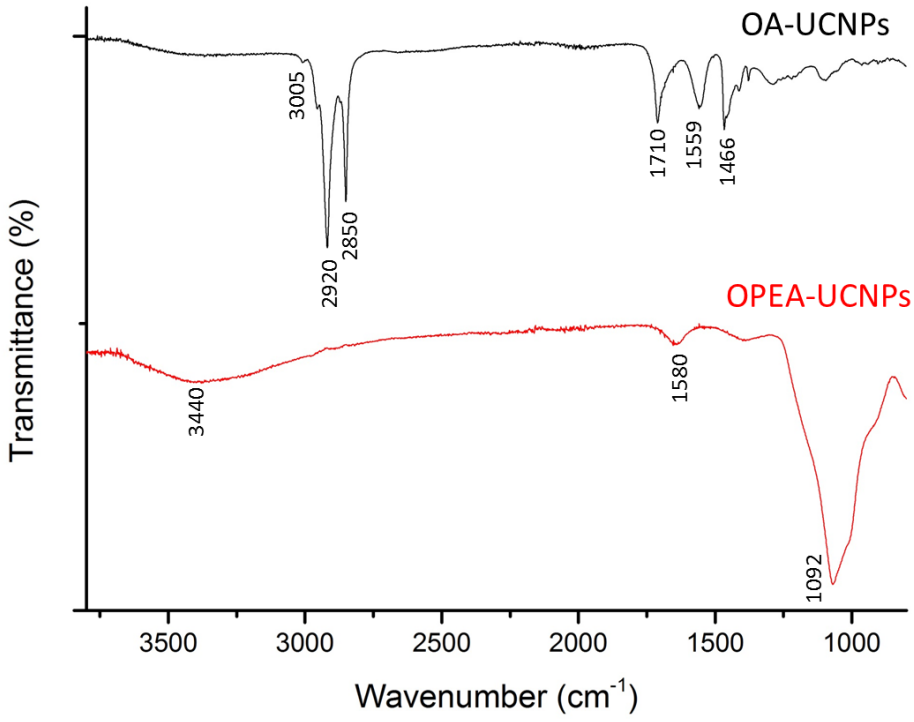

Figure 5.2 FT-IR spectra of OA-UCNP (black trace) and OPEA-UCNPs (red trace).

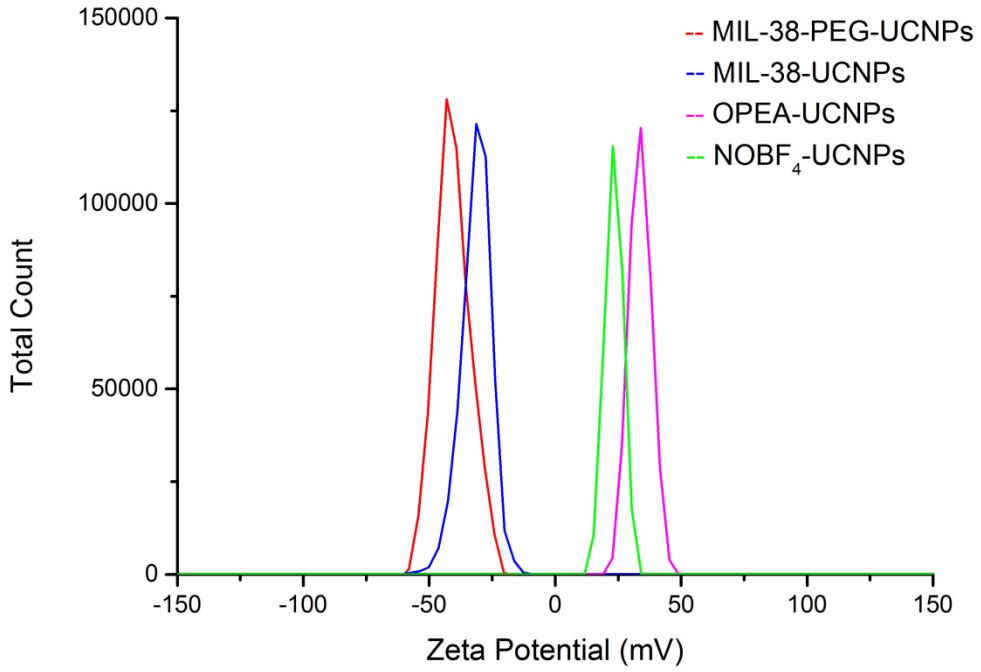

Figure 5.3 (A) Zeta potential of $NOBF_4$-UCNPs (green trace), OPEA-UCNPs (purple trace), MIL-38-UCNPs (blue trace) and MIL-38-PEG-UCNPs (red trace) dispersed in PBS buffer was measured at 23 mV, 33.8 mV, -31.4 mV and -40.5 mV, respectively.

5.3.2 MIL-38 Antibody Carbohydrate Modification and PEGylation

The monoclonal antibody MIL-38 (provided by Minomic Pty. Ltd, AU) was employed as a specific reagent for targeting prostate cancer cells. The specificity of MIL-38 antibody has been confirmed as shown in Chapter 4 (**Figure 5.4A**). The positive binding cell line DU145 and the negative cell line LNCaP were chosen for the following cell imaging study. As shown in Scheme 1, oligosaccharides located on Fc region of MIL-38 antibody were firstly oxidized by sodium periodate ($NaIO_4$) to generate active aldehyde groups for subsequent conjugation with amino functionalized UCNPs (OPEA-UCNPs). After $NaIO_4$ oxidation, the oxidized antibody MIL-38 (Oxi-MIL-38) maintains its specificity through a immunofluorescence assay (IFA) which was

visualizing the specific targeting on DU145 cells by using a FITC conjugated secondary antibody (2^{nd}-FITC) (**Figure 5.4B**).

The Oxi-MIL-38 was alternatively functionalized by introducing a bifunctional PEG linker (HZ-PEG-PO_4). The hydrazide groups on PEG linkers react with active aldehyde groups on Oxi-MIL-38 to form a stable covalent bond, while the –PO_4 groups coordinated with lanthanide ions on the surface of $NOBF_4$-UCNPs to form a linkage. Electrophoresis analysis (**Figure 5.5**) showed that the molecular weight of the PEGylated antibody MIL-38 (PEG-Oxi-MIL-38) increased after PEGylation process. In the SAS-PAGE reducing conditions, the antibody MIL-38 dissociated into 50,000 kDa (heavy chains) and 25,000 kDa (light chains). As shown in Figure 5, Lane 4, a new band at approximately 60 kDa can be observed in PEG-Oxi-MIL-38 sample indicating, based on mass, that 2 PEG linkers have been conjugated to the antibody heavy chain. Another band, meanwhile, was seen at a lower mass position suggests a heterogeneous PEG labelling of antibody. The antibody PEGylation mixture was used for UCNP bioconjugation without further purification. In addition, the IFA result shows that PEGylated antibody PEG-Oxi-MIL-38 still specifically binds to DU145 cells which was visualized by using 2^{nd}-FITC (**Figure 5.4C**).

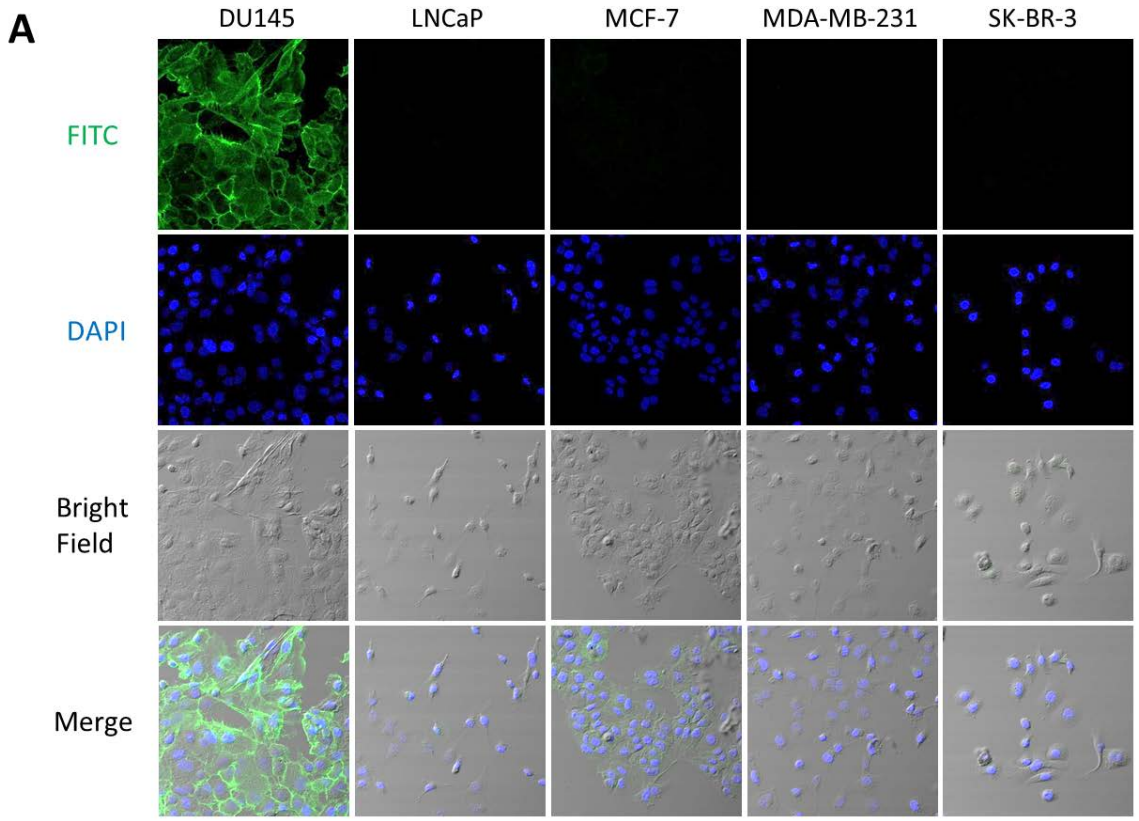
A
DU145
LNCaP
MCF-7
MDA-MB-231
SK-BR-3
FITC
DAPI
Bright Field
Merge

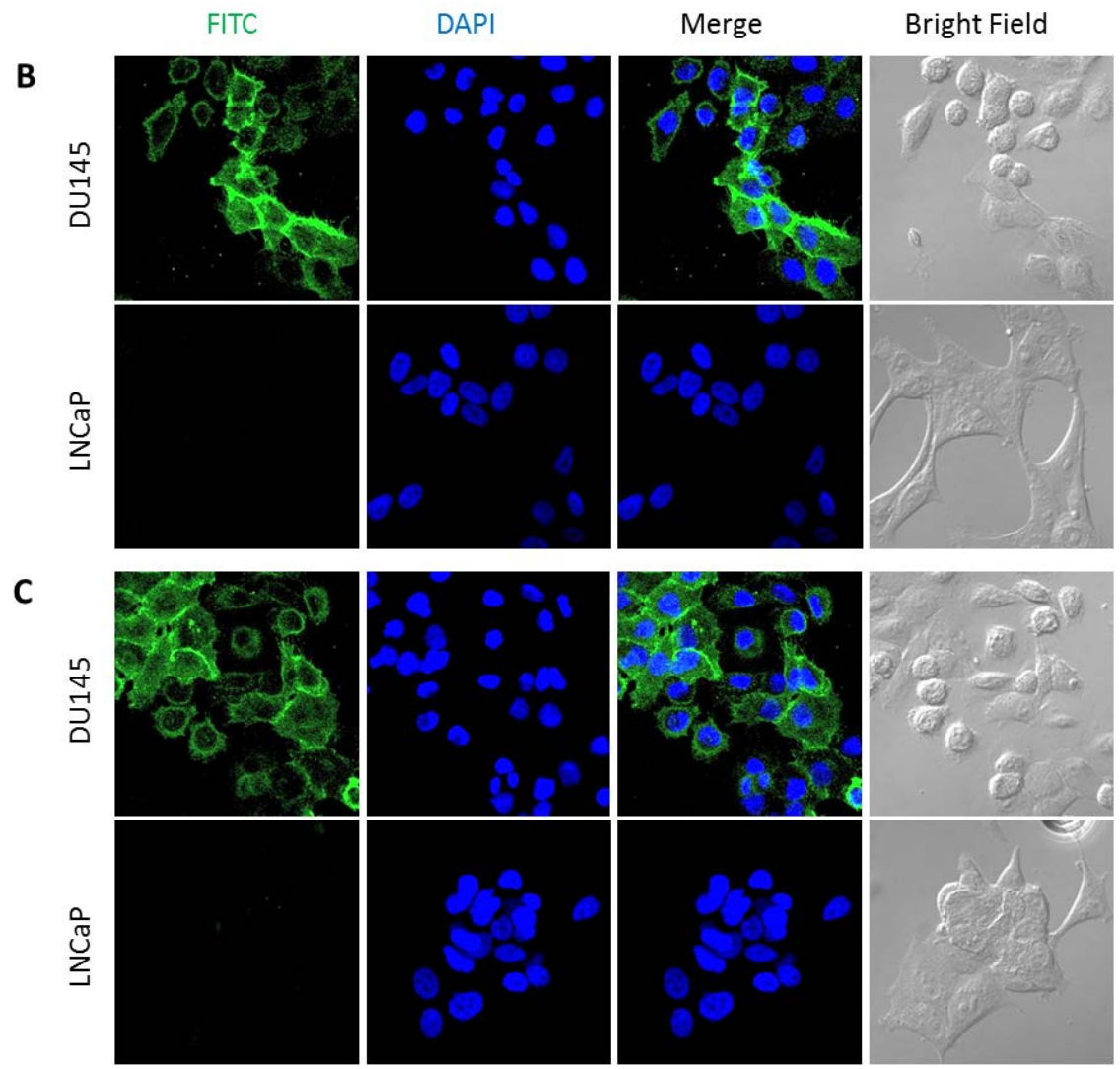

Figure 5.4 Confocal luminescence imaging of (A) the specificity verification of antibody MIL-38 incubate with prostate cancer cell lines DU145 and LNCaP and breast cancer cell lines MCF-7, MDA-MB-231 and SK-BR-3 *. (B) the verification of oxidized antibody MIL-38 (Oxi-MIL-38) specific targeting ability. (C) the verification of PEGylated antibody MIL-38 (PEG-Oxi-MIL-38) specific targeting ability. Green and blue colors represent green and blue fluorescence from FITC conjugated secondary antibody attached to MIL-38 antibody and DAPI stained nucleus, respectively. *: Panel A is included as **Figure S6** as in the manuscript presented in Chapter 4.

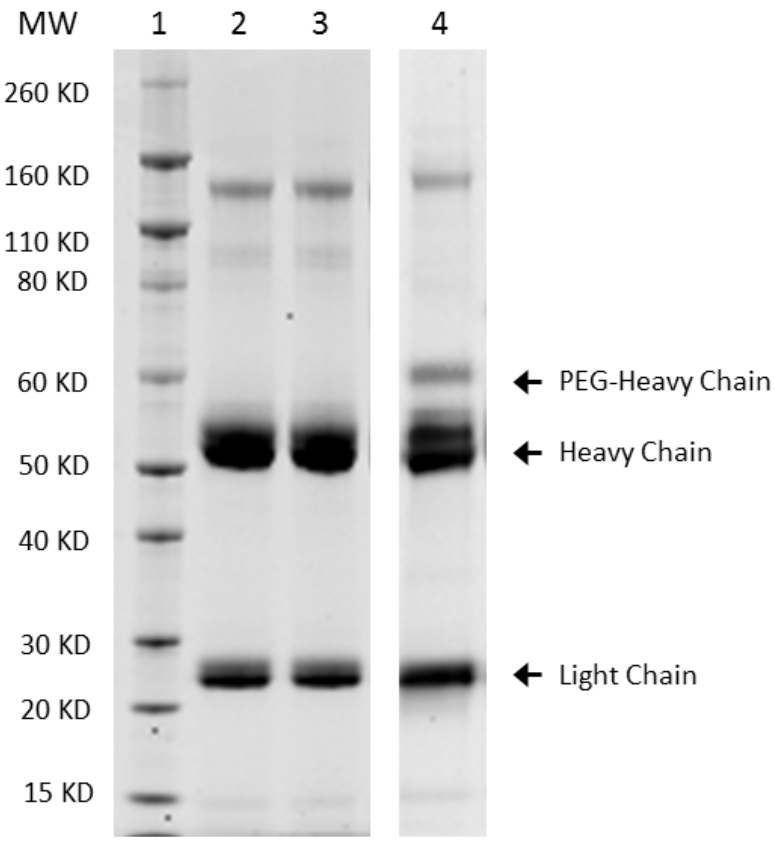

Figure 5.5 SDS-PAGE analysis of MIL-38 and PEG-Oxi-MIL-38 in reducing condition and stained with Coomassie Brilliant Blue. Lane 1: molecular mass marker. Lane 2: MIL-38 (20 μg). Lane 3: Oxi-MIL-38 (20 μg). Lane 4: PEG-Oxi-MIL-38 (20 μg).

5.3.3 Conjugation of Oxi-MIL-38 to Amino Functionalized UCNPs

After $NaIO_4$ oxidation, Oxi-MIL-38 with active carbohydrate aldehyde were mixed with OPEA-UCNPs via reductive amination reaction with the primary amine groups. After MIL-38-UCNPs bioconjugation, aggregation of the UCNPs was observed when resuspended in PBS buffer as shown by TEM imaging (**Figure 5.1D**). Dynamic light scattering (DLS) measurements **(Figure 5.6**) were performed to visualize the changing of hydrodynamic diameter of MIL-38-UCNPs before and after conjugation. The OA-UCNPs dispersed in cyclohexane were measured to have an average diameter of

42.9 nm that corresponds to the average size of the same sample by TEM measurement since DLS takes into account the length of the ligands on the nanoparticle surface. After $NOBF_4$ treatment, the hydrodynamic diameter does not change much (44.6 nm) but greatly increased to 86.2 nm after OPEA modification. The significantly increased diameter of MIL-38-UCNPs was found to be 2653 nm, which indicated the aggregation after the MIL-38-UCNPs conjugation. Meanwhile, the zeta potential of MIL-38-UCNPs was measured at -31.4 mV (**Figure 5.3**).

The aggregated MIL-38-UCNPs sample was tested in cell labeling assay and DU145 and LNCaP were chosen as antibody positive and negative cell line (**Figure 5.7**). MIL-38-UCNPs were firstly incubated with DU145 and LNCaP cells and goat anti-mouse IgG (H+L) secondary antibody, FITC conjugate was then added to provide additional fluorescent signal which was used to monitor the co-localization of UCNPs and MIL-38 antibody in cell labeling. As shown in Figure 7A, strong green fluorescent signal was detected from UCNPs under 980 nm laser scanning; however, the aggregated MIL-38-UCNPs were found to be non-specifically attaching to both DU145 and LNCaP cells. The similar pattern of fluorescence from FITC under 473 nm laser scanning model has proved the non-specific binding. No fluorescence signal can be detected when labeling with only OPEA-UCNPs on DU145 and LNCaP cells (**Figure 5.7B**), which suggesting the non-specific binding properties occur only after bioconjugation. To sum up, MIL-38-UCNPs conjugation causes aggregation and the MIL-38 antibody loses its specific antigen binding ability.

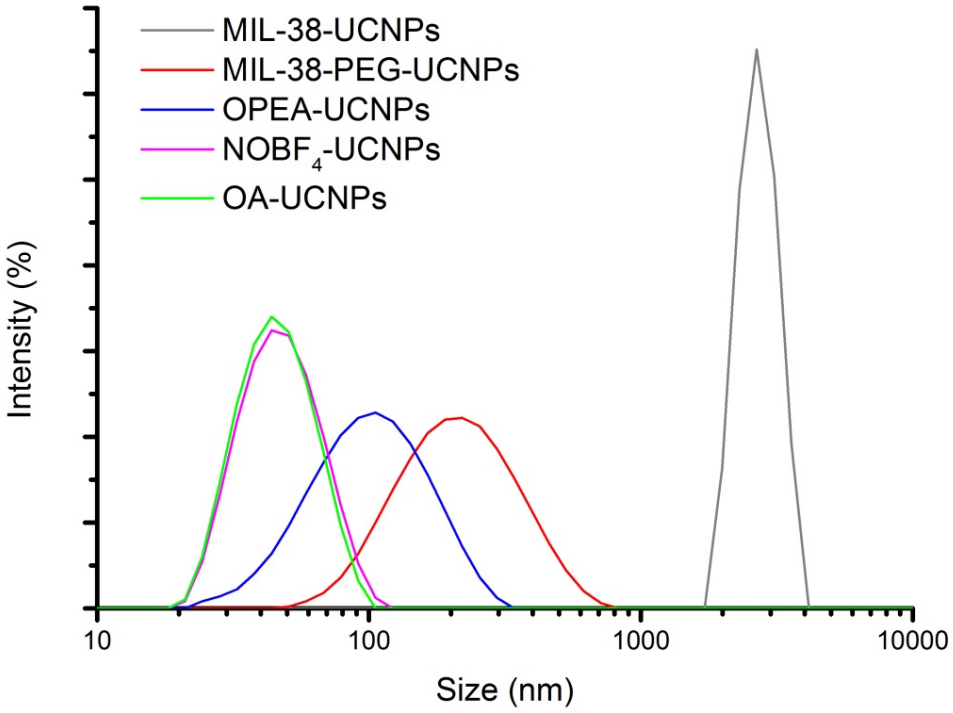

Figure 5.6 Hydrodynamic diameter of (A) OA-UCNPs (green trace), (B) $NOBF_4$-UCNPs (purple trace), (C) OPEA-UCNPs (blue trace), (D) MIL-38-UCNPs (grey trace) and (E) MIL-38-PEG-UCNPs (red trace) were measured at 42.9, 44.6, 86.2, 195.8 and 2653 nm, respectively.

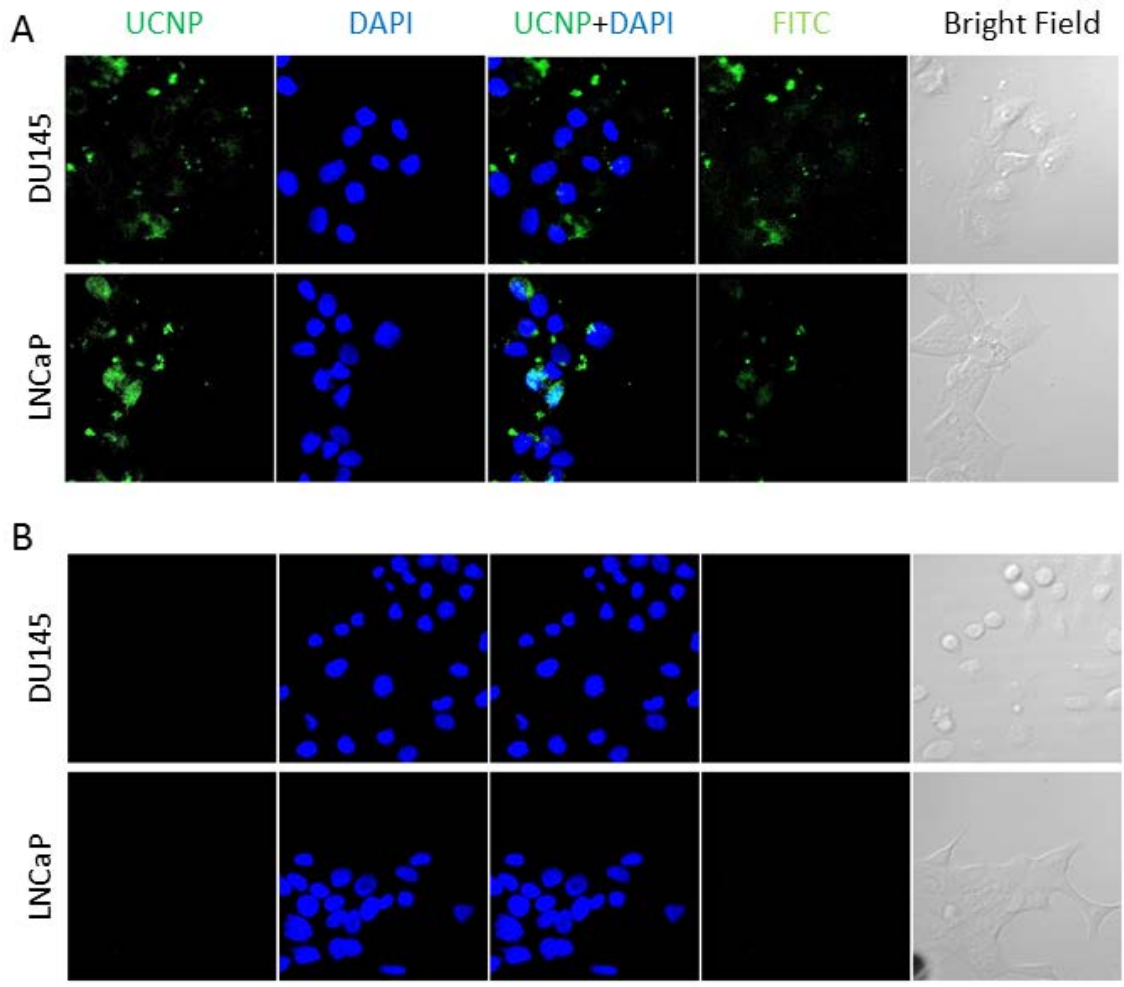

Figure 5.7 Confocal upconversion luminescence (UCL) imaging of (A) PEGylated antibodies conjugated UCNPs (MIL-38-PEG-UCNP) labeling; (B) $NOBF_4$/OPEA functionalized UCNPs (OPEA-UCNP) labeling on DU145 and LNCaP prostate cancer cells, respectively.

5.3.4 Conjugation of PEG-Oxi-MIL-38 to $NOBF_4$ Functionalized UCNPs

To overcome the limitation of aggregation and non-specific binding after UCNPs and antibody direct conjugation through the oligosaccharides, a new approach was developed through a one-step conjugation method. PEGylated antibody Oxi-MIL-38

(PEG-Oxi-MIL-38) with free $-PO_4$ groups conjugated to $NOBF_4$-UCNPs by replacing the BF_4^- counter-ions on UCNPs to form a stable bond. TEM images shows no noticeable agglomeration after bioconjugation when dispersed in PBS buffer (**Figure 5.1E**). The hydrodynamic diameter of PEG-Oxi-MIL-38 conjugated UCNPs (MIL-38-PEG-UCNPs) was measured at 195.8 nm (**Figure 5.2**). Comparing with $NOBF_4$-UCNPs (size at 44.6 nm), the increased particle size after bioconjugation can be attributed to the presence of MIL-38 molecules attaching on UCNPs surface and the length of PEG chains. The zeta potential of MIL-38-PEG-UCNPs was measured at -40.5 mV (**Figure 5.3**) which is lower than that of MIL-38-UCNPs. In addition, the successful MIL-38-PEG-UCNPs conjugation was also demonstrated by the OD_{280nm} absorbance peak. The antibody MIL-38 has strong absorption at 280 nm while UCNPs do not. After conjugation, the absorption profile of the MIL-38-PEG-UCNPs showed an increased absorbance at 280 nm (**Figure 5.8**); together with the increase of hydrodynamic diameter and decrease of zeta potential, this evidence indicates the successful antibodies-UCNPs linkage.

The change of optical properties of UCNPs before and after bioconjugation is important to evaluate the modification procedure. A successful method is expected to maintain the upconversion efficiency of the products in aqueous environments after surface functionalization. The upconversion luminescence (UCL) emission spectra and visible luminescence photographs excited by a 980 nm laser were compared to quantify the luminescence intensity between OA-UCNPs, $NOBF_4$-UCNPs, and MIL-38-PEG-UCNPs at the same concentration (10 mg/mL) dispersed in cyclohexane, DMF and PBS, respectively (**Figure 5.9**). Under continuous excitation at 980 nm, the luminescence in solution appears green in color due to the green emission from doped ion Er^{3+} in UCNPs. Compared to OA-UCNPs, $NOBF_4$-UCNPs have a significant increase in luminescence emission intensity. After $NOBF_4$-UCNPs bioconjugation, there was no obvious change in UCL intensity of MIL-38-PEG-UCNPs sample. The

luminescence photographs of UCNPs before and after bioconjugation, shown in the upper panel of **Figure 5.9**, gave the same degree of the change of upconversion intensity in each sample. It is clear from the luminescence photos of the conjugated UCNPs, that the visible light emitted under 980 nm laser excitation presented a similar intensity change as observed in UCL emission spectral comparison. As a result, the modification and conjugation method used in this study appears not to compromise the upconversion efficiency of the conjugated UCNPs.

The specific antigen binding ability of MIL-38-PEG-UCNPs was validated by a cell labeling assay. MIL-38-PEG-UCNPs labeling displays strong UCL signal on the DU145 cell surface while no obvious fluorescence can be observed from labeling of the MIL-38 negative cell line, LNCaP, under the same conditions (**Figure 5.10**). Fluorescence signal from 2^{nd}-FITC incubation can be detected on DU145 cell membrane and proves the co-localization of UCNPs and the MIL-38 antibodies. When compared with the directly labelled MIL-38-UCNP cell labeling, no aggregation and non-specific binding was observed with the MIL-38-PEG-UCNPs. To sum up, MIL-38-PEG-UCNPs cell labelling was effective with the MIL-38-antibody maintaining its antigen binding activity with no non-specific binding to cells.

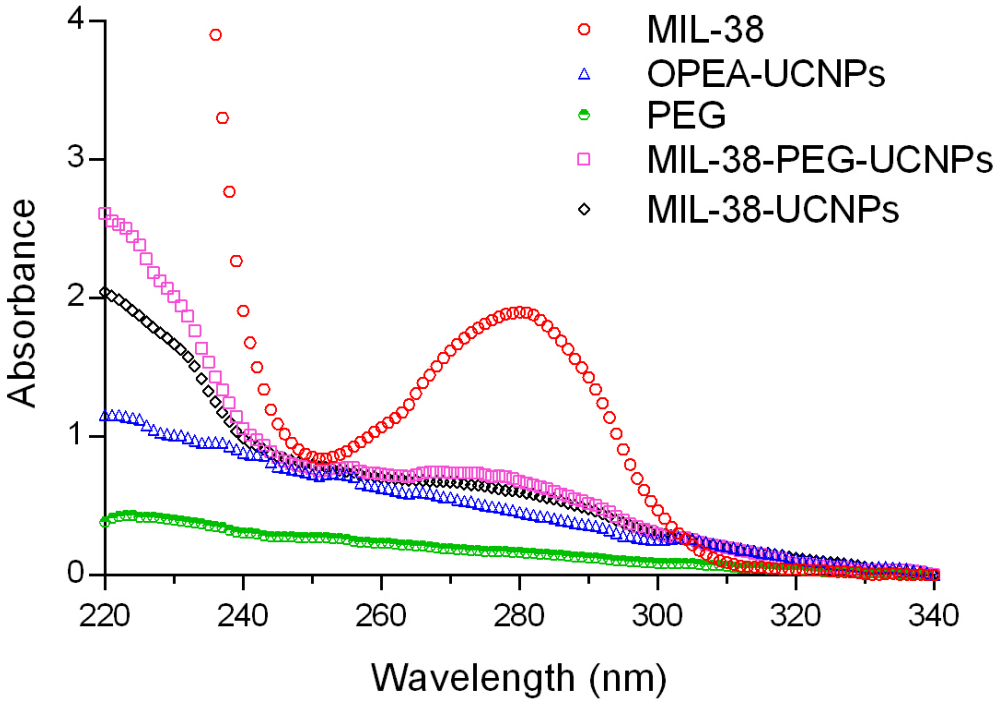

Figure 5.8 The comparison of absorption profile of OA-UCNPs, $NOBF_4$-UCNPs and MIL-38-PEG-UCNPs.

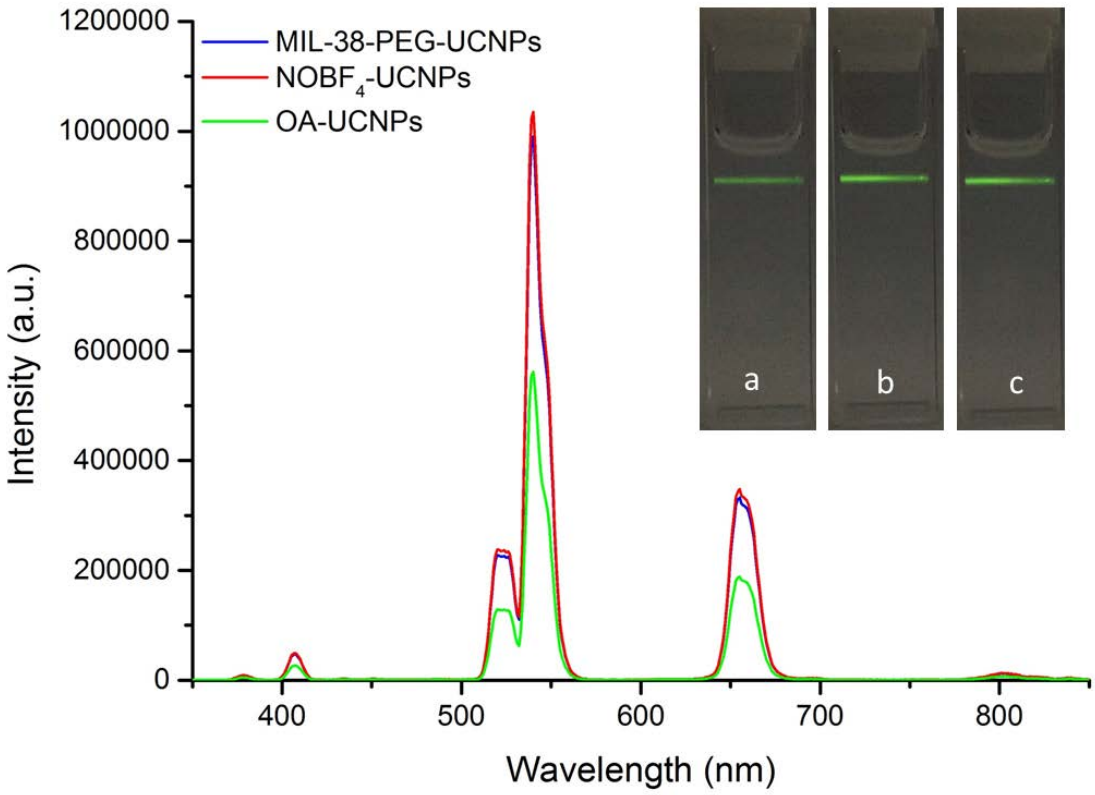

Figure 5.9 Comparison of UCL emission spectra between (black trace) OA-capped UCNPs (OA-UCNP) dispersed in cyclohexane, (red trace) $NOBF_4$ treated UCNPs ($NOBF_4$-UCNP) dispersed in DMF, (blue trace) PEGylated antibodies conjugated UCNPs (IgG-PEG-UCNP) dispersed in PBS buffer under 980 nm excitation. The upper panel displays the luminescence photographs of UCNP solution excited with a 980 nm laser of OA-UCNP (a), $NOBF_4$-UCNP (b) and IgG-PEG-UCNP (c). All spectra and photographs were obtained with the same concentration of UCNPs (10 mg/mL).

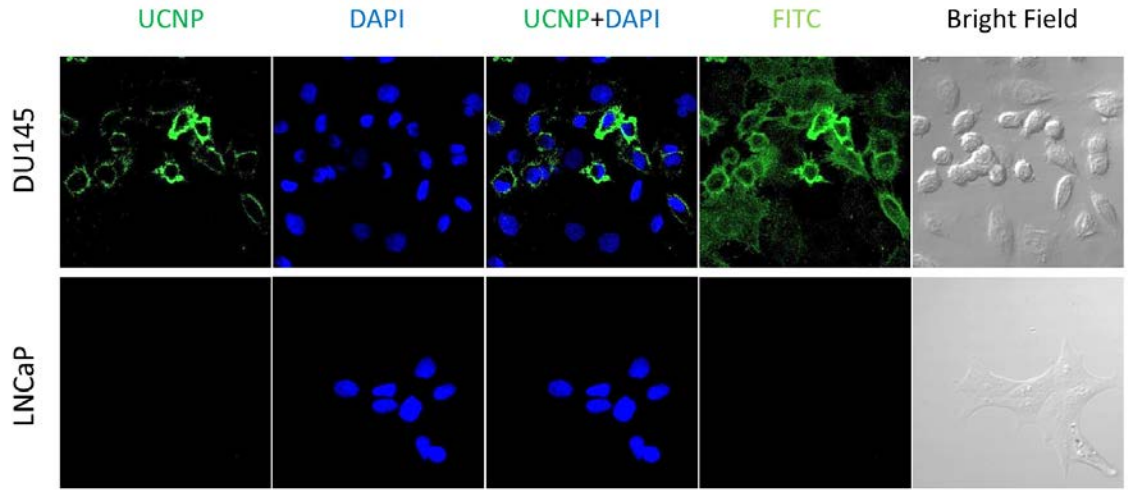

Figure 5.10 Confocal UCL imaging of MIL-38-PEG-UCNPs labeling on DU145 and LNCaP prostate cancer cells, respectively.

5.3.5 Water Stability, Optical Stability and Biocompatibility of MIL-38-PEG-UCNPs

After the PEG-Oxi-MIL-38 conjugated UCNPs were successfully achieved, the water solubility and stability in aqueous solutions is critical before utilizing in biological applications. The difference between good and poor water stability of UCNP-antibody conjugates can be easily compared. When MIL-38-UCNP sample aggregated, nanoparticles settled down to the bottom of the UCNP solution and emitted strong fluorescence under a NIR 980 nm laser; and the top layer of solution has undetectable fluorescence when giving the same excitation (**Figure 5.11**). UCNP antibody bioconjugated samples with perfect solubility and stability in aqueous solutions for enough time can be regarded as a powerful targeting probe for biological applications. DLS analysis served as a tool to monitor and evaluate the solubility and stability of MIL-38-PEG-UCNPs in different environments and times. The MIL-38-PEG-UCNPs exhibited good colloid stability in aqueous solutions (ultrapure water, PBS buffer and

DMEM cell culture medium with 10 (w/v) % FBS) without agglomeration and discernible settling for at least 24 h. DLS results displayed that the size distribution of MIL-38-PEG-UCNPs show no obvious change while dispersed in water, PBS and DMEM for 24 h (**Figure 5.12A**). The images of luminescence photographs of UCNP solution under 980 nm excitation also showed a corresponding result, in which the MIL-38-PEG-UCNPs were stable in the above solutions for 24 h and did not show obvious aggregation. A wide range of pHs in physiological buffer conditions were tested. MIL-38-PEG-UCNPs were dispersed in PBS at pHs from 4.0 to 9.0 for 1 h and the hydrodynamic diameters remained roughly unchanged (**Figure 5.12B**), indicating their great potential for biological applications in different physiological conditions.

The photostability of fluorescence probes is another critical issue for application of these probes. As show in **Figure 5.13**, the fluorescence images of traditional organic dyes (e.g. FITC conjugated MIL-38 antibody) and UCNPs (MIL-38-PEG-UCNPs) labeling on DU145 cells were compared. With continuous scanning mode and the same excitation power (20 mW) of a 473 nm and 980 nm laser for FITC and UCNPs respectively, images over different scanning times were acquired. The photostability of FITC is weak as the FITC fluorescence decreased significantly after laser scanning for 3 min (**Figure 5.13**, upper panel). On the contrary, the fluorescence intensity of UCNPs showed no obvious decrease after laser scanning for 60 min (**Figure 5.13**, lower panel), thus showing good photostability and indicating the bioapplication potential for long time imaging by UCNPs probes.

Furthermore, the cytotoxicity of MIL-38-PEG-UCNPs was evaluated by MTT assay (**Figure 5.14**). The viability of DU145 cells was approximately 90% even when cultured at a concentration of as high as 200 μg/mL after incubation for 48 h. From these results, MIL-38-PEG-UCNPs have good water stability, optical stability and

biocompatibility and hold great promise for biological applications.

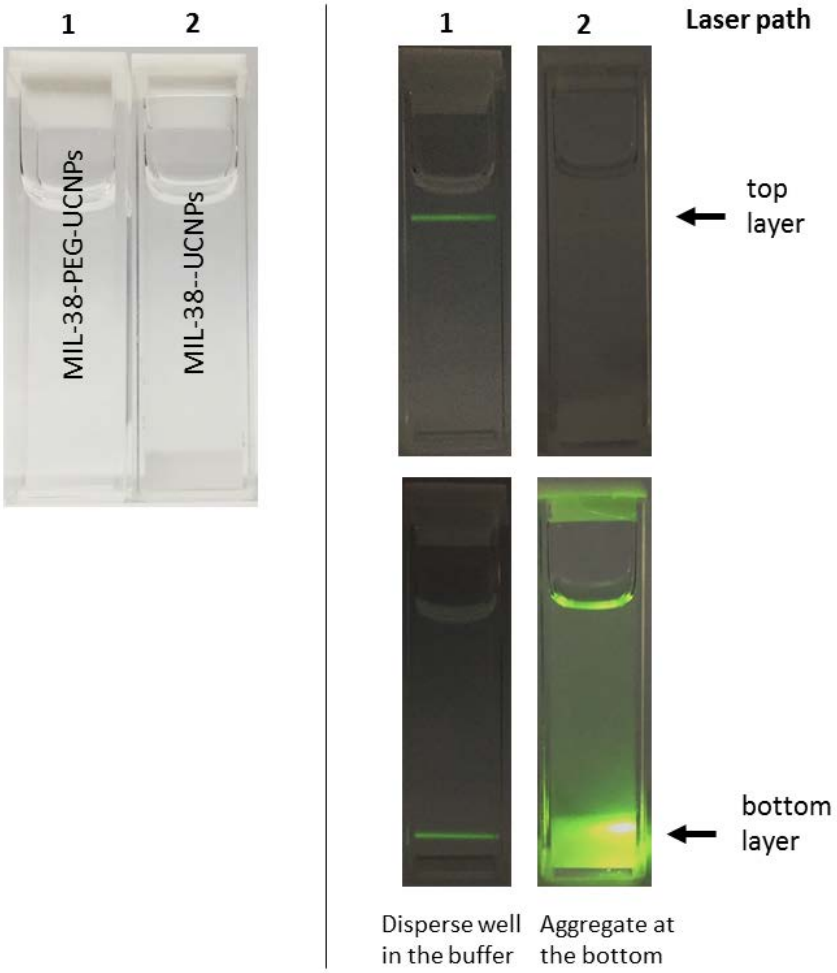

Figure 5.11 Comparison of aggregated MIL-38-UCNPs sample (2) and well-dispersed MIL-38-PEG-UCNPs (1) in PBS buffer. Bright-field photographs are compared in left panel. Luminescence photographs under 980 nm excitation are compared in right panel. Top and bottom layer of UCNP solution was excited by NIR laser respectively to visualize UCNP dispersion in PBS buffer.

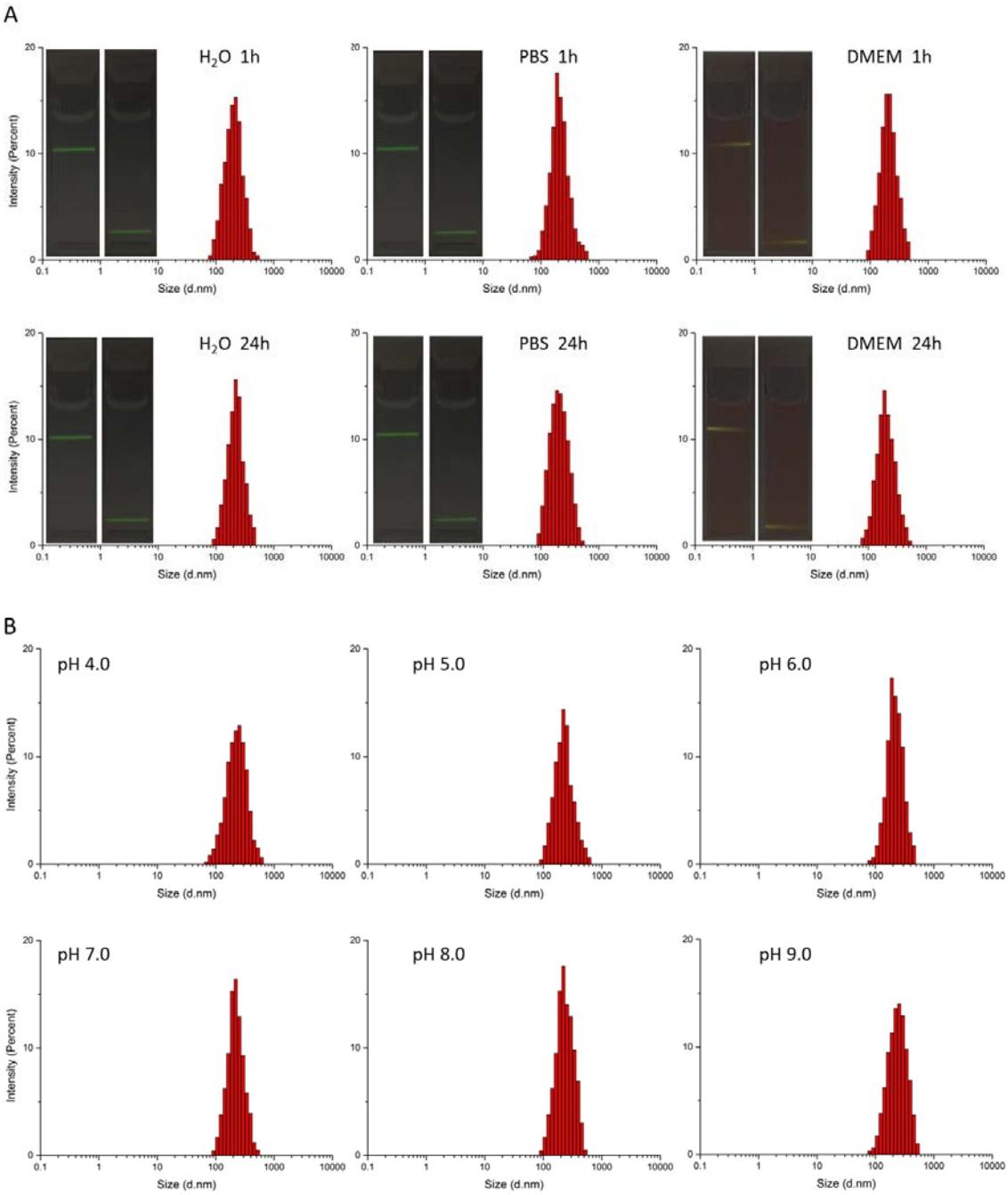

Figure 5.12 (A) The dynamic light scattering of PEGylated antibodies conjugated UCNPs dispersed in H_2O, PBS buffer and DMEM cell culture medium at 1 h and 24 h. Left panel in each diagram is luminescence photographs of PEGylated antibodies conjugated to UCNPs dispersed in H_2O, PBS and DMEM for 1 h and 24 h after preparation. The top layer and bottom layer are excited at 980 nm laser to monitor the emission water stability. (B) The dynamic light scattering of PEGylated antibodies

conjugated to UCNPs dispersed in PBS buffer at different pH from 4.0 to 9.0.

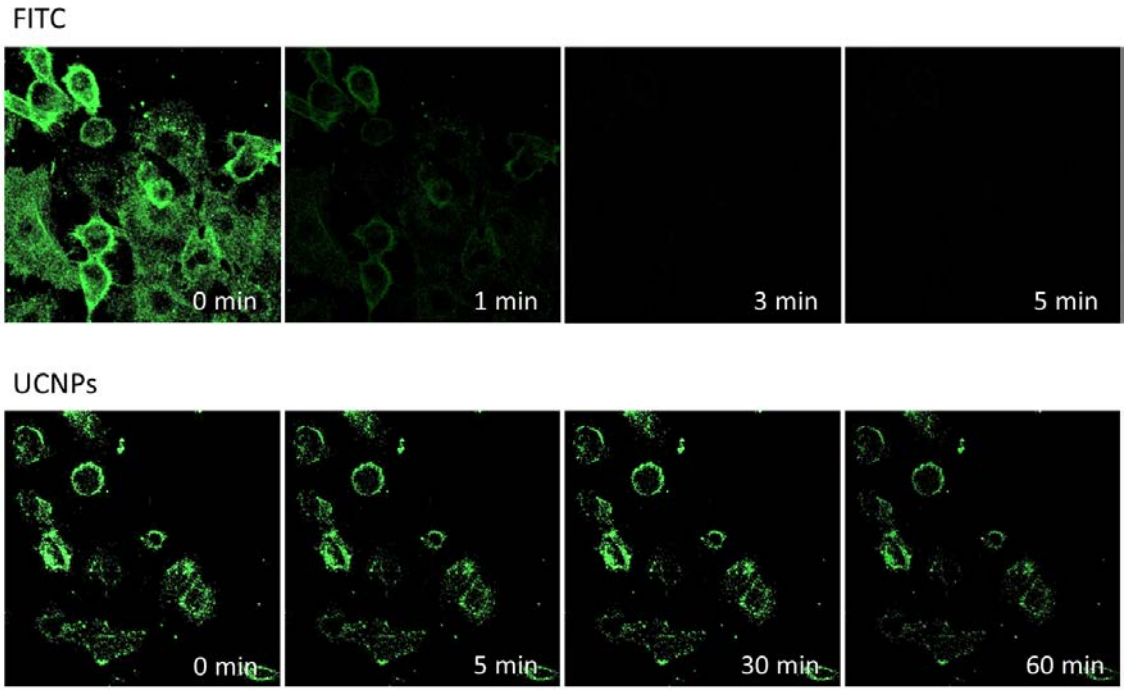

Figure 5.13 The comparison of photo-bleaching of fluorescence between FITC and UCNPs under the excitation of 473 nm (for FITC) and 980 nm (for UCNPs), respectively, with a continuous laser scanning mode. (A) The upper panel is the serial fluorescence imaging of FITC on DU145 cells with the scanning time. Green color represents green fluorescence from FITC. (B) The bottom panel is the serial fluorescence imaging of UCNPs on DU145 cells with the scanning time. Green color represents UCL signals from UCNPs.

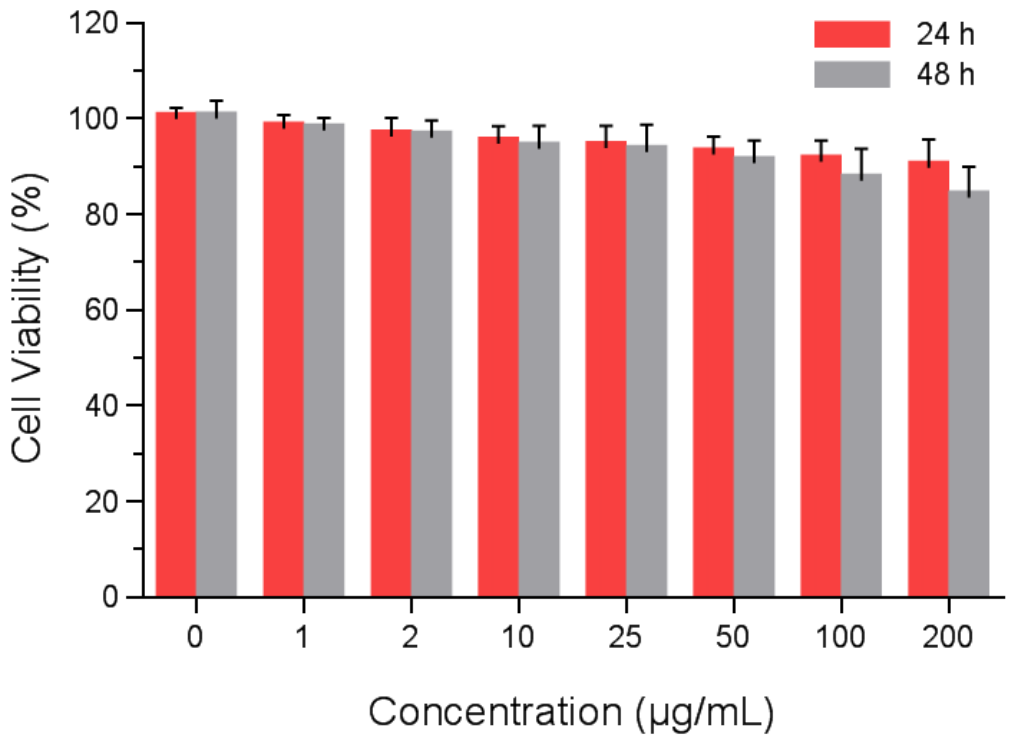

Figure 5.14 Cell Viability of DU145 cells in the presence of MIL-38-PEG-UCNPs with different concentration for 24 h and 48 h at 37 °C as measured by MTT assay.

5.4 Conclusions

In this chapter, the strategy which amino functionalizes UCNPs by direct conjugation to $NaIO_4$ oxidized oligosaccharides on IgG antibodies via reductive amination was initially carried out; however, low reproducibility, antibody inactivation and nanoparticle aggregation after conjugation restricted further applications. A new one-step strategy for the direct conjugation between UCNPs and antibody MIL-38 has been demonstrated here. By taking advantage of the $NOBF_4$ based UCNP ligand exchange approach as shown in Chapter 4 and by using the bifunctional PEG linker (HZ-PEG-PO_4), this strategy displays simplicity in a one-step conjugation process producing high stability of the antibody conjugated UCNPs and prevention of

agglomeration after reaction and in storage. More importantly, the specific conjugation site which is chosen at the oligosaccharides on the Fc constant region of the MIL-38 antibody was shown not to compromise the antigen-antibody binding ability and provided an orientation control of the UCNP-antibody conjugation. In addition, introducing the PEG linker to functionalize the MIL-38 antibody improved the physiological stability and added a spacer “arm” between the UCNPs and antibodies which could reduce any space steric-hindrance-effect. Thus, by applying such specific, orientation modified and biocompatible antibodies and one-step conjugation, this approach provides biologically active, highly water stable and reliable UCNP-antibody conjugate probes that give great promise in bioapplications such as immunolabeling and imaging.

Chapter 6: Conclusions and Future Perspectives

6.1 Conclusions

Studies focusing on upconversion nanoparticles (UCNPs)-based nanotechnology have been motivated by the requirement for overcoming some major limitations of the current detection techniques and facilitating the diagnosis of cancer at an early stage to save lives (see Chapter 1). The unique optical properties, such as anti-Stokes shift, non-photobleaching and long fluorescence lifetime, provide UCNPs with enhanced sensitivity as detection probes which is crucial for recognizing residual cancer cells in blood or circulating tumor cells (CTCs). However, most studies regarding application of UCNPs are still in proof-of-concept stage. Here I add to the advancement of the field by having developed reliable and effective UCNPs-based cancer targeting probes.

The studies in this dissertation mainly focus on developing UCNPs as fluorescent probes for the detection of cancer cells by confocal microscopy. To address the main goal, several critical steps were taken. First, preparation of uniform and monodispersed UCNPs is the basic requirement for the entire project. Second, a suitable and effective method for UCNP surface modification is required to successfully transfer hydrophobic UCNPs into hydrophilic ones. Third, improved design of UCNP-antibody conjugates is important to achieve water dispersible and bioactive UCNP targeting probes. The following paragraphs will outline the key accomplishments made in each step of this development process.

(1) $NaYF_4$ UCNPs co-doped with lanthanide ions Yb^{3+}/Er^{3+} and Yb^{3+}/Tm^{3+} were prepared by the thermal decomposition method. Using different times and

temperatures in the synthesis procedure, the size of UCNPs $NaYF_4$: Yb^{3+}/Er^{3+} can be tuned to range from 7 to 41 nm. The synthesized UCNPs were uniform and monodispersed under transmission electron microscopy (TEM) and exhibited strong visible fluorescence excited by 980 nm laser.

(2) A $NaYF_4$: Yb^{3+}/Er^{3+}@$NaGdF_4$ core-shell structure was obtained to enhance the upconversion luminescence (UCL) intensity by 3.5 times compared to $NaYF_4$: Yb^{3+}/Er^{3+}. This procedure can be applied when the confocal microscope setup is lacking power density.

(3) Seven surface modification approaches selected from highly cited literature were tested. These included ligand attraction by (a) α-cyclodextrin (α-CD) coating and (b) 1,2-distearoyl-sn-glycero-3-phosphoethanolamine-N-[carboxy(polyethylene glycol)-2000] (DSPE-PEG-COOH) coating; (c) ligand oxidation by Lemieux-von Rudloff reagent; (d) single-step ligand exchange by poly(acrylic acid) (PAA); two-step ligand exchange by $NOBF_4$ and other functional ligands (e, O-Phosphorylethanolamine and f, PO_4-PEG_{5000}-COOH) and (g) surface silanization. Among these well-investigated approaches, the two-step ligand exchange strategy by $NOBF_4$ and OPEA/PO_4-PEG_{5000}-COOH was proven to be a good choice. Oleic acid (OA)-capped UCNPs modified with $NOBF_4$ and OPEA/PO_4-PEG_{5000}-COOH showed good water dispersibility and stability, exhibited strong UCL emission intensity and displayed a clean background in fluorescence signal detection in near infrared (NIR) laser confocal microscopy. The absence of detectable non-specific binding and aggregation of the surface modified UCNPs developed in this work in a cell-based assay has opened an opportunity for further functionalization of the nanoparticles with specific targeting molecules in various bioapplications.

(4) UCNP streptavidin (SA) conjugates were successfully prepared by ligand exchange-based method. Unlike the other bioconjugation strategies which use covalent bonds (e.g. EDC/NHS chemistry), this conjugation design introduced a multifunctional PEG linker PO_4-PEG_{5000}-COOH to modify the SA prior to interact with the $NOBF_4$ treated UCNPs through a ligand exchange manner. The SA-UCNP conjugates were shown to be stable in water, PBS buffer and the DMEM cell culture medium for at least 24 h; they were also well dispersed on a large pH range (4.0 to 9.0) in PBS buffer for 1 h without detectable agglomeration. Conjugation of the antibody MIL-38 to the SA conjugated UCNPs was performed via biotin-SA interaction system to obtain the upconversion immune-nanohybrids (UINBs). Besides the optical stability and non-toxicity, UINBs displayed highly specific targeting capability in detecting prostate cancer cells DU145 in an immunofluorescence assay (IFA) without non-specific binding.

(5) A site-directed strategy was used to conjugate UCNPs to the antibody MIL-38. Bifuncitonal PEG linker Hydrazide-PEG-Phosphate (HZ-PEG-PO_4) was introduced to covalently bind to the oxidized polysaccharide residues on the Fc region of MIL-38 antibodies. The PEGylated MIL-38 was then conjugated to $NOBF_4$ modified UCNPs via a ligand exchange. This orientation-controlled binding allowed maximum exposure of the MIL-38 epitopes to the antigen on the surface of DU145 prostate cancer cells. In comparison with the traditional MIL-38-UCNP conjugation through covalent bonding and without the PEG spacer arm, the new MIL-38-PEG-UCNP conjugates exhibited good water dispersibility and stability in aqueous environment (water, PBS and DMEM) and at different pH (4.0 to 9.0). Differently to the IFA with MIL-38-UCNP conjugates that showed non-specific binding, the MIL-38-PEG-UCNP complex can be used to specifically target to DU145 cells without obvious non-specific binding.

6.2 Future Perspectives

In this dissertation, the successful construction of reliable and effective UCNP-antibody targeting probes has proven to be a robust tool to specifically detect cancer cells. However, a number of additional improvements will need to be accomplished in this UCNP-based detection technique as discussed below.

Conjugation of UCNPs with biomolecules is still at the forefront of the UCNP research. After studies into specific targeting of cancer cells with UCNP-antibody conjugates *in vitro*, UCNP-antibody conjugates will be used for *in vivo* tumor tissue imaging, as therapy agents and for drug delivery due to their deep penetration of the tissue and relatively low toxicity. The *in vivo* experiments require UCNP-antibody conjugates with higher stability and bioactivity to survive and function in the more complicated and "rigorous" internal environment of animals or the human body. However, studies showing successful targeting of the tumor tissue with UCNP-antibody conjugates in small animal models have rarely been reported. Thus, more studies on the conjugation of UCNPs to antibodies are still needed.

In addition, if the UCNP-antibody conjugates are expected to be used *in vivo*, the cytotoxicity and biodistribution of UCNPs also need to be studied in-depth. Although many studies claim non-toxicity or low toxicity of UCNPs, no consensus has been reached by these reports so more comprehensive studies are required. In terms of the UCNP *in vivo* distribution, the long term fate of UCNPs circulating in biofluids is still unknown despite UCNPs have been reported to be biocompatible and readily clear from the body. Therefore, the toxicity and biodistribution studies may be the further directions in this field.

Finally, to facilitate cancer diagnosis at an early stage, particularly in the screening of CTCs or prostate cancer cells in urine, trace amounts of abnormal cells in large sample volumes must be detected sensitively and rapidly. The CTCs or residual cancer cells in blood only occur at frequencies on the order of 1-10 CTCs per mL of whole blood that contains a billion red blood cells and a few million white blood cells in patients with metastatic disease. In some cases, ten cells or even less need to be found in 10 mL of biofluids (e.g. blood, urine, saliva and latex) for useful diagnosis and current tests frequently lack the sensitivity and selectivity required for the detection. Ultrasensitivity of UCNP-based detection probes can be obtained, on one hand, by the unique property of the anti-Stokes shift which eliminates the background noise originating from the test sample. On the other hand, their long lifetime, which extends the emission period by the order of tens of microseconds, provides an opportunity for time-gated detection to remove autofluorescence and excitation scattering. Combined with NIR excitation and time-gated detection, a background-free detection probe can be used to capture rare-event cancer cells in blood or urine samples. As microscopy cannot screen cancer cells in large sample volumes, a high throughput detection technique is also needed to facilitate the diagnostic procedure. A flow cytometer equipped with a 980 nm laser and time-gated instrument could bring about enhanced detection speed for rapid cancer screening. Therefore, a novel cancer detection method should simultaneously satisfy the sensitivity requirement by minimizing the background noise and detection speed to handle a large quantity of samples. To achieve this ultimate goal, successful construction a water dispersible, stable, bioactive UCNP-antibody conjugates with non-specific binding has just begun.

References

Agrawal P., G. J. Strijkers and K. Nicolay 2010. Chitosan-based systems for molecular imaging. Advanced Drug Delivery Reviews 62(1): 42-58.

Ai Y., D. Tu, W. Zheng, et al. 2013. Lanthanide-doped NaScF 4 nanoprobes: crystal structure, optical spectroscopy and biodetection. Nanoscale 5(14): 6430-6438.

Akers W. J., M. Y. Berezin, H. Lee, et al. 2010. Biological applications of fluorescence lifetime imaging beyond microscopy. BiOS, International Society for Optics and Photonics.

Alazemi A. M. 2014. Effect of metal coating on NaYF4: Yb3+, Tm3+ upconversion nanoparticles, University of Cincinnati.

Alford R., H. M. Simpson, J. Duberman, et al. 2009. Toxicity of organic fluorophores used in molecular imaging: literature review. Molecular Imaging 8(6): 341-354.

Alitalo A. and M. Detmar 2012. Interaction of tumor cells and lymphatic vessels in cancer progression. Oncogene 31(42): 4499-4508.

Alivisatos A. P., W. Gu and C. Larabell 2005. Quantum dots as cellular probes. Annu. Reviews of Biomedical Engineering 7: 55-76.

Alok A., S. Panat, A. Aggarwal, et al. 2013. Nanotechnology: A boon in oral cancer diagnosis and therapeutics. SRM Journal of Research in Dental Sciences 4(4): 154.

Altinoglu E. I., T. J. Russin, J. M. Kaiser, et al. 2008. Near-infrared emitting fluorophore-doped calcium phosphate nanoparticles for in vivo imaging of human breast cancer. Acs Nano 2(10): 2075-2084.

Anker J. N., W. P. Hall, O. Lyandres, et al. 2008. Biosensing with plasmonic nanosensors. Nature materials 7(6): 442-453.

Backman V., M. Wallace, L. Perelman, et al. 2000. Detection of preinvasive cancer cells. Nature 406(6791): 35-36.

Bagwe R. P., L. R. Hilliard and W. Tan 2006. Surface modification of silica nanoparticles to reduce aggregation and nonspecific binding. Langmuir 22(9): 4357-4362.

Bangham A. D. and R. Horne 1964. Negative staining of phospholipids and their structural modification by surface-active agents as observed in the electron microscope. Journal of Molecular Biology 8(5): 660IN662-668IN610.

Bao Y., Q. A. N. Luu, C. Lin, et al. 2010. Layer-by-layer assembly of freestanding thin films with homogeneously distributed upconversion nanocrystals. Journal of Materials Chemistry 20(38): 8356-8361.

Barreto J. A., W. O'Malley, M. Kubeil, et al. 2011. Nanomaterials: applications in cancer imaging and therapy. Advanced Materials 23(12).

Begent R., M. Verhaar, K. Chester, et al. 1996. Clinical evidence of efficient tumor targeting based on single-chain Fv antibody selected from a combinatorial library. Nature Medicine 2(9): 979-984.

Benyettou F., J. Hardouin, M. Lecovey, et al. 2012. PEGylated versus non-PEGylated γ Fe2O3@ alendronate nanoparticles. Journal of Bioanalysis & Biomedicine 4: 039-045.

Berezin M. Y. and S. Achilefu 2010. Fluorescence lifetime measurements and biological imaging. Chemical Reviews 110(5): 2641-2684.

Bertrand N., J. Wu, X. Xu, et al. 2014. Cancer nanotechnology: the impact of passive and active targeting in the era of modern cancer biology. Advanced Drug Delivery Reviews 66: 2-25.

Bharali D. J., I. Klejbor, E. K. Stachowiak, et al. 2005. Organically modified silica

nanoparticles: a nonviral vector for in vivo gene delivery and expression in the brain. Proceedings of the National Academy of Sciences of the United States of America 102(32): 11539-11544.

Bogdan N., E. M. Rodríguez, F. Sanz-Rodríguez, et al. 2012. Bio-functionalization of ligand-free upconverting lanthanide doped nanoparticles for bio-imaging and cell targeting. Nanoscale 4(12): 3647-3650.

Bogdan N., F. Vetrone, G. A. Ozin, et al. 2011. Synthesis of ligand-free colloidally stable water dispersible brightly luminescent lanthanide-doped upconverting nanoparticles. Nano Letters 11(2): 835-840.

Bogdan N., F. Vetrone, R. Roy, et al. 2010. Carbohydrate-coated lanthanide-doped upconverting nanoparticles for lectin recognition. Journal of Materials Chemistry 20(35): 7543-7550.

Boyer J. C., M. P. Manseau, J. I. Murray, et al. 2009. Surface modification of upconverting NaYF4 nanoparticles with PEG-phosphate ligands for NIR (800 nm) biolabeling within the biological window. Langmuir 26(2): 1157-1164.

Boyer J. C., F. Vetrone, L. A. Cuccia, et al. 2006. Synthesis of colloidal upconverting NaYF4 nanocrystals doped with Er3+, Yb3+ and Tm3+, Yb3+ via thermal decomposition of lanthanide trifluoroacetate precursors. Journal of the American Chemical Society 128(23): 7444-7445.

Budd G. T., M. Cristofanilli, M. J. Ellis, et al. 2006. Circulating tumor cells versus imaging-predicting overall survival in metastatic breast cancer. Clinical Cancer Research 12(21): 6403-6409.

Budijono S. J., J. Shan, N. Yao, et al. 2009. Synthesis of stable block-copolymer-protected NaYF4: Yb3+, Er3+ up-converting phosphor nanoparticles. Chemistry of Materials 22(2): 311-318.

Burda C., X. B. Chen, R. Narayanan, et al. 2005. Chemistry and properties of nanocrystals of different shapes. Chemical Reviews 105(4): 1025-1102.

Cai W., T. Gao, H. Hong, et al. 2008. Applications of gold nanoparticles in cancer nanotechnology. Nanotechnology, Science and Applications 2008(1).

Cao T., T. Yang, Y. Gao, et al. 2010. Water-soluble NaYF 4: Yb/Er upconversion nanophosphors: Synthesis, characteristics and application in bioimaging. Inorganic Chemistry Communications 13(3): 392-394.

Cao T., Y. Yang, Y. Gao, et al. 2011. High-quality water-soluble and surface-functionalized upconversion nanocrystals as luminescent probes for bioimaging. Biomaterials 32(11): 2959-2968.

Carter P. J. 2006. Potent antibody therapeutics by design. Nature Reviews Immunology 6(5): 343-357.

Carter T., K. Sterling-Levis, K. Ow, et al. 2004. Biodistributions of intact monoclonal antibodies and fragments of BLCA-38, a new prostate cancer directed antibody. Cancer Immunology, Immunotherapy 53(6): 533-542.

Cazalis C. S., C. A. Haller, L. Sease-Cargo, et al. 2004. C-terminal site-specific PEGylation of a truncated thrombomodulin mutant with retention of full bioactivity. Bioconjugate Chemistry 15(5): 1005-1009.

Cen Y., Y. M. Wu, X. J. Kong, et al. 2014. Phospholipid-modified upconversion nanoprobe for ratiometric fluorescence detection and imaging of phospholipase D in cell lysate and in living cells. Analytical Chemistry 86(14): 7119-7127.

Chan W. C. W. and S. M. Nie 1998. Quantum dot bioconjugates for ultrasensitive nonisotopic detection. Science 281(5385): 2016-2018.

Chatterjee D. K., A. J. Rufaihah and Y. Zhang 2008. Upconversion fluorescence imaging of cells and small animals using lanthanide doped nanocrystals.

Biomaterials 29(7): 937-943.

Chen G., H. Liu, H. Liang, et al. 2008. Upconversion emission enhancement in Yb3+/Er3+-codoped Y2O3 nanocrystals by tridoping with Li+ ions. The Journal of Physical Chemistry C 112(31): 12030-12036.

Chen G., T. Y. Ohulchanskyy, R. Kumar, et al. 2010. Ultrasmall monodisperse NaYF4: Yb3+/Tm3+ nanocrystals with enhanced near-infrared to near-infrared upconversion photoluminescence. ACS Nano 4(6): 3163-3168.

Chen G., T. Y. Ohulchanskyy, W. C. Law, et al. 2011. Monodisperse NaYbF 4: Tm 3+/NaGdF 4 core/shell nanocrystals with near-infrared to near-infrared upconversion photoluminescence and magnetic resonance properties. Nanoscale 3(5): 2003-2008.

Chen G., H. Qiu, P. N. Prasad, et al. 2014. Upconversion nanoparticles: design, nanochemistry, and applications in theranostics. Chemical Reviews 114(10): 5161-5214.

Chen H., Y. Guan, S. Wang, et al. 2014. Turn-on detection of a cancer marker based on near-infrared luminescence energy transfer from NaYF4: Yb, Tm/NaGdF4 core-shell upconverting nanoparticles to gold nanorods. Langmuir 30(43): 13085-13091.

Chen H., F. Yuan, S. Wang, et al. 2013. Aptamer-based sensing for thrombin in red region via fluorescence resonant energy transfer between NaYF 4: Yb, Er upconversion nanoparticles and gold nanorods. Biosensors and Bioelectronics 48: 19-25.

Chen H., Z. Zhen, W. Tang, et al. 2013. Label-free luminescent mesoporous silica nanoparticles for imaging and drug delivery. Theranostics 3(9): 650.

Chen J., C. R. Guo, M. Wang, et al. 2011. Controllable synthesis of NaYF4 : Yb,Er

upconversion nanophosphors and their application to in vivo imaging of Caenorhabditis elegans. Journal of Materials Chemistry 21(8): 2632-2638.

Chen Q., X. Wang, F. Chen, et al. 2011. Functionalization of upconverted luminescent NaYF4: Yb/Er nanocrystals by folic acid–chitosan conjugates for targeted lung cancer cell imaging. Journal of Materials Chemistry 21(21): 7661-7667.

Chen W. 2008. Nanoparticle fluorescence based technology for biological applications. Journal of Nanoscience and Nanotechnology 8(3): 1019-1051.

Chen Y. Y., P. A. Ma, D. M. Yang, et al. 2014. Multifunctional core-shell structured nanocarriers for synchronous tumor diagnosis and treatment in vivo. Chemistry-an Asian Journal 9(2): 506-513.

Chen Z., H. Chen, H. Hu, et al. 2008. Versatile synthesis strategy for carboxylic acid-functionalized upconverting nanophosphors as biological labels. Journal of the American Chemical Society 130(10): 3023-3029.

Cheng L., C. Wang and Z. Liu 2013. Upconversion nanoparticles and their composite nanostructures for biomedical imaging and cancer therapy. Nanoscale 5(1): 23-37.

Cheng L., K. Yang, Y. G. Li, et al. 2011. Facile preparation of multifunctional upconversion nanoprobes for multimodal imaging and dual-targeted photothermal therapy. Angewandte Chemie-International Edition 50(32): 7385-7390.

Cheng L., K. Yang, Y. G. Li, et al. 2012. Multifunctional nanoparticles for upconversion luminescence/MR multimodal imaging and magnetically targeted photothermal therapy. Biomaterials 33(7): 2215-2222.

Cheng L., K. Yang, M. Shao, et al. 2011. Multicolor in vivo imaging of upconversion nanoparticles with emissions tuned by luminescence resonance energy transfer.

The Journal of Physical Chemistry C 115(6): 2686-2692.

Cheng L., K. Yang, S. Zhang, et al. 2010. Highly-sensitive multiplexed in vivo imaging using PEGylated upconversion nanoparticles. Nano Research 3(10): 722-732.

Chien Y. H., Y. L. Chou, S. W. Wang, et al. 2013. Near-infrared light photocontrolled targeting, bioimaging, and chemotherapy with caged upconversion nanoparticles in vitro and in vivo. ACS Nano 7(10): 8516-8528.

Chikkaveeraiah B. V., A. A. Bhirde, N. Y. Morgan, et al. 2012. Electrochemical Immunosensors for Detection of Cancer Protein Biomarkers. ACS Nano 6(8): 6546-6561.

Cho K., X. Wang, S. Nie, et al. 2008. Therapeutic nanoparticles for drug delivery in cancer. Clinical Cancer Research 14(5): 1310-1316.

Choi K. Y., K. H. Min, H. Y. Yoon, et al. 2011. PEGylation of hyaluronic acid nanoparticles improves tumor targetability in vivo. Biomaterials 32(7): 1880-1889.

Choi Y. E., J. W. Kwak and J. W. Park 2010. Nanotechnology for early cancer detection. Sensors 10(1): 428-455.

Collins F. S. and H. Varmus 2015. A new initiative on precision medicine. New England Journal of Medicine 372(9): 793-795.

Crawley A. S. and R. J. O'Kennedy 2015. The need for effective pancreatic cancer detection and management: a biomarker-based strategy. Expert Review of Molecular Diagnostics 15(10): 1339-1353.

Cristofanilli M., D. F. Hayes, G. T. Budd, et al. 2005. Circulating tumor cells: a novel prognostic factor for newly diagnosed metastatic breast cancer. Journal of Clinical Oncology 23(7): 1420-1430.

DaCosta M. V., S. Doughan, Y. Han, et al. 2014. Lanthanide upconversion nanoparticles and applications in bioassays and bioimaging: A review. Analytica Chimica Acta 832: 1-33.

Dai Y., D. Yang, X. Kang, et al. 2012. Doxorubicin conjugated NaYF 4: Yb 3+/Tm 3+ nanoparticles for therapy and sensing of drug delivery by luminescence resonance energy transfer. Biomaterials 33(33): 8704-8713.

Danhier F., O. Feron and V. Préat 2010. To exploit the tumor microenvironment: passive and active tumor targeting of nanocarriers for anti-cancer drug delivery. Journal of Controlled Release 148(2): 135-146.

Dayaker G., T. Durand and L. Balas 2014. A versatile and stereocontrolled total synthesis of dihydroxylated docosatrienes containing a conjugated E, E, Z-triene. Chemistry–A European Journal 20(10): 2879-2887.

Deng R., X. Xie, M. Vendrell, et al. 2011. Intracellular glutathione detection using MnO2-nanosheet-modified upconversion nanoparticles. Journal of the American Chemical Society 133(50): 20168-20171.

DeSantis C. E., C. C. Lin, A. B. Mariotto, et al. 2014. Cancer treatment and survivorship statistics, 2014. CA: A Cancer Journal for Clinicians 64(4): 252-271.

Devi R. V., M. Doble and R. S. Verma 2015. Nanomaterials for early detection of cancer biomarker with special emphasis on gold nanoparticles in immunoassays/sensors. Biosensors & Bioelectronics 68: 688-698.

Dong A., X. Ye, J. Chen, et al. 2010. A generalized ligand-exchange strategy enabling sequential surface functionalization of colloidal nanocrystals. Journal of the American Chemical Society 133(4): 998-1006.

Dong B., S. Xu, J. Sun, et al. 2011. Multifunctional NaYF4: Yb 3+, Er 3+@ Ag

core/shell nanocomposites: integration of upconversion imaging and photothermal therapy. Journal of Materials Chemistry 21(17): 6193-6200.

Dong C., A. Korinek, B. Blasiak, et al. 2012. Cation exchange: a facile method to make NaYF4: Yb, Tm-NaGdF4 core–shell nanoparticles with a thin, tunable, and uniform shell. Chemistry of Materials 24(7): 1297-1305.

Duan N., S. Wu, C. Zhu, et al. 2012. Dual-color upconversion fluorescence and aptamer-functionalized magnetic nanoparticles-based bioassay for the simultaneous detection of salmonella typhimurium and staphylococcus aureus. Analytica Chimica Acta 723: 1-6.

Ehdaie B. 2007. Application of nanotechnology in cancer research: review of progress in the National Cancer Institute's Alliance for Nanotechnology. International Journal of Biological Sciences 3(2): 108-110.

Faure A. C., C. Hoffmann, R. Bazzi, et al. 2008. Functionalization of luminescent aminated particles for facile bioconjugation. ACS Nano 2(11): 2273-2282.

Fedoryshin L. L., A. J. Tavares, E. Petryayeva, et al. 2014. Near-infrared-triggered anticancer drug release from upconverting nanoparticles. Acs Applied Materials & Interfaces 6(16): 13600-13606.

Ferrari M. 2005. Cancer nanotechnology: Opportunities and challenges. Nature Reviews Cancer 5(3): 161-171.

Fletcher J. 1971. The plasma clearance and liver uptake of iron from transferrin of low and high iron saturation. Clinical Science 41(5): 395-402.

Gatter K. C., G. Brown, I. Trowbridge, et al. 1983. Transferrin receptors in human tissues: their distribution and possible clinical relevance. Journal of Clinical Pathology 36(5): 539-545.

Giljohann D. A., D. S. Seferos, W. L. Daniel, et al. 2010. Gold nanoparticles for biology

and medicine. Angewandte Chemie International Edition 49(19): 3280-3294.

Gnach A. and A. Bednarkiewicz 2012. Lanthanide-doped up-converting nanoparticles: Merits and challenges. Nano Today 7(6): 532-563.

Gu Z., L. Yan, G. Tian, et al. 2013. Recent advances in design and fabrication of upconversion nanoparticles and their safe theranostic applications. Advanced Materials 25(28): 3758-3779.

Haase M. and H. Schäfer 2011. Upconverting nanoparticles. Angewandte Chemie International Edition 50(26): 5808-5829.

Hanahan D. and R. A. Weinberg 2000. The hallmarks of cancer. Cell 100(1): 57-70.

Hanahan D. and R. A. Weinberg 2011. Hallmarks of cancer: the next generation. Cell 144(5): 646-674.

Hardman R. 2006. A toxicologic review of quantum dots: toxicity depends on physicochemical and environmental factors. Environmental Health Perspectives: 165-172.

Haun J. B., N. K. Devaraj, S. A. Hilderbrand, et al. 2010. Bioorthogonal chemistry amplifies nanoparticle binding and enhances the sensitivity of cell detection. Nature Nanotechnology 5(9): 660-665.

Hayat M. 2008. Methods of Cancer Diagnosis, Therapy and Prognosis: General Methods and Overviews, Lung Carcinoma and Prostate Carcinoma, Springer Science & Business Media.

Hayes D. F., M. Cristofanilli, G. T. Budd, et al. 2006. Circulating tumor cells at each follow-up time point during therapy of metastatic breast cancer patients predict progression-free and overall survival. Clinical Cancer Research 12(14): 4218-4224.

He M. and Z. Liu 2013. Paper-based microfluidic device with upconversion fluorescence assay. Analytical Chemistry 85(24): 11691-11694.

He X. X., K. M. Wang and Z. Cheng 2010. In vivo near-infrared fluorescence imaging of cancer with nanoparticle-based probes. Wiley Interdisciplinary Reviews-Nanomedicine and Nanobiotechnology 2(4): 349-366.

Hermanson G. T. 2013. Bioconjugate techniques, Academic Press.

Higgins M. J. and D. S. Ettinger 2009. Chemotherapy for lung cancer: the state of the art in 2009. Expert Review of Anticancer Therapy 9(10): 1365-1378.

Hlavacek A., A. Sedlmeier, P. Skládal, et al. 2014. Electrophoretic characterization and purification of silica-coated photon-upconverting nanoparticles and their bioconjugates. Acs Applied Materials & Interfaces 6(9): 6930-6935.

Hoffman R. M. 2005. The multiple uses of fluorescent proteins to visualize cancer in vivo. Nature Reviews Cancer 5(10): 796-806.

Homola J. 2008. Surface plasmon resonance sensors for detection of chemical and biological species. Chemical Reviews 108(2): 462-493.

Hu H., Z. Chen, T. Cao, et al. 2008. Hydrothermal synthesis of hexagonal lanthanide-doped LaF3 nanoplates with bright upconversion luminescence. Nanotechnology 19(37): 375702.

Hu H., L. Xiong, J. Zhou, et al. 2009. Multimodal-luminescence core-shell nanocomposites for targeted imaging of tumor cells. Chemistry–A European Journal 15(14): 3577-3584.

Hu H., M. Yu, F. Li, et al. 2008. Facile epoxidation strategy for producing amphiphilic up-converting rare-earth nanophosphors as biological labels. Chemistry of Materials 20(22): 7003-7009.

Huang P., D. Tu, W. Zheng, et al. 2015. Inorganic lanthanide nanoprobes for background-free luminescent bioassays. Science China Materials 58(2): 156-177.

Huang P., W. Zheng, S. Zhou, et al. 2014. Lanthanide-doped LiLuF4 upconversion nanoprobes for the detection of disease biomarkers. Angewandte Chemie International Edition 53(5): 1252-1257.

Huang X., P. K. Jain, I. H. El-Sayed, et al. 2007. Gold nanoparticles: interesting optical properties and recent applications in cancer diagnostics and therapy. Nanomedicine 2(5): 681-693.

Hutter E. and J. H. Fendler 2004. Exploitation of localized surface plasmon resonance. Advanced Materials 16(19): 1685-1706.

Idris N. M., M. K. Gnanasammandhan, J. Zhang, et al. 2012. In vivo photodynamic therapy using upconversion nanoparticles as remote-controlled nanotransducers. Nature Medicine 18(10): 1580-1585.

Ito A., M. Shinkai, H. Honda, et al. 2005. Medical application of functionalized magnetic nanoparticles. Journal of Bioscience and Bioengineering 100(1): 1-11.

Jain K. K. 2007. Applications of nanobiotechnology in clinical diagnostics. Clinical Chemistry 53(11): 2002-2009.

Jain P. K., X. Huang, I. H. El-Sayed, et al. 2008. Noble metals on the nanoscale: optical and photothermal properties and some applications in imaging, sensing, biology, and medicine. Accounts of Chemical Research 41(12): 1578-1586.

Jaiswal J. K. and S. M. Simon 2004. Potentials and pitfalls of fluorescent quantum dots for biological imaging. Trends in Cell Biology 14(9): 497-504.

Jalil R. A. and Y. Zhang 2008. Biocompatibility of silica coated NaYF 4 upconversion fluorescent nanocrystals. Biomaterials 29(30): 4122-4128.

Jameson J. L. and D. L. Longo 2015. Precision medicine-personalized, problematic, and promising. New England Journal of Medicine 372(23): 2229-2234.

Jares-Erijman E. A. and T. M. Jovin 2003. FRET imaging. Nature Biotechnology 21(11): 1387-1395.

Jiang G., J. Pichaandi, N. J. Johnson, et al. 2012. An effective polymer cross-linking strategy to obtain stable dispersions of upconverting NaYF4 nanoparticles in buffers and biological growth media for biolabeling applications. Langmuir 28(6): 3239-3247.

Jiang S., K. Y. Win, S. Liu, et al. 2013. Surface-functionalized nanoparticles for biosensing and imaging-guided therapeutics. Nanoscale 5(8): 3127-3148.

Jiang S., Y. Zhang, K. M. Lim, et al. 2009. NIR-to-visible upconversion nanoparticles for fluorescent labeling and targeted delivery of siRNA. Nanotechnology 20(15): 155101.

Johnson N. J., N. M. Sangeetha, J.-C. Boyer, et al. 2010. Facile ligand-exchange with polyvinylpyrrolidone and subsequent silica coating of hydrophobic upconverting β-NaYF 4: Yb3+/Er3+ nanoparticles. Nanoscale 2(5): 771-777.

Ju Q., D. Tu, Y. Liu, et al. 2011. Amine-functionalized lanthanide-doped KGdF4 nanocrystals as potential optical/magnetic multimodal bioprobes. Journal of the American Chemical Society 134(2): 1323-1330.

Juan J., L. Cheng, M. Shi, et al. 2015. Poly-(allylamine hydrochloride)-coated but not poly (acrylic acid)-coated upconversion nanoparticles induce autophagy and apoptosis in human blood cancer cells. Journal of Materials Chemistry B 3(28): 5769-5776.

Kairdolf B. A., A. M. Smith, T. H. Stokes, et al. 2013. Semiconductor Quantum Dots for Bioimaging and Biodiagnostic Applications. Annual Review of Analytical

Chemistry, Vol 6. R. G. Cooks and J. E. Pemberton. Palo Alto, Annual Reviews. 6**:** 143-162.

Kelly K. L., E. Coronado, L. L. Zhao, et al. 2003. The optical properties of metal nanoparticles: the influence of size, shape, and dielectric environment. The Journal of Physical Chemistry B 107(3): 668-677.

Khatri A., T. Ho, L. Lindholm, et al. 2010. Promise of BLCA-38 as a targeting antibody for tissue specific gene delivery to prostate cancer. Austral - Asian Journal of Cancer 9(3): 195-203.

Kim W. J., M. Nyk and P. N. Prasad 2009. Color-coded multilayer photopatterned microstructures using lanthanide (III) ion co-doped NaYF4 nanoparticles with upconversion luminescence for possible applications in security. Nanotechnology 20(18): 185301.

Kobayashi H., M. Ogawa, R. Alford, et al. 2009. New strategies for fluorescent probe design in medical diagnostic imaging. Chemical Reviews 110(5): 2620-2640.

Kodama R. 1999. Magnetic nanoparticles. Journal of Magnetism and Magnetic Materials 200(1): 359-372.

Kumar C. S. 2005. Biofunctionalization of nanomaterials. Biofunctionalization of Nanomaterials, by Challa SSR Kumar (Editor), pp. 377. ISBN 3-527-31381-8. Wiley-VCH, November 2005. 1.

Kumar R., M. Nyk, T. Y. Ohulchanskyy, et al. 2009. Combined optical and MR bioimaging using rare earth ion doped NaYF4 nanocrystals. Advanced Functional Materials 19(6): 853-859.

Kumar S., J. Aaron and K. Sokolov 2008. Directional conjugation of antibodies to nanoparticles for synthesis of multiplexed optical contrast agents with both delivery and targeting moieties. Nature Protocol 3(2): 314-320.

Lee J., T. S. Lee, J. Ryu, et al. 2013. RGD Peptide-Conjugated Multimodal NaGdF4:Yb3+/Er3+ Nanophosphors for Upconversion Luminescence, MR, and PET Imaging of Tumor Angiogenesis. Journal of Nuclear Medicine 54(1): 96-103.

Lee J., T. S. Lee, J. Ryu, et al. 2013. RGD peptide–conjugated multimodal NaGdF4: Yb3+/Er3+ nanophosphors for upconversion luminescence, MR, and PET imaging of tumor angiogenesis. Journal of Nuclear Medicine 54(1): 96-103.

Li L. and Y. Lu 2013. Functional DNA-Integrated Nanomaterials for Biosensing. DNA Nanotechnology, Springer**:** 277-305.

Li L. L. and Y. Lu 2015. Regiospecific hetero-assembly of DNA-functionalized plasmonic upconversion superstructures. Journal of the American Chemical Society 137(16): 5272-5275.

Li L. L., R. Zhang, L. Yin, et al. 2012. Biomimetic surface engineering of lanthanide-doped upconversion nanoparticles as versatile bioprobes. Angewandte Chemie 124(25): 6225-6229.

Li X. M., F. Zhang and D. Y. Zhao 2015. Lab on upconversion nanoparticles: optical properties and applications engineering via designed nanostructure. Chemical Society Reviews 44(6): 1346-1378.

Li X. M., D. Y. Zhao and F. Zhang 2013. Multifunctional upconversion-magnetic hybrid nanostructured materials: synthesis and bioapplications. Theranostics 3(5): 292-305.

Li Z., H. Guo, H. Qian, et al. 2010. Facile microemulsion route to coat carbonized glucose on upconversion nanocrystals as high luminescence and biocompatible cell-imaging probes. Nanotechnology 21(31): 315105.

Li Z., L. Wang, Z. Wang, et al. 2011. Modification of NaYF4: Yb, Er@ SiO2

nanoparticles with gold nanocrystals for tunable green-to-red upconversion emissions. The Journal of Physical Chemistry C 115(8): 3291-3296.

Li Z. and Y. Zhang 2006. Monodisperse silica-coated polyvinylpyrrolidone/NaYF4 nanocrystals with multicolor upconversion fluorescence emission. Angewandte Chemie 118(46): 7896-7899.

Li Z. and Y. Zhang 2008. An efficient and user-friendly method for the synthesis of hexagonal-phase NaYF4: Yb, Er/Tm nanocrystals with controllable shape and upconversion fluorescence. Nanotechnology 19(34): 345606.

Li Z. Q., Y. Zhang and S. Jiang 2008. Multicolor core/shell-structured upconversion fluorescent nanoparticles. Advanced Materials 20(24): 4765-4769.

Lian W., S. A. Litherland, H. Badrane, et al. 2004. Ultrasensitive detection of biomolecules with fluorescent dye-doped nanoparticles. Analytical Biochemistry 334(1): 135-144.

Lim S. F., R. Riehn, W. S. Ryu, et al. 2006. In vivo and scanning electron microscopy imaging of upconverting nanophosphors in Caenorhabditis elegans. Nano Letters 6(2): 169-174.

Lim S. F., R. Riehn, C.-k. Tung, et al. 2009. Upconverting nanophosphors for bioimaging. Nanotechnology 20(40): 405701.

Lin M., Y. Zhao, S. Wang, et al. 2012. Recent advances in synthesis and surface modification of lanthanide-doped upconversion nanoparticles for biomedical applications. Biotechnology Advances 30(6): 1551-1561.

Liu C., Z. Wang, X. Wang, et al. 2011. Surface modification of hydrophobic NaYF4: Yb, Er upconversion nanophosphors and their applications for immunoassay. Science China Chemistry 54(8): 1292-1297.

Liu F., Q. Zhao, H. You, et al. 2013. Synthesis of stable carboxy-terminated NaYF 4: Yb

3+, Er 3+@ SiO 2 nanoparticles with ultrathin shell for biolabeling applications. Nanoscale 5(3): 1047-1053.

Liu F. Y., X. X. He, L. Liu, et al. 2013. Conjugation of NaGdF4 upconverting nanoparticles on silica nanospheres as contrast agents for multi-modality imaging. Biomaterials 34(21): 5218-5225.

Liu J. A., W. B. Bu, S. J. Zhang, et al. 2012. Controlled synthesis of uniform and monodisperse upconversion core/mesoporous silica shell nanocomposites for bimodal imaging. Chemistry-a European Journal 18(8): 2335-2341.

Liu Q., M. Chen, Y. Sun, et al. 2011. Multifunctional rare-earth self-assembled nanosystem for tri-modal upconversion luminescence/fluorescence/positron emission tomography imaging. Biomaterials 32(32): 8243-8253.

Liu Q., Y. Sun, C. G. Li, et al. 2011. F-18-labeled magnetic-upconversion nanophosphors via rare-earth cation-assisted ligand assembly. ACS Nano 5(4): 3146-3157.

Liu S., G. Chen, T. Y. Ohulchanskyy, et al. 2013. Facile synthesis and potential bioimaging applications of hybrid upconverting and plasmonic NaGdF 4: Yb 3, Er 3/silica/gold nanoparticles. Theranostics 3(4): 275-281.

Liu Y., M. Chen, T. Cao, et al. 2013. A cyanine-modified nanosystem for in vivo upconversion luminescence bioimaging of methylmercury. Journal of the American Chemical Society 135(26): 9869-9876.

Liu Y., D. Tu, H. Zhu, et al. 2013. Lanthanide-doped luminescent nanoprobes: controlled synthesis, optical spectroscopy, and bioapplications. Chem Soc Rev 42(16): 6924-6958.

Liu Y., D. Tu, H. Zhu, et al. 2010. A strategy to achieve efficient dual-mode luminescence of Eu3+ in lanthanides doped multifunctional NaGdF4

nanocrystals. Advanced Materials 22(30): 3266-3271.

Liu Y., D. Tu, H. Zhu, et al. 2013. Lanthanide-doped luminescent nano-bioprobes: from fundamentals to biodetection. Nanoscale 5(4): 1369-1384.

Liu Y., S. Zhou, D. Tu, et al. 2012. Amine-functionalized lanthanide-doped zirconia nanoparticles: optical spectroscopy, time-resolved fluorescence resonance energy transfer biodetection, and targeted imaging. Journal of the American Chemical Society 134(36): 15083-15090.

Lowe A. R., J. J. Siegel, P. Kalab, et al. 2010. Selectivity mechanism of the nuclear pore complex characterized by single cargo tracking. Nature 467(7315): 600-603.

Lu A. H., E. e. L. Salabas and F. Schüth 2007. Magnetic nanoparticles: synthesis, protection, functionalization, and application. Angewandte Chemie International Edition 46(8): 1222-1244.

Lü Q., F. Guo, L. Sun, et al. 2008. Surface modification of ZrO2: Er3+ nanoparticles to attenuate aggregation and enhance upconversion fluorescence. The Journal of Physical Chemistry C 112(8): 2836-2844.

Lü Q., A. Li, F. Guo, et al. 2008. Experimental study on the surface modification of Y2O3: Tm3+/Yb3+ nanoparticles to enhance upconversion fluorescence and weaken aggregation. Nanotechnology 19(14): 145701.

Luo S., E. Zhang, Y. Su, et al. 2011. A review of NIR dyes in cancer targeting and imaging. Biomaterials 32(29): 7127-7138.

Luo S. L., E. L. Zhang, Y. P. Su, et al. 2011. A review of NIR dyes in cancer targeting and imaging. Biomaterials 32(29): 7127-7138.

Ma J., P. Huang, M. He, et al. 2012. Folic acid-conjugated LaF3: Yb, Tm@ SiO2 nanoprobes for targeting dual-modality imaging of upconversion luminescence and X-ray computed tomography. The Journal of Physical Chemistry B 116(48):

14062-14070.

Mader H. S., P. Kele, S. M. Saleh, et al. 2010. Upconverting luminescent nanoparticles for use in bioconjugation and bioimaging. Current Opinion in Chemical Biology 14(5): 582-596.

Mayer A., E. Tsiompanou, D. O'Malley, et al. 2000. Radioimmunoguided surgery in colorectal cancer using a genetically engineered anti-CEA single-chain Fv antibody. Clinical Cancer Research 6(5): 1711-1719.

Mettlin C., F. Lee, J. Drago, et al. 1991. The American cancer society national prostate cancer detection project. Findings on the detection of early prostate cancer in 2425 men. Cancer 67(12): 2949-2958.

Mi C., J. Zhang, H. Gao, et al. 2010. Multifunctional nanocomposites of superparamagnetic (F3O4) and NIR-responsive rare earth-doped up-conversion fluorescent (NaYF4: Yb, Er) nanoparticles and their applications in biolabeling and fluorescent imaging of cancer cells. Nanoscale 2(7): 1141-1148.

Mi Y., K. Li, Y. Liu, et al. 2011. Herceptin functionalized polyhedral oligomeric silsesquioxane–conjugated oligomers–silica/iron oxide nanoparticles for tumor cell sorting and detection. Biomaterials 32(32): 8226-8233.

Michalet X., F. F. Pinaud, L. A. Bentolila, et al. 2005. Quantum dots for live cells, in vivo imaging, and diagnostics. Science 307(5709): 538-544.

Min Y. Z., J. M. Li, F. Liu, et al. 2014. Recent advance of biological molecular imaging based on lanthanide-doped upconversion-luminescent nanomaterials. Nanomaterials 4(1): 129-154.

Misra R., S. Acharya and S. K. Sahoo 2010. Cancer nanotechnology: application of nanotechnology in cancer therapy. Drug Discovery Today 15(19): 842-850.

Miyawaki A., J. Llopis, R. Heim, et al. 1997. Fluorescent indicators for Ca2+ based on

green fluorescent proteins and calmodulin. Nature 388(6645): 882-887.

Moghimi S. M., A. C. Hunter and J. C. Murray 2005. Nanomedicine: current status and future prospects. Faseb Journal 19(3): 311-330.

Muhr V., S. Wilhelm, T. Hirsch, et al. 2014. Upconversion nanoparticles: from hydrophobic to hydrophilic surfaces. Accounts of Chemical Research 47(12): 3481-3493.

Nichkova M., D. Dosev, S. J. Gee, et al. 2005. Microarray immunoassay for phenoxybenzoic acid using polymer encapsulated Eu: Gd2O3 nanoparticles as fluorescent labels. Analytical Chemistry 77(21): 6864-6873.

Nie S., Y. Xing, G. J. Kim, et al. 2007. Nanotechnology applications in cancer. Annual Review of Biomedical Engineering 9: 257-288.

Nyk M., R. Kumar, T. Y. Ohulchanskyy, et al. 2008. High contrast in vitro and in vivo photoluminescence bioimaging using near infrared to near infrared up-conversion in Tm3+ and Yb3+ doped fluoride nanophosphors. Nano Letters 8(11): 3834-3838.

Pankhurst Q. A., J. Connolly, S. Jones, et al. 2003. Applications of magnetic nanoparticles in biomedicine. Journal of physics D: Applied Physics 36(13): R167.

Pantel K., R. H. Brakenhoff and B. Brandt 2008. Detection, clinical relevance and specific biological properties of disseminating tumour cells. Nature Reviews Cancer 8(5): 329-340.

Park Y. I., K. T. Lee, Y. D. Suh, et al. 2015. Upconverting nanoparticles: a versatile platform for wide-field two-photon microscopy and multi-modal in vivo imaging. Chemical Society Reviews 44(6): 1302-1317.

Pastorino U., M. Bellomi, C. Landoni, et al. 2003. Early lung-cancer detection with

spiral CT and positron emission tomography in heavy smokers: 2-year results. The Lancet 362(9384): 593-597.

Peer D., J. M. Karp, S. Hong, et al. 2007. Nanocarriers as an emerging platform for cancer therapy. Nature Nanotechnology 2(12): 751-760.

Pepe M. S., R. Etzioni, Z. D. Feng, et al. 2001. Phases of biomarker development for early detection of cancer. Journal of the National Cancer Institute 93(14): 1054-1061.

Pierschbacher M., E. G. Hayman and E. Ruoslahti 1983. Synthetic peptide with cell attachment activity of fibronectin. Proceedings of the National Academy of Sciences 80(5): 1224-1227.

Piliarik M. and V. Sandoghdar 2014. Direct optical sensing of single unlabelled proteins and super-resolution imaging of their binding sites. Nature Communications 5.

Pollnau M., D. Gamelin, S. Lüthi, et al. 2000. Power dependence of upconversion luminescence in lanthanide and transition-metal-ion systems. Physical Review B 61(5): 3337.

Qian H. S. and Y. Zhang 2008. Synthesis of hexagonal-phase core-shell NaYF4 nanocrystals with tunable upconversion fluorescence. Langmuir 24(21): 12123-12125.

Ramasamy P., P. Chandra, S. W. Rhee, et al. 2013. Enhanced upconversion luminescence in NaGdF 4: Yb, Er nanocrystals by Fe 3+ doping and their application in bioimaging. Nanoscale 5(18): 8711-8717.

Rantanen T., M.-L. Järvenpää, J. Vuojola, et al. 2009. Upconverting phosphors in a dual-parameter LRET-based hybridization assay. Analyst 134(8): 1713-1716.

Resch-Genger U., M. Grabolle, S. Cavaliere-Jaricot, et al. 2008. Quantum dots versus organic dyes as fluorescent labels. Nature Methods 5(9): 763-775.

Roychowdhury S. and A. M. Chinnaiyan 2013. Advancing precision medicine for prostate cancer through genomics. Journal of Clinical Oncology 31(15): 1866-1873.

Rusling J. F., C. V. Kumar, J. S. Gutkind, et al. 2010. Measurement of biomarker proteins for point-of-care early detection and monitoring of cancer. Analyst 135(10): 2496-2511.

Russell P., K. Ow, P. Tam, et al. 2004. Immunohistochemical characterisation of the monoclonal antibody BLCA-38 for the detection of prostate cancer. Cancer Immunology, Immunotherapy 53(11): 995-1004.

Ryu J., H. Y. Park, K. Kim, et al. 2010. Facile synthesis of ultrasmall and hexagonal NaGdF4: Yb3+, Er3+ nanoparticles with magnetic and upconversion imaging properties. The Journal of Physical Chemistry C 114(49): 21077-21082.

Santra S., P. Zhang, K. M. Wang, et al. 2001. Conjugation of biomolecules with luminophore-doped silica nanoparticles for photostable biomarkers. Analytical Chemistry 73(20): 4988-4993.

Schäfer H., P. Ptacek, K. Kömpe, et al. 2007. Lanthanide-doped NaYF4 nanocrystals in aqueous solution displaying strong up-conversion emission. Chemistry of Materials 19(6): 1396-1400.

Sedlmeier A. and H. H. Gorris 2015. Surface modification and characterization of photon-upconverting nanoparticles for bioanalytical applications. Chemical Society Reviews 44(6): 1526-1560.

Shan J. N., S. J. Budijono, G. H. Hu, et al. 2011. PEGylated composite nanoparticles containing upconverting phosphors and meso-tetraphenyl porphine (TPP) for photodynamic therapy. Advanced Functional Materials 21(13): 2488-2495.

Shen B.-Q., K. Xu, L. Liu, et al. 2012. Conjugation site modulates the in vivo stability

and therapeutic activity of antibody-drug conjugates. Nature Biotechnology 30(2): 184-189.

Shen J., G. Chen, T. Y. Ohulchanskyy, et al. 2013. Tunable near infrared to ultraviolet upconversion luminescence enhancement in (α-NaYF4: Yb, Tm)/CaF2 core/shell nanoparticles for in situ real-time recorded biocompatible photoactivation. Small 9(19): 3213-3217.

Shen J., L. D. Sun, Y. W. Zhang, et al. 2010. Superparamagnetic and upconversion emitting Fe3O4/NaYF4: Yb, Er hetero-nanoparticles via a crosslinker anchoring strategy. Chemical Communications 46(31): 5731-5733.

Shi J. Y., F. Tian, J. Lyu, et al. 2015. Nanoparticle based fluorescence resonance energy transfer (FRET) for biosensing applications. Journal of Materials Chemistry B 3(35): 6989-7005.

Siegel R. L., K. D. Miller and A. Jemal 2015. Cancer statistics, 2015. CA: A Cancer Journal for Clinicians 65(1): 5-29.

Sivakumar S., P. R. Diamente and F. C. van Veggel 2006. Silica-coated Ln3+-doped LaF3 nanoparticles as robust down-and-pconverting biolabels. Chemistry–A European Journal 12(22): 5878-5884.

Sivakumar S., F. C. M. van Veggel and M. Raudsepp 2005. Bright white light through up-conversion of a single NIR source from sol-gel-derived thin film made with Ln3+-doped LaF3 nanoparticles. Journal of the American Chemical Society 127(36): 12464-12465.

Smith A. M., H. Duan, A. M. Mohs, et al. 2008. Bioconjugated quantum dots for in vivo molecular and cellular imaging. Advanced Drug Delivery Reviews 60(11): 1226-1240.

Srinivas P. R., P. Barker and S. Srivastava 2002. Nanotechnology in early detection of

cancer. Laboratory Investigation 82(5): 657-662.

Srinivas P. R., B. S. Kramer and S. Srivastava 2001. Trends in biomarker research for cancer detection. Lancet Oncology 2(11): 698-704.

Stewart B. and C. P. Wild 2015. World cancer report 2014. World.

Sukhorukov G. B., E. Donath, H. Lichtenfeld, et al. 1998. Layer-by-layer self assembly of polyelectrolytes on colloidal particles. Colloids and Surfaces A: Physicochemical and Engineering Aspects 137(1): 253-266.

Szymanski C., C. Wu, J. Hooper, et al. 2005. Single molecule nanoparticles of the conjugated polymer MEH-PPV, preparation and characterization by near-field scanning optical microscopy. The Journal of Physical Chemistry B 109(18): 8543-8546.

Tartaj P., M. del Puerto Morales, S. Veintemillas-Verdaguer, et al. 2003. The preparation of magnetic nanoparticles for applications in biomedicine. Journal of physics D: Applied physics 36(13): R182.

Tsang M. K., C. F. Chan, K.-L. Wong, et al. 2015. Comparative studies of upconversion luminescence characteristics and cell bioimaging based on one-step synthesized upconversion nanoparticles capped with different functional groups. Journal of Luminescence 157: 172-178.

Tsuda M., K. Soga, H. Inoue, et al. 1999. Upconversion mechanism in Er3+-doped fluorozirconate glasses under 800 nm excitation. Journal of Applied Physics 85: 29-37.

Tu D., L. Liu, Q. Ju, et al. 2011. Time-resolved FRET biosensor based on amine-functionalized lanthanide-doped NaYF4 nanocrystals. Angewandte Chemie International Edition 50(28): 6306-6310.

Tuncel D. and H. V. Demir 2010. Conjugated polymer nanoparticles. Nanoscale 2(4):

484-494.

Vennerberg D. and Z. Q. Lin 2011. Upconversion Nanocrystals: Synthesis, Properties, Assembly and Applications. Science of Advanced Materials 3(1): 26-40.

Vetrone F., J. C. Boyer, J. A. Capobianco, et al. 2004. Significance of Yb3+ concentration on the upconversion mechanisms in codoped Y2O3: Er3+, Yb3+ nanocrystals. Journal of Applied Physics 96: 661-667.

Vinhas R., M. Cordeiro, F. Carlos, et al. 2015. Gold nanoparticle-based theranostics: disease diagnostics and treatment using a single nanomaterial. Nanobiosensors Disease Diagnosis 4: 11-23.

Wagh A. and B. Law 2013. Methods for conjugating antibodies to nanocarriers. Antibody-Drug Conjugates: 249-266.

Wang C., L. Cheng and Z. Liu 2011. Drug delivery with upconversion nanoparticles for multi-functional targeted cancer cell imaging and therapy. Biomaterials 32(4): 1110-1120.

Wang C., L. Cheng and Z. Liu 2013. Upconversion nanoparticles for photodynamic therapy and other cancer therapeutics. Theranostics 3(5): 317-330.

Wang C., L. Cheng, H. Xu, et al. 2012. Towards whole-body imaging at the single cell level using ultra-sensitive stem cell labeling with oligo-arginine modified upconversion nanoparticles. Biomaterials 33(19): 4872-4881.

Wang F., D. Banerjee, Y. Liu, et al. 2010. Upconversion nanoparticles in biological labeling, imaging, and therapy. Analyst 135(8): 1839-1854.

Wang F., D. K. Chatterjee, Z. Li, et al. 2006. Synthesis of polyethylenimine/NaYF4 nanoparticles with upconversion fluorescence. Nanotechnology 17(23): 5786.

Wang F., R. R. Deng, J. Wang, et al. 2011. Tuning upconversion through energy

migration in core-shell nanoparticles. Nature Materials 10(12): 968-973.

Wang F., Y. Han, C. S. Lim, et al. 2010. Simultaneous phase and size control of upconversion nanocrystals through lanthanide doping. Nature 463(7284): 1061-1065.

Wang F. and X. Liu 2008. Upconversion multicolor fine-tuning: visible to near-infrared emission from lanthanide-doped NaYF4 nanoparticles. Journal of the American Chemical Society 130(17): 5642-5643.

Wang F. and X. G. Liu 2009. Recent advances in the chemistry of lanthanide-doped upconversion nanocrystals. Chemical Society Reviews 38(4): 976-989.

Wang F., J. Wang and X. Liu 2010. Direct evidence of a surface quenching effect on size-dependent luminescence of upconversion nanoparticles. Angewandte Chemie 122(41): 7618-7622.

Wang F., X. Yang, L. Ma, et al. 2012. Multifunctional up-converting nanocomposites with multimodal imaging and photosensitization at near-infrared excitation. Journal of Materials Chemistry 22(47): 24597-24604.

Wang G. F., Q. Peng and Y. D. Li 2011. Lanthanide-doped nanocrystals: synthesis, optical-magnetic properties, and applications. Accounts of Chemical Research 44(5): 322-332.

Wang J., T. Wei, X. Li, et al. 2014. Near-infrared-light-mediated imaging of latent fingerprints based on molecular recognition. Angewandte Chemie International Edition 126(6): 1642-1646.

Wang L., R. Yan, Z. Huo, et al. 2005. Fluorescence resonant energy transfer biosensor based on upconversion-luminescent nanoparticles. Angewandte Chemie International Edition 44(37): 6054-6057.

Wang L., W. Zhao and W. Tan 2008. Bioconjugated silica nanoparticles: development

and applications. Nano Research 1(2): 99-115.

Wang M., G. Abbineni, A. Clevenger, et al. 2011. Upconversion nanoparticles: synthesis, surface modification and biological applications. Nanomedicine: Nanotechnology, Biology and Medicine 7(6): 710-729.

Wang M., C. C. Mi, W. X. Wang, et al. 2009. Immunolabeling and NIR-excited fluorescent imaging of HeLa cells by using NaYF4: Yb, Er upconversion nanoparticles. ACS Nano 3(6): 1580-1586.

Wang M., C. Mi, Y. Zhang, et al. 2009. NIR-responsive silica-coated NaYbF4: Er/Tm/Ho upconversion fluorescent nanoparticles with tunable emission colors and their applications in immunolabeling and fluorescent imaging of cancer cells. The Journal of Physical Chemistry C 113(44): 19021-19027.

Wang M. and M. Thanou 2010. Targeting nanoparticles to cancer. Pharmacol Research 62(2): 90-99.

Wang M. D., D. M. Shin, J. W. Simons, et al. 2007. Nanotechnology for targeted cancer therapy. Expert Eeview of Anticancer Therapy 7(6): 833-837.

Wang X. D., O. S. Wolfbeis and R. J. Meier 2013. Luminescent probes and sensors for temperature. Chemical Society Reviews 42(19): 7834-7869.

Wang X., Y. Bu, S. Xiao, et al. 2008. Upconversion in Ho3+-doped YbF3 particle prepared by coprecipitation method. Applied Physics B 93(4): 801-807.

Wegner K. D. and N. Hildebrandt 2015. Quantum dots: bright and versatile in vitro and in vivo fluorescence imaging biosensors. Chemical Society Reviews 44(14): 4792-4834.

Wilhelm S., T. Hirsch, W. M. Patterson, et al. 2013. Multicolor upconversion nanoparticles for protein conjugation. Theranostics 3(4): 239.

Wolfbeis O. S. 2015. An overview of nanoparticles commonly used in fluorescent bioimaging. Chemical Society Reviews 44(14): 4743-4768.

Wolfe C. A. and D. S. Hage 1995. Studies on the rate and control of antibody oxidation by periodate. Analytical Biochemistry 231(1): 123-130.

Wong H. T., H. L. W. Chan and J. Hao 2010. Towards pure near-infrared to near-infrared upconversion of multifunctional GdF 3: Yb 3+, Tm 3+ nanoparticles. Optics Express 18(6): 6123-6130.

Wu C., B. Bull, C. Szymanski, et al. 2008. Multicolor conjugated polymer dots for biological fluorescence imaging. ACS Nano 2(11): 2415-2423.

Wu C. and D. T. Chiu 2013. Highly fluorescent semiconducting polymer dots for biology and medicine. Angewandte Chemie International Edition 52(11): 3086-3109.

Wu C., H. Peng, Y. Jiang, et al. 2006. Energy transfer mediated fluorescence from blended conjugated polymer nanoparticles. The Journal of Physical Chemistry B 110(29): 14148-14154.

Wu C., T. Schneider, M. Zeigler, et al. 2010. Bioconjugation of ultrabright semiconducting polymer dots for specific cellular targeting. Journal of the American Chemical Society 132(43): 15410-15417.

Wu C., C. Szymanski, Z. Cain, et al. 2007. Conjugated polymer dots for multiphoton fluorescence imaging. Journal of the American Chemical Society 129(43): 12904-12905.

Wu S., N. Duan, Z. Wang, et al. 2011. Aptamer-functionalized magnetic nanoparticle-based bioassay for the detection of ochratoxin a using upconversion nanoparticles as labels. Analyst 136(11): 2306-2314.

Wu X., G. Y. Chen, J. Shen, et al. 2015. Upconversion nanoparticles: a versatile solution

to multiscale biological imaging. Bioconjugate Chemistry 26(2): 166-175.

Wu Y. M., Y. Cen, L. J. Huang, et al. 2014. Upconversion fluorescence resonance energy transfer biosensor for sensitive detection of human immunodeficiency virus antibodies in human serum. Chemical Communications 50(36): 4759-4762.

Wulfkuhle J. D., L. A. Liotta and E. F. Petricoin 2003. Proteomic applications for the early detection of cancer. Nature Reviews Cancer 3(4): 267-275.

Xia A., M. Chen, Y. Gao, et al. 2012. Gd3+ complex-modified NaLuF4-based upconversion nanophosphors for trimodality imaging of NIR-to-NIR upconversion luminescence, X-Ray computed tomography and magnetic resonance. Biomaterials 33(21): 5394-5405.

Xing H., W. Bu, S. Zhang, et al. 2012. Multifunctional nanoprobes for upconversion fluorescence, MR and CT trimodal imaging. Biomaterials 33(4): 1079-1089.

Xing L., N. W. Todd, L. Yu, et al. 2010. Early detection of squamous cell lung cancer in sputum by a panel of microRNA markers. Modern Pathology 23(8): 1157-1164.

Xing Y. and J. H. Rao 2008. Quantum dot bioconjugates for in vitro diagnostics & in vivo imaging. Cancer Biomarkers 4(6): 307-319.

Xiong L. Q., Z. G. Chen, M. X. Yu, et al. 2009. Synthesis, characterization, and in vivo targeted imaging of amine-functionalized rare-earth up-converting nanophosphors. Biomaterials 30(29): 5592-5600.

Xiong L., Z. Chen, Q. Tian, et al. 2009. High contrast upconversion luminescence targeted imaging in vivo using peptide-labeled nanophosphors. Analytical Chemistry 81(21): 8687-8694.

Xiong L., T. Yang, Y. Yang, et al. 2010. Long-term in vivo biodistribution imaging and toxicity of polyacrylic acid-coated upconversion nanophosphors. Biomaterials

31(27): 7078-7085.

Xu C. T., Q. Q. Zhan, H. C. Liu, et al. 2013. Upconverting nanoparticles for pre-clinical diffuse optical imaging, microscopy and sensing: Current trends and future challenges. Laser & Photonics Reviews 7(5): 663-697.

Xu W., H. Zhao, Y. Li, et al. 2013. Optical temperature sensing through the upconversion luminescence from Ho 3+/Yb 3+ codoped CaWO 4. Sensors and Actuators B: Chemical 188: 1096-1100.

Yang J., Y. Deng, Q. Wu, et al. 2010. Mesoporous silica encapsulating upconversion luminescence rare-earth fluoride nanorods for secondary excitation. Langmuir 26(11): 8850-8856.

Yang J. L., S. J. An, W. I. Park, et al. 2004. Photocatalysis using ZnO thin films and nanoneedles grown by metal–organic chemical vapor deposition. Advanced Materials 16(18): 1661-1664.

Yang W., Y. Wang, L. Chang, et al. 2014. Highly sensitive detection of protein kinase activity using upconversion luminescent nanoparticles. RSC Advances 4(28): 14546-14549.

Yang Y., Q. Zhao, W. Feng, et al. 2012. Luminescent chemodosimeters for bioimaging. Chemical Reviews 113(1): 192-270.

Yang Y. M., B. Velmurugan, X. G. Liu, et al. 2013. NIR photoresponsive crosslinked upconverting nanocarriers toward selective intracellular drug release. Small 9(17): 2937-2944.

Yao C., P. Wang, L. Zhou, et al. 2014. Highly biocompatible zwitterionic phospholipids coated upconversion nanoparticles for efficient bioimaging. Analytical Chemistry 86(19): 9749-9757.

Yao J., M. Yang and Y. Duan 2014. Chemistry, biology, and medicine of fluorescent

nanomaterials and related systems: New insights into biosensing, bioimaging, genomics, diagnostics, and therapy. Chemical Reviews 114(12): 6130-6178.

Yi G. S. C., Gan-Moog 2007. Water-soluble NaYF: Yb, Er (Tm)/NaYF4/polymer core/shell/shell nanoparticles with significant enhancement of upconversion fluorescence. Chemistry of Materials 19(3): 341-343.

Yi G., Y. Peng and Z. Gao 2011. Strong red-emitting near-infrared-to-visible upconversion fluorescent nanoparticles. Chemistry of Materials 23(11): 2729-2734.

Yi G. S. and G. M. Chow 2006. Synthesis of hexagonal-phase NaYF4: Yb, Er and NaYF4: Yb, Tm nanocrystals with efficient upconversion fluorescence. Advanced Functional Materials 16(18): 2324-2329.

Yi G. S. and G. M. Chow 2007. Water-soluble NaYF4 : Yb,Er(Tm)/NaYF4/polymer core/shell/shell nanoparticles with significant enhancement of upconversion fluorescence. Chemistry of Materials 19(3): 341-343.

Yu X. F., Z. Sun, M. Li, et al. 2010. Neurotoxin-conjugated upconversion nanoprobes for direct visualization of tumors under near-infrared irradiation. Biomaterials 31(33): 8724-8731.

Zako T., H. Nagata, N. Terada, et al. 2009. Cyclic RGD peptide-labeled upconversion nanophosphors for tumor cell-targeted imaging. Biochemical and Biophysical Research Communications 381(1): 54-58.

Zeng S. J., Z. G. Yi, W. Lu, et al. 2014. Simultaneous realization of phase/size manipulation, upconversion luminescence enhancement, and blood vessel imaging in multifunctional nanoprobes through transition metal Mn2+ doping. Advanced Functional Materials 24(26): 4051-4059.

Zhan Q., J. Qian, H. Liang, et al. 2011. Using 915 nm laser excited

Tm3+/Er3+/Ho3+-doped NaYbF4 upconversion nanoparticles for in vitro and deeper in vivo bioimaging without overheating irradiation. ACS Nano 5(5): 3744-3757.

Zhang F. 2015. Surface Modification and Bioconjugation of Upconversion Nanoparticles. Photon Upconversion Nanomaterials, Springer**:** 159-185.

Zhang Y., W. Wei, G. K. Das, et al. 2014. Engineering lanthanide-based materials for nanomedicine. Journal of Photochemistry and Photobiology C-Photochemistry Reviews 20: 71-96.

Zhao J., D. Jin, E. P. Schartner, et al. 2013. Single-nanocrystal sensitivity achieved by enhanced upconversion luminescence. Nature Nanotechnology 8(10): 729-734.

Zhou H. P., C. H. Xu, W. Sun, et al. 2009. Clean and flexible modification strategy for carboxyl/aldehyde-functionalized upconversion nanoparticles and their optical applications. Advanced Functional Materials 19(24): 3892-3900.

Zhou J., Z. Liu and F. Y. Li 2012. Upconversion nanophosphors for small-animal imaging. Chemical Society Reviews 41(3): 1323-1349.

Zhou J., L. Yao, C. Li, et al. 2010. A versatile fabrication of upconversion nanophosphors with functional-surface tunable ligands. Journal of Materials Chemistry 20(37): 8078-8085.

Zhou J., M. X. Yu, Y. Sun, et al. 2011. Fluorine-18-labeled Gd3+/Yb3+/Er3+ co-doped NaYF4 nanophosphors for multimodality PET/MR/UCL imaging. Biomaterials 32(4): 1148-1156.

Zhou L., B. Z. He, J. C. Huang, et al. 2014. Multihydroxy dendritic upconversion nanoparticles with enhanced water dispersibility and surface functionality for bioimaging. Acs Applied Materials & Interfaces 6(10): 7719-7727.

Zhu X. J., J. Zhou, M. Chen, et al. 2012. Core-shell Fe3O4@NaLuF4:Yb,Er/Tm

nanostructure for MRI, CT and upconversion luminescence tri-modality imaging. Biomaterials 33(18): 4618-4627.

Zijlmans H., J. Bonnet, J. Burton, et al. 1999. Detection of cell and tissue surface antigens using up-converting phosphors: a new reporter technology. Analytical biochemistry 267(1): 30-36.

Zitzmann S., V. Ehemann and M. Schwab 2002. Arginine-glycine-aspartic acid (RGD)-peptide binds to both tumor and tumor-endothelial cells in vivo. Cancer research 62(18): 5139-5143.

Contribution to Published Work

In addition to the work described in the thesis, I have provided contribution to the following papers：

[1] **Yu Shi**, Bingyang Shi, Arun V. Everest Dass, Yiqing Lu, Nima Sayyadi, Liisa Kautto, Robert D. Willows, Roger Chung, James Piper, Helena Nevalainen, Bradley Walsh, Dayong Jin and Nicolle H. Packer. 2016. Stable Upconversion nanohybrid particles for specific prostate cancer cell immunodetection. Scientific Reports 6, 37533; doi: 10.1038/srep37533

[2] Jie Lu, Yinghui Chen, Deming Liu, Wei Ren, Yiqing Lu, **Yu Shi**, James Piper, Ian Paulsen and Dayong Jin. 2015. One-step protein conjugation to upconversion nanoparticles. Analytical Chemestry 87: 10406−10413

[3] Hongmin Jia, Xue Gao, **Yu Shi**, Nima Sayyadi, Zhiqiang Zhang, Qi Zhao, Qingtao Meng, Run Zhang. 2015. Fluorescence detection of Fe 3+ ions in aqueous solution and living cells based on a high selectivity and sensitivity chemosensor. Spectrochimica Acta Part A: Molecular and Biomolecular Spectroscopy 149: 674-681

[4] Qingtao Meng, **Yu Shi**, Cuiping Wang, Hongmin Jia, Xue Gao, Run Zhang, Yongfei Wang, Zhiqiang Zhang. 2015. NBD-based fluorescent chemosensor for the selective quantification of copper and sulfide in an aqueous solution and living cells. Organic & Biomolecular Chemistry 13(10): 2918-2926

[5] Qingtao Meng, Run Zhang, Hongmin Jia, Xue Gao, Cuiping Wang, **Yu Shi**, Arun V Everest-Dass, Zhiqiang Zhang. 2015. A reversible fluorescence chemosensor for sequentially quantitative monitoring copper and sulfide in living cells. Talanta 143(2015): 294–301

[6] Yiqing Lu, Jiangbo Zhao, Run Zhang, Yujia Liu, Deming Liu, Ewa M Goldys, Xusan Yang, Peng Xi, Anwar Sunna, Jie Lu, **Yu Shi**, Robert C Leif, Yujing Huo, Jian Shen, James A Piper, J Paul Robinson, Dayong Jin. 2014. Tunable lifetime multiplexing using luminescent nanocrystals. Nature Photonics 8(1): 32-36